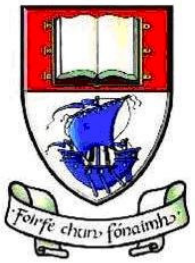

An Investigation into the Mechanisms of Heavy Metal Binding by Selected Seaweed Species

Submitted in partial fulfilment of the requirements for the degree of Doctor of Philosophy

Based on work carried out by Vanessa Murphy

under the supervision of Dr. Helen Hughes and Dr Peter McLoughlin

Submitted to Waterford Institute of Technology

May 2007

Declaration

No element of the work described in this thesis, except where otherwise acknowledged, has been previously submitted for a degree at this or any other institution. The work in this thesis has been performed entirely by the author.

Signed : _____

Date : _____

Acknowledgements

Firstly, I would like to sincerely thank my fantastic supervisors Dr. Helen Hughes and Dr. Peter McLoughlin for their encouragement, guidance and enthusiasm during my time in W.I.T.

To the staff of W.I.T. especially Drs Jim Stack and Joe O' Mahony for their boundless enthusiasm (even when confronted with a subject like seaweed!!).

To my fellow postgrads for their friendship throughout the years.

To the Irish Research Council for Science, Engineering and Technology without whose generous funding this research would not have taken place.

To the Tyndall National Institute, Cork for the use of their SEM/EDX facilities as part of the National Access Programme and the Materials and Surface Science Institute (Tofail Syed and Balazs Azalos) for their XPS analysis.

To Cora McGrath (RIP) who taught me not to worry about the "ifs" and "ands".

And last, but not least, to my friends and family especially my wonderful and extraordinary mother for her unwavering love and support through the ups, the downs and the in-betweens.

Publications

1. Cu (II) binding by dried biomass of red, green and brown macroalgae. *Water Research* **41** 731-740 (2007)

   Vanessa Murphy, Helen Hughes, Peter McLoughlin

2. Comparative study of chromium biosorption by red, green and brown seaweed biomass. *Chemosphere* (In Press)

   Vanessa Murphy, Helen Hughes, Peter McLoughlin

Abstract

The Irish Marine Institute has identified the potential of marine natural resources to be exploited as high value-added products. Marine biotechnology is at an early stage of development, and therefore, more of the potential global market is open for development by Ireland than is the case for other sectors. A key area of growth, both in Ireland and Europe is the use of seaweeds for various applications including bioremediation of heavy metal contaminated waters.

This thesis has demonstrated a method for identifying the most promising seaweeds for metal biosorption through the use of multiple analytical techniques. A comprehensive study of dead biomass of six locally derived seaweeds (*Fucus vesiculosus*, *Fucus spiralis*, *Ulva lactuca*, *Ulva* spp., *Palmaria palmata* and *Polysiphonia lanosa*) and three regionally significant metals (Cu (II), Cr (III) and Cr (VI)) was carried out. Fundamental investigations into metal binding were undertaken in order to determine the potential binding capacity of the seaweeds, the factors influencing binding and their potential mechanisms of binding. This work has adapted a number of analytical techniques previously used for seaweed analysis and modified them so that binding information supplementary to that found in the literature could be obtained.

Studies indicated that seaweed is polyfunctional in nature with groups of varying affinities for metal ions. The quantity and distribution of these groups varied between species. Variations in experimental parameters were shown to influence the quantity of metal bound to the seaweeds, with optimum conditions dependent on the metal under investigation. Isotherm modelling revealed that *Fucus vesiculosus* and *Polysiphonia lanosa* were most effective in removing cations and anions respectively from solutions containing high residual metal concentrations while *Palmaria palmata* was superior for both cation and anion removal at low residual concentrations. Therefore, this implied that the most suitable seaweed biosorbent was ultimately dependent upon its final application. Changes in seaweed functional groups after metal binding were monitored using FTIR analysis with novel information on the timescale of Cu (II) binding presented.

Ion-exchange and complexation mechanisms were shown to occur for cation binding while a surface reduction mechanism was also apparent during anion binding. The use of multiple chemical modification techniques confirmed binding mechanisms and identified a methodology for capacity enhancement of the seaweeds. Important changes in surface morphology and binding mechanism were established using surface analysis techniques such as SEM/EDX and XPS while a novel methodology for seaweed surface analysis using SFM was also demonstrated.

Table of Contents

Chapter 3: Factors affecting metal biosorption

Chapter 4: FTIR Analysis

Chapter 5: SEM/EDX and XPS analysis

Chapter 8: Conclusions and Future Work

Appendices

Chapter 1
Literature Review

1.1 Seaweeds

1.1.1 What are seaweeds?

Seaweeds are marine algae: saltwater-dwelling, simple organisms that fall into the general category of "plants" [1]. They are found throughout the world's oceans and are classified into brown, red and green seaweeds [2] as illustrated in Figure 1.1.

Figure 1.1 Commonly found seaweed species (a) *Fucus vesiculosus* (brown) (b) *Palmaria palmata* (red) (c) *Ulva lactuca* (green) [3].

The mixture of pigments in their chloroplasts lends characteristic colours to the algae and many of their common and scientific names are based on these colours. Although their pigment composition is often used in their classification, the actual colour of seaweeds tends to vary a great deal.

1.1.2 Classification

Bold and Wynne [4] have carried out extensive work on the classification of algae. Seaweeds may be classified as follows:

The largest and most comprehensive taxonomic group within plants is called the **division**. There are seven divisions of algae, four of which contain seaweeds as members. Divisions which include the larger visible seaweeds are the Cyanophyta (blue-green algae), Chlorophyta (green algae), Rhodophyta (red algae) and Phaeophyta (brown algae)

[5]. However, the Cyanophyta are eubacteria, and are therefore evolutionarily distinct from macroalgae [6].

These divisions are subdivided into **orders** (e.g. Fucales), which are subsequently divided into **families** (e.g. Fucaceae), and then into **genus** (e.g. *Fucus*) and **species** (e.g. *vesiculosus*) [4].

1.1.3 Seaweed Ecology

Seaweeds are very important ecologically as they dominate the rocky intertidal zone in most oceans. However in temperate and polar regions they dominate rocky surfaces in the shallow subtidal. They are typically found only in shallow waters of depths of less than 200m because of the light requirement for photosynthesis but some may be found to depths of 250m in particularly clear waters.

The distributions of various seaweed species are related to temperature, light and tides while quality of light that reaches different depths may play some minor role in the vertical distribution of seaweeds [7].

Other functions controlling seaweed distribution are the amount of chlorophylls and accessory pigments present, the type of substrate, the presence of certain herbivores, tolerance to certain levels of irradiance or desiccation, and temperature and salinity fluctuations.

1.1.3.1 Phaeophyta

The largest and most complex members of the algae are members of the Phaeophyta (brown seaweeds) which contains approximately 2200 species, most of which are marine [1]. All are multi-cellular and they occur mainly in the marine environment, where they appear as an inter-tidal component being especially common along temperate coasts [8]. The brown colour of the Phaeophyta results from the dominance of the pigment fucoxanthin which masks the other pigments (including chlorophyll a and c, beta-carotene and other xanthophylls) [9].

1.1.3.2 Rhodophyta

There are about 6500 species of red algae, most of which are marine. These seaweeds are found in the intertidal zone but can be found in the subtidal to depths of up to 40, or occasionally, 250 m [1]. They are most abundant in the warm coastal waters of the tropics and the structure of the thallus of red algae does not show the wide variation in complexity and size that is observed in the brown algae.

The red colour of these algae results from the dominance of the pigments phycoerythrin and phycocyanin which masks the other pigments. These pigments reflect red light and absorb blue light [9].

1.1.3.3 Chlorophyta

Green algae may be unicellular, multicellular, colonial or coenocytic (composed of one large cell without cross-walls) [1] but few green algae are as complex as the brown and red algae in terms of the structure of the thallus. Most species are aquatic and are found commonly in freshwater and marine habitats while some are terrestrial, growing on soil, trees, or rocks. Some are symbiotic with fungi giving lichens. Others are symbiotic with animals, e.g. the freshwater coelentrate *Hydra* has a symbiotic species of *Chlorella*.

There are approximately 1200 marine species [1] with many species being dominant in environments with wide variations in salinity such as bays and estuaries.

1.1.4 Seaweed Structure and Morphology

The complete body of the seaweed is known as the thallus. The main parts of the thallus are: (1) the holdfast which anchors the plant to a surface and (2) the blades which are the principal sites of photosynthesis but also remove nutrients from water.

Figure 1.2 illustrates the corresponding components of seaweeds and land plants. The structural differences between them are as a result of their differing biological needs [5].

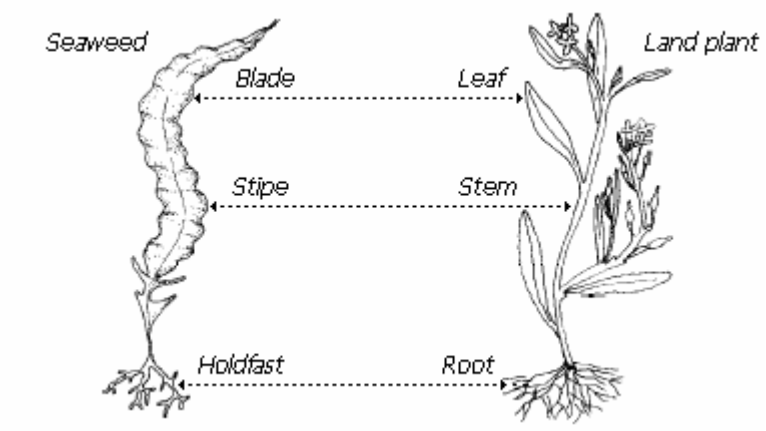

Figure 1.2 The corresponding components of land plants and seaweeds [10].

From Figure 1.2 it is seen that while land plants need roots for attachment as well as the absorption of water and mineral nutrients from the soil, seaweeds are immersed in their own water and nutrient supply and therefore absorb these materials directly into their cells.

Land plants also need firm stems to hold themselves upright and transfer the material absorbed through the roots to the leaves while seaweeds require secure attachment by a holdfast.

Certain seaweed species have a stipe, a cylindrical flexible shaft rising from the holdfast and supporting the remainder of the plant. Also, air bladders in some seaweeds assist in the flotation of the photosynthetic tissues [5].

1.1.5 Cell Wall Composition

Typical algal cell walls of Phaeophyta, Rhodophyta, and many Chlorophyta are comprised of at least two different layers- a fibrillar skeleton and an amorphous embedding matrix [6]. Figure 1.3 illustrates the cell wall structure in brown algae.

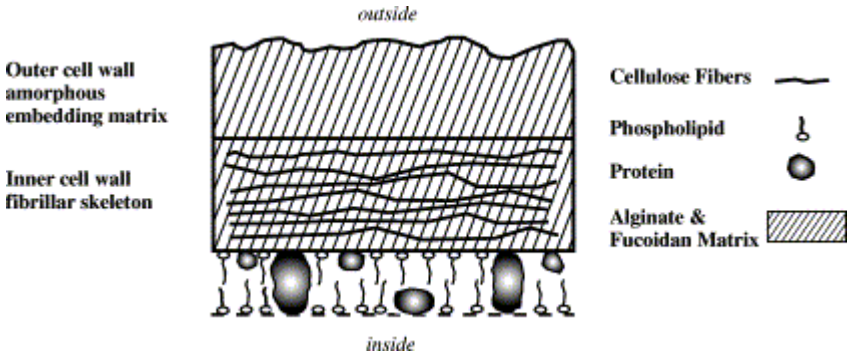

Figure 1.3 Cell wall structure in Phaeophyta [11].

The most common fibrillar skeleton material is cellulose which imparts rigidity to the cell wall [12]. It can be replaced by xylan in the Chlorophyta and Rhodophyta in addition to mannan in the Chlorophyta [6].

The Phaeophyta algal embedding matrix is predominately alginic acid (a long-chained heteropolysaccharide), with smaller amounts of the sulphated polysaccharide fucoidan, while the Rhodophyta contain a number of sulphated galactans (e.g. agar, carrageenan, porphyran, etc.). Both the Phaeophyta and Rhodophyta contain the largest amount of amorphous embedding matrix polysaccharides making them potentially excellent materials for heavy metal binding [6].

The main storage products in seaweeds are laminaran in the Phaeophyta, starch in the Chlorophyta and floridean starch in the Rhodophyta.

1.1.6 The Seaweed Industry in Ireland

It has been reported that Ireland has approximately 501 species of seaweed comprising 274 red, 147 brown and 80 green. The Irish seaweed industry employs nearly 500 people, exports 85-90% of its produce, and had a turnover of over €12 million in 2003 [1].

The industry is broadly based with product being supplied to agriculture/horticulture, cosmetics, thalassotherapy, the biopharma sector (functional foods/ nutraceuticals) and for human consumption [13]. There is also considerable interest in the use of algae in bioremediation processes associated with sewage treatment plants, tanneries and aquaculture onshore production units where excess nutrients can be dramatically reduced in any discharge waters.

1.1.7 Marine Biotechnology

Biotechnology is fundamentally based on using nature's own technology for the production of goods and services [13]. The seas are a major source of organisms with unique metabolic mechanisms and novel biological materials. Marine biotechnology is unlike other areas of biotechnology in that it is defined in terms of its source material rather than the market it serves.

It is anticipated that it will eventually contribute to nearly every industry, from healthcare to bioremediation and from cosmetics to nutraceuticals. The fact that marine biotechnology is at an early stage of development means that more of the potential global market is open for development by Ireland than is the case for other sectors. The global marine biotechnology market is projected to surpass $3.2 billion by the end of 2007 with the non-U.S. segment comprising the bulk of the market [13].

1.1.8 The use of seaweeds and seaweed products

1.1.8.1 As a food source

The major utilisation of seaweeds as food is in Asia, where seaweed cultivation has become a major industry. The main food species grown by aquaculture in China, Korea

and Japan are Nori (*Porphyra*, a red alga), Kombu or Kunbu (*Laminaria*, a brown alga) and Wakame (*Undaria*, also a brown alga). In Japan alone, the total annual production value of Nori amounts to >US$1 billion making it one of the most valuable marine crops produced by aquaculture in the world [1]. In most western countries, food and animal consumption is relatively restricted and there has not been any great pressure to develop mass cultivation techniques.

1.1.8.2 Gelling Polysaccharides

Some of the most commercially important products extracted from seaweeds are the hydrocolloids or gelling polysaccharides which are chains of simple sugars.

The food industry uses three common types of hydrocolloid extensively when thickening or gelling properties are required: alginic acid from brown algae and agar and carrageenan from red algae [14]. Alginates and carrageenans are also used as non-dairy stabilisers in many dairy products [15].

Agar's best-known use is as a solid microbiological culture substrate [14]. Modern agar is a purified form consisting largely of the neutral fraction known as agarose; the non-ionic nature of the latter makes it more suitable for a wide range of laboratory applications. Agar in a crude or purified form also finds wide usage in the food industry where it is used in a huge range of ices, canned foods and bakery products as a coagulant, emulsifying agent, and stabilising agent [16].

1.1.8.3 As Medical Products

In recent years, the biomedical and pharmaceutical industries have shown increased interest in the use of biopolymers extracted from seaweeds [17]. Some examples are discussed below.

Calcium alginate is often used as a dressing for exudative wounds. It is an effective absorbable haemostatic and is often used to pack sinuses, bleeding wounds of various types and burns [14]. Sodium alginate is also used for this purpose.

Alginate based raft-forming formulations for the symptomatic treatment of heartburn and oesophagitis have been marketed word-wide for over 30 years [18]. These formulations work by effectively providing physical barriers to acidic gastric contents.

Recent work by de Sousa *et al.* [19] showed that two alginates (SVHV and SVLV) extracted from *Sargassum vulgare* possessed anti-tumour activity against the murine tumour Sarcoma 180 while carrageenans (sulphated polysaccharides) from the red algae *Meristiella gelidium* have shown a potent antiviral activity against the herpes simplex virus types 1 and 2 (HSV-1 and HSV-2) and dengue virus (DENV) [20,21]. Crude extracts from *Polysiphonia* spp. have also shown some anti-herpetic and anti-oxidant properties [22] while those from *Codium* have shown anti-coagulant properties [23].

1.1.8.4 As Biosorption Products

Seaweeds have developed a reputation as one of the most promising types of biosorbents in view of their rigid macro-structure and high uptake capacity as well as the ready abundance of the biomass in many parts of the world's oceans [24]. Seaweeds offer many advantages for biosorption because their macroscopic structures offer a convenient basis for the production of biosorbent particles suitable for sorption process applications. Many authors have reported the excellent performance of seaweeds as biosorption products for a variety of heavy metals [25-28] and this shall be discussed extensively in later sections.

1.1.8.5 Other applications of seaweed-derived compounds

In addition to polysaccharides, a variety of other bioactive substances from seaweeds have been characterised and tested for other potential applications. Observations of natural seaweed systems, such as self-protection against bio-fouling and damaging ultra-violet (UV) radiation, have initiated research into their potential applications for human use including: (1) Development of algal anti-fouling substances with no toxicity on for example fish larvae, for replacing common anti-fouling paints [29,30] and (2) development of sunscreens using seaweed-derived compounds (mycosporine-like amino acids (MAAs) and polyphenols), which act as UV filters and anti-oxidants to prevent skin-cell damage when the skin is exposed to UV radiation [30].

1.2 Metals

1.2.1 Sources of metals in the environment

Metals in the aquatic environment may exist in dissolved or particulate forms. They may be dissolved as free hydrated ions or as complex ions chelated with inorganic ligands such as OH^-, Cl^- or CO_3^{2-} or they may be complexed with organic ligands such as amines, humic or fulvic acids and proteins [31].

Knowledge about metal speciation i.e. the different physical or chemical forms in which a metal occurs is widely regarded as crucial to the understanding and prediction of metal behaviour and impact in any environmental system [32]. The chemical speciation of a metal depends upon its oxidation state and its interactions with other components in the system as well as other parameters including pH, redox potential, ionic strength, salinity and alkalinity [31]. Changes in these variables can result in transformation of the metal's chemical form and can alter its availability and toxicity.

Modern industry is to a large degree responsible for contamination of the environment. Among the toxic substances reaching hazardous levels are heavy metals [33]. Recovery of heavy metals from industrial waste streams is becoming increasingly important as society realises the necessity for recycling and conservation of essential metals. Increasingly strict discharge limits on heavy metals have also accelerated the search for highly efficient yet economically attractive treatment methods for their removal [9].

When assessing pollution, a distinction must be made between natural sources of metals and those due to human activity. Metals in minerals and rocks are generally harmless, becoming potentially toxic only when they dissolve in water. They can enter the environment through natural weathering of rocks, leaching of soils and vegetation and through volcanic activity. Most of the metal load is transported by water in a dissolved or particulate state, and reaches the ocean via rivers or land runoff.

Humans, on the other hand, contribute metals to the environment during a variety of activities including mining activities, burning fossil fuels and disposing of industrial waste [34].

1.2.2 Impact of metals in the environment

Depending on the angle of interest and the environmental impacts, metals can be divided into four major categories: (1) Toxic heavy metals (2) strategic metals (3) precious metals and (4) radionuclides [31]. In terms of environmental threat it is mainly categories 1 and 4 that are of interest for removal from the environment. The classification of metals according to toxicity and availability has previously been demonstrated by Wood [35].

According to Duffus [36], the term "heavy metal" is often used in the literature as a group name for metals and semi-metals (metalloids) that have been associated with contamination and potential toxicity. However the term has never been defined by any authoritative body such as IUPAC.

Research shows that the term "heavy metals" has been used inconsistently. Some authors define it in relation to density or specific gravity [37], others define it in terms of atomic mass [38] or atomic number [39] while some definitions have no clear basis except toxicity [40]. This term is misleading because they are not all "heavy" in terms of atomic weight, density, or atomic number and are not even entirely metallic in character e.g. arsenic. For the purposes of this work, a rough generalisation of the term "heavy metals" shall include all the metals of the Periodic Table except those in Groups I and II [41].

Ten industrially significant metals were ranked by Volesky [24] in terms of the priority for their recovery and these have been summarised in Table 1.1. The considerations required when choosing the metals of interest for removal and/or recovery rank the metals into three general priority categories:

1. Environmental Risk (ER)
2. Reserve Depletion Risk (RDR)
3. Combination of the above factors

Table 1.1 Ranking of metal interest priorities [24].

Relative Priority	Environmental Risk (ER)	Reserve Depletion Risk (RDR)	Combination
High	Cd	Cd	Cd
	Pb	Pb	Pb
	Hg	Hg	Hg
	-	Zn	Zn
Medium	-	Al	-
	Cr	-	-
	Co	Co	Co
	Cu	Cu	Cu
	Ni	Ni	Ni
	Zn	-	(See High)
Low	Al	-	Al
	-	Cr	Cr
	Fe	Fe	Fe

It was shown that the environmental risk, ER, assessment could be based on a number of different factors. The RDR category was used as an indicator of probable future increase in the market price of the metal. Also, changes in the technological uses of these metals could change the priority sequence among the metals considered.

When the RDR was coupled with the ER above, it indicated that Cd, Pb, Hg and Zn are high priority metals. However, when considering the environmental impact of mobilised metals it is the first three that are to the forefront [24].

In humans, lead is extremely toxic and can damage the nervous system, kidneys, and reproductive system, particularly in children while chronic exposure to elevated levels of cadmium is known to cause renal dysfunction, bone degeneration, liver damage, and blood damage [42]. The EPA requires lead and cadmium in drinking water not to exceed 0.015 and 0.005 mg L^{-1}, respectively. Exposure to mercury may cause allergic skin

reactions, possible negative reproductive effects as well as disruption of the nervous system and damage to brain function [43].

1.2.3 Heavy metals under investigation

The metals under investigation in this study are copper and chromium. However, from Table 1.1 it is seen that both of these metals pose only a medium risk to the environment. So, the question is, why study these specific metals? The reasons behind the selection of these particular metals are outlined below.

With an increase in urbanisation and ongoing construction in Ireland, the prevalence of copper in the environment is expected to increase due to the increased use of copper piping in these new structures. Therefore, the identification of materials that can effectively remove copper from aqueous environments is desirable. As well as its industrial significance, copper also has a historical importance in this region (52° 8'17.06"N, 7°22'22.83"W) due to intensive mining of the metal in the 19th century. This present work also builds on that of Fitzgerald *et al.* [44] who studied accumulation of copper in various salt marsh plants and the red seaweed *Polysiphonia lanosa* within this region.

Chromium too has historical significance in this geographic region, as it has traditionally been used for tanning. A tannery using chromium in its leather processing was historically located in Portlaw (52°17'6.02"N, 7°18'53.17"W) on the Clodiagh River (a tributary of the Suir). Set up in 1934 by Irish Tanners Ltd, the site was at one stage the largest in Europe [45]. The tannery was closed in 1985 but reports by the EPA in 1995, showed that, although chromium pollution had decreased after the closure, some traces were still evident in the Clodiagh River. Michell Ireland Ltd also operated a tannery in Killowen Portlaw (near the site of the former tannery) from 1993-2003. Thus, the environmental impact of chromium in the area cannot be underestimated.

The ready availability of a number of chromium oxidation states makes it especially desirable in order to study the mechanisms of binding of these oxidation states as well as the relationship between them. In this case, Cr (III) and Cr (VI), as the most common forms of chromium, have been selected for analysis.

1.2.3.1 Copper -Cu (II)

Copper is one of the most common industrial metals with effluents resulting from various industries including mining operations, metal processing and coal fired power generation [24].

Cu (II) is also widely used in household plumbing materials and contamination of drinking water generally occurs from corrosion of household pipes [42]. Therefore, it cannot be directly removed from the water system.

People with Wilson's disease have been found to be especially at risk from prolonged exposure to copper [42]. The liver of a person with Wilson's disease does not release copper into bile as it should, so this leads to an accumulation of copper in the body which can result in severe damage to the liver, kidneys, brain, and eyes.

The US EPA requires copper in drinking water not to exceed a limit of 1.3 mg L^{-1} [43]. It has been shown that short periods of exposure can cause gastrointestinal disturbance, including nausea and vomiting while use of water exceeding the safe limit over many years could result in liver or kidney damage.

1.2.3.2 Chromium – Cr (III) and Cr (VI)

Chromium is a transition metal located in group VI-B of the periodic table. This toxic metal is commonly used in industrial applications such as in tanning, electroplating, pigmentation, catalysis for corrosion inhibitors and wood preservatives [46].

Although it is able to exist in several oxidation states, the most common forms are the trivalent (III) and hexavalent (VI) states, which display quite different chemical properties.

Cr (VI) is usually associated with oxygen as chromate (CrO_4^{2-}) or dichromate ($Cr_2O_7^{2-}$) while Cr (III) is in the form of oxides, hydroxides ($CrOH^{2+}$) or sulphates. Cr (III) is much less mobile than Cr (VI) and mainly exists bound to organic matter in soil and aquatic environments [47].

While both chromium species are prevalent in industrial waste streams, the hexavalent form is considered more hazardous to public health due to its greater mobility and its mutagenic and carcinogenic properties [48]. Although Cr (III) is less toxic than Cr (VI), long term exposure to Cr (III) is known to cause allergic skin reactions and cancer [49].

It is well known that Cr (VI) is toxic to living systems and prolonged exposure may cause cancer in the digestive tract and lungs. Chromium (VI) compounds may also cause epigastric pain, nausea, vomiting, severe diarrhoea and haemorrhage [50] and as a result, the US EPA has set the maximum contaminate level for Cr (VI) in domestic water supplies at 0.05 mg L^{-1} [43]. Acar and Malkoc [51] also reported that the maximum chromium levels permitted in wastewaters were 5 mg L^{-1} for Cr (III) and 0.05 mg L^{-1} for Cr (VI).

1.2.4 Removal of Metals from the Environment

As previously discussed, the removal of metals from the environment is extremely important. Industrial wastewaters containing heavy metals require efficient and cost effective treatment [52] to remove these metals. The major target industrial sectors as outlined by Volesky [24] are mining and electroplating operations, metal processing, coal-fired power generation and the nuclear industry.

Conventional methods of heavy metal removal include chemical precipitation, electrochemical techniques, reverse osmosis, evaporation and ion-exchange [53]. However, these processes may be ineffective or extremely expensive especially when the metals in solution are present in the range of 1–100 mg L^{-1} [54-56]. These techniques may also cause secondary environmental problems due to the creation of metal-bearing sludges which are extremely difficult to dispose of.

For example, conventional Cr (VI) removal from wastewaters has traditionally been carried out using ion-exchange resins, filtration and chemical treatment [57,58]. However, these methods are not completely satisfactory as they generate large amounts of secondary waste due to the various reagents used in treatments such as reduction of Cr (VI), neutralisation of acidic solution and precipitation. The instability of ion-exchange resins due to serious oxidation by Cr (VI) also points to the need for alternative removal methodologies.

For these reasons, alternative technologies that are practical, efficient and cost effective at low metal concentrations are being investigated.

The most prominent alternative technology for heavy metal removal is biosorption. Biosorption is the removal of heavy metals from an aqueous solution by passive binding to non-living biomass [6]. This technique is competitive, effective and economically attractive [24]. The use of biological materials is extremely appealing since they

sequester heavy metals in substantial quantities, are relatively cheap, widely available, fast growing and from sustainable sources.

The biosorption process also offers the advantages of (1) minimisation of the volume of chemical and/or biological sludge to be disposed of (2) high efficiency in detoxifying very dilute effluents, and (3) possibility of reusability of the biomass.

The biosorption potential of various biomass types has been widely investigated. Different biomass types such as bacteria [59,60], fungi [61,62], microalgae [63,64] and macroalgae [9,27,65,66] have been screened and studied extensively in the last decade with the aim of identifying highly efficient biosorbents.

Some types of biosorbents are broad range, binding and collecting the majority of heavy metals with no specific priority while others can be specific for certain metal types [67]. Although many biological materials bind heavy metals, only those with sufficiently high metal-binding capacity and selectivity for heavy metals are suitable for use in a full-scale biosorption process [68].

Metal sequestration by this diverse group of biosorbents was comprehensively summarised by Volesky and Holan [69]. The various biosorbent types showed levels of metal uptake in the order of 0.1-2 mmol g^{-1}. Among the different biosorbents studied, algal biomass (seaweed) has received much attention due to the cost saving, low sensitivity to environmental and impurity factors, possible metal recovery and its elevated metal binding capacity which has been shown to be higher than activated carbon and comparable to synthetic ion-exchange resins [55].

Table 1.2 illustrates some of the results found for cadmium and lead biosorption in the comparative biosorbent study of Volesky and Holan [69].

Table 1.2 Cadmium and lead biosorption by various biosorbent materials [69].

	Biomass type	Biomass class	Metal uptake		Ref.
			(mg g^{-1})	(mmol g^{-1})	
Cd					
	Ascophyllum nodosum	marine algae	215	1.91	[70]
	Fucus vesiculosus	marine algae	73	0.65	[71]
	Rhizopus arrhizus	fungus	30	0.27	[72]
	Saccharomyces cerevisiae	yeast	20-40	0.18-0.36	[73]
Pb					
	Ascophyllum nodosum	marine algae	270-360	1.30-1.74	[70]
	Fucus vesiculosus	marine algae	220-370	1.06-1.79	[70]
	Rhizopus arrhizus	fungus	91	0.44	[72]
	Streptomyces longwoodensis	yeast	100	0.48	[74]

From Table 1.6, it is clear that marine algae were among the most promising biosorbents for cadmium and lead. Metal uptake by the brown seaweed species was significantly larger than that observed for fungal or yeast biomass pointing to its suitability as a biosorbent material.

As well as the benefits outlined above, another advantage of using seaweed biosorbents is that they possess rigid physical shapes and structures which make their application in biosorption processes particularly suitable [52]. Unlike microorganisms, the size of seaweed biomass is large enough to facilitate its application without a cumbersome solid-liquid separation process [49]. Morphologically, the seaweed thallus particles approximate flat chips rather than having a spherical shape [75] which thereby facilitates rapid metal ion mass transfer and effective metal binding.

However, biological materials are complex and the binding mechanisms are often unclear [76]. The unique capabilities of certain types of biomass to concentrate and immobilise heavy metals can depend on [24]:

- The type of biomass.
- The metal mixture in the solution.
- The physico-chemical environment.

It is therefore extremely important to investigate the environmental parameters that influence biosorption behaviour. Some parameters affecting metal biosorption are given in Section 1.3.2.2.

1.3 Mechanisms of Metal Biding to Seaweeds

1.3.1 Bioaccumulation by living seaweeds

Although the primary focus of this work is the biosorption of metals by dead seaweed biomass, some consideration must also be given to the mechanisms of heavy metal binding by live seaweeds in order to differentiate between the two. In the case of biosorption by non-living seaweed, the mechanisms can be thought of as occurring discretely at the cell wall while bioaccumulation normally implies intracellular binding by a living organism [6].

Even though both living and dead cells are capable of metal accumulation, there are differences in the mechanisms involved, depending on the extent of metabolic dependence in live seaweeds [77]. The parameters affecting performance of living biosorbents are as follows:

- The physiological state of the organism.
- The age of the cells
- The availability of micronutrients during their growth.
- The environmental conditions during uptake (pH, temperature, light intensity etc.).

Accumulation of heavy metals by living seaweeds has been shown to occur in two phases: (1) a rapid surface reaction followed by (2) a much slower metal uptake over a period of hours [78]. An initial rapid uptake will correspond to extracellular adsorption and/or to passive intracellular uptake (metabolism-independent) involving cell surface adsorption and simple diffusion into cells or intercellular spaces. A slower uptake will correspond to metabolism-dependent incorporation into the cell body or, in some cases, to a continuous or non-continuous excretion taking place in the macro-algae [78].

In parallel experiments, extracellular adsorption and intracellular uptake of metals may be analysed separately by washing the algae with EDTA [79]. The metal in the algae after

the EDTA wash is defined as the intracellular metal while the metal in the extraction solution is defined as the adsorbed metal.

Because few studies on tolerance to metal toxicity have been carried out on seaweeds, some of those used for micro-organisms can be used to discuss the basic mechanisms that may be applied to seaweeds [80,81]. Figure 1.4 illustrates the routes of uptake for potentially toxic metal cations and possible tolerance mechanisms.

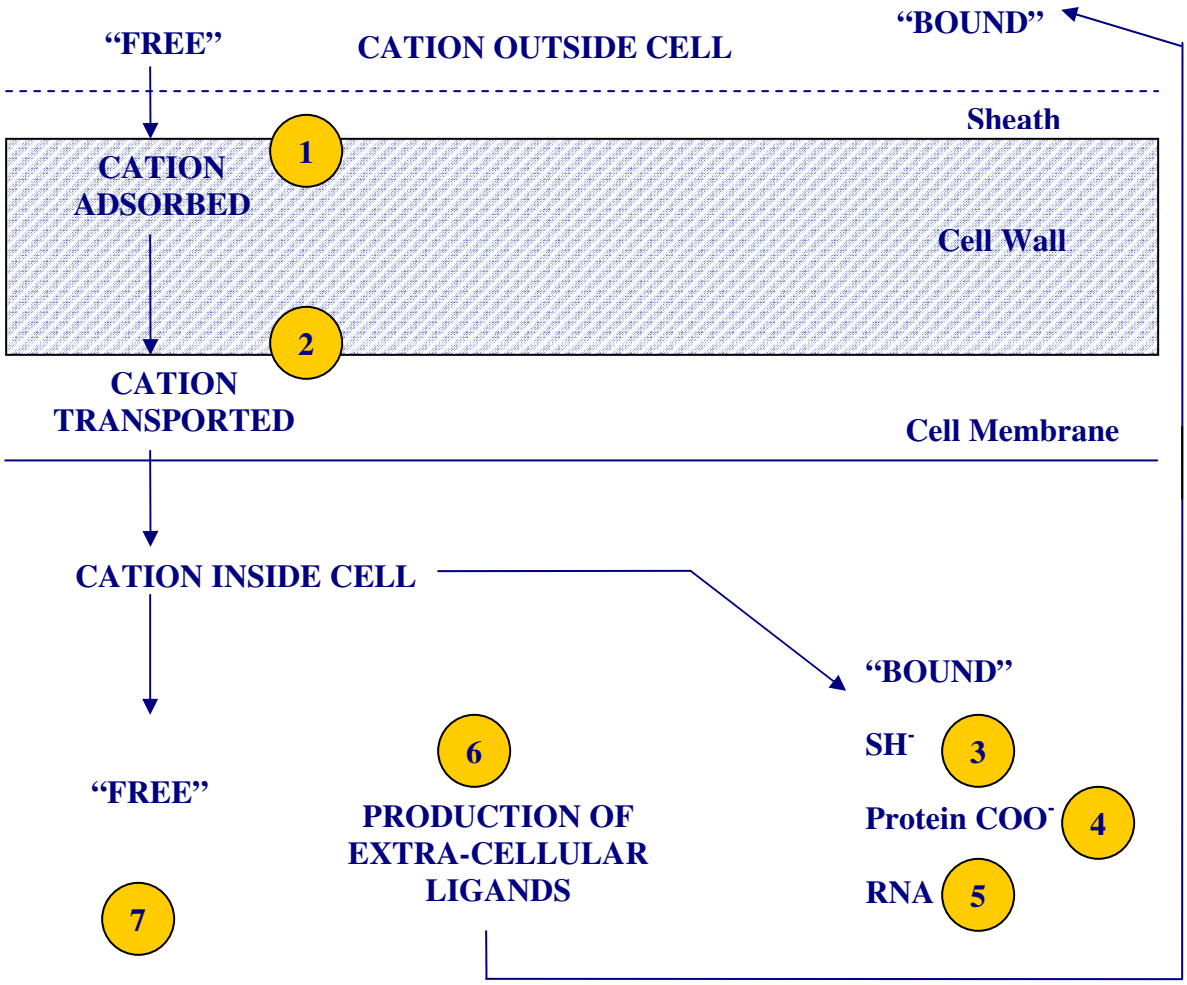

Figure 1.4 Routes of uptake for potentially toxic cations and possible sites (1-7) of tolerance mechanisms [80].

Algae may produce extracellular compounds [82], compounds in the cell wall [83] or on the cell wall [84] that can bind to certain metals rendering them non-toxic. Detoxification

of metal ions at the cell surface is referred to as an exclusion mechanism because the metal ions do not cross the cell membrane (Mechanism 1).

Another possible exclusion metal is adsorption or detoxification of a metal ion by surface-living micro-organisms (Mechanism 2). It is possible that epiphytes such as diatoms or bacteria may sequester the metal ion before it reaches the membrane surface of the seaweed [31].

If no exclusion mechanism is operating, a metal ion can enter the cytoplasm. Several detoxification mechanisms are then possible inside the cell. Mechanisms 3-5 refer to metal binding to –SH residues, protein carboxyl groups and RNA respectively.

Mechanism 6 (production of extracellular ligands in Figure 1.4) refers to the production of phytochelatins. Grill *et al.* [85] showed that phytochelatins are cysteine-rich peptides that can be induced in higher plants when exposed to a range of heavy metals. Gekeler *et al*. later extended these findings to the microalga *Chlorella fusca* [86] and the marine macroalga *Sargassum muticum* [83].

If neither exclusion nor inclusion mechanisms take place, the metal cation remains “free” within the cell and a toxic effect takes place (Mechanism 7).

1.3.2 Biosorption by dead seaweed biomass

As previously outlined in Section 1.2.4, biosorption is a passive process of metal uptake whereby the metal is sequestered by chemical sites naturally present and functional even when the biomass is dead [24].

Singh *et al*. [87] reported that dead biomass could bind metal ions to the same or a greater extent as living biomass. This agrees with the work of Abu al-Rub *et al*. [88] who compared the binding of nickel by live and dead *Chlorella vulgaris* cells. With an initial metal concentration of 100 mg L^{-1}, 15.4 and 15.6 mg g^{-1} nickel were bound by the live and dead cells respectively.

It is important to note that biosorption of metals by seaweed is not based solely on a single mechanism. It consists of several mechanisms that quantitatively and qualitatively differ according to the species used. Therefore the differences in metal uptake capacities of the seaweeds may be related to compositional differences among the cell walls, as well as different binding mechanisms involved for different heavy metal ions [65].

Metal sequestration follows complex mechanisms including ion-exchange and complexation with oxidation/reduction reactions also a possibility in some cases [69]. Due to the complexity of biomaterials such as seaweed it is quite possible that at least some of these mechanisms are acting simultaneously to varying degrees depending on the seaweed, the metal ion and the solution environment [65].

For example, results have shown that the main cadmium sequestration mechanism by macroalgae was apparently chelation [89], while nickel cation sequestration was mainly due to ion-exchange [90]. The binding mechanism of lead cations included a combination of ion-exchange, chelation and reduction reactions, accompanied by metallic lead precipitation on the cell wall matrix [91].

1.3.2.1 Key Functional Groups

The constituents of the cell wall provide an extensive array of ligands with various functional groups capable of binding metallic ions. However, the actual role that any functional group plays in metal binding depends on factors such as the number of sites on the biosorbent material, their accessibility and chemical state (i.e. availability), and the affinity between site and metal (i.e. binding strength) [6]. The various key structures (and their component functionalities) within each algal division are discussed below.

1.3.2.1.1 Phaeophyta

1.3.2.1.1.1 Alginic acid

Alginic acid is an extracellular polysaccharide that occurs in all brown algae [8]. It is the most abundant cell wall polysaccharide in brown algae and offers carboxyl (-COOH) groups for metal binding [6]. It is a linear polysaccharide containing 1,4-linked β-D-mannuronic acid (M) and α-L-guluronic acid residues arranged in a non-regular block wise order along the chain [92]. The residues typically occur as $(\text{-M-})_n$, $(\text{-G-})_n$ and $(\text{-MG-})_n$ sequences or blocks [6]. The carboxylic acid dissociation constants have been determined as pK_a=3.38 and pK_a=3.65 for M and G respectively with similar values obtained for the polymers [93].

Figure 1.5 illustrates the structure of β-D-mannuronic acid (M) and α-L-guluronic acid (G).

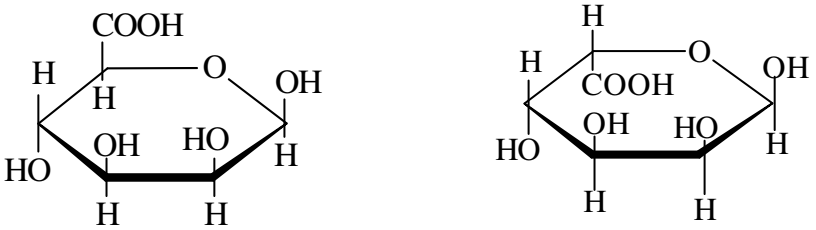

(M) **(G)**

Figure 1.5 Constituent acids of alginic acid, where (M) is β-D-Mannuronic Acid and (G) is α-L-Guluronic Acid [6].

Mannuronic and guluronic acids are classed as uronic acids. The uronic acids are simple monosaccharides in which the primary hydroxyl group at C_6 has been oxidized to the corresponding carboxylic acid. Their names retain the root of the monosaccharides, but the *-ose* sugar suffix is changed to *-uronic acid*. For example, galact**uronic acid** has the same configuration as galact**ose**, and the structure of gluc**uronic acid** corresponds to that of gluc**ose**.

Uronic acids are present in all three algal divisions [94]. Figure 1.6 illustrates the possible cadmium binding sites on polyuronic acids as proposed by Schweiger [95].

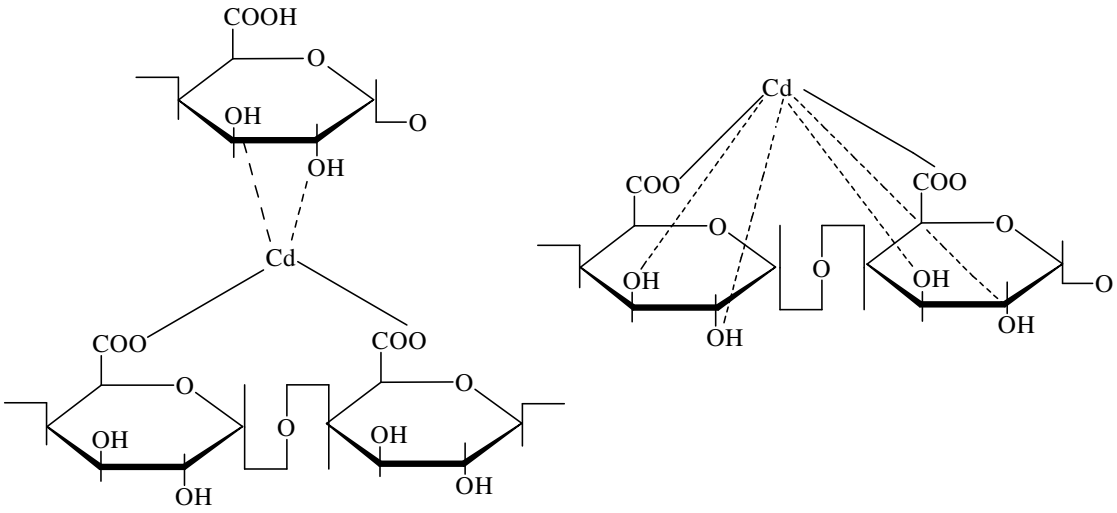

Figure 1.6 Possible cadmium binding sites on polyuronic acids [95].

Alginic acid usually constitutes about 10–40% of brown algal dry weight [94] but for *Sargassum*, alginate contents between 17% and 45% have been reported [14,96] which corresponds to 0.85–1.25 meq g^{-1} of carboxyl groups per dry weight, where meq g^{-1} (milliequivalents per gram of dry biomass) is a concentration term corrected for active site valence.

It is important to note that while carboxyl groups have been identified as the main metal-sequestration sites they are not likely to be the only strongly active sites [97].

1.3.2.1.1.2 Fucoidan

The second most abundant acidic functional group in brown algae is the sulphonic acid of fucoidan [14]. Fucoidan is a branched matrix polysaccharide sulphate ester with L-fucose building blocks as the major component with predominantly α (1→ 2)-linkages [98]. Brown algae contain about 5–20% fucoidan [14], about 40% of which are sulphate esters. The structure of fucoidan is shown in Figure 1.7.

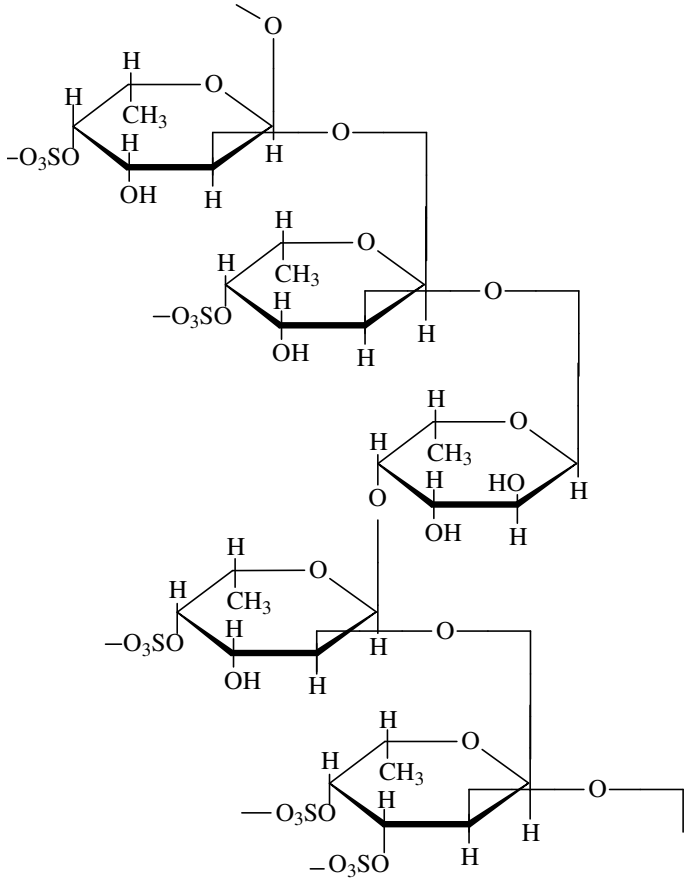

Figure 1.7 Fucoidan: Branched polysaccharide sulphate ester with L-fucose building blocks as the major component with predominantly α (1→ 2)-linkages [6].

The concentration of R-OSO_3^- detected in *Sargassum* was estimated to range from 0.2 to 0.3 meq g^{-1}, representing approximately 10% of the overall metal binding sites in this seaweed [96].

Sulphonic acid groups are present in the three algal divisions but typically play a secondary role in metal binding, except when metal binding takes place at low pH [6]. Hydroxyl groups are also present in all polysaccharides but they are less abundant and only become negatively charged at pH >10 thus playing a secondary role in metal binding at lower pH values. [99].

1.3.2.1.1.3 Proteins

The protein content of seaweed varieties varies greatly and demonstrates a dependence on such factors as season and environmental growth conditions [100]. In brown algae the protein content has been shown to be less than 30% [101]. For *Sargassum* 10% protein was reported comprising ~0.17 meq g^{-1} carboxyl groups and ~0.07 meq g^{-1} amino groups [102]. This means that in brown algae the carboxyl groups of alginic acid are more abundant than either carboxyl or amino groups of the protein and are therefore likely to be the main binding sites [103].

1.3.2.1.2 Chlorophyta

1.3.2.1.2.1 Polysaccharides

The cell wall matrix of Chlorophyta contains highly complex sulphated hetero-polysaccharides, which offer carboxyl and sulphonate groups for metal binding [8]. The extracted polysaccharides from *Ulva* (12% of the algal dry weight) were found to contain 16% sulphate and 15–19% uronic acids [104,105].

Each molecule of these heteropolysaccharides is made up of several different residues with the major sugars being glucuronic acid, rhamnose, arabinose and galactose made up in several combinations [94]. Figure 1.8 shows the structure of rhamnose and glucuronic acid, two of the constituent sugars of some green seaweed polysaccharides

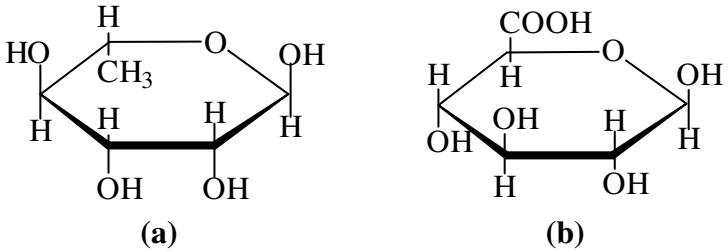

Figure 1.8 Green seaweed constituents: (a) α-L- rhamnose and (b) glucuronic acid [94].

A polysaccharide, ulvan, has been found to be easily extracted from *Ulva rigida* [106,107]. This polysaccharide corresponds to water-soluble dietary fibre and is resistant to both human digestive track enzymes and degradation by colonic bacteria [108] and is composed of β-(1-4)-xyloglucan, glucuronan and cellulose in a linear arrangement [94,107].

1.3.2.1.2.2 Proteins

Protein can constitute 10–70% of the green algal cell wall [101]. The presence of these proteins is important for binding as it has been previously shown that both amino and carboxyl groups play significant roles in metal binding to seaweeds [12].

In some green seaweeds such as the species belonging to the genus *Ulva*, the protein content can represent between 10 and 26% (dry weight) of the plant [109], whereby aspartic and glutamic acid account for 12% of the protein giving 0.15 meq g^{-1} of carboxyl groups per dry weight [8]. Lysine and arginine on the other hand make up 13% of the protein, yielding approximately 0.08 meq g^{-1} of amino groups [110]. These constituent amino acids are illustrated in Figure 1.9

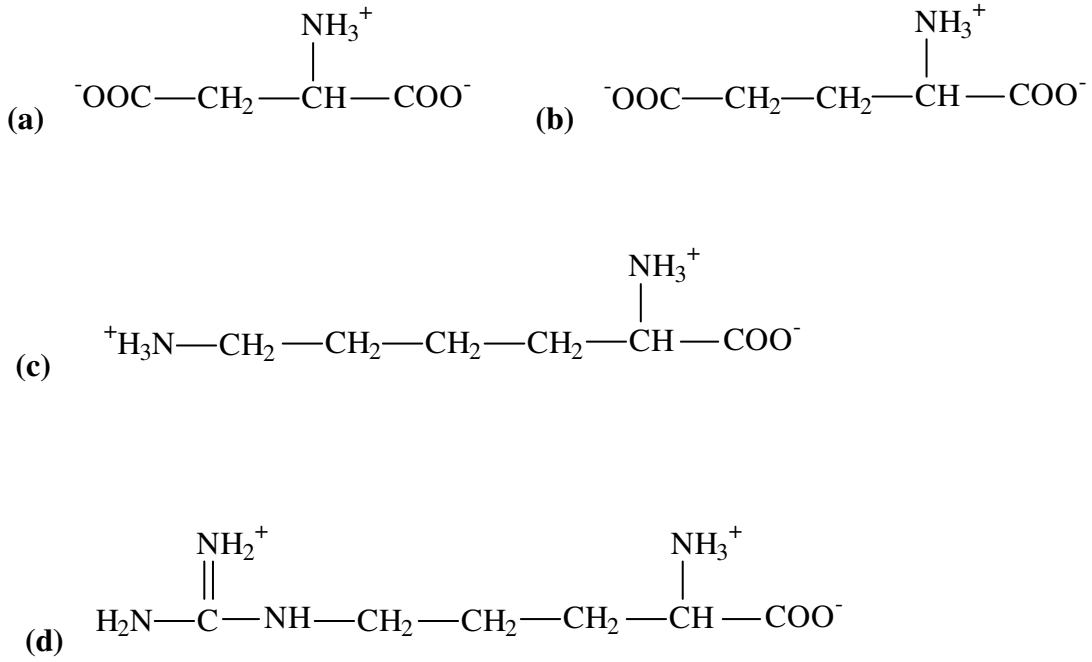

Figure 1.9 Some constituent amino acids found in green seaweed proteins (a) Aspartic acid (b) Glutamic acid (c) Lysine (d) Arginine [111].

1.3.2.1.3 Rhodophyta

1.3.2.1.3.1 Polysaccharides

Most red algal polysaccharides are galactans in which α (1→ 3) and β (1→ 4) links alternate [94]. Variety in the polysaccharides comes from sulphation, pyruvation and methylation of some of the hydroxyl groups and from the formation of an anhydride bridge between C_3 and C_6. In many red seaweeds, the sulphonate groups of carrageenan and sulphated galactans (at C_2, C_4 or C_6) of agar offer many anionic sites for the binding of polyvalent cations.

Agars consist of alternating β-D-galactose and α-L-galactose with relatively little sulphation [112] (Figure 1.10).

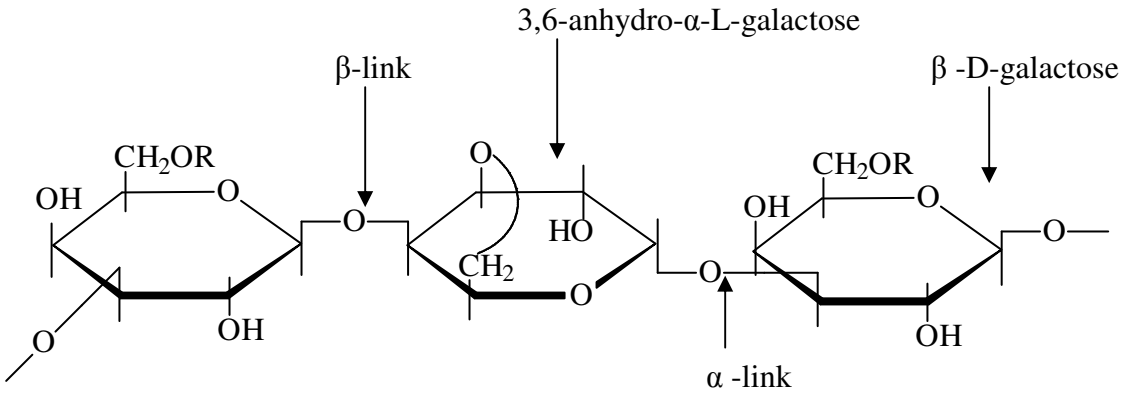

R=H or CH_3

Figure 1.10 Red algal matrix polysaccharide agar [94].

In carrageenans, β-D-galactose alternates with α-D-galactose and not α-L-galactose. The degree of sulphation in carrageenans is much greater than that in agars. Paskins-Hurlburt *et al*. [113] reported that the level of sulphation in carrageenans may contribute significantly to heavy metal binding. The principal carrageenans are called kappa-carrageenan, lambda-carrageenan and iota-carrageenan. The structure of kappa-carrageenan is shown in Figure 1.11.

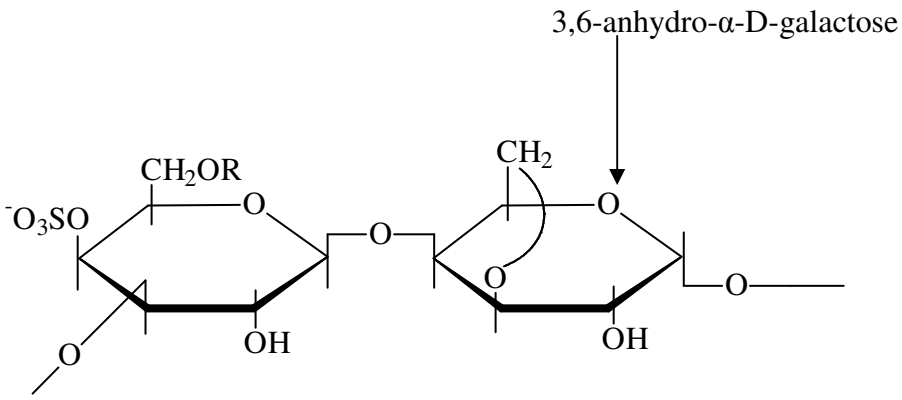

Figure 1.11 κ-carrageenan structure

The presence of uronic acids in red seaweeds polysaccharides has also been reported in some cases. From *Palmaria decipiens*, a neutral xylan and a xylogalactan with 4.8 % uronic acids were obtained [114].

1.3.2.1.3.2 Proteins

It has been shown that red seaweeds possesses a high levels of protein [115] with *Porphyra tenera* and *Palmaria palmata* revealing especially high levels, with as much as 47.5% and 30%, found respectively [109,116].

All of the essential amino acids i.e. methionine, leucine, lysine, cysteine, phenylalanine, tyrosine, arginine, isoleucine, threonine and valine and six non-essential amino acids were found to be present in *Gracilaria changii* [117]. Many seaweeds have relatively high content of free amino acids which provide flavour in foodstuffs e.g. glycine and alanine which give a sweet flavour [118].

1.3.2.2 Factors affecting heavy metal biosorption

Although, there are many variables which can influence metal biosorption, experimental parameters such as pH, ionic strength and competition between metal ions can have a significant effect on metal binding to seaweeds. Some of the most important factors affecting metal binding are discussed below.

1.3.2.2.1 pH

The dependence of metal uptake on pH is related to both the surface functional groups on the cell walls of the biomass and to metal chemistry in solution. Both carboxyl and sulphonate groups are acidic and therefore the optimum solution pH for maximum metal uptake is related to the pK_a of these surface groups. At low pH, they are protonated and therefore are less available for the binding of heavy metals. However, as pH increases, dissociation of these groups occurs, (pK_a of sulphonate groups is pH 1.5-2.5 and pK_a of carboxyl groups is pH 3.5-5) [68] resulting in increased negative charge which will increase biosorption of metal cations onto the surface [119]. This explains why the binding of many metals increases with increasing pH [103,120,121].

Many divalent metals e.g. Cd^{2+}, Cu^{2+} and Pb^{2+} displayed almost maximal binding at pH values close to the apparent pK_a value of the seaweed carboxyl groups (pK_a near 5) thus pointing to the importance of these groups in metal binding [55,65,121]. However, it is important to note that the pH at which maximum uptake is achieved is not the same for all heavy metals. This is as expected on the basis of the varying affinity of the metals for the various acidic functional groups.

Similar pH dependence was observed for biomass amino groups but the pH values at which the metal uptake increases sharply and reaches its maximum are generally higher for the amino groups than for the carboxyl groups [68]. As previously discussed, biomass hydroxyl groups become negatively charged at high pH, thereby contributing to metal removal at higher pH values [65].

1.3.2.2.2 Ionic Strength

Apart from pH, another important parameter for metal uptake is the ionic strength. Changing ionic strength or background electrolyte concentration influences metal binding by:

1. Altering the interfacial potential and therefore the activity of the electrolyte ions.
2. Changing the competition of the electrolyte ions and adsorbing ions for sorption sites [122].

Sodium is common in many industrial wastewaters and high concentrations lead to high ionic strengths at which the amount of heavy metal bound is reduced. Sodium is typically bound by ionic attraction [123] and therefore does not compete directly with the covalent binding of heavy metals by the biosorbent. However, the effect of ionic strength is explained as the result of competition of Na^+ with the heavy metals for electrostatic binding to the biomass. Since deprotonated free carboxyl or sulphonate groups are negatively charged, they will electrostatically attract any cation, be it Na^+ or the heavy metal of interest.

The effect of Na^+ is more pronounced during the uptake of weakly bound metals such as Zn^{2+} or Ni^{2+}. Strongly bound metals such as Cu^{2+} are generally less affected by solution ionic strength [103]. Tsui *et al.* [27] showed that as the ionic strength of the solution increases, binding of a variety of metals including Ag, Cd, Co, Mn, Ni and Zn decreased.

The presence of the corresponding anions e.g. chloride, nitrate, sulphate, and acetate can also affect metal uptake by seaweeds [9]. This is especially true for anion binding.

1.3.2.2.3 Competition between metal ions

An actual industrial wastewater contains many ions, not just a single ion which may affect the biosorptive capacity of the biomass [124]. As a result, there have been extensive studies on the biosorption of multi-metal components onto various biosorbents [125-127]. Singh *et al*. [87] studied the effect of multi-metallic systems on the microalgae *Lemna*, *Microcystis* and *Spirogyra* using Differential Pulse Anodic Stripping Voltammetry (DPASV). Saeed *et al*. have also investigated multi-metallic systems in black gram husk [128] while Pagnanelli *et al*. [129] dealt with *Arthrobacter* sp. biomass.

In bimetallic combinations, sorption of metals is a competitive process between ions in solution and those sorbed onto the biomass surface [87,130]. Antagonistic interactions of two metals may be due to the fact that different cations have different affinities to cell binding sites thus reducing the effective binding sites available for a single metal e.g. Cd^{2+} uptake has been shown to be suppressed by increasing concentrations of Zn^{2+}, Mn^{2+} and Cu^{2+} [87].

Chlorella vulgaris was sequentially exposed to a solution containing an equimolar mixture of nine metal ions at pH 5.0 [131]. The order of selectivity in biosorption of the nine metal ions is as follows:

Al (III) = Ag (I) >> Cu (II) > Cd (II) >> Ni (II) >> Pb (II) > Zn (II) = Co (II) ≥ Cr (III)

The authors showed that the binding of Al (III) and Ag (I) was essentially unaffected by the presence of the other metal ions. However, in contrast, the binding of all other metal ions was decreased in multi-metallic systems. Kuyucak and Volesky [132] also found that the presence of competing ions had little effect on gold uptake by *Sargassum natans*.

Therefore, it is seen that biosorption in multi-metallic system depends not only on the physicochemical nature of the solution but also on the surface properties of the biosorbent material as well as interactions between metals. Additional parameters influencing metal biosorption are discussed in Section 1.3.2.3.

1.3.2.3 Mechanisms of Heavy Metal Binding

1.3.2.3.1 Ion-exchange

Davis *et al*. [6] indicated that ion-exchange is an important concept in biosorption, because it explains many of the observations made during heavy metal uptake experiments. It was noted that the term ion-exchange does not explicitly identify the mechanism of heavy metal binding to seaweeds, as the precise mechanism(s) may range from physical (i.e. electrostatic or London–van der Waals forces) to chemical binding (i.e. ionic and covalent), but that it is effective in describing the experimental observations.

1.3.2.3.1.1 Background

The term *sorption* refers to the binding of a metal cation to a *free* site as opposed to one that was previously occupied by another cation [6].

The Langmuir adsorption model [133] assumes that all the binding sites on the sorbent are free sites that are ready to accept the sorbate from solution [69]. Therefore an adsorption reaction can be described as:

$$B^- + M^+ \longleftrightarrow BM \qquad \textbf{(Equation 1.1)}$$

Where, B represents the free binding site, M represents the sorbate (metal) and BM is the adsorbed sorbate M bound on B.

The ion-exchange model describes the reaction as:

$$BH + M^+ \longleftrightarrow BM + H^+ \qquad \textbf{(Equation 1.2)}$$

Where B, the binding site is already occupied by a proton (H) that can take part in ion-exchange with a metal cation. However, a one-to-one stoichiometry is not complied with as typically two protons are released upon the binding of one divalent heavy metal ion. Figure 1.12 illustrates schematic representations of both adsorption and ion-exchange mechanisms for a biosorbent material.

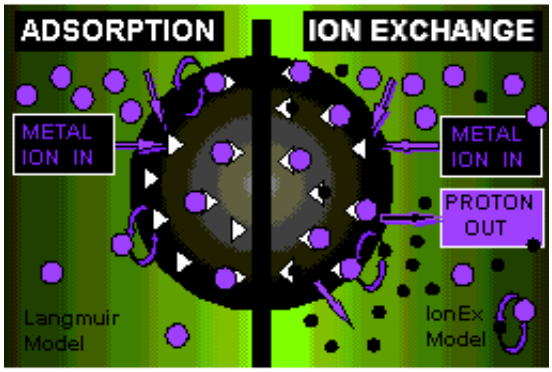

Figure 1.12 Comparison of adsorption and ion-exchange mechanisms for metal binding [134].

The ion-exchange approach is probably somewhat closer to the reality than the simple Langmuir model, but does not completely and accurately describe biosorption [6]. This is because the assumption of a constant number of free sites may be reasonable for a constant pH system, but, may not hold for systems with varying pH values.

1.3.2.3.1.2 Ion-exchange in seaweeds

Seaweed can be viewed as a natural ion-exchange material that primarily contains weakly acidic and basic groups. It follows from the theory of acid-base equilibrium that, in the pH range 2.5-5, the binding of heavy metal cations is determined primarily by the state of dissociation of the weakly acidic groups [68].

Untreated algal biomass generally contains alkali and alkaline earth metal ions such as K^+, Na^+, Ca^{2+} and Mg^{2+} which are originally present from seawater. These ions are bound to the surface acidic functionalities. It has been reported that where the non-treated

Sargassum was reacted with a heavy metal-bearing solution, a pH increase and the release of light metal ions were observed [135]. This also was explained in terms of ion-exchange, whereby the observed release of light metals balanced the uptake of protons and heavy metals [136].

It was also reported by da Costa *et al*. [137] that alkali and alkaline earth ions played a key role in the ion-exchange properties of the biosorbent irrespective of the metal solute to be sorbed. Various authors have demonstrated this ion-exchange behaviour for numerous seaweed-metal combinations [121,138-141]. It therefore appears that ion-exchange plays an important role in heavy metal binding to seaweeds.

1.3.2.3.2 Complexation

A complex is formed by the donation of electrons from a complexing ligand to a metal. As the ligand is the electron pair donor it is described as being a Lewis base while the electron pair acceptor (the metal) is, by this definition a Lewis acid [142]. Complexation is therefore a Lewis acid-Lewis base neutralisation process [41].

A metal ion in aqueous solution represents an example of a metal complex. For example metal ions such as zinc are in fact surrounded by a shell of water molecules. Each water molecule is bound to the metal by donation of electrons originating from the lone pairs on the oxygen [142].

A complexation reaction such as the following:

$$Zn^{2+} + 4Cl^- \rightleftharpoons ZnCl_4^{2-} \qquad \textbf{(Equation 1.3)}$$

is in fact a substitution reaction with chloride ions replacing coordinated water

$$Zn(H_2O)_6^{2+} + 4Cl^- \rightleftharpoons Zn\,(H_2O)_2Cl_4^{2-} + 4H_2O \qquad \textbf{(Equation 1.4)}$$

Any combination of cations with molecules or anions containing free electron pairs (bases) is termed coordination, also known as complex formation [123]. The heavy metal cation that is bound is often designated as the central atom, and is distinguished from the anions or molecules (ligands) with which it forms a coordination compound [6].

1.3.2.3.2.1 Denticity

Ligands are distinguished by the number of groups they contain which are capable of binding to a metal. Unidentate ligands attach through only one coordinating group and in general, these tend to result in the formation of ionic water soluble complexes.

Polydentate or multidentate ligands are molecules that contain more than one group that is capable of binding to the metal centre [123]. A reagent that attaches to a single metal centre in this way is termed a chelating agent [142], and the complexes are referred to as chelates where ring closure with a metal ion occurs. A majority of chelating ligands contain the three most important donors, nitrogen, oxygen and sulphur [143].

The coordination number refers to the number of ligand atoms surrounding the central atom [6]. Most metal cations engage in coordination of 2, 4, 6 and 8 with 4 and 6 being the most common. However, for polymers these values may be lower due to steric effects [6,123]. The effects metal ionic radius and coordination number on seaweed surface morphology is investigated in Chapter 5.

To summarise, it is the number of groups in the chelating agent and the number of available coordination sites on the metal that will govern the stoichiometry of the final compound.

1.3.2.3.2.2 Complex Formation with biomaterials

Metal sequestration can be viewed as the complexation (or coordination) of a central heavy metal to a multidentate ligand (the surface of the algae) [6]. The algal surface is a complicated system, since it behaves as a heterogeneous ligand and can be treated as a

polyfunctional macromolecule [144]. The surface groups are not identical and it is not possible to determine the complexation constants for each group [145].

Binding of different metal ions on biomaterials having different functional groups depends on ionic properties such as electronegativity, ionisation potential, ionic radius and redox potential of these metals [146]. Allen and Brown [146] proposed that more electronegative metal ions will be more strongly attracted to the surface. Their results also showed that the sorption capacity for Cu^{2+} was smaller than that for Pb^{2+} due to its lower electronegativity.

Tobin *et al.* [72] established a relationship between sorption capacity and ionic radii of several metal ions. This suggested that molecules having smaller ionic radii could be more quickly sorbed onto a fixed surface area of sorbent (in this case, macroalgae). For example, the smaller ionic radius of Zn^{2+} (0.74 Å) than Cd^{2+} (0.95 Å) may be responsible for its higher biosorption [147].

Heavy metal complexation to alginate polymers has been extensively studied by Haug, Smidsrød and Larsen [92,92,148]. Figure 1.13 gives a structural representation of the conformation of the alginate polymer showing both mannuronic (M) and guluronic (g) acid residues [6].

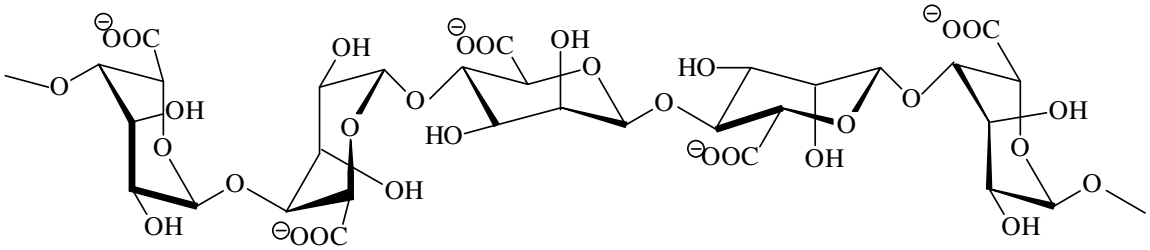

Figure 1.13 Alginate structural data for the alginate polymer showing orientation of M and G residues [149].

Early work by Haug [150] demonstrated that, in alginates with different M:G ratios, as the guluronic content increased, so too did the affinity of the alginate for divalent metal ions. The higher specificity of polyguluronic acid residues for divalent metals may be explained by its "zigzag" structure (Figure 1.13) which can accommodate the ions more easily [6] .

It has been shown that regions of the alginate polymer rich in 'G' residues display a higher selectivity for divalent metal ions over mannuronic rich regions. This is due to the fact that they provide a multidentate environment for complexation. On the other hand, in regions rich in mannuronic acid ("M" residues) complexation would be predominantly monodentate and therefore weaker [6]. It would therefore be expected that the coordination number of the metal bound to guluronic acid residues should be larger than that for mannuronic acid. This appears to be supported by the higher selectivity observed in regions rich in guluronic acid [6].

1.3.2.3.2.3 Hard Soft Acid Base Theory (HSAB)

There are two components to any complexation reaction i.e. the metal and the complexing agent; both contribute to the formation of the complex and both have their own characteristics. Only if these characteristics match is a strong bond formed between the two [142].

Predicting which metal will be bound strongly by which ligand requires an understanding of the factors controlling the bond formation. From a consideration of the nature of the participating metals and ligands it is possible to break these down into two extreme cases. Metals are thereby categorised as being hard or soft acids while ligands are categorised as being hard or soft bases [136].

The basis of the Hard Soft Acid Base Theory is that "in a competitive situation, hard acids tend to form complexes with hard bases and soft acids tend to form complexes with soft bases" [142]. In other words, metals that tend to bond covalently preferentially form complexes with ligands that tend to bond covalently, and similarly, metals that tend to bond electrostatically preferentially form complexes with ligands that tend to bond electrostatically. Intermediate acids will bind with harder or softer bases depending on their oxidation state.

The degree of hardness or softness refers to the electron mobility or polarisability of a species [41]. Table 1.3 illustrates the classification of metals (acids) according to the HSAB Theory.

Table 1.3 Classification of metals according to the HSAB Theory [142].

Property	Hard	Soft	Intermediate
Polarisability	Low	High	
Electropositivity	High	Low	
Positive charge (Oxidation state)	Large	Small	
Bonding	Ionic/electrostatic	Covalent	
Outer electrons on donor	Few and not easily excited	Several and easily excited	
Examples	K^+, Li^+, Na^+, Cr^{3+}, Ca^{2+}, Mg^{2+}, Cr^{6+}	Ag^+, Au^+, Tl^+, Hg^+, Hg^{2+}, Cu^+, Cd^{2+}	Fe^{2+}, Co^{2+}, Ni^{2+}, Cu^{2+}, Zn^{2+}, Pb^{2+}

According to the HSAB Theory, Cr (III) and Cr (VI) are hard acids while Cu (II) is an intermediate acid (i.e. it is a hydrogen bonding molecule taking the form HX) [69]. Table 1.4 shows the classification of ligands (bases) according to the HSAB Theory.

Table 1.4 Classification of ligands according to the HSAB Theory [142].

Property	Hard	Soft
Polarisability	Low	High
Electropositivity	High	Low
Positive charge (Oxidation state)	Large	Small
Bonding	Ionic/electrostatic	Covalent
Available empty orbitals or donor atom	High energy/ inaccessible	Several and easily excited
Examples	COO^-, H_2O, OH^-, RNH_2, SO_4^{2-}	RSH, SCN^-, CN^-

On the basis of the HSAB Theory, it would therefore be expected that Cr (III) and Cr (VI) would involve binding to groups such as carboxyl and ether groups while Cu (II) should be bound to sulphur and nitrogen containing groups. The agreement of results with HSAB theory is examined in later chapters.

1.3.2.4 Biosorption of heavy metal anions

Although much of the current biosorption research is oriented towards the removal of heavy-metal cations [65,151-153], the binding of anions to biomass is a growing area of study [154-156].

Effluents from major industrial activities such as mining, electroplating and power generation often contain heavy metals in anionic complex forms such as chromate (CrO_4^{2-}), vanadate (VO_4^{3-}), selenate (SeO_4^{2-}) and gold cyanide ($AuCN_2^-$) [154]. These species have been conventionally recovered by precipitation, ion-exchange or activated carbon sorption [157].

However, anionic metal complexes may also be effectively bound by biomass types containing an abundance of amino groups such e.g. chitin-containing biosorbents [68]. Chitin is a natural polysaccharide consisting of (1,4) 2-acetamide-2-deoxy-D-glucose units some of which are deacetylated (chitosan). The structures of chitin and chitosan are shown in Figure 1.14.

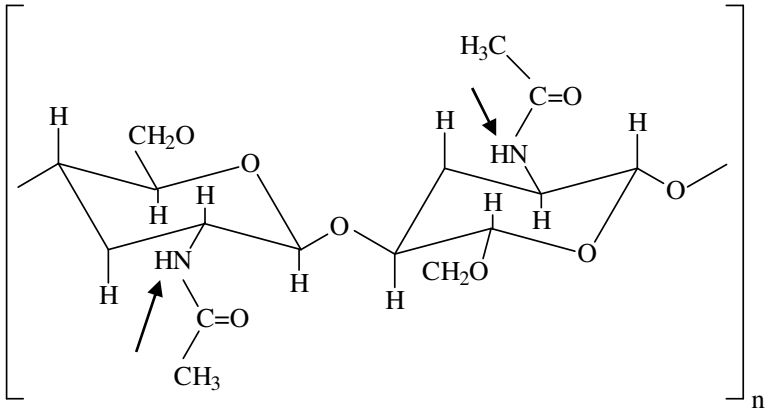

(a)

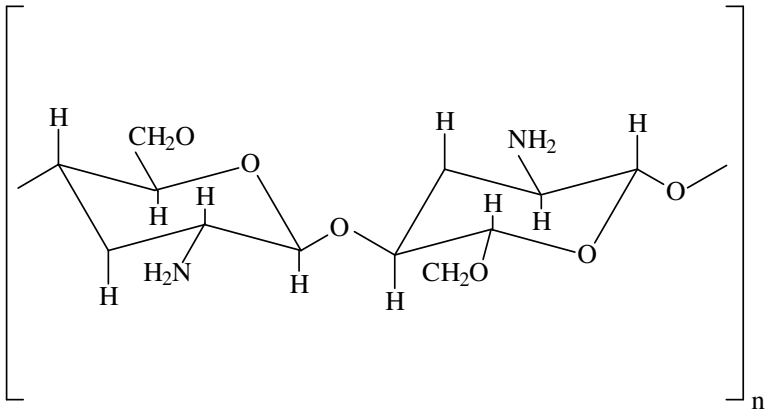

(b)

Figure 1.14 The structure of (a) Chitin and (b) Chitosan [158].

Chitin can be obtained from fungi, insect, lobster, shrimp and krill but the most important sources are crab exoskeletons obtained from sea-food processing waste [159]. The removal of molybdate (MoO_4^{2-}) by chitosan beads has recently been reported [68] with an uptake of 700 mg g^{-1} found.

The conjugated acid dissociation constant pK_a of the chitin amide group is lower than 3.5 [160]. Therefore, only when the solution pH is lower than this, the amide sites (as highlighted in Figure 1.14) could be effectively protonated with a positive charge and an anion could thus be bound.

The removal of anionic Cr (VI) by various other biomaterials e.g. peat-moss [161], corn-cob [162], fungi [62] and seaweed (including *Ecklonia* sp. and *Ulva lactuca*) [163,164] has also been studied with promising results. The optimum pH for Cr (VI) removal by all of these biomasses was reported to lie in the pH range 1.5–2.5. Moreover, the studies revealed that, although some Cr (VI) was taken up by the biomass, considerable quantities of Cr (VI) were reduced to Cr (III).

However, more research is needed to assess the proposed mechanisms and develop mathematical models for the sorption of anions. Because some highly toxic metals occur in anionic forms (As, Se, Cr, Mo, Va etc.), studies of anion biosorption remains a relevant challenge.

1.4 Quantifying Metal-Biomass Interactions

1.4.1 Sorption Isotherms

The first step towards elucidating metal binding mechanisms and determining the relative affinity of heavy metals for the biomass is to determine the binding capacity of the biomass. This is usually done by characterising the equilibrium state after the biomass has been allowed to react with an aqueous solution of the metal of interest [6]. The reaction may be monitored by measuring the amount of metal remaining in solution until it becomes time invariant. The model used to describe the results should be capable of predicting heavy metal binding at both low and high concentrations.

Comparison of different sorbent types must always be done under the same conditions e.g. pH, temperature, ionic strength etc. If these external parameters are carefully controlled during experiments then the models chosen may be capable of satisfactorily reflecting the experimental data.

Binding isotherms have been widely applied in biosorption since they are simple, give a good description of experimental behaviour in a large range of operating conditions and are characterised by a limited number of adjustable parameters [165].

Biosorption equilibrium isotherms are plotted for the metal uptake ($\boldsymbol{q}$) against the residual metal concentration ($\boldsymbol{C_f}$). It has been shown that the metal uptake by marine algae typically does not exceed 2.5 mmol g^{-1} [52,141,166].

Figure 1.15 illustrates the experimental isotherm plots for lead sorption as determined by Jalali *et al*. [167] for eight brown, red and green seaweed species.

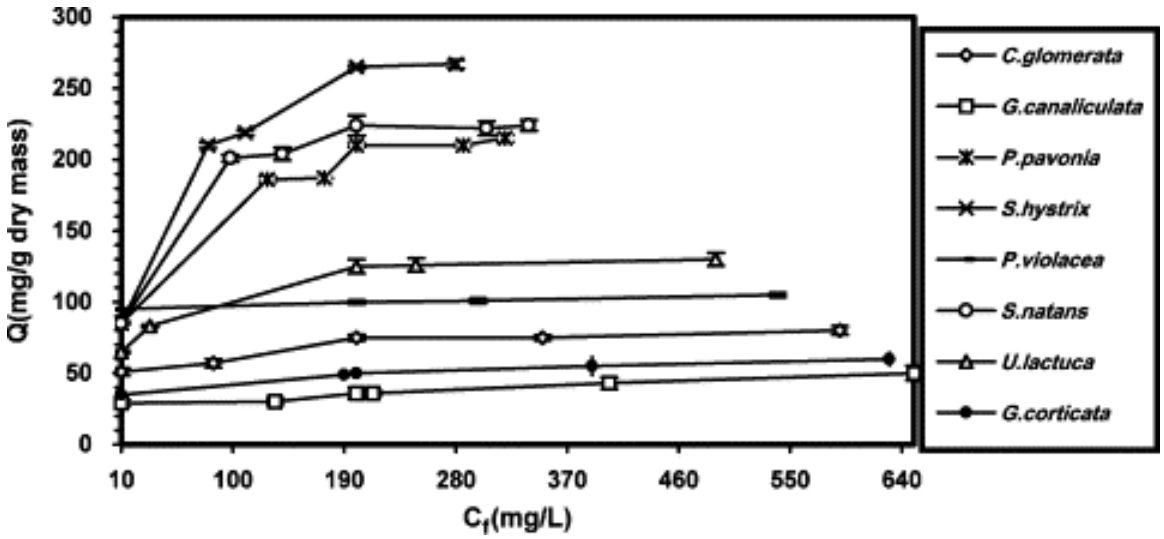

Figure 1.15 Experimental Isotherm Plot of lead uptake for eight brown, red and green seaweed species [167].

The Langmuir [133] and Freundlich [168] Isotherms are the models most commonly used in biosorption to describe the q vs. C_f relationship [61,169-171]. However, they were developed under many assumptions that are known not to be met in biosorption. For instance, they do not take into account that metal ion biosorption is mainly an ion-exchange phenomenon [78].

The main reason for the extended use of these isotherms is that they incorporate constants that are easily interpretable [169]. These constants reflect the nature of the sorbent and can be used to compare biosorbent performance. Equation 1.5 shows the form of the Langmuir equation commonly used for biosorption work.

$$q = q_{\max} \frac{bC_f}{1 + bC_f} \qquad \textbf{(Equation 1.5)}$$

Where,

q represents the equilibrium metal uptake (mmol heavy metal /gram biosorbent), q_{max} is the maximum uptake (mmol heavy metal/ gram biosorbent), C_f is the equilibrium

solution concentration of the heavy metal (mmol heavy metal / L solution) and ***b*** is an affinity parameter (L $mmol^{-1}$).

The Freundlich Isotherm is given in Equation 1.6.

$$q = kC_f^{1/n} \qquad \textbf{(Equation 1.6)}$$

Where,

n is an empirical parameter that relates to the sorption intensity and ***k*** (expressed in mmol heavy metal/ gram biosorbent) relates to the biosorption capacity. The parameters ***q*** and $\boldsymbol{C_f}$ are as above.

A more detailed discussion of each isotherm, an interpretation of their respective constants and their potential uses and limitations is given in Chapter 3.

1.5 Instrumental Analysis of Heavy Metal Binding

Many techniques have been used to study metal binding to biomaterials. These include potentiometric titration [52,96], infrared spectroscopy [96,121], scanning electron microscopy [89], X-ray photoelectron spectroscopy [65,172] and Scanning Probe Microscopy [173,174].

Knowledge of the chemical composition of the algal cell wall as well as the use of a variety of analytical techniques may help to elucidate metal binding mechanisms. The use of a single technique will not yield a complete picture of binding and therefore a range of techniques must be used to characterise the metal-biomass interactions. This work uses variety of complementary analytical techniques to give an overall picture of metal binding with further information on these techniques given in later chapters.

1.5.1 Potentiometric and Conductimetric Titrations

Potentiometric titrations have been used by various authors to determine the quantity and nature of acidic binding sites on the seaweed surface [52,96,121]. Once the quantity of available functional groups has been established, its relationship with the maximum metal binding capacity of the seaweeds can be established.

Fourest and Volesky [96] showed that simultaneous potentiometric and conductimetric titrations provided information concerning the amounts of "strong" and "weak" acidic functional groups in the biomass as well as allowing the pK_a characteristics of the algae to be determined. "Strong" acidic groups usually refer to sulphonate functionalities while "weak" acidities are surface carboxyl groups.

Protonated biomass is titrated with a base, usually NaOH and the concentrations of strong and weak acidic groups in the biomass are determined through estimating the position of inflection points on the resulting titration curve. The first inflection point on the curve

represents the number of strong acidic groups, the final represents the total number of acidic groups with the number of weak groups calculated by difference.

Figure 1.16 illustrates the potentiometric and conductimetric titration curves of three *Sargassum* species as determined by Davis *et al.* [52].

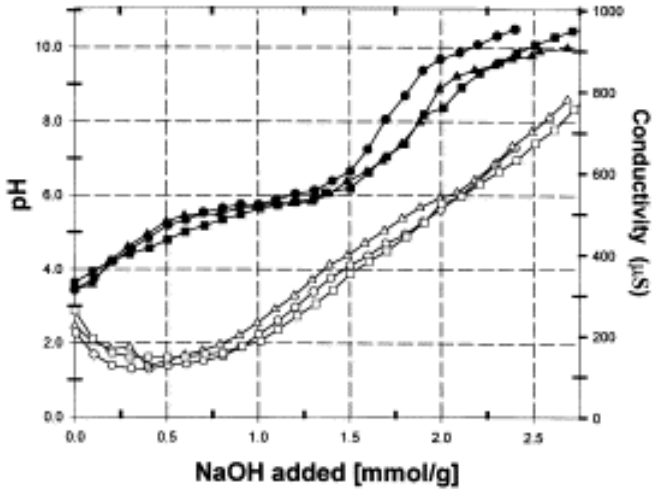

Figure 1.16 Potentiometric and conductimetric titration curves of three *Sargassum* species. Potentiometric titration: (●) *S. fluitans*, (▲) *S. filipendula* I, (▪) *S. vulgare*. Conductimetric titration: (○) *S. fluitans*, (Δ) *S. filipendula* I, (□) *S. vulgare*. [52].

The quantity of strong and weak acidic groups obtained from the potentiometric curves in Figure 1.16 as well as the seaweeds' cadmium binding capacity is summarised in Table 1.5.

Table 1.5 Acidic group content in selected *Sargassum* species in comparison with maximum cadmium uptake.

Seaweed	strong (mmol g^{-1})	weak (mmol g^{-1})	weak. 0.5 (mmol g^{-1})	q_{max} Cd (II) (mmol g^{-1})
Sargassum vulgare	0.5	1.5	0.75	0.79
Sargassum fluitans	0.3	1.5	0.75	0.71
Sargassum filipendula	0.3	1.6	0.75	0.66

From Table 1.5 it is clearly seen that carboxyl groups are significantly more abundant than sulphonate groups. It is also apparent that any correlation between metal binding capacity and the amount of acidic groups is related to the number of weak acidic groups. This is due to the fact that carboxyl groups have been shown to play a dominant role in metal binding to brown seaweeds [96]. The relationship between weak acidic groups and metal uptake is very good if assuming a two-to-one stoichiometry between protons released and divalent metals bound [52].

Further interpretation of potentiometric and conductimetric titration curves is given in Chapter 2.

1.5.2 Fourier Transform Infrared Spectroscopy (FTIR)

As previously discussed, numerous chemical groups have been proposed to be responsible for metal biosorption by seaweeds. These include carboxyl, amino, sulphonate and hydroxyl and their respective importance in metal binding depends on factors such as the quantity of sites, their accessibility and the affinity between the site and the metal [175]. Once the quantity of available sites has been determined, say by potentiometric titration, other techniques such as Fourier transform Infrared Spectroscopy (FTIR) may be used to assess the interaction of the surface functional groups with metal ions.

Various authors have used FTIR spectroscopy to detect vibrational frequency changes in seaweeds [65,121,176]. FTIR offers excellent information on the nature of the bonds present on the surface of the algae and also presents three main advantages as an analytical technique: It is fast, non-destructive and requires only small sample quantities [177].

Several intense characteristic bands in the IR spectra [96] can be attributed to functional groups present in seaweed proteins and in polysaccharides. For example, bands at approximately 1740, 1640, 1420 and 1240 cm^{-1} can be attributed to various carboxyl stretches (free C=O, chelate/ asymmetric C=O, symmetric C=O and C-O respectively) while polysaccharide ether and hydroxyl groups exhibit stretches of around 1160 and 1030 cm^{-1} respectively. On the other hand, seaweed proteins exhibit –NH stretches at approximately 1540 cm^{-1}. Changes in band intensity and frequency after metal binding can be used to identify the functionalities involved in binding. A comprehensive summary of the typical bands observed in seaweed FTIR spectra is given in Chapter 4.

Figure 1.17 illustrates sample FTIR spectra obtained by Lodeiro *et al*. [55] for Cd (II) and Pb (II) binding by *Cystoseira baccata* and by Chen and Yang [121] for Cr (III) and Cr (VI) binding to *Sargassum* sp.

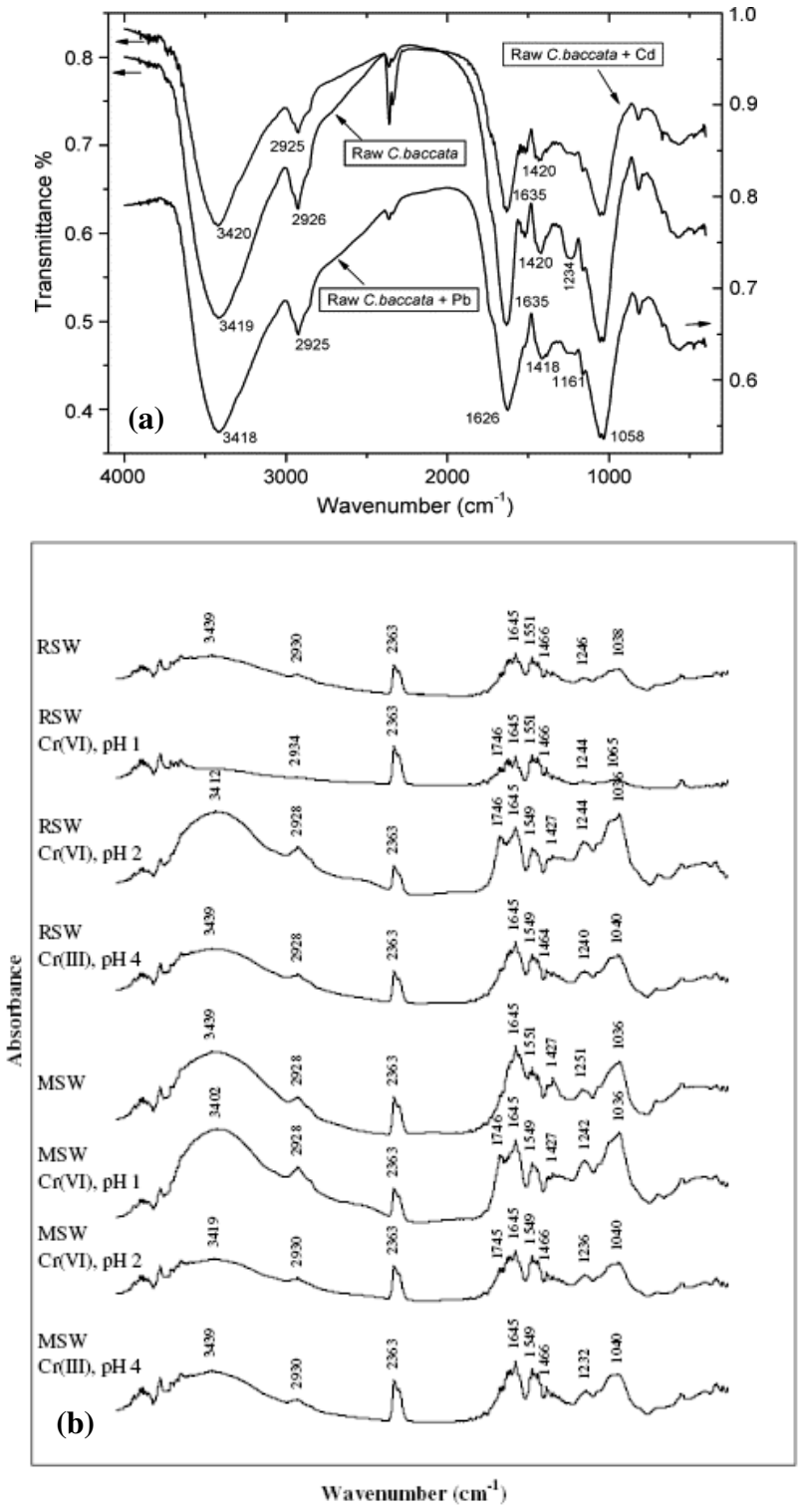

Figure 1.17 **Typical FTIR spectra obtained for (a) raw and metal loaded *Cystoseira baccata* [55] and (b) Raw (RSW), modified (MSW) and metal loaded *Sargassum* sp. [121].**

Lodeiro *et al*. [55] found that cadmium and lead binding to *Cystoseira baccata* involved significant interaction of biomass carboxyl groups as well as amino groups while sulphonate groups did not appear to play a role in binding of these metals. Yang and Chen [28] also found that carboxyl and amino groups were involved in chromium binding to *Sargassum* sp. but, in addition to this, sulphonate groups also played a role in metal binding. Therefore, it is apparent that the groups involved in metal binding depend on both the metal ion involved and the seaweed species under consideration.

FTIR analysis has been carried out in this work in order to determine the functionalities involved in Cu (II), Cr (III) and Cr (VI) binding to the selected seaweeds. A detailed discussion of binding behaviour is given in Chapter 4.

1.5.3 Scanning Electron Microscopy / Energy Dispersive X-ray analysis (SEM/EDX)

Scanning electron microscopy is a powerful techniques that can be used to investigate binding of metals to seaweed [28,89,176]. SEM allows us to evaluate morphological changes in the surface i.e. changes in the cell wall composition after metal binding, but when combined with EDX techniques it can provide valuable inputs in determining the distribution of various elements over the seaweed surface [176]. However, it is worth noting that SEM provides only a qualitative estimation of the surface structure. To obtain quantitative information regarding morphological changes, a supplementary technique such as scanning probe microscopy is required.

Yang and Chen [28] evaluated the surface of *Sargassum* sp. before and after metal loading. The SEM micrographs obtained by these authors are shown in Figure 1.18.

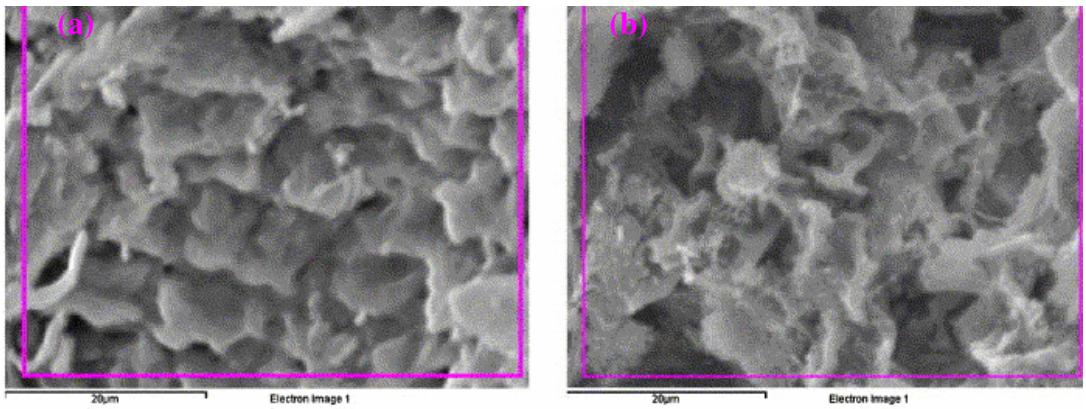

Figure 1.18 SEM Micrographs of (a) Raw (b) Cr (VI) loaded *Sargassum* sp. (Leaf). Magnification 2000X. Scale bar correspond to 20 µm [28].

The authors observed surface protuberance and microstructures in the raw seaweed (Figure 1.18a) and suggested that this may be due to calcium and other salt crystalloid deposition. This was in agreement with their EDX analysis which showed that calcium was a major component of the seaweed surface.

Raize *et al*. [89] also used SEM to evaluate the surface of *Sargassum vulgaris* before and after cadmium, nickel and lead binding. After metal binding, minor morphological changes including shrinking and layer sticking were seen in the cell wall matrix. Changes in surface morphology are usually related to disruption of the cross-linking between the metal ions and negatively charged chemical groups e.g. carboxyl groups in the cell wall polymers. Raw seaweeds usually contain high concentrations of calcium and magnesium (naturally present from seawater) in the cell wall, which creates a net of cross-linking [94]. When the seaweed is exposed to metal solutions e.g. cadmium, the cadmium cations replace some of the calcium and magnesium ions thus changing the nature of the cross-linking on the surface and resulting in morphological changes.

SEM/EDX analysis is used in this present work to establish changes in morphology and elemental composition of each of the seaweeds with a view to establishing a mechanism of metal binding.

1.5.4 X-ray photoelectron spectroscopy (XPS)

X-ray photoelectron spectroscopy (XPS) involves irradiating a sample under vacuum with mono-energetic X-rays. The electrons produced are then analysed according to energy. Because each element has a unique set of binding energies for electrons, XPS can therefore be used to identify and determine the concentration of the elements on the surface [178]. This technique facilitates quantitative elemental surface analysis, chemical state surface analysis, and determination of the molecular environment and/or oxidation state of metals [179]. A more detailed description of the technique is given in Chapter 5.

Venkata Mohan *et al*. [180] showed that XPS was a suitable technique for the surface analysis of various biosorbents due to its sensitivity and chemical specificity. The technique has been used by a number of authors to determine interactions between seaweed functional groups and the metals bound to them in order to elucidate a metal binding mechanism [65,89,181].

Figure 1.19 illustrates the binding energy (BE) profiles of the carbon atom (C 1s) and the oxygen (O 1s) in raw *Sargassum* sp. before and after Cu (II) binding (as determined by Chen and Yang [121]). Analysis of these profiles before and after metal binding gives an indication of the degree of interaction between the various carbon and oxygen containing functionalities with metal ions. Similar BE profiles may be obtained for sulphur and nitrogen.

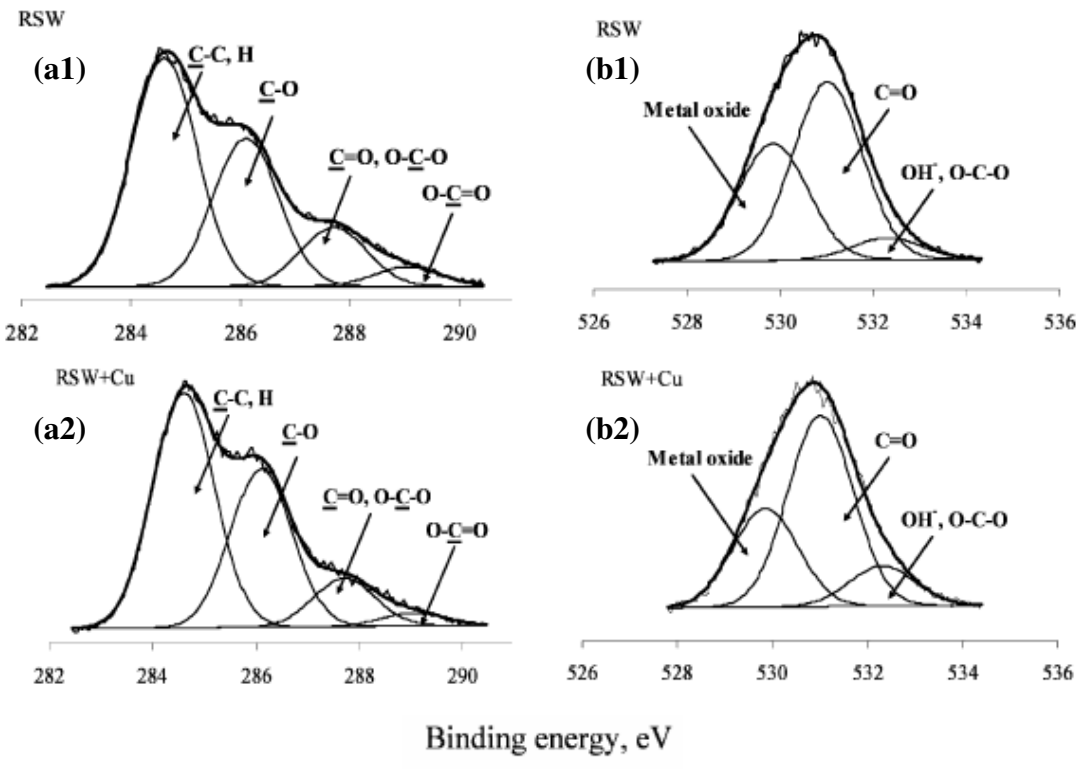

Figure 1.19 Carbon 1s (a1 and a2) and oxygen 1s (b1 and b2) XPS binding profiles of raw and Cu (II)-loaded *Sargassum* sp. [121] where, a1 and b1 refer to the raw seaweed and a2 and b2 refer to the Cu (II)-loaded seaweed.

From Figure 1.19 it is seen that the various carbon-containing functionalities such as hydrocarbons, alcohol, ether and carboxyl groups can be identified based on their respective binding energies [121]. Deconvolution of the oxygen peak also reveals the presence of numerous oxygen species including alcohol, ether, carboxyl as well as metal oxides. Analysis of the area under each peak gives an estimate of the atomic percentage the functionalities in the biomass.

Apart from identifying the constituent elements contained within a sample; XPS is also a powerful tool for elucidating metal binding mechanism. This is especially important if differentiation between metal oxidation states is required.

Figueira *et al*. [176] used XPS to gather chemical information on the interaction of iron with specific binding sites in the biomass. *Sargassum* biomass was exposed to sulphate solutions of either ferrous (II) or ferric (III) iron. XPS results indicated the presence of iron in two oxidation states in the biomass exposed to ferrous solution whereas only Fe (III) was present in the ferric-iron exposed biomass. This suggested a partial oxidation of Fe (II) when in contact with the biomass.

Dambies *et al*. [172] also studied the binding mechanism of various metals to chitosan. These authors not only confirmed the predominance of amino interactions during metal ion sorption but also showed that during molybdate sorption, Mo (VI) was reduced to Mo (V). Chromate sorption was shown to follow a similar mechanism with Cr (VI) reduced to Cr (III) upon contact with chitosan.

XPS is used in this work to investigate the binding of Cu (II) and Cr (VI) to various seaweeds and to elucidate possible binding mechanisms for the metals.

1.5.5 Scanning Probe Microscopy

Scanning Probe Microscopy (SPM) refers to the growing number of instruments for the exploration and investigation of surfaces from the micrometer level down to atomic dimensions. The use of this technique relies on a mechanical probe for generation of magnified images [182].

An SPM instrument is operable in ambient air, liquid or vacuum; and resolves features in three dimensions, down to a fraction of an angstrom [183]. It is comprised of a sensing probe, piezoelectric ceramics for positioning the probe, an electronic control unit, and a computer for controlling the scan parameters as well as generating and presenting images.

An essential component in the SPM is a sensor with very high spatial resolution. These sensors can routinely sense height changes as small as 0.1 Å. Two common types of sensors are the tunneling sensor and force sensor. The related techniques are known respectively as scanning tunneling microscopy (STM) and scanning force microscopy (SFM). The use of scanning force microscopy is discussed below and in Chapter 7.

A wide range of biological materials have been imaged with scanning force microscopy, from bio-molecules to entire cells. In the last decade, the scanning force microscope has emerged as a powerful tool for cell biology research giving ultrahigh resolution in real time under near physiological conditions [184]. Dammer *et al*. [185] directly bound antibodies to SFM tips in order to probe active sites on antigen surfaces.

Scanning force microscopy has also previously been used in biosorption studies. Ahinou *et al*. [186] used chemically functionalised probes to investigate the local electrostatic properties of microbial cells while Macaskie *et al*. [187] used the technique in conjunction with transmission electron microscopy and electron-probe X-ray microanalysis to visualise deposition of uranyl phosphate at the cell surface.

Various authors have used scanning force microscopy to investigate the polysaccharide networks present in some seaweed polymers. For example, Decho [173] previously used scanning force microscopy to image an alginate polymer gel matrix derived from *Macrocystis pyrifera* in order to measure polymer thickness while Gunning *et al*. [174] studied the iota-carrageenan networks extracted from some sun-dried red seaweeds. The high resolution of the SFM offers the potential to develop methodologies for imaging structural irregularity, branching or block structures in these polysaccharides [188].

The gel-forming properties of alginate were used to manipulate gel and solution states of alginate in order to observe the structure of single molecules and polymer networks (gels). Figure 1.20 shows an enlarged scanning force micrograph of alginate molecules and an alginate gel in seawater [173].

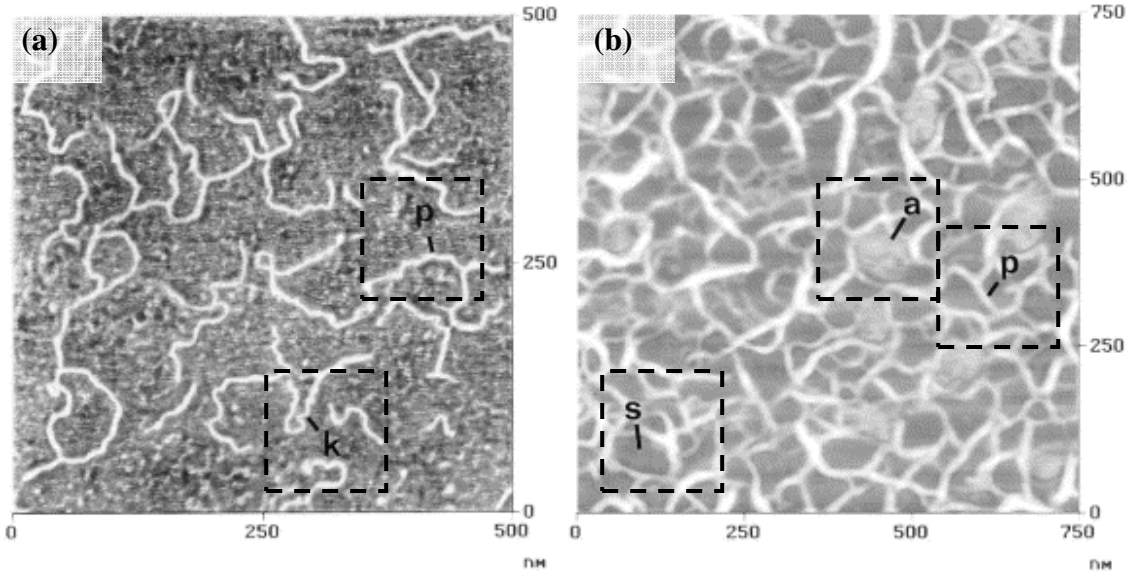

Figure 1.20 Enlarged SFM image of (a) alginate molecules (500 X 500) on mica surface (b) alginate gel (2%) in seawater (30 ppt salinity) where highlighted structures are: k, kink; s, solvent cavity; p, polymer; a, artefact.

The measured thickness of individual polymer strands in (a) was estimated to be 1-3 nm while those in the gel matrix (b) ranged from 3.74 to 18.2 nm. This suggested that the gel strands may represent several polymer molecules arranged as an aggregate. This work demonstrated the suitability of SFM for examining the structure and gel conformation of a plant polymeric matrix and may be applied to other seaweed polymers.

In this present work, a protocol for seaweed analysis by SFM has been developed. SFM represents a method of quantifying changes in the seaweed surface morphology before and after metal binding. Specific morphological data such as degree of surface roughness can be obtained from this technique, thus allowing comparisons with the qualitative data obtained from scanning electron microscopy.

1.6 Chemical Modification

In order to determine the mechanism of metal binding, it is necessary to determine the relative importance of each functional group in binding. One approach to gaining this information is chemical modification of the metal binding functional groups on the algal surface. For example, if Cu (II) binding occurs through interaction with carboxyl groups, then chemical modification that reduces the availability of the carboxyl groups for metal complexation should cause a reduction in Cu (II) binding [96]. If this happens, the participation of this functionality in metal binding is confirmed and its relative importance compared to other groups can then be estimated.

Various authors have used chemical modification to identify the functionalities involved in metal binding. Gardea-Torresday *et al*. [138] investigated the effect of carboxyl esterification on metal uptake. The carboxyl groups of five different biomasses were esterified using acidic methanol. It was found that all modified biomasses showed major decreases in Cu (II) and Al (III) binding although the decrease varied among algal species. However, it was seen that Au (III) binding capacities slightly increased as the algal carboxyl groups were esterified. These results indicated that carboxyl groups played a positive role in Cu (II) and Al (III) binding and an inhibitory role in Au (III) binding. Thus, possible differences in the binding mechanism of these metals were identified.

Chojnacka *et al*. [189] carried out chemical modifications on the functional groups of the blue-green algae *Spirulina* sp. to determine the role of each group in binding. Modifications included esterification of the carboxyl groups, methylation of the amino or hydroxyl groups as well as esterification of phosphate groups to block their participation in metal binding. It was shown that biosorption of Cr (III) ions was hindered when carboxyl and phosphate groups were esterified showing their important role in metal binding. On the other hand, methylation of the biomass hydroxyl groups brought about little or no change in the biosorption properties of the biomass thus indicating that these groups did not contribute significantly to the biosorption process.

The microorganism *Zoogloea ramigera* was subjected to a variety of chemical treatments by Xie *et al.* [190] in order to determine if its metal binding capacity could be enhanced and/or unique binding capabilities produced. The metals studied included Cu^{2+}, Cr^{3+}, Ni^{2+}, Pb^{2+} and Zn^{2+}. Table 1.5 summarises the observed effects of various chemical treatments on metal ion binding in *Zoogloea ramigera.*

Table 1.5 Effect of chemical treatment on metal binding as observed by Xie *et al.* [190].

Treatment	Observations
Acid	Strong acids (>1M) destroyed the metal binding capacity of the biomass.
Alkali	Strong bases can dissolve biomass and destroy metal binding.
$Na_2S_2O_3$	Sodium thiosulphate yields biomass with additional sulphydryl groups resulting in as much as 155% improvement in metal binding capacity.
$NaCO_2CH_2Cl$	Sodium chloroacetic acid adds carboxyl groups to biomass to yield about 33% improvement in metal binding capacity.
CS_2	Treatment of the biomass with carbon disulphide can yield a 74% improvement in metal binding capacity.
$POCl_3$	Phosphorus oxychloride yields phosphotated biosorbents with as much as a 133% improvement in binding capacity.
$HOC_6H_6SO_3$	Phenylsulphonate neither increases nor decreases the capacity of the biosorbents.

Although the work of Xie *et al.* [190] discussed the beneficial effects on capacity brought about by chemical modification, it did not establish the specific sites responsible for metal binding.

Park *et al*. [12] on the other hand, also carried out a number of treatments on *Ecklonia* biomass in order to alter the binding capacity of the seaweed as well as identify the functional groups involved in Cr (VI) binding. Modification techniques included treatment with acid, alkali, organic solvents, chelating agents as well as modification of the amino and carboxyl groups. Chemical treatment brought about both increases and decreases in metal binding capacity but in all cases, blocking of the carboxyl and amino groups resulted in decreased metal binding capacity. Thus the importance of these groups in Cr (VI) binding was proven.

In this work, the most suitable modification method for enhancement of the seaweeds' metal binding capacity was identified. Confirmation of the functionalities involved in metal binding was also achieved through modification of the seaweed functional groups.

1.7 Seaweeds under Investigation

Investigations by various groups have shown that selected species of seaweeds possess impressive sorption capacities for a range of heavy metal ions [6,65,69]. Many of the studies to date on metal biosorption by seaweeds have largely been restricted to various species of brown seaweeds [27,52,56,121,191]. On the other hand, green and red seaweed species have been evaluated to a much lesser extent [9,164,167].

This study attempts to give equal attention to each seaweed division and the seaweeds under investigation represent examples from brown (*Fucus vesiculosus* and *Fucus spiralis*), green (*Ulva lactuca* and *Ulva* spp.) and red (*Palmaria palmata* and *Polysiphonia lanosa*) seaweeds.

The seaweeds in this study were chosen because of their relative abundance in the selected geographic location (52°11'53.68"N, 6°49'34.64"W) in addition to the fact they have not previously been studied comparatively. Also, initial work by Fitzgerald *et al.* [44] pointed to the potential of *Polysiphonia lanosa* as a biosorbent material which could bind significant quantities of metal from the environment thus making it a suitable candidate for further study.

The seaweeds under investigation are discussed below. Seaweed images were obtained from www.algaebase.org [3]. An illustration of the sampling location from which these seaweeds were taken is given in Chapter 2.

1.7.1 *Fucus vesiculosus* (Brown)

Fucus vesiculosus (Figure 1.21) grows on the mid-shore, usually just below *Fucus spiralis* but sometimes with *Ascophyllum nodosum* in between. The repeatedly forked dark olive-brown fronds are joined to a disc-shaped holdfast by cylindrical stalks. The branches have wavy margins and contain air bladders which are usually in pairs, one on either side of the midrib.

Figure 1.21 *Fucus vesiculosus* [3]

It is the most common and most adaptable of all the seaweeds. For example, in exposed places, plants with very few or no bladders may be found.

1.7.2 *Fucus spiralis* (Brown)

The species *Fucus spiralis* (Figure 1.22) is located in the higher levels of the inter-tidal zone and is covered with water only for a few hours in the day. Hence, it is quite resistant to damage from drying out [5]. The branches of the olive brown fronds are spirally twisted. They have a prominent midrib and fronds are often worn away down to the midrib towards the base of the plant.

Figure 1.22 *Fucus spiralis* [3]

This seaweed has paler swollen tips containing pits with the reproductive structure inside them. These bodies do not extend to the extreme rim and thus a sterile margin remains.

1.7.3 *Ulva lactuca* (Green)

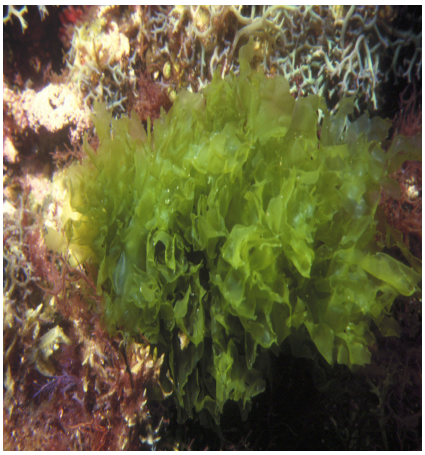

The green seaweed *Ulva lactuca* (Figure 1.23) is found at all times of year on all types of shore. The green sheets of *Ulva lactuca* are only 2 cells in thickness and may be up 2 feet long and almost as broad, but are usually much smaller [5]. It can be found attached to stones or rocks by a small disc but plants which have come adrift may continue to thrive in sheltered situations. The fronds are irregular, wavy and translucent.

Figure 1.23 *Ulva lactuca* [3]

Ulva lactuca will grow in places where fresh water runs into the sea and also where there is a moderate amount of pollution [192].

1.7.4 *Ulva* spp. (Green)

Most species of the green seaweed *Ulva* (Figure 1.24) may flourish in polluted areas and can tolerate wide fluctuations in salinity [140]. Many species of *Ulva* are practically impossible to distinguish without a microscope. In this study, the plural form, *Ulva* spp. shall be used as there is more than one species present, namely *Ulva intestinalis*, *Ulva linza* and *Ulva compressa*. These species are discussed below.

Figure 1.24 *Ulva* spp. [3]

1.7.4.1 *Ulva intestinalis*

This seaweed has long, unbranched, tubular fronds, which develop from a very small disc holdfast but frequently become detached and form free-floating masses. It varies from size from about the thickness and length of a pencil to three or four times as large and

when fully grown is irregularly inflated and constricted at intervals. It is abundant in salt marshes and is also found in pools on the upper shore of rocky coasts [192].

1.7.4.2 *Ulva linza*

This seaweed grows attached by a small disc holdfast to rocks and stones, and also to other seaweeds in pools on the middle and upper shore. It has a short cylindrical, hollow stalk, expanding into a bright-green, flat, narrow frond which is usually spirally twisted and often crimped at the margins [192].

1.7.4.3 *Ulva compressa*

Ulva compressa differs from the other two species in that it possesses branches near the base of its green long tubular fronds. The fronds are narrow at the base and flattened towards the blunt tip.

1.7.5 *Palmaria palmata* (Red)

Palmaria palmata (Figure 1.25) is one of the most common red seaweeds and is easily recognised. It is a flat, leathery purple-red frond which may branch several times and often has small outgrowths along the edge, particularly towards the base of the seaweed [5]. It grows directly from a disc-shaped holdfast on various large brown seaweeds and also on rocks at the low water mark.

Figure 1.25 ***Palmaria palmata*** **[3]**

1.7.6 *Polysiphonia lanosa* (Red)

Polysiphonia lanosa (Figure 1.26) is a thread-like seaweed which grows almost exclusively on *Ascophyllum nodosum* but is occasionally found on some *Fucus* species. It consists of repeatedly branched, hair-like threads, at the tips of which the reproductive structures are produced in small swellings [192].

Figure 1.26 ***Polysiphonia lanosa*** **[3]**

There are approximately twenty species of *Polysiphonia* that grow on the mid-shore level around the British and Irish coast.

1.8 Objectives of the Research

A comprehensive study of six seaweeds has been carried out with three metal ions namely Cu (II), Cr (III) and Cr (VI). These six seaweeds in their entirety have not been studied thus demonstrating the novelty of this approach. To date, many seaweeds biosorption studies have focused on either (1) binding of a single metal ion to a single seaweed species [169,193] (2) binding of a variety of metals to a single seaweed [27,89] or alternatively (3) binding of a single metal to a variety of seaweeds [9,167]. This work encompasses the study of a number of seaweeds and metals coupled with a wide variety of complementary analytical techniques to enhance knowledge of metal binding to seaweeds and hence attempt to elucidate the potential binding mechanisms.

The metals above were chosen not only because of their industrial significance in the region (as previously outlined) but, also because of the threat they pose to both plant and animal life when present in the environment.

This research is focussed on novel, fundamental investigations into metal sequestration by seaweeds. Such research although fundamental in nature has positive economic implications for society through the potential exploitation of our natural resources as biosorption products.

The main objectives of this work are:

- To further develop techniques that have been used in the literature to enhance knowledge of metal biosorption by seaweeds.
- To characterise the seaweeds in terms of the number of available binding sites on the surface and to hence determine the relationship between these sites and the maximum metal uptake of the seaweeds.
- To investigate the extent to which physicochemical parameters such as pH, equilibration time, ionic strength and the presence of competing ions influence metal binding.
- To investigate (using isotherm analysis) the binding capacity and binding strength/affinity of each seaweed for the metal ions under study, and to hence determine the most suitable seaweed for use as a potential biosorption product.

- To elucidate the functional groups responsible for metal binding using a variety of analytical techniques and to determine their relative importance in each seaweed-metal combination.
- To characterise the seaweed surface morphology and identify qualitative changes in the surface using SEM.
- To identify potential binding mechanisms for cation and anion binding using EDX and XPS analyses.
- To identify a modification method that can enhance the seaweeds' overall metal binding capacity and to examine the effect of chemical modification on seaweed composition.
- To develop a preliminary scanning force microscopy protocol for seaweed analysis.

1.9 References

[1] Guiry, M., www.seaweed.ie, (2007).

[2] Chan, C. X., Ho, C. L. and Phang, S. M. *Trends in Plant Science*, **11**, 165-166 (2006).

[3] www.algaebase.org, (2007).

[4] Bold, H. C. and Wynne, M. J., Introduction to the algae: Structure and Reproduction, Prentice-Hall, Englewood Cliffs, NJ, 516 (1985).

[5] Lee, T. F., The Seaweed Handbook, Dover Publications Inc., New York, 43-210 (1986).

[6] Davis, T. A., Volesky, B. and Mucci, A. *Water Research*, **37**, 4311-4330 (2003).

[7] Lobban, C. S. and Haritonidis, S., Light and Photosynthesis, In: Seaweed Ecology and Physiology, Cambridge University Press, Cambridge, UK, 123-159 (1997).

[8] Lee, R. E., Phycology, Cambridge University Press, Cambridge, UK, 3-66 (1980).

[9] Hashim, M. A. and Chu, K. H. *Chemical Engineering Journal*, **97**, 249-255 (2004).

[10] Fisheries and Oceans Canada Online., Seaweeds on The Sea Floor http://www.dfo-mpo.gc.ca/, (2005).

[11] Schiewer, S. and Volesky, B., Biosorption by marine algae, In: Remediation, Valdes, J. J. (Ed.), Kluwer Academic Publishers, Dordrecht, The Netherlands, 139-169 (2000).

[12] Park, D., Yun, Y. S. and Park, J. M. *Chemosphere*, **60**, 1356-1364 (2005).

[13] Marine Institute., Sea Change-A Marine Knowledge, Research and Innovation Strategy for Ireland (2007-2013). Part II: Research Measures, Research Programmes and Research Outcomes, Marine Institute, Galway, 58-112 (2006).

[14] Chapman, V. J. and Chapman, D. J., Seaweeds and their uses, Kluwer Academic Publishers, Dordrecht, The Netherlands, 194-240 (1980).

[15] Lal, S. N. D., O'Connor, C. J. and Eyres, L. *Advances in Colloid and Interface Science*, **123-126**, 433-437 (2006).

[16] Marinho-Soriano, E. and Bourret, E. *Bioresource Technology*, **96**, 379-382 (2005).

[17] Shilpa, A., Agrawal, S. S. and Ray, A. R. *Journal of Macromolecular Science-Polymer Review*, **C43**, 187-221 (2003).

[18] Oztekin, N., Baskan, S. and Erim, F. B. *Journal of Chromatography B*, **850**, 488-492 (1-5-2007).

[19] de Sousa, A. P. A., Torres, M. R., Pessoa, C., de Moraes, M. O., Filho, F. D. R., Alves, A. P. N. N. and Costa-Lotufo, L. V. *Carbohydrate Polymers*, **69**, 7-13 (2007).

[20] de S.F-Tischer, P. C., Talarico, Laura B., Noseda, Miguel D., Pita, B. Guimaraes, Damonte, Elsa B. and Duarte, Maria Eugenia. *Carbohydrate Polymers*, **63**, 459-465 (2006).

[21] Talarico, L. B., Pujol, C. A., Zibetti, R. G. M., Faria, P. C. S., Noseda, M. D., Duarte, M. E. R. and Damonte, E. B. *Antiviral Research*, **66**, 103-110 (2005).

[22] Colwell, R. R. *Biotechnology Advances*, **20**, 215-228 (2002).

[23] Athukorala, Y., Lee, K. W., Kim, S. K. and Jeon, Y. J. *Bioresource Technology*, **98**, 1711-1716 (2007).

[24] Volesky, B. *Hydrometallurgy*, **59**, 203-216 (2001).

[25] Senthilkumar, R., Vijayaraghavan, K., Thilakavathi, M., Iyer, P. V. R. and Velan, M. *Biochemical Engineering Journal*, **33**, 211-216 (2007).

[26] Prasanna Kumar, Y., King, P. and Prasad, V. S. R. K. *Chemical Engineering Journal*, **129**, 161-166 (2007).

[27] Tsui, M. T. K., Cheung, K. C., Tam, N. F. Y. and Wong, M. H. *Chemosphere*, **65**, 51-57 (2006).

[28] Yang, L. and Chen, J. P. *Bioresource Technology*, **In Press, Corrected Proof**, (2007).

[29] Hellio, C., De La Broise, D., Dufosse, L., Le Gal, Y. and Bourgougnon, N. *Marine Environmental Research*, **52**, 231-247 (2001).

[30] de Nys, R. and Steinberg, P. D. *Current Opinion in Biotechnology*, **13**, 244-248 (2002).

[31] Lobban, C. S. and Harrison, P. J., Pollution, In: Seaweed Ecology and Physiology, Cambridge University Press, Cambridge, UK, 255-281 (1997).

[32] Cornelis, R., Caruso, J., Crews, H. and Heumann, K., Handbook of Elemental Speciation, John Wiley & Sons Ltd., Chichester, 1-6 (2005).

[33] European Environment Agency., The European Environment- State and Outlook 2005, Office for Official Publications of the European Communities, Copenhagen, 28-232 (2005).

[34] Bradl, H., Sources and Origins of Heavy Metals, In: Heavy Metals in the Environment: Origin, Interaction and Remediation, Elsevier Academic Press, Amsterdam, 1-11 (2005).

[35] Wood, J. M. *Science*, **183**, 1049-1052 (1974).

[36] Duffus, J. H. *Chemistry International*, **23**, 161-167 (2001).

[37] Scott, T. A. and Mercer, E. I., Concise Encyclopedia Biochemistry and Molecular Biology, Jakube, H. D. (Ed.), W. de Gruyter & Co., Berlin; New York, 245-306 (1996).

[38] Rand, G. M., Wells, P. G. and McCarty, S. L., Introduction to aquatic toxicology, In: Fundamentals of Aquatic Toxicology; Effects, Environmental Fate And Risk Assessment, Rand, G. M. (Ed.), Taylor and Francis, Washington DC, 449-492 (1995).

[39] Lyman, W. J., Transport and transformation processes, In: Fundamentals of Aquatic Toxicology; Effects, Environmental Fate And Risk Assessment, Rand, G. M. (Ed.), Taylor and Francis, Washington DC, 449-492 (1995).

[40] Crompton, T. R., Pollution of Potable Water, In: Toxicants in the Aqueous Ecosystem, John Wiley & Sons, Chichester, 291-298 (1997).

[41] Volesky, B., Removal and recovery of heavy metals by biosorption, In: Biosorption of Heavy Metals, CRC Press, Boca Raton, FL, 7-44 (1990).

[42] United States Department of Health & Human Services, Public Health Service., Agency for Toxic Substances and Disease Registry (ATSDR) Toxicological Profiles, http://www.atsdr.cdc.gov/toxprofiles/, (1999).

[43] United States Environmental Protection Agency., http://www.epa.gov/, (2007).

[44] Fitzgerald, E. J., Caffrey, J. M., Nesaratnam, S. T. and McLoughlin, P. *Environmental Pollution*, **123**, 67-74 (2003).

[45] Inland Waterways Association of Ireland. *Newsletter of the Inland Waterways Association of Ireland*, **29**, 1-6 (2002).

[46] Barnhart, J. *Regulatory Toxicology and Pharmacology*, **26**, S3-S7 (1997).

[47] Cervantes, C., Campos-Garcia, J., Devars, S., Gutierrez-Corona, F., Loza-Tavera, H., Torres-Guzman, J. C. and Moreno-Sanchez, R. *Fems Microbiology Reviews*, **25**, 335-347 (2001).

[48] Costa, M. *Toxicology and Applied Pharmacology*, **188**, 1-5 (2003).

[49] Yun, Y. S., Park, D., Park, J. M. and Volesky, B. *Environmental Science & Technology*, **35**, 4353-4358 (2001).

[50] Browning, E., Toxicity of Industrial Metals, Butterworths, London, 119-131 (1969).

[51] Acar, F. N. and Malkoc, E. *Bioresource Technology*, **94**, 13-15 (2004).

[52] Davis, T. A., Volesky, B. and Vieira, R. H. S. F. *Water Research*, **34**, 4270-4278 (2000).

[53] Ahluwalia, S. S. and Goyal, D. *Bioresource Technology*, **98**, 2243-2257 (2007).

[54] Nourbakhsh, M., Sag, Y., Ozer, D., Aksu, Z., Kutsal, T. and Caglar, A. *Process Biochemistry*, **29**, 1-5 (1994).

[55] Lodeiro, P., Barriada, J. L., Herrero, R. and De Vicente, M. E. S. *Environmental Pollution*, **142**, 264-273 (2006).

[56] Lodeiro, P., Cordero, B., Barriada, J. L., Herrero, R. and Sastre de Vicente, M. E. *Bioresource Technology*, **96**, 1796-1803 (2005).

[57] Singh, V. K. and Tiwari, P. N. *Journal of Chemical Technology and Biotechnology*, **69**, 376-382 (1997).

[58] Sengupta, A. K. and Clifford, D. *Industrial & Engineering Chemistry, Fundamentals*, **25**, 249-258 (1986).

[59] Cabuk, A., Akar, T., Tunali, S. and Tabak, O. *Journal of Hazardous Materials*, **136**, 317-323 (2006).

[60] Ozturk, A. *Journal of Hazardous Materials*, **In Press, Corrected Proof**, (2007).

[61] Akar, T. and Tunali, S. *Bioresource Technology*, **97**, 1780-1787 (2006).

[62] Park, D., Yun, Y. S., Hye, J. J. and Park, J. M. *Water Research*, **39**, 533-540 (2005).

[63] Han, X., Wong, Y. S., Wong, M. H. and Tam, Nora F. Y. *Journal of Hazardous Materials*, **146**, 65-72 (19-7-2007).

[64] Fraile, A., Penche, S., Gonzalez, F., Blazquez, M. L., Munoz, J. A. and Ballester, A. *Chemistry and Ecology*, **21**, 61-75 (2005).

[65] Sheng, P. X., Ting, Y. P., Chen, J. P. and Hong, L. *Journal of Colloid and Interface Science*, **275**, 131-141 (2004).

[66] Murphy, V., Hughes, H. and McLoughlin, P. *Water Research*, **41**, 731-740 (2007).

[67] Hosea, M., Greene, B., McPherson, R., Henzl, M., Alexander, M. D. and Darnall, D. W. *Inorganic Chimica Acta*, **123**, 161-165 (1986).

[68] Kratochvil, D. and Volesky, B. *Trends in Biotechnology*, **16**, 291-300 (1998).

[69] Volesky, B. and Holan, Z. R. *Biotechnology Progress*, **11**, 235-250 (1995).

[70] Holan, Z. R. and Volesky, B. *Biotechnology and Bioengineering*, **43**, 1001-1009 (1994).

[71] Holan, Z. R., Volesky, B. and Prasetyo, I. *Biotechnology and Bioengineering*, **41**, 819-825 (1993).

[72] Tobin, J. M., Cooper, D. G. and Neufeld, R. J. *Applied and Environmental Microbiology*, **47**, 821-824 (1984).

[73] Volesky, B., May, H. and Holan, Z. R. *Biotechnology and Bioengineering*, **41**, 826-829 (1993).

[74] Friis, N. and Myers-Keith, P. *Biotechnology and Bioengineering*, **28**, 21-28 (1986).

[75] Yang, J. and Volesky, B. *Environmental Science and Technology*, **33**, 4079-4085 (1999).

[76] Cordero, B., Lodeiro, P., Herrero, R. and De Vicente, M. E. S. *Environmental Chemistry*, **1**, 180-187 (2004).

[77] Webster, E. A. and Gadd, G. M. *Biometals*, **9**, 241-244 (1996).

[78] Crist, R. H., Oberholser, K., Mcgarrity, J., Crist, D. R., Johnson, J. K. and Brittsan, J. M. *Environmental Science & Technology*, **26**, 496-502 (1992).

[79] Knauer, K., Behra, R. and Sigg, L. *Environmental Toxicology and Chemistry*, **16**, 220-229 (1997).

[80] Stokes, P. M. *Progress in Phycological Research*, **2**, 87-112 (1983).

[81] Gadd, G. M. and Griffiths, A. J. *Microbial Ecology*, **4**, 303-317 (1977).

[82] Huntsman, S. A. and Sunda, W. G., The role of trace metals in regulating phytoplankton growth, In: The Physiological Ecology of Phytoplankton, Morris, I. (Ed.), Blackwell Scientific, Oxford, 285-328 (1980).

[83] Gekeler, W., Grill, E., Winnacker, E. L. and Zenk, M. H. *Zeitschrift fur Naturforschung C-A Journal of Biosciences*, **44**, 361-369 (1989).

[84] Francke, J. A. and Hillebrand, H. *Aquatic Botany*, **8**, 285-289 (1980).

[85] Grill, E., Winnacker, E. L. and Zenk, M. H. *Proceedings of the National Academy of Sciences of the United States of America*, **84**, 439-443 (1987).

[86] Gekeler, W., Grill, E., Winnacker, E. L. and Zenk, M. H. *Archives of Microbiology*, **150**, 197-202 (1988).

[87] Singh, S., Pradhan, S. and Rai, L. C. *Process Biochemistry*, **36**, 175-182 (2000).

[88] Abu Al-Rub, F. A., El Naas, M. H., Benyahia, F. and Ashour, I. *Process Biochemistry*, **39**, 1767-1773 (2004).

[89] Raize, O., Argaman, Y. and Yannai, S. *Biotechnology and Bioengineering*, **87**, 451-458 (2004).

[90] Volesky, B. and Holan, Z. R. *Biotechnology Progress*, **11**, 235-250 (1995).

[91] Brown, D. H. and Bates, J. W. *Journal of Bryology*, **7**, 187-193 (1972).

[92] Haug, A., Larsen, B. and Smidsrod, O. *Acta Chemica Scandinavica*, **21**, 691-& (1967).

[93] Haug, A. *Acta Chemica Scandinavica*, **15**, 1794-1795 (1961).

[94] Percival, E. G. V. and McDowell, R. H., Chemistry and Enzymology of Marine Algal Polysaccharides, Academic Press, London, UK, 99-126 (1967).

[95] Schweiger, R. G. *Journal of Organic Chemistry*, **27**, 1789-& (1962).

[96] Fourest, E. and Volesky, B. *Environmental Science & Technology*, **30**, 277-282 (1996).

[97] Majidi, V., Laude, D. A. and Holcombe, J. A. *Environmental Science & Technology*, **24**, 1309-1312 (1990).

[98] Mackie, W. and Preston, R. D., Cell wall and intercellular region polysaccharides, In: Algal physiology and biochemistry, Stewart, W. D. P. (Ed.), Blackwell Scientific Publications, Oxford, 58-64 (1974).

[99] Haug, A. and Smidsrod, O. *Acta Chemica Scandinavica*, **24**, 843-847 (1970).

[100] Dawczynski, C., Schubert, R. and Jahreis, G. *Food Chemistry*, **103**, 891-899 (2007).

[101] Siegel, B. Z. and Siegel, S. M. *CRC Critical Reviews in Microbiology*, **3**, 1-26 (1973).

[102] Chan, J. C. C., Cheung, P. C. K. and Ang, P. O. *Journal of Agricultural and Food Chemistry*, **45**, 3056-3059 (1997).

[103] Schiewer, S. and Wong, M. H. *Chemosphere*, **41**, 271-282 (2000).

[104] Mckinnell, J. P. and Percival, E. *Journal of the Chemical Society*, 2082-2083 (1962).

[105] Lahaye, M. and Axelos, M. A. V. *Carbohydrate Polymers*, **22**, 261-265 (1993).

[106] Paradossi, G., Cavalieri, F. and Chiessi, E. *Macromolecules*, **35**, 6404-6411 (2002).

[107] Ray, B. and Lahaye, M. *Carbohydrate Research*, **274**, 313-318 (1995).

[108] Andrieux, C., Hibert, A., Houari, A. M., Bansaada, M., Popot, F. and Szylit, O. *Journal of the Science of Food and Agriculture*, **77**, 25-30 (1998).

[109] Fujiwara-Arasaki, T., Mino, N. and Kuroda, M. *Hydrobiologia*, **116-117**, 513-516 (1984).

[110] Chan, J. C. C., Cheung, P. C. K. and Ang, P. O. *Journal of Agricultural and Food Chemistry*, **45**, 3056-3059 (1997).

[111] Zubay, G. L., Parson, W. W and Vance, D. E., The Building Blocks of Proteins: Amino Acids, Peptides and Polypeptides, In: Principles of Biochemistry, Wm. C. Brown Publishers, Dubuque, IA, 49-76 (1995).

[112] Lobban, C. S. and Harrison, P. J., Light and Photosynthesis, In: Seaweed Ecology and Physiology, Cambridge University Press, Cambridge, 123-159 (1997).

[113] Paskins-Hurlburt, A. J., Tanaka, Y. and Skoryna, S. C. *Botanica Marina*, **19**, 59-60 (1976).

[114] Percival, E. G. V. *British Phycological Journal*, **14**, 103-117 (1979).

[115] Fleurence, J., Gutbier, G., Mabeau, S. and Leray, C. *Journal of Applied Phycology*, **6**, 527-532 (1994).

[116] Rupérez, P. and Saura-Calixto, F. *European Food Research Technology*, **212**, 349-354 (2001).

[117] Norziah, M. H. and Ching, C. Y. *Food Chemistry*, **68**, 69-76 (2000).

[118] McLachlan, J., Craigie, J. S., Chen, L. C. M. and Ogetze, E. *Proceedings of the International Seaweed Symposium*, **7**, 473-476 (1972).

[119] Aksu, Z. *Separation and Purification Technology*, **21**, 285-294 (2001).

[120] Vijayaraghavan, K., Jegan, J., Palanivelu, K. and Velan, M. *Separation and Purification Technology*, **44**, 53-59 (2005).

[121] Chen, J. P. and Yang, L. *Langmuir*, **22**, 8906-8914 (2006).

[122] Tien, C., In: Adsorption Calculations and Modeling, Butterworth-Heinemann, Boston, 29-40 (1994).

[123] Stumm, W. and Morgan, J. J., Aquatic Chemistry, Wiley Interscience, New York, 3-32 (1996).

[124] Park, D., Yun, Y. S., Yim, K. H. and Park, J. M. *Bioresource Technology*, **97**, 1592-1598 (2006).

[125] Aksu, Z., Acikel, U. and Kutsal, U. *Journal of Chemical Technology and Biotechnology*, **70**, 378 (1997).

[126] Schiewer, S. and Volesky, B. *Environmental Science & Technology*, **31**, 2478-2485 (1997).

[127] Yun, Y. S. and Volesky, B. *Environmental Science & Technology*, **37**, 3601-3608 (2003).

[128] Saeed, A., Iqbal, M. and Akhter, M. W. *Journal of Hazardous Materials*, **117**, 65-73 (2005).

[129] Pagnanelli, F., Trifoni, M., Beolchini, F., Esposito, A., Toro, L. and Veglio, F. *Process Biochemistry*, **37**, 115-124 (2001).

[130] Kramer, K. J. M., Biomonitoring of Coastal Waters and Estuaries, CRC Press, Boca Raton, FL (1994).

[131] Greene, B., McPherson, R. and Darnall, D. W., Algal sorbents for selective metal ion recovery, In: Metals Speciation, Separation and Recovery, Patterson, J. W. and Pasino, R. (Ed.), Lewis, Chelsea, MI, 315-338 (1987).

[132] Kuyucak, N. and Volesky, B. *Biorecovery*, **1**, 189-204 (1989).

[133] Langmuir, I. *Journal of the American Chemical Society*, **40**, 1361-1403 (1918).

[134] Volesky, B., Equilibrium Biosorption Performance, In: Sorption and Biosorption, BV-Sorbex, Inc., St.Lambert, Quebec, 103-116 (2004).

[135] Lee, H. S. and Volesky, B. *Water Research*, **31**, 3082-3088 (1997).

[136] Schiewer, S. and Volesky, B. *Environmental Science & Technology*, **29**, 3049-3058 (1995).

[137] da Costa, A. C. A., Tavares, A. P. M. and de Franca, F. P. *Electronic Journal of Biotechnology*, **4**, 125-129 (2001).

[138] Gardea-Torresdey, J. L., Becker-Hapak, M. K., Hosea, J. M. and Darnall, D. W. *Environmental Science & Technology*, **24**, 1372-1378 (1990).

[139] Kratochvil, D., Volesky, B. and Demopoulos, G. *Water Research*, **31**, 2327-2339 (1997).

[140] Crist, D. R., Crist, R. H., Martin, J. R. and Watson, J. R. *Fems Microbiology Reviews*, **14**, 309-313 (1994).

[141] Kuyucak, N. and Volesky, B. *Biotechnology and Bioengineering*, **33**, 809-814 (1989).

[142] Howard, A. J., Aquatic Environmental Chemistry, Oxford University Press, Oxford, 36-51 (1998).

[143] Marcus, Y. and Kertes, A. S., Ion Exchange and Solvent Extraction of Metal Complexes, Wiley, New York (1969).

[144] Andrade, A. D., Rollemberg, M. C. E. and Nobrega, J. A. *Process Biochemistry*, **40**, 1931-1936 (2005).

[145] Botelho, C. M. S., Boaventura, R. A. R. and Goncalves, M. L. S. S. *Analytica Chimica Acta*, **462**, 73-85 (2002).

[146] Allen, S. J. and Brown, P. A. *Journal of Chemical Technology and Biotechnology*, **62**, 17-24 (1995).

[147] Cho, D. Y., Lee, S. T., Park, S. W. and Chung, A. S. *Journal of Environmental Science and Health Part A-Environmental Science and Engineering & Toxic and Hazardous Substance Control*, **29**, 389-409 (1994).

[148] Haug, A. and Smidsrod, O. *Nature*, **215**, 1167-1168 (1967).

[149] Smidsrod, O and Draget, K. I. *Carbohydr.Eur.*, **14**, 6-13 (1996).

[150] Haug, A. *Acta Chemica Scandinavica*, **15**, 1794-& (1961).

[151] Seki, H. and Suzuki, A. *Journal of Colloid and Interface Science*, **246**, 259-262 (2002).

[152] Gupta, V. K., Rastogi, A., Saini, V. K. and Jain, N. *Journal of Colloid and Interface Science*, **296**, 59-63 (2006).

[153] Naja, G. and Volesky, B. *Colloids and Surfaces A: Physicochemical and Engineering Aspects*, **281**, 194-201 (2006).

[154] Niu, H. and Volesky, B. *Hydrometallurgy*, **71**, 209-215 (2003).

[155] Udaybhaskar, P., Iyengar, L. and Prabhakara Rao, A. V. S. *Journal of Applied Polymer Science*, 739-747 (2003).

[156] Sharma, D. C. and Forster, C. F. *Bioresource Technology*, **47**, 257-264 (1994).

[157] Marsden, J. and House, L., In: Chemistry of Gold Extraction, Ellis Horwood, Hartnoll, UK, 100-150 (1993).

[158] Niu, C. H., Volesky, B. and Cleiman, D. *Water Research*, **41**, 2473-2478 (2007).

[159] Roberts, G. A. F., Chitin Chemistry, Macmillan, London, 55-58 (1992).

[160] Roberts, G. A. F., Chitin Chemistry, Macmillan, London, 204-206 (1992).

[161] Sharma, D. C. and Forster, C. F. *Water Research*, **27**, 1201-1208 (1993).

[162] Bosinco, S., Roussy, J., Guibal, E. and LeCloirec, P. *Environmental Technology*, **17**, 55-62 (1996).

[163] Park, D., Yun, Y. S., Ahn, C. K. and Park, J. M. *Chemosphere*, **66**, 939-946 (2007).

[164] El-Sikaily, A., Nemr, A. El, Khaled, A. and Abdelwehab, O. *Journal of Hazardous Materials*, **In Press, Corrected Proof**, -113 (2007).

[165] Veglio, F., Esposito, A. and Reverberi, A. P. *Process Biochemistry*, **38**, 953-961 (2003).

[166] Figueira, M. M., Volesky, B., Ciminelli, V. S. T. and Roddick, F. A. *Water Research*, **34**, 196-204 (2000).

[167] Jalali, R., Ghafourian, H., Asef, Y., Davarpanah, S. J. and Sepehr, S. *Journal of Hazardous Materials*, **92**, 253-262 (2002).

[168] Freundlich, H. *Z Phys Chem*, **57**, 385-470 (1907).

[169] Lodeiro, P., Cordero, B., Grille, Z., Herrero, R. and De Vicente, M. E. S. *Biotechnology and Bioengineering*, **88**, 237-247 (2004).

[170] Hanif, M. A, Nadeem, R., Bhatti, H. N., Ahmad, N. R. and Ansari, T. M. *Journal of Hazardous Materials*, **139**, 345-355 (2007).

[171] Agarwal, G. S., Bhuptawat, H. K. and Chaudhari, S. *Bioresource Technology*, **97**, 949-956 (2006).

[172] Dambies, L., Guimon, C., Yiacoumi, S. and Guibal, E. *Colloids and Surfaces A: Physicochemical and Engineering Aspects*, **177**, 203-214 (2001).

[173] Decho, A. W. *Carbohydrate Research*, **315**, 330-333 (1999).

[174] Gunning, A. P., Cairns, P., Kirby, A. R., Round, A. N., Bixler, H. J. and Morris, V. J. *Carbohydrate Polymers*, **36**, 67-72 (1998).

[175] Wase, J. and Forster, C. F., Biosorbents for metal ions, Taylor and Francis, London, 11-38 (1997).

[176] Figueira, M. M., Volesky, B. and Mathieu, H. J. *Environmental Science & Technology*, **33**, 1840-1846 (1999).

[177] Pereira, L., Sousa, A., Coelho, H., Amado, A. M. and Ribeiro-Claro, P. J. A. *Biomolecular Engineering*, **20**, 223-228 (2003).

[178] Skoog, D. A., Holler, F. J. and Nieman, T. A., Surface Characterization by Spectroscopy and Microscopy, In: Principles of Instrumental Analysis, Saunders College Publishing, 535-566 (1992).

[179] Briggs, D., Applications of XPS in Polymer Technology, In: Practical Surface Analysis, Briggs, D. and Seah, M. P. (Ed.), 436-483 (1990).

[180] Venkata Mohan, S., Ramanaiah, S. V., Rajkumar, B. and Sarma, P. N. *Bioresource Technology*, **98**, 1006-1011 (2007).

[181] Yang, L. and Chen, J. P. *Bioresource Technology*, **In Press, Corrected Proof**, (2007).

[182] Simon, A. and Durrieu, M. C. *Micron*, **37**, 1-13 (2006).

[183] Dupres, V., Verbelen, C. and Dufrene, Y. F. *Biomaterials*, **28**, 2393-2402 (2007).

[184] Heinrich Horber, J. K., Local Probe Techniques, In: Atomic Force Microscopy in Cell Biology, Jena, B. P. and Heinrich Horber, J. K. (Ed.), Academic Press, San Diego, 1-31 (2002).

[185] Dammer, U., Hegner, M., Anselmetti, D., Wagner, P., Dreier, M., Huber, W. and Guntherodt, H. J. *Biophysical Journal*, **70**, 2437-2441 (1996).

[186] Ahimou, F., Denis, F. A., Touhami, A. and Dufrene, Y. F. *Langmuir*, **18**, 9937-9941 (2002).

[187] Macaskie, L. E., Bonthrone, K. M., Yong, P. and Goddard, D. T. *Microbiology UK*, **146**, 1855-1867 (2000).

[188] Morris, V. J., Gunning, A. P., Kirby, A. R., Round, A., Waldron, K. and Ng, A. *International Journal of Biological Macromolecules*, **21**, 61-66 (1997).

[189] Chojnacka, K., Chojnacki, A. and Gorecka, H. *Chemosphere*, **59**, 75-84 (2005).

[190] Xie, J. Z., Chang, H. L. and Kilbane, J. J. *Bioresource Technology*, **57**, 127-136 (1996).

[191] Park, D., Yun, Y. S., Cho, H. Y. and Park, J. M. *Industrial & Engineering Chemistry Research*, **43**, 8226-8232 (2004).

[192] Brightman, F. H., The Illustrated Book of Flowerless Plants, Oxford University Press, Oxford, 2-27 (1966).

[193] Luo, F., Liu, Y., Li, X., Xuan, Z. and Ma, J. *Chemosphere*, **64**, 1122-1127 (2006).

Chapter 2 Physical Characterisation of the Seaweed

2.1 Introduction

The knowledge of the chemical structure of biosorbents is essential for modelling and predicting their metal binding performance and biosorption behaviour in water purification systems. The work in this chapter examines seaweed surface in terms of the quantity of binding sites present as well as the specific surface area of the seaweeds. The effect of Cu (II) binding on the availability of these sites is also established while the relationship between quantity of acidic sites, surface area and maximum metal uptake is established in Chapter 3.

2.1.1 Potentiometric and Conductimetric Titrations

Various authors have used potentiometric titrations in order to establish the number of acidic functionalities on the biomass surface [1,2] and hence to predict heavy metal binding to the surface. The analysis of potentiometric titration curves shows the influence of pH on the deprotonation of the surface functional groups which are capable of binding metals [3,4]. For pH values greater than the pK_a, the sites are mainly in dissociated form and can exchange H^+ with metal ions in solution. To quantify the potential metal cation uptake by the seaweeds, the number of functional groups and their associated pK_a values must be determined.

In general, protonated biomass may be titrated with a base, usually sodium hydroxide. The analysis of results shows that the cell wall seems to have two or more main functional groups responsible for metal sorption [1,2]. If the only active sites are those titrated, the metal sorption abilities of the selected biosorbents are strongly influenced by pH as reported by the following equilibrium equation:

$$Me^{2+} + 2B\text{-}H \longleftrightarrow B_2Me + 2H^+ \qquad \textbf{(Equation 2.1)}$$

Where Me^{2+} is the heavy metal in solution (i.e. in divalent form), B-H represents the protonated biomass and B_2Me represents the complex biomass-metal [4].

2.1.3 Objectives of the Research

The main objectives of the work in this chapter are:

- To characterise the biomass in terms of the number and type of acidic binding sites present on the surface and hence investigate the effect of metal binding on the availability of these sites.

2.2 Experimental

2.2.1 Materials and Methods

2.2.1.1 Biomass Preparation

Seaweeds were identified [5] and collected from Fethard-on-Sea, Co. Wexford, Ireland (52°11'53.68"N, 6°49'34.64"W) (Figure 2.2).

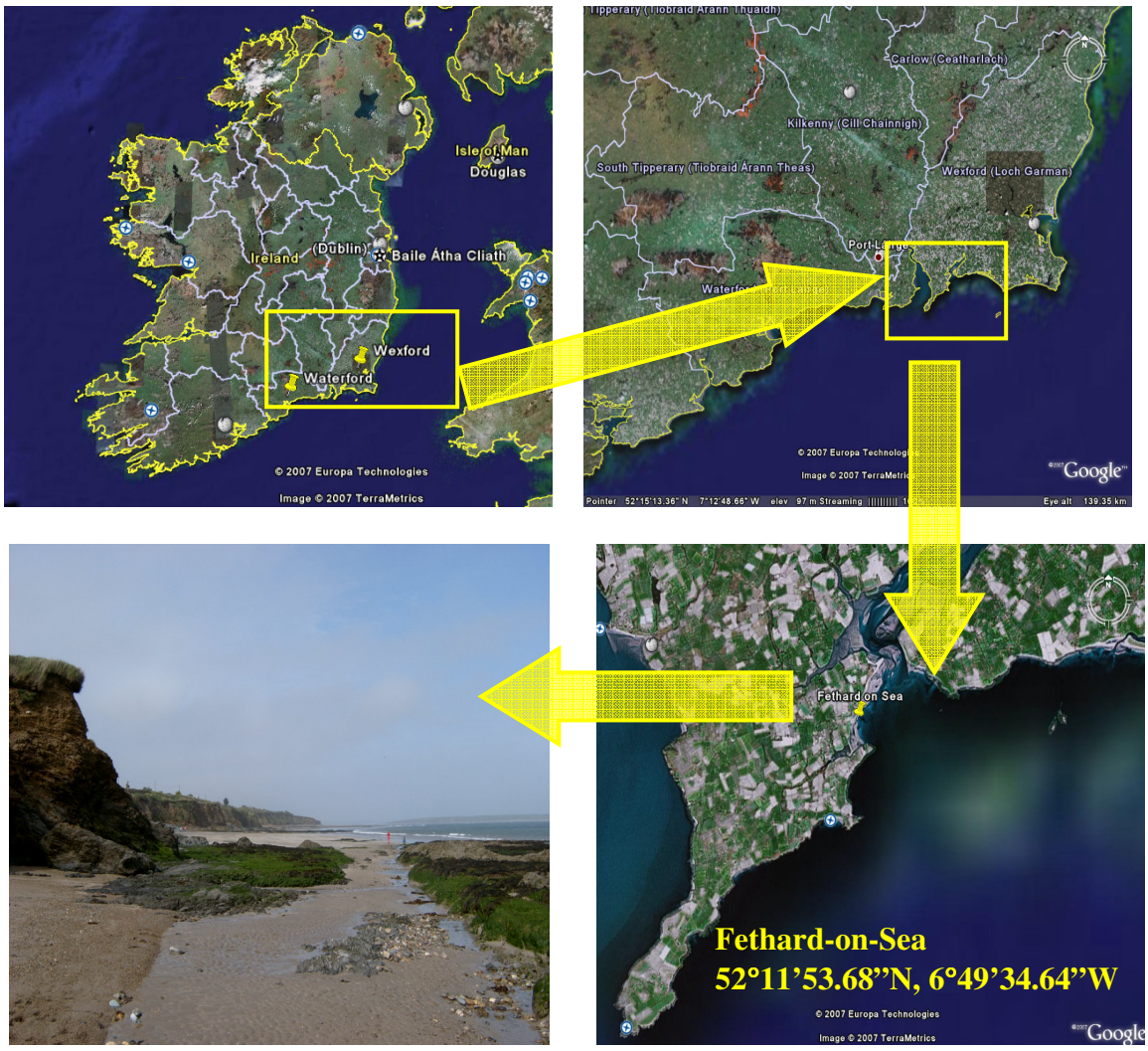

Figure 2.2 Clean Seaweed Collection Site, Fethard-on-Sea, Co. Wexford, Ireland. (Source: Google Earth).

This sampling location was chosen due to the low background metal concentration in both seawater and seaweeds and also because of the relative abundance of the seaweed species in the area.

The seaweed samples were rinsed thoroughly with distilled water in order to remove any adhering debris. Washing also allows the removal of common ions such as Ca^{2+}, Mg^{2+}, Na^{2+} and K^{+} that are present in seawater. The various plants collected within each species, from various locations on the sampling site were combined to give composite batches. Samples were oven-dried at 60°C for 24h, then subsequently ground and sieved to a particle size of 500-850 μm. This particle size fraction was used for all experiments. The biomass was stored in airtight polyethylene bottles until required.

The use of dead seaweed biomass in this work offers various advantages such as no toxicity effects, no requirement for growth media and nutrients, easy desorption of metal ions and reusability of biomass [6].

2.2.1.2 Chemicals

- 1000mg L^{-1} Cu (II) as Cu $(NO_3)_2$ (analytical grade) - Sigma-Aldrich Ltd., Dublin, Ireland.
- Sodium Hydroxide (solid) - Ridel de Haën, Germany.
- Sodium Chloride (solid) - Ridel de Haën, Germany.
- Hydrochloric Acid (37%) - LabScan Ltd., Dublin, Ireland.
- Buffers pH 4 (± 0.02) and 7 (± 0.02) - Ridel de Haën, Germany.

2.2.1.3 Instrumentation

- Glove Box- Plas Labs Inc. Model Number 818GB

2.2.2 Potentiometric and Conductimetric Titrations

2.2.2.1 Protonation of the Biomass

Biomass particles (5g) were protonated (from procedure by Fourest and Volesky [1]) by washing with 250mL of 0.1M HCl. This treatment ensured that any remaining salts e.g. Ca^{2+}, Mg^{2+}, $Na^{2+,}$ K^{+} were removed from the seaweed surface. The suspension was allowed to stir for 6h to ensure that equilibrium had been reached. The biomass was filtered under vacuum and washed with distilled water until a constant conductance was obtained for the filtrate. The protonated biomass was oven-dried at 60˚C for 24h and stored in airtight polyethylene bottles until required.

2.2.2.2 Titration of biomass

For each titration, 200mg of protonated biomass was dispersed in 100mL of a 1mM NaCl solution. Titration was carried out by stepwise addition of 0.25mL of 0.1M NaOH (prepared with boiled distilled water) to the flask while the suspension was stirred under a nitrogen atmosphere in a glove box. After each addition of titrant, the system was allowed to equilibrate until a stable pH reading was obtained. Conductivity was measured using a WTW LF 538 Conductivity meter with WTW TetraCon® 325 probe while pH measurements were recorded using a Mettler Toledo MP 220 pH meter with a Mettler Toledo Inlab® 413 pH electrode. The pH electrode was calibrated with buffers pH 4 (± 0.02) and pH 7 (± 0.02) prior to use and the conductivity probe was checked by measuring the conductivity of a 0.01M KCl solution. Potentiometric titrations were carried out in triplicate with errors bars calculated to 95% confidence intervals. Conductimetric titrations were carried out singly to act as verification for potentiometric titration results.

2.2.3 Titration of metal bound seaweeds

In order to determine the effects of metal binding on the number of available acidic sites on the biomass surface, 100 mg of protonated *Fucus vesiculosus* (Section 2.2.2.1) was exposed to 50mL of metal solutions containing 200µg L^{-1} and 10 mg L^{-1} of Cu (II)

respectively. Solution pH was maintained at pH 5 while flasks were shaken at 200rpm and room temperature (21 ± 1°C). The biomass was then filtered under vacuum and oven dried at 60°C for 24h. Titration of the biomass was carried out as in Section 2.2.2.2. Triplicate analyses were carried out in all cases.

2.3 Results and Discussion

2.3.1 Potentiometric & Conductimetric Titrations

Figure 2.3 shows the potentiometric titration curves obtained for the six seaweeds under investigation.

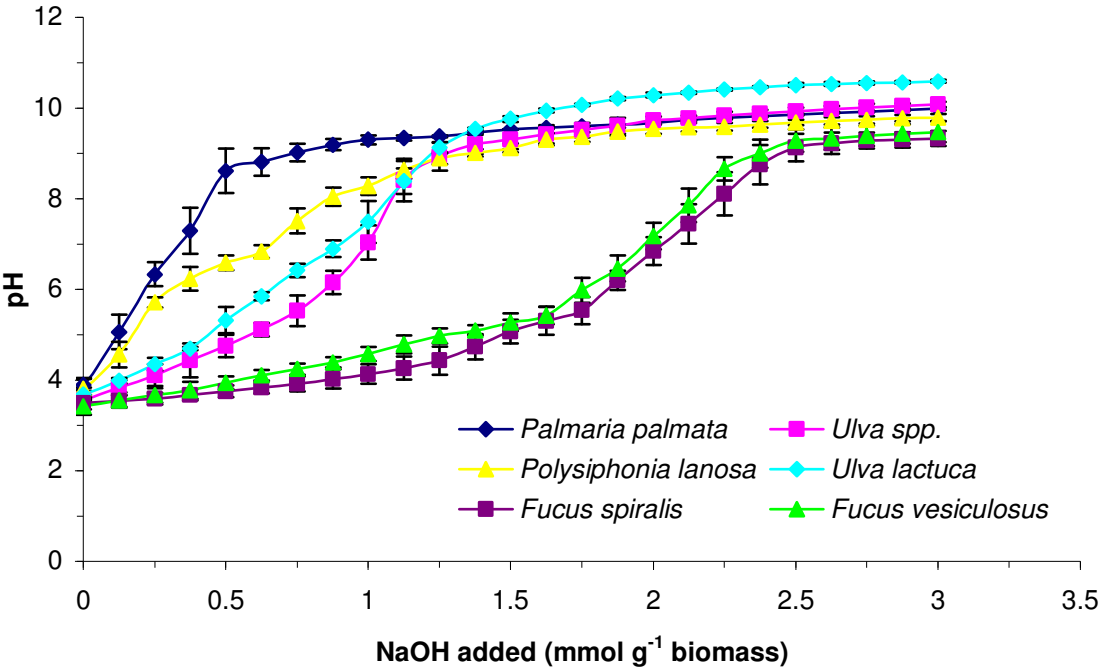

Figure 2.3 Potentiometric Titration Curves for six seaweed species. Error bars are calculated based on triplicate runs with 95% Confidence Intervals.

Figure 2.3 shows that there are large variations in the potentiometric titration curves of the six seaweeds. While *Fucus vesiculosus* and *Fucus spiralis* followed similar patterns, significant differences were apparent between the green and red seaweeds.

The various amounts of acidic groups in the biomass and their corresponding pK_a values were evaluated by identifying the inflection points of the titration curves (Figure 2.3). However, this may be difficult and a better indication of the position of these inflections was obtained from first derivative plots of average pH titration data. The use of first derivative plots for seaweed potentiometric titrations has not previously been demonstrated.

The first derivative plots consist of the midpoint of successive amounts of NaOH added (x-axis) versus dpH/dV (y-axis). The location of each peak on the x-axis gives the number of acidic groups on the biomass surface.

Figure 2.4 illustrates the first derivative plots obtained for the six seaweeds. The number of strong acidic groups was determined from the first peak in each of the first derivative plots while the total number of acidic groups for a given weight of biomass was determined from the final peak. The number of weak acidic groups was then calculated by difference (Total-Strong = Weak). Only peaks over a dpH/dV limit of 0.66 were considered to be significant with values lower than this approximating baseline. Biomass leaching was found to occur (especially in the case of the brown seaweeds) as the titration progressed at higher alkalinity and this may have introduced some error into the measurement.

First derivative peaks from Figure 2.4 were compared with the inflection points on the original titration curves and both were found to be in agreement. Once these values were established, the corresponding apparent pK_a values were then identified from the original titration curves. The pK_a values and the number of acidic groups on the biomass surface are summarised in Table 2.1.

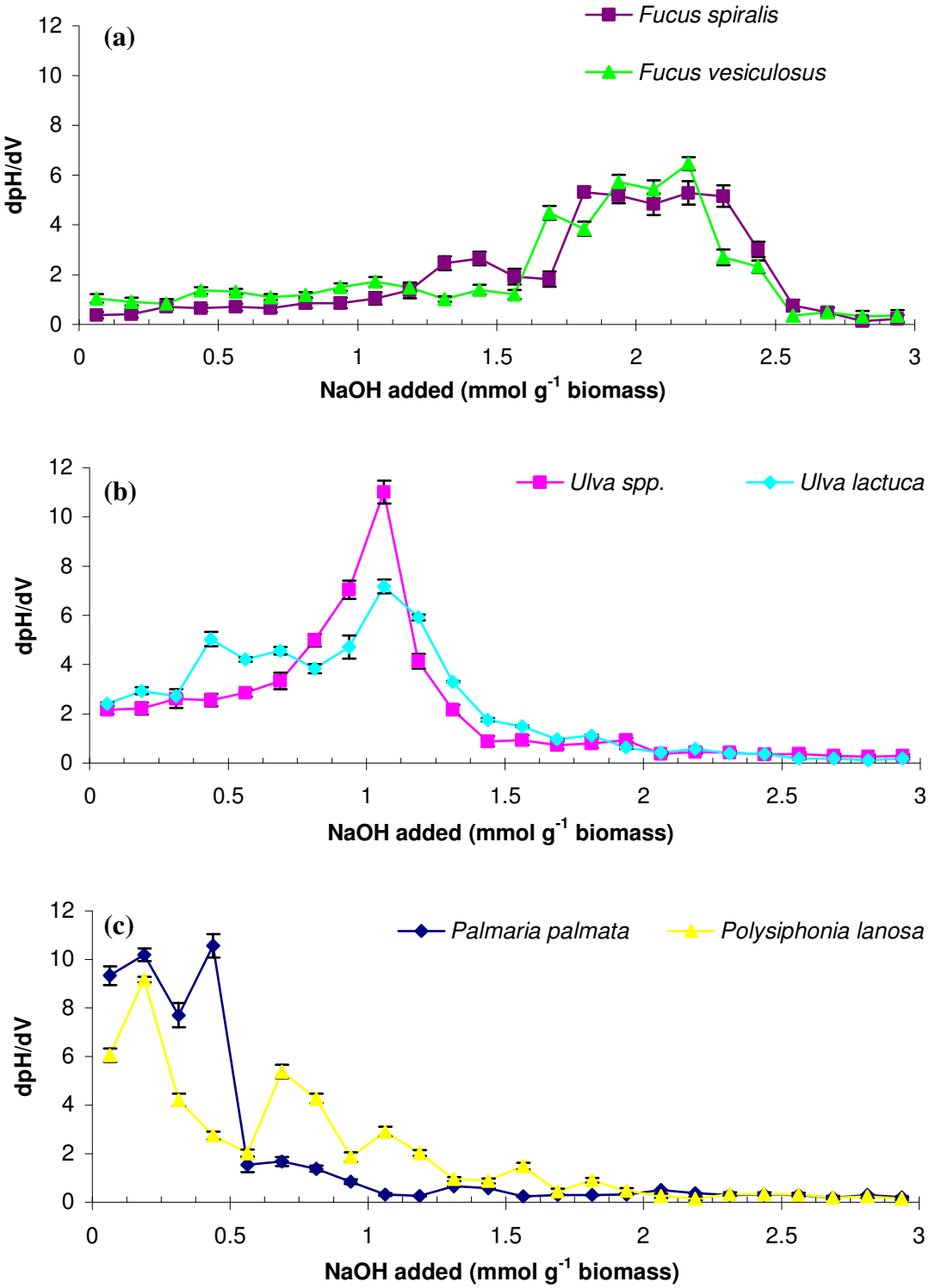

Figure 2.4 **First Derivative plots of average pH titration data for (a) Brown (b) Green (c) Red seaweed species. Error bars are calculated based on triplicate runs with 95% Confidence Intervals.**

Table 2.1 **pK_a values and number of acidic groups of the various seaweeds as determined by titration. Error bars are calculated based on triplicate runs with 95% Confidence Intervals.**

Seaweed	pK_a Values	Acidic Groups (mmol g^{-1})		
		Total	Strong	Weak
Fucus vesiculosus	3.85 ± 0.1 4.68 ± 0.2 5.70 ± 0.2 6.82 ± 0.3 8.25 ± 0.2	2.44 ± 0.22	0.44 ± 0.16	2.00 ± 0.20
Fucus spiralis	3.60 ± 0.1 4.30 ± 0.2 5.30 ± 0.3 8.11 ± 0.3	2.31 ± 0.12	0.31 ± 0.08	2.00 ± 0.14
Ulva lactuca	3.83 ± 0.1 4.52 ± 0.2 6.66 ± 0.3 8.76 ± 0.3 10.01 ± 0.2	1.81 ± 0.03	0.19 ± 0.03	1.62 ± 0.11
Ulva spp.	3.69 ± 0.3 4.59 ± 0.2 7.20 ± 0.3 9.25 ± 0.2	1.94 ± 0.13	0.44 ± 0.11	1.50 ± 0.22
Palmaria palmata	4.47 ± 0.2 8.71 ± 0.3 9.35 ± 0.2	1.31 ± 0.16	0.19 ± 0.01	1.12 ± 0.08
Polysiphonia lanosa	4.19 ± 0.1 6.71 ± 0.2 8.16 ± 0.2 9.06 ± 0.1	1.81 ± 0.09	0.19 ± 0.06	1.62 ± 0.11

In general, potentiometric titrations have been carried out for brown seaweeds and even then, mostly for *Sargassum* species [1,2,7]. On the other hand, details of potentiometric titration analyses for red and green seaweeds have not been found in the literature, thus, illustrating the novelty of approach in this work.

Figueira *et al*. [8] used potentiometric titrations to evaluate the number of total acidic groups in four brown seaweeds, *Laminaria* sp., *Durvillaea* sp., *Ecklonia* sp. and *Homosira* sp. The seaweeds contained 2.40, 2.24, 2.00 and 2.10 mmol g^{-1} of acidic groups respectively and these results were well aligned with the results found for the brown seaweeds (2.44 ± 0.22 and 2.31 ± 0.12 mmol g^{-1} for *Fucus vesiculosus* and *Fucus spiralis* respectively) in this study.

Results in Table 2.1 indicate that the total quantity of acidic groups in the remaining seaweeds decreased in the order: *Ulva* spp. > *Ulva lactuca* = *Polysiphonia lanosa* > *Palmaria palmata*.

From Table 2.1, it is also seen that the brown seaweeds contained the greatest number of weak acidic groups on the seaweed surface. Given this finding, and the fact that carboxyl groups (weak) are primarily responsible for cation sorption [9], it would be expected that the brown seaweeds would exhibit superior metal biosorption performance. Subsequent pH experiments (Chapter 3) show that the brown seaweeds do in fact exhibit superior cation uptake relative to the other seaweeds. This finding is also in agreement with the work of various authors comparing cation uptake by brown, red and green seaweeds [9-11].

For all seaweeds, Figures 2.3 and 2.4 indicate the presence of multiple inflection points and peaks respectively in the carboxyl region of the curves. It is possible that these inflection points may represent the different orientations of constituent carboxyl groups thus leading to more than one observed pK_a for these groups (Table 2.1). This is a reasonable explanation when the different carboxyl orientations in mannuronic and guluronic acid residues in brown seaweeds are considered. It is also possible that

carboxyl groups in different environments in the red and green species could contribute to the observed results. The repeatability of these inflections over triplicate runs also indicates that these are not artifacts of the experiment.

In their study on three *Sargassum* species, Davis *et al*. [2] found that the quantity of strong acidic groups in *S. vulgare*, *S. fluitans* and *S. filipendula* was 0.5, 0.3 and 0.3 mmol g^{-1} respectively. Again, these values were comparable with the results obtained in this study, with *Fucus vesiculosus* and *Fucus spiralis* having 0.44 and 0.31 mmol g^{-1} strong acidic groups respectively (Table 2.1).

No literature comparison can be used for the potentiometric titration curves of the green and red seaweeds at this time, but results indicated that *Ulva* spp. had the same quantity of strong acidic groups as *Fucus vesiculosus* (0.44 ± 0.11 mmol g^{-1}). This value was significantly larger than those observed for *Ulva lactuca*, *Palmaria palmata* and *Polysiphonia lanosa*, each of which contained 0.19 mmol g^{-1} strong acidities (Table 2.1).

The various pK_a values observed in Table 2.1 illustrate that the seaweed is polyfunctional in nature, with each functional group having a different pK_a value. The observed values and their corresponding functional groups are discussed below.

Sulphonate groups usually only contribute to metal binding at low pH and their typical pK_a values are in the range 1.0-2.5 [12]. Apparent pK_a values in this range were not detected by titration, but the presence of sulphonate groups on the seaweed surface was later confirmed by FTIR analysis (Chapter 4).

From Table 2.1, it was seen that the apparent carboxyl pK_a values obtained for the brown seaweeds in this study (pK_a 3.85 ± 0.1 and 4.68 ± 0.2 for *Fucus vesiculosus* and pK_a 3.60 ± 0.1 and 4.30 ± 0.2 for *Fucus spiralis*) were above the intrinsic pK_a values of mannuronic and guluronic acids (~3.38 and ~3.65 respectively) [13] . This may be explained by the effects of electrostatic interactions between adjacent acidic groups in the biomass or conformational transitions [14]. Small quantities of sulphated polysaccharides

may also result in a shift in the observed pK_a values of the various functionalities. This has been shown to be a common phenomenon in the titration of polyelectrolyte gels [15].

As previously discussed, a number of peaks were also observed in the carboxyl region of the green and red seaweed curves (Figure 2.4). The pK_a values obtained for the green seaweeds were similar to those obtained for the brown seaweeds with values of 3.83 ± 0.1 and 4.52 ± 0.2 obtained for *Ulva* spp. and 3.69 ± 0.3 and 4.59 ± 0.2 for *Ulva lactuca* (Table 2.1). However, for *Polysiphonia lanosa,* apparent pK_a values were slightly higher at 4.19 ± 0.1 and 6.71 ± 0.2. On the other hand, only one pK_a value was observed in this region for *Palmaria palmata* (4.47 ± 0.2). Thus, these findings may illustrate possible differences in the polysaccharide composition of the red seaweeds.

Between pH 6 and 9, algal proteins may interact with metal ions. Protonated amino groups have been shown to have pK_a values of around 8 [13]. From Table 2.1 it is seen that each of the seaweeds displayed at least one pK_a value in this region e.g. *Fucus vesiculosus* (8.25 ± 0.2), *Ulva lactuca* (8.76 ± 0.3) and *Palmaria palmata* (8.71 ± 0.3).

Hydroxyl groups in seaweed cell wall polysaccharides are considerably weaker than carboxyl groups and therefore may only interact with cations at a higher pH. This usually occurs at pH >10. Therefore surface hydroxyl groups only play a significant role in binding at very high pH values [9]. Apparent pK_a values in the range 9-10 were found for the green and red seaweeds but were not detected for the brown seaweeds. This may have been due to lower concentration of these groups on the surface or their inaccessibility during titration.

Conductimetric curves have been used in previous investigations as a standard procedure [1,2] and have been included in this work for comparative purposes only using a single replicate. The general trends observed in the conductimetric curves were similar to those observed previously by various authors [1,8]. The conductimetric curves obtained for the six seaweeds are shown in Figure 2.5.

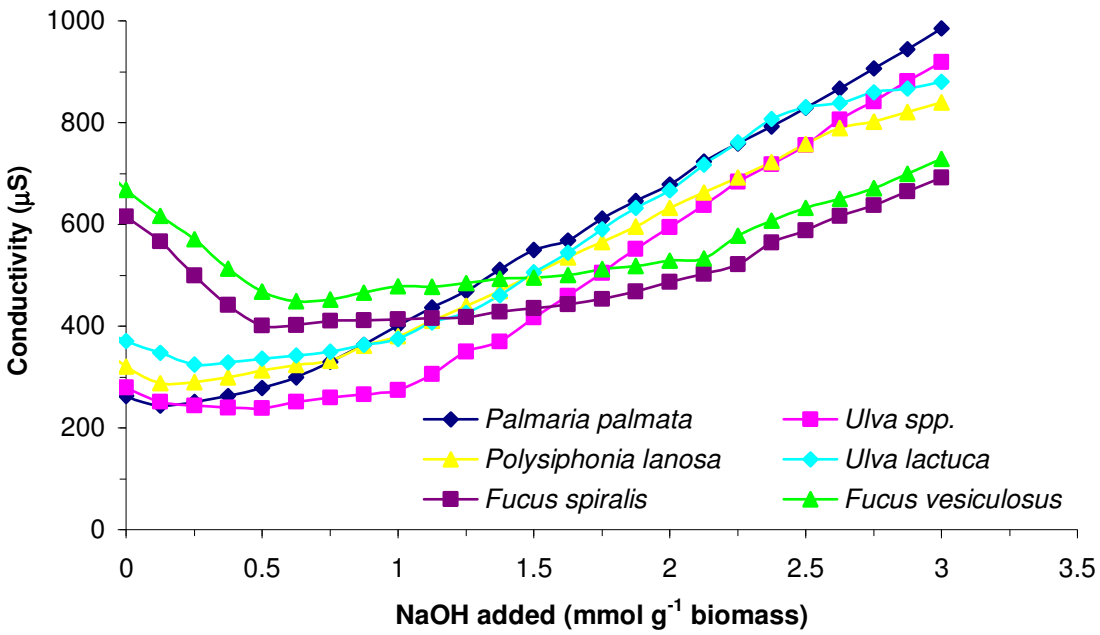

Figure 2.5 Conductimetric Titration Curves for six seaweed species.

From Figure 2.5 it is seen that solution conductivity initially decreased quite sharply. This was due to the neutralisation of free protons from strongly acidic groups [2]. When all of the strong acidic groups were neutralised, the weaker acidic groups began to dissociate and contribute to measured conductivity. The neutralisation of weak acids was characterised by a gentle increase in solution conductivity. When all the weak acidic groups were neutralised, the conductivity of the solution increased in proportion to the excess sodium hydroxide added.

According to Davis *et al.* [2], the transition between the decreasing and increasing portion of the conductivity curve should correspond to the first equivalence point on the potentiometric titration curve and thus give the quantity of strong acidic groups. However, in most cases an equivalence range rather than a specific point was obtained. Approximate values were as follows: *Fucus vesiculosus* (0.60 ± 0.1), *Fucus spiralis* (0.60 ± 0.1), *Ulva* spp. (0.50 ± 0.1), *Ulva lactuca* (0.25 ± 0.1), *Palmaria palmata* (0.13 ± 0.1), and *Polysiphonia lanosa* (0.13 ± 0.1). Comparing these values to those obtained from potentiometric curves, it is seen that conductimetric titrations slightly overestimated the

strong acidic groups for the brown seaweeds, but that results were comparable (within error) to the potentiometric titrations of the green and red seaweeds.

2.3.2 Titration of metal bound samples

Figure 2.6 illustrates the first derivative plots of protonated and Cu (II)-loaded *Fucus vesiculosus*. The quantity of acidic binding sites before and after metal binding is summarised in Table 2.2.

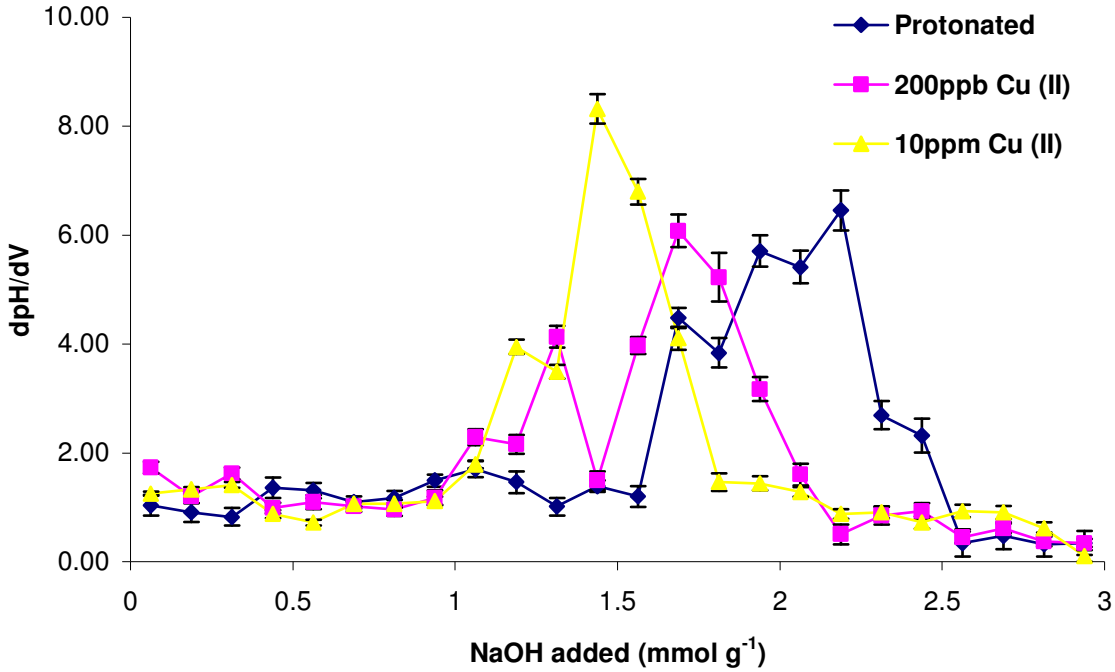

Figure 2.6 **First derivative plots of protonated and Cu (II)-loaded *Fucus vesiculosus*. Error bars are calculated based on triplicate runs with 95% Confidence Intervals.**

Table 2.2 **Variation in the number of acidic groups in protonated and Cu (II)-loaded *Fucus vesiculosus*. Error bars are calculated based on triplicate runs with 95% Confidence Intervals.**

	Peaks in 1st Derivative Plots (mmol g^{-1} biomass)		
	Protonated	**200 µg L^{-1} Cu (II)**	**10 mg L^{-1} Cu (II)**
Strong	0.44 ± 0.16	0.31 ± 0.11	0.31 ± 0.13
Total	2.44 ± 0.22	2.19 ± 0.18	1.94 ± 0.09
Weak	2.00 ± 0.20	1.88 ± 0.18	1.63 ± 0.11

An apparent reduction in the number of available acidic sites in metal loaded biomass was observed in Table 2.2. Decreases in the quantity of strong and weak acidic groups indicate that both sulphonate and carboxyl groups take part in Cu (II) binding at μg L^{-1} and mg L^{-1} metal levels.

In 200μg L^{-1} Cu (II)-loaded biomass, there is a reduction of 0.25 mmol g^{-1} of which 0.12 mmol g^{-1} was attributed to the weak acidic groups. Exposure of the biomass to 10 mg L^{-1} Cu (II) resulted in a decrease of 0.50 mmol g^{-1} of which 0.37 mmol g^{-1} were weak acidic groups. This shows that, as expected, there is significant contribution of the biomass carboxyl groups to Cu (II) binding at both concentrations. This is also demonstrated by the loss of complexity in the carboxyl region of the plot.

The same reduction in strong acidic groups (0.13 mmol g^{-1}) was observed at both 200 μg L^{-1} and 10 mg L^{-1} perhaps implying that all accessible strong acid groups are occupied initially and that, after this point, Cu (II) binding is then primarily due to carboxyl interactions.

2.4 Conclusions

Of the seaweeds studied, the brown seaweeds possessed the greatest number of total and weak acidic binding sites while *Palmaria palmata* contained the least. The importance of the weak acidic sites for cation binding is demonstrated in Chapter 3.

Ulva spp. showed an elevated quantity of acidic groups relative to the other green and red seaweeds. The effect of this on metal binding is investigated in later chapters.

The polyfunctional nature of the seaweed surface was demonstrated by the variety of pK_a values observed for each species. Apparent pKa values were detected for carboxyl, amino and hydroxyl groups.

Both strong and weak acidities take part in Cu (II) binding to *Fucus vesiculosus* at $\mu g\ L^{-1}$ and $mg\ L^{-1}$ levels of the metal. The relative contribution of the sulphonate groups was the same for both concentrations perhaps indicating that all accessible strong acid groups are occupied initially and that the remaining sites are not available for metal binding at these concentrations.

The seaweed surface has been described in terms of the quantity of acidic binding sites. Therefore, the next steps are to determine the factors which affect metal biosorption by seaweeds, to investigate the quantity of metal which may be bound to the seaweed and to establish the relationship between the seaweed surface and its binding capacity.

2.5 References

[1] Fourest, E. and Volesky, B. *Environmental Science & Technology*, **30**, 277-282 (1996).

[2] Davis, T. A., Volesky, B. and Vieira, R. H. S. F. *Water Research*, **34**, 4270-4278 (2000).

[3] Pagnanelli, F., Beolchini, F., Esposito, A., Toro, L. and Veglio, F. *Hydrometallurgy*, **71**, 201-208 (2003).

[4] Esposito, A., Pagnanelli, F. and Veglio, F. *Chemical Engineering Science*, **57**, 307-313 (2002).

[5] Brightman, F. H., The Illustrated Book of Flowerless Plants, Oxford University Press, Oxford, 2-27 (1966).

[6] Kapoor, A. and Viraraghavan, T. *Bioresource Technology*, **61**, 221-227 (1997).

[7] Chen, J. P. and Yang, L. *Langmuir*, **22**, 8906-8914 (2006).

[8] Figueira, M. M., Volesky, B., Ciminelli, V. S. T. and Roddick, F. A. *Water Research*, **34**, 196-204 (2000).

[9] Davis, T. A., Volesky, B. and Mucci, A. *Water Research*, **37**, 4311-4330 (2003).

[10] Volesky, B. and Holan, Z. R. *Biotechnology Progress*, **11**, 235-250 (1995).

[11] Holan, Z. R. and Volesky, B. *Biotechnology and Bioengineering*, **43**, 1001-1009 (1994).

[12] Sheng, P. X., Ting, Y. P., Chen, J. P. and Hong, L. *Journal of Colloid and Interface Science*, **275**, 131-141 (2004).

[13] Percival, E. G. V. and McDowell, R. H., Chemistry and Enzymology of Marine Algal Polysaccharides, Academic Press, London, UK, 99-126 (1967).

[14] Rey-Castro, C., Lodeiro, P., Herrero, R. and De Vicente, M. E. S. *Environmental Science & Technology*, **37**, 5159-5167 (2003).

[15] Marinsky, J. A. and Ephraim, J. *Environmental Science & Technology*, **20**, 349-354 (1986).

Chapter 3
Factors Affecting Metal Biosorption

3.1 Introduction

In Chapter 2 the seaweeds were defined in terms of the quantity of acidic sites while Chapter 1 described some of the experimental parameters affecting metal biosorption by seaweeds. These parameters included pH and ionic strength as well as the presence of competing ions. The influence of these and other factors on Cu (II), Cr (III) and Cr (VI) binding to the seaweeds is described in this chapter.

Isotherm analysis is used to describe the capacity and affinity of the seaweeds for the metal ions. The relationship between capacity and the quantity of acidic binding sites is also studied.

3.1.1 Optimum pH determination

The pH of the aqueous phase governs the speciation of metals and also the dissociation of the active functional sites on the sorbent [1]. Hence, metal sorption is critically linked with pH. Various authors have observed that solution pH is an important parameter affecting heavy metal biosorption by seaweed species [2-4]. The surface groups of seaweed species e.g. carboxyl and sulphonate display acidic characteristics and the optimum pH for metal uptake is therefore related to the pK_a of these functionalities. For cationic metals, the availability of negatively charged groups at the biosorbent surface is necessary for the sorption of metals to proceed [5].

However, the solution chemistry of the metal complexes involved must also be considered, as the speciation of metals in solution is pH dependent. Figure 3.1 illustrates the influence of solution pH on metal uptake as observed by Kratochvil and Volesky [6].

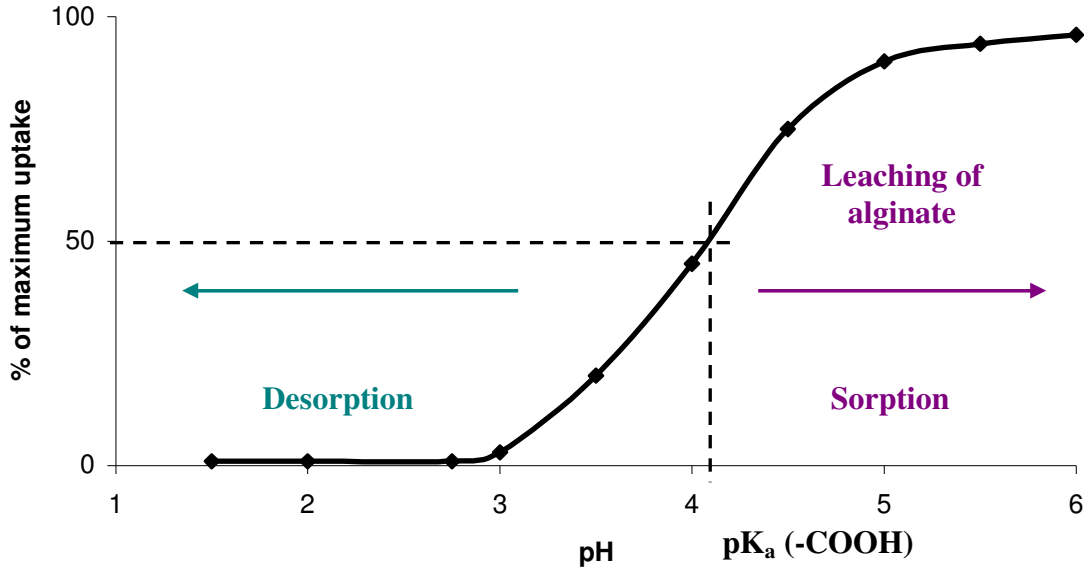

Figure 3.1 pH profile of metal uptake capacity illustrating the influence of carboxyl group dissociation on metal binding [6].

From Figure 3.1, it is clear that the biomass can be regenerated at lower pH with desorption occurring at pH values less than 3. As pH increases, so too does the percentage of maximum uptake with almost 100% achieved at pH 6. The pK_a value of the carboxyl groups are highlighted since it is thought that carboxyl groups are primarily responsible for metallic cation sorption in brown seaweeds. At increased pH values, some leaching of alginate was observed due to solubilisation of the biomass under alkaline conditions.

3.1.2 Equilibrium Binding Time

In any biosorption experiment it is necessary to allow sufficient contact time between the sorbent and sorbate to ensure that equilibrium conditions have been reached. Equilibrium times of 24 h have been proposed for cadmium binding to various biomaterials including: chitin [7], chitosan beads [8], Baker's yeast [9] or *Pinus pinaster* bark [10]. Even longer times have been reported for some carbonaceous materials (72 h) [11] or activated carbon (3-5 days) [12]. Therefore, the rapid metal uptake observed by some authors for sorption onto macroalgae [13-15] makes algal biomass desirable from a practical industrial perspective as its use will facilitate shorter columns thus ensuring efficiency and

economy. For example, batch experiments carried out by Lodeiro *et al*. [16], at an initial metal concentration of 2 mmol L^{-1}, showed that over 90% of total binding is reached within 17 minutes for Cd (II) sorption (50% in 1 minute) and in around 47 minutes for Pb (II) (50% in 5 min).

3.1.3 Ionic Strength

Industrial effluents often contain large amounts of light metal ions such as Ca^{2+}, Mg^{2+}, Na^{+} and K^{+} along with the heavy metal ions. These light metal ions can affect the performance of the biosorption system. Schiewer and Wong [17] observed that, with an increase in ionic strength, metal binding can be reduced due to the strong competitiveness of the electrolyte ions for binding sites on the biomass.

Generally, hard ions like sodium, which are bound weakly through mostly electrostatic interaction (HSAB, Table 1.3) are effective in competing only with other weakly bound ions [18]. However, even heavy metals that tend to form complexes are partially bound through electrostatic attraction as a consequence of the higher metal concentration near binding sites than in the bulk solution [17]. Therefore, their binding is consequently reduced when background salts are added to solution.

Schiewer and Wong [17] studied the effects of ionic strength on binding of Ni^{2+} and Cu^{2+}. Cu^{2+} is known to bind strongly to many biomaterials whereas Ni^{2+} binds weakly mainly through electrostatic interactions. It is therefore expected that these two metals would display very different binding behaviour at increased ionic strength. For Ni^{2+} binding the importance of electrostatic effects was evident, as a much higher binding capacity was determined at low ionic strength while lesser effects were seen for Cu^{2+}.

It is therefore important to evaluate metal binding under conditions of both low and high ionic strength as metal binding behaviour under these conditions may give an indication of the binding mechanism.

3.1.4 Adsorption Isotherms

The performance of many biosorbents in the removal of heavy metals from aqueous solutions has been reported by various authors [4,14,19,20]. Typically, the Langmuir [14,18] and Freundlich [21,22] isotherms, or a combination of both [1,16], have been used to describe this performance.

Although the Langmuir and Freundlich isotherms have found widespread use in biosorption studies, these models are simply mathematical functions and do not provide any mechanistic understanding of the sorption phenomenon [23]. They can, however, conveniently be used to indicate binding capacities and strengths for various metal-biosorbent systems.

Conformity to the Freundlich model suggests adsorption in a multilayer fashion while the Langmuir model explains a monolayer type of sorption [24]. A description of each isotherm is given below.

3.1.4.1 Langmuir Isotherm

The Langmuir isotherm represents a simple and widespread equation for quantitative comparison of the sorption performance of different biosorbent materials [18].

The Langmuir Isotherm incorporates constants that are easily interpretable and has traditionally been used to quantify and contrast the performance of different biosorbents [25]. However, in order to evaluate the suitability of the model is it necessary to look at its underlying assumptions.

Compliance with Langmuir Isotherm Theory [26] requires that the following conditions are met:

(1) Adsorption of the solute is limited to the formation of a monolayer i.e. the number of adsorbed species does not exceed the total sites.

(2) All sites have the same energy or equal affinity for the sorbate i.e. the sorbent surface is homogeneous and contains only one type of binding site.

In the case of biosorption, condition (2) is not met. The literature has shown that there is more than one type of functional group contributing to the process of biosorption, each of which has a different affinity for heavy metals [25]. This is apparent when the pK_a values of the various surface functionalities are considered (Table 2.1). It has also been shown that the relative affinity of these groups for metal ions is dependent on the experimental pH. Furthermore, the one-to-one stoichiometry is not complied with because ion-exchange has been shown to be the dominant mechanism and typically two protons are released upon the binding of one divalent heavy metal [25].

Despite these factors, the Langmuir Isotherm has found widespread use in biosorption work. This is due to the fact that it contains two parameters that are useful and easily interpretable [27]. The parameter $\boldsymbol{q_{max}}$ is the maximum sorbate (metal) uptake under the given conditions e.g. mmol g^{-1}, and $\boldsymbol{b}$ is a coefficient related to the affinity between the sorbent and sorbate. Variations in affinity between seaweeds could be explained by differences in their chemical constitution, since different types of polysaccharides would present different affinities for the metal ions.

According to the Langmuir model, sorption occurs uniformly on active sites of the sorbent, and once a sorbate occupies a site, no further sorption can take place at this site [28].

Thus, the Langmuir model is given by:

$$q = q_{max} \frac{bC_f}{1 + bC_f} \qquad \textbf{(Equation 3.1)}$$

Where q is the equilibrium metal uptake (mmol g^{-1}) , q_{max} is the maximum metal uptake (mmol g^{-1}), C_f is the residual equilibrium metal concentration in solution (mmol L^{-1}) and b is an affinity parameter (L $mmol^{-1}$) [13].

Figure 3.2 gives an illustration of Langmuir model for a sorption isotherm adapted from Volesky [27].

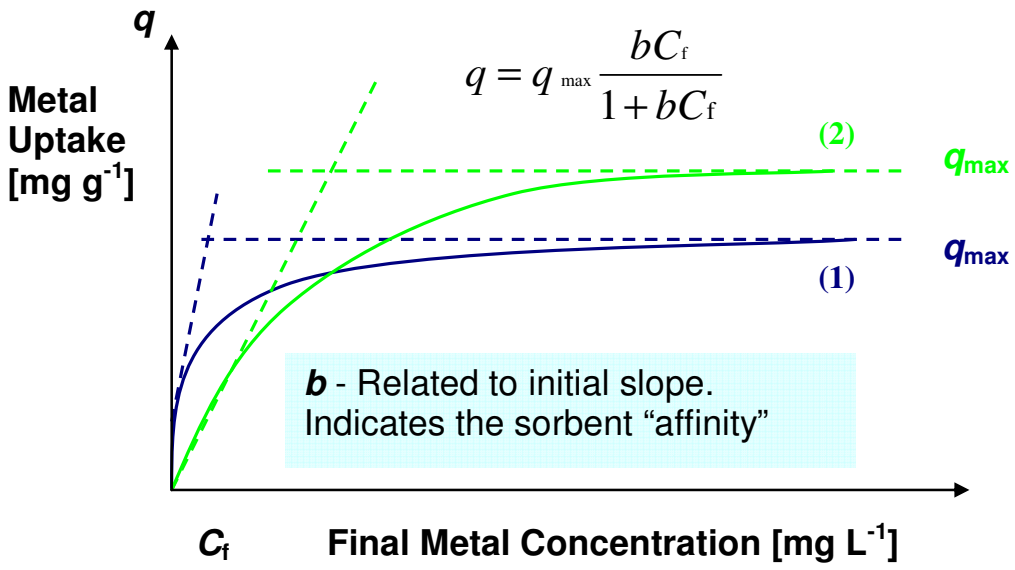

Figure 3.2 Comparison of Langmuir isotherm curves for two sorbents (1) and (2).

The linear form of the Langmuir equation is:

$$\frac{1}{q} = \frac{1}{q_{max}} \left(\frac{1}{b C_f} + 1 \right) \qquad \textbf{(Equation 3.2)}$$

Thus, a plot of $\mathbf{1/}\boldsymbol{q}$ vs. $\mathbf{1/}\boldsymbol{C}_\mathbf{f}$ results in a straight line with a slope of $(\mathbf{1/(}\boldsymbol{b}\mathbf{.}\boldsymbol{q}_\mathbf{max}\mathbf{)})$ and an intercept of $(\mathbf{1/}\boldsymbol{q}_\mathbf{max}\mathbf{)}$.

Table 3.1 illustrates the Langmuir parameters obtained by Hashim *et al*. [29] for their work on cadmium biosorption by various brown, green and red seaweed species.

Table 3.1 Langmuir parameters for cadmium biosorption by seven seaweed species obtained by Hashim *et al*. [29].

Seaweed species	q_{max} (mmol g^{-1})	b (L $mmol^{-1}$)
Sargassum baccularia (brown)	0.74	4.67
Sargassum siliquosum (brown)	0.73	6.60
Padina tetrastomatica (brown)	0.53	4.65
Chaetomorpha linum (green)	0.48	1.43
Gracilaria changii (red)	0.23	9.65
Gracilaria edulis (red)	0.24	4.82
Gracilaria salicornia (red)	0.16	9.04

These authors [29] also demonstrated that the performance of a biosorbent is dependent upon both Langmuir parameters $\boldsymbol{q}_\mathbf{max}$ and $\boldsymbol{b}$, with high values of $\boldsymbol{q}_\mathbf{max}$ values being desirable.

The value $\boldsymbol{q}_\mathbf{max}$ represents a practical limiting adsorption capacity corresponding to the surface of sorbent fully covered by metal ions (Figure 3.2). This quantity is particularly useful in the assessment of the sorption performance, especially in cases where the sorbent does not reach its full saturation as it enables comparison between different sorbents [30] .

Various authors have shown that high values of $\boldsymbol{b}$ are reflected by steep initial slopes (Curve 1 in Figure 3.2) of isotherm curves and indicate a high affinity of the sorbent for the sorbate [13,14,18,29,31,32]. A curve with a steep initial slope also indicates a sorbent which has a capacity for the sorbate in the low residual concentration range.

Hashim *et al.* [29] found that the red seaweeds often possessed larger ***b*** values than either the greens or browns. This indicates that they have a greater affinity for metals in the lower residual concentration ranges than the brown or green seaweeds.

A biosorbent with a low q_{max} value and a high ***b*** could display superior performance over a biosorbent with a high q_{max} and a low ***b***, especially in cases where the metal ion to be removed is at trace levels. However, as previously outlined, it has been predicted in the literature that the most efficient seaweed biosorbent would have high values of both q_{max} and ***b*** [25,29]. The most suitable seaweed therefore depends on the application for which it is to be used.

3.1.4.2 Freundlich Isotherm

The Freundlich isotherm [33] attempts to interpret sorption of materials to heterogeneous surfaces and surfaces containing sites of varying affinities. The pK_a values observed for the various seaweed functional groups indicate that the seaweed surface does indeed contain sites with varying affinities for metal ions (Table 2.1). Therefore, the Freundlich isotherm can be used in an attempt to describe heavy metal binding to the seaweed surface.

The Freundlich model does not predict surface saturation but instead considers the existence of a multilayered structure [34]. It is assumed that the stronger binding sites are occupied first and that the binding strength decreases with increasing degree of site occupation [25].

The Freundlich Isotherm is given by:

$$q = kC_f^{1/n} \qquad \textbf{(Equation 3.3)}$$

Where ***q*** is the equilibrium metal uptake (mmol g^{-1}), C_f is the equilibrium solution concentration of the heavy metal (mmol L^{-1}), ***k*** (mmol g^{-1}) relates to the biosorption capacity and ***n*** is an empirical parameter that relates to the sorption intensity.

The linear form of this equation is:

$$\ln q = \ln k + \left(\frac{1}{n}\right) \ln C_{\mathrm{f}} \qquad \textbf{(Equation 3.4)}$$

A plot of $\ln q$ versus $\ln C_{\mathrm{f}}$ results in a straight line with a slope of $(1/n)$ and intercept of $\ln k$.

Similarly to the Langmuir Isotherm, the values of the Freundlich parameters can also be used to predict the affinity between the sorbent and sorbate [35]. A high value of n indicates that there is high affinity between sorbent and sorbate while a large k value indicates that the sorbent has a large metal uptake capacity.

3.1.5 Competition between metal ions

Multi-component adsorption systems are extremely complicated because of solute-surface interactions. In bimetallic combination, sorption of metals is a competitive process between ions in solution and those sorbed onto the biomass surface. Antagonistic interaction of the two metals may be due to the fact that different cations have different affinities to cell binding sites, therefore the effective binding sites available are reduced [36].

Due to the presence of the competitive metal ions, the uptake of the metal ions is generally negatively affected. Chen and Yang [36] found that simultaneous sorption of Pb (II) and Cu (II) lead to decreased uptake of both metals. It was shown that Pb (II) could form stronger complexes than Cu (II) and as a result the competitive effect from Pb (II) ions was more significant on Cu (II) binding than vice versa.

3.1.6 Objectives of the Research

The main objectives of the work in this chapter are:

- To investigate the effect of manipulation of experimental parameters such as pH, equilibrium time, ionic strength and competition between ions on the metal uptake.
- To compare the use of Langmuir and Freundlich Isotherms for describing the biosorption process.
- To define the optimum seaweed for metal uptake based on the calculation of Langmuir ($\boldsymbol{q}_{\mathbf{max}}$ and $\boldsymbol{b}$) and Freundlich (k and $\boldsymbol{n}$) parameters.

3.2 Experimental

3.2.1 Materials and Methods

3.2.1.1 Chemicals

- Sodium Hydroxide (solid) - Ridel de Haën, Germany.
- Hydrochloric Acid (37%) - LabScan Ltd., Dublin, Ireland.
- Analytical grade metal solutions (1000 mg L^{-1}) of Cu (II), Cr (III) and Cr (VI) as nitrate salts- Sigma-Aldrich Ltd., Dublin, Ireland.
- Buffers pH 4 (± 0.02) and 7 (± 0.02) - Ridel de Haën, Germany.
- NIST Standard Reference Material 1573a Tomato Leaves.
- BCR (certified reference material) No. 279 *Ulva lactuca* – LGC Promochem

3.2.1.2 Instrumentation

3.2.1.2.1 Atomic Absorption Spectrophotometer

Metal concentrations were measured using a VARIAN SpectrAA-600 atomic absorption spectrophotometer with SpectrAA software 4.10 (Figure 3.3) using the parameters specified in Table 3.2

Figure 3.3 Varian SpectrAA 600 Atomic Absorption Spectrophotometer (Flame Mode).

Table 3.2 Operating parameters for metal analysis using Varian SpectrAA 600 AAS.

	Cu (II)	Cr (III) and Cr (VI)
Flame Type	Air/acetylene	Air/acetylene
Wavelength	324.8 nm	357.9nm
Slit Width	0.5nm	0.2nm
Background correction	Off	Off
Standards	0, 1, 5, 10 and 20 mg L^{-1}	0, 1, 5, 10 and 20 mg L^{-1}
Certified Reference Material	BCR CRM No. 279 *Ulva lactuca*	NIST Standard Reference Material 1573a Tomato Leaves

3.2.2 Optimum pH Determination

Working solutions were prepared by appropriate dilution of the metal standards with distilled water. In order to investigate the effect of pH on Cu (II) sorption, 50 mg L^{-1} solutions of various initial pH values were prepared using 0.1M NaOH or 0.1M HCl. 100mg of biomass was added to 100 mL conical flasks containing 50mL of Cu (II) solution at the required pH. Flasks were shaken for 6 h at 200rpm at room temperature (21±1°C). Solutions were unbuffered but pH was monitored periodically, and small amounts of HCl and NaOH were added as necessary in order to keep solution pH constant. The equilibrium metal uptake $\boldsymbol{q}$ (mmol g^{-1}) was calculated from the metallic ion concentration in the solution according to Equation 3.5 [13].

$$q = \frac{V.(C_i - C_f)}{1000.m_s} \qquad \textbf{(Equation 3.5)}$$

Where V is the volume of the copper solution (mL), $\boldsymbol{C_i}$ and $\boldsymbol{C_f}$ are the initial and equilibrium concentration of copper in solution (mmol L^{-1}) respectively and m_s is the mass of the algae (g). Calcium release upon Cu (II) binding was also measured for the six

seaweeds. Error bars were calculated based on triplicate runs with 95% confidence intervals. Distilled water blanks were run between each sample to ensure that there was no carryover effect in the flame with metal-free and biomass-free blanks used as controls. Solution pH was monitored over the course of the experiment and was controlled by the addition of small amounts of either 0.1M HCl or NaOH as appropriate. Triplicate samples were run in all cases.

3.2.3 Determination of Equilibrium Binding Time

In the equilibrium experiments the pH was maintained at the optimum pH for each of the seaweeds as determined in pH trials (Section 3.2.2). The biomass (100mg) was added to 50mL of a 50mg L^{-1} Cu (II) solution adjusted to the appropriate pH (pH 5 for Cu (II), pH 4.5 for Cr (III) and pH 2 for Cr (VI)). Flasks were shaken at 200rpm and room temperature (21±1°C). Samples were taken at periodic time intervals and analysed via AAS. The equilibrium metal uptake $\boldsymbol{q}$ (mmol g^{-1}) was calculated according to Equation 3.5. Solution pH was monitored over the course of the experiment and was controlled by the addition of small amounts of either 0.1M HCl or NaOH as appropriate. Triplicate samples were run in all cases.

3.2.4 Ionic Strength Effects

100 mg of biomass was exposed to 50 mL of the metal solution at low (0mM), medium (1 and 10 mM) and high (50 and 100 mM) ionic strength, adjusted to the optimum pH as above. Metal solutions containing 0, 1, 10, 50 and 100 mM $NaNO_3$ were prepared with pH adjustments made using 0.1 M HCl and 0.1 M NaOH. Nitrate was chosen as the anion because of its low tendency for complex formation with most metals [37]. Flasks were shaken for 4h at room temperature (21±1°C) and 200rpm. The samples were then filtered under vacuum and analysed via AAS. The equilibrium metal uptake $\boldsymbol{q}$ (mmol g^{-1}) was calculated according to Equation 3.5. Solution pH was monitored over the course of the experiment and was controlled by the addition of small amounts of either 0.1M HCl or NaOH as appropriate. Triplicate samples were run in all cases.

3.2.5 Adsorption Isotherms

A volume of 50mL of metal solutions of several concentrations (5, 10, 20, 50, 75, 100, 150, 200 and 250 mg L^{-1}) prepared by dilution of the 1000 mg L^{-1} metal stock, were placed in 100 mL conical flask and adjusted to the appropriate pH using 0.1 M HCl and 0.1 M NaOH as appropriate. 100 mg of biomass was placed in each flask and the flasks were shaken at room temperature (21 ± 1 °C) and 200rpm for 4h. The algal biomass was then filtered under vacuum and after appropriate dilution the metal uptake was measured using AAS. Triplicate analyses were carried out in all cases. The equilibrium metal uptake $\boldsymbol{q}$ (mmol g^{-1}) was calculated according to Equation 3.5. Solution pH was monitored over the course of the experiment and was controlled by the addition of small amounts of either 0.1M HCl or NaOH as appropriate. Triplicate samples were run in all cases.

3.2.6 Competitive Binding Studies

100mg of biomass (*Fucus vesiculosus*) was added to 50mL of solution containing Cu (II) and Cr (III) at various concentrations [36]. In each experiment, the initial concentration of one heavy metal ion was fixed while that of the other one was varied. The initial fixed metal concentration was 40 mg L^{-1} while the concentration of the remaining metal was varied in the region of 5-150 mg L^{-1}. The solutions were adjusted to pH 4.5 using 0.1M HCl and 0.1M NaOH. Samples were shaken at 200rpm and room temperature (21±1°C) for 4h. Samples were then filtered under vacuum and the filtrate (after appropriate dilution) was analysed via AAS. Solution pH was monitored over the course of the experiment and was controlled by the addition of small amounts of either 0.1M HCl or NaOH as appropriate. The equilibrium metal uptake $\boldsymbol{q}$ (mmol g^{-1}) was calculated according to Equation 3.5. Triplicate samples were run in all cases.

3.3 Results & Discussion

3.3.1 Optimum pH Determination

3.3.1.1 Cu (II)

Figure 3.4 illustrates the relationship between Cu (II) uptake and solution pH for the six seaweed species under investigation. The formation of soluble Cu $(OH)^{+}$ and $Cu_2(OH)_2^{2+}$ has been shown to occur at pH values of pH 5.2-6 [14] while Kratochvil and Volesky [6] reported that most heavy metals tend to precipitate out at pH > 5.5. In this study, precipitation of insoluble copper hydroxide at pH values greater than 6 was observed and thus, a pH range from pH 2-6 was selected as a suitable experimental range.

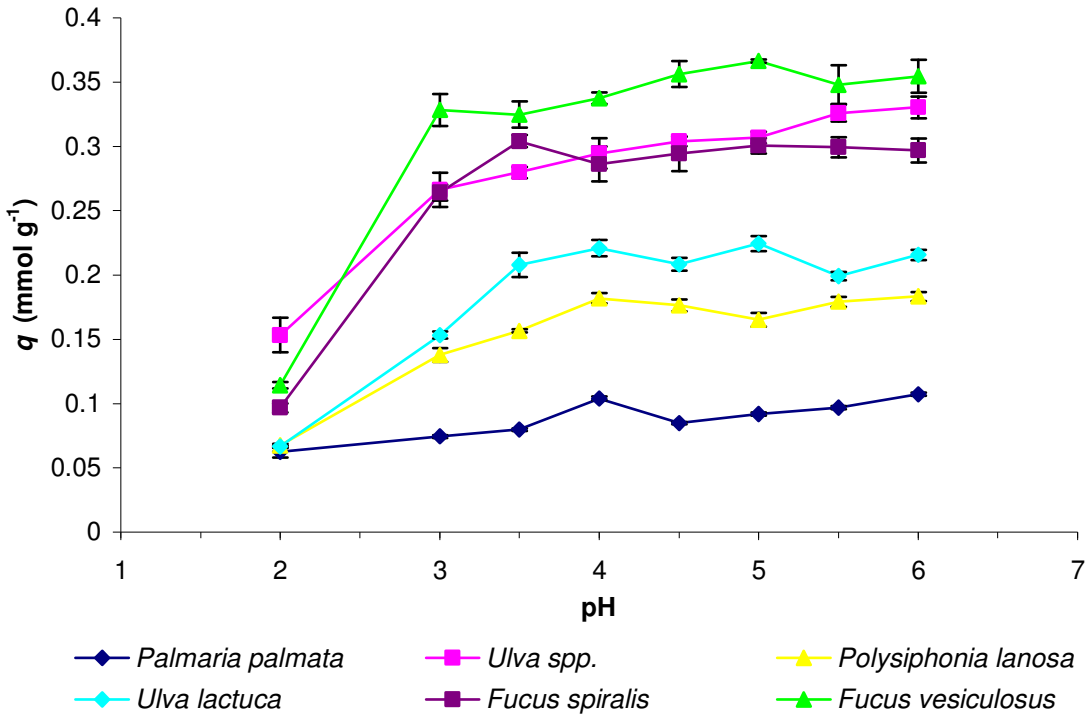

Figure 3.4 Optimum pH determination for Cu (II) sorption. Initial Cu (II) ion concentration = 50mg L^{-1}, concentration of biomass = 2mg mL^{-1}, Equilibration Time = 360 minutes. Error bars are calculated based on triplicate runs with 95% Confidence Intervals.

It can be seen from Figure 3.4, that, higher pH values generally led to higher metal uptake. The uptake capacities of the six seaweeds generally demonstrated a similar trend where an increase was distinctly seen in the lower pH range (from pH 2 to 3) but this effect was seen to level off at higher pH.

At low pH, the positively charged hydrogen ions may compete with metal ions for binding ligands on the cell wall and this effectively leads to fewer sites being available to bind metal ions. As the pH increases there are fewer H^+ ions in solution resulting in less competition for binding sites. As a consequence more ligands are freed up thus leading to enhanced biosorption.

At pH 2 the metal uptake is low but not negligible which may be as a consequence of the presence of sulphonate groups on the seaweed surface. Sulphonate groups have a pK_a value of about 1-2.5, are therefore dissociated at lower pH values and can only contribute to metal binding at low pH values [14].

It was shown in Chapter 2 that *Ulva lactuca*, *Polysiphonia lanosa* and *Palmaria palmata* contained an equal number of strongly acidic groups (0.19 ± 0.03, ± 0.06 and ± 0.01 mmol g^{-1} respectively). Figure 3.4 shows that each of these seaweeds binds approximately 0.07 mmol g^{-1} (± 0.07, ± 0.04 and ± 0.01) of Cu (II) at pH 2. Similarities in initial uptake reflect the similarity in the number of binding sites obtained in titration work. At pH 2 *Ulva* spp. showed the greatest metal uptake with approximately 0.15 (± 0.1) mmol Cu (II) bound per gram biomass. By contrast *Fucus vesiculosus* bound only 0.11 (± 0.02) mmol g^{-1} Cu (II). Although both *Ulva* spp. and *Fucus vesiculosus* contain the same number of strong acidic groups, these groups may not have been available in *Fucus vesiculosus*. Titration results predicted that *Fucus spiralis* possessed only 0.31 (± 0.08) mmol g^{-1} of strongly acidic groups and as a result, Cu (II) uptake at pH 2 was lower than that of either *Ulva* spp. or *Fucus vesiculosus*.

At pH 3.5-5 carboxyl groups on the seaweed generate an increasingly negatively charged surface and electrostatic interactions between cationic species and this surface can be responsible for increased metal biosorption seen in this pH range. As a result, in subsequent experiments the pH was maintained at a value of pH 5. Although Cu (II) sorption generally reached a plateau above pH 3.5, this value of pH 5 was chosen to ensure that complete dissociation of carboxyl groups had taken place.

Although *Fucus vesiculosus* had the highest overall Cu (II) uptake (0.37 ± 0.01 mmol g^{-1}) at pH 5, *Ulva* spp. also performed extremely efficiently in sequestering Cu (II) (0.33 ± 0.02 mmol g^{-1}). The high binding capacity of non-living *Ulva* spp. has not previously been investigated, but Dodson and Aronson [38] found that specific fractions of *Ulva* (formerly *Enteromorpha* as classified by Hayden *et al*. [39]) were high in uronic acid content. This may account for the increased metal uptake observed for *Ulva* spp. in this study.

In this study, *Ulva* spp. are plentiful in the geographic location of this study relative to some of the other seaweeds. The abundance of these species as well as their increased Cu (II) uptake points to their potential usage as a biosorbent. It is therefore proposed that *Ulva* spp. warrants further study as potential biosorption products for heavy metal removal.

Figure 3.5 illustrates the relationship between Cu (II) uptake at equilibrium and the quantity of acidic sites as observed from a 50 mg L^{-1} Cu (II) solution. Each point on the x-axis represents the number of total acidic groups as determined by titration for each seaweed species (Table 2.1).

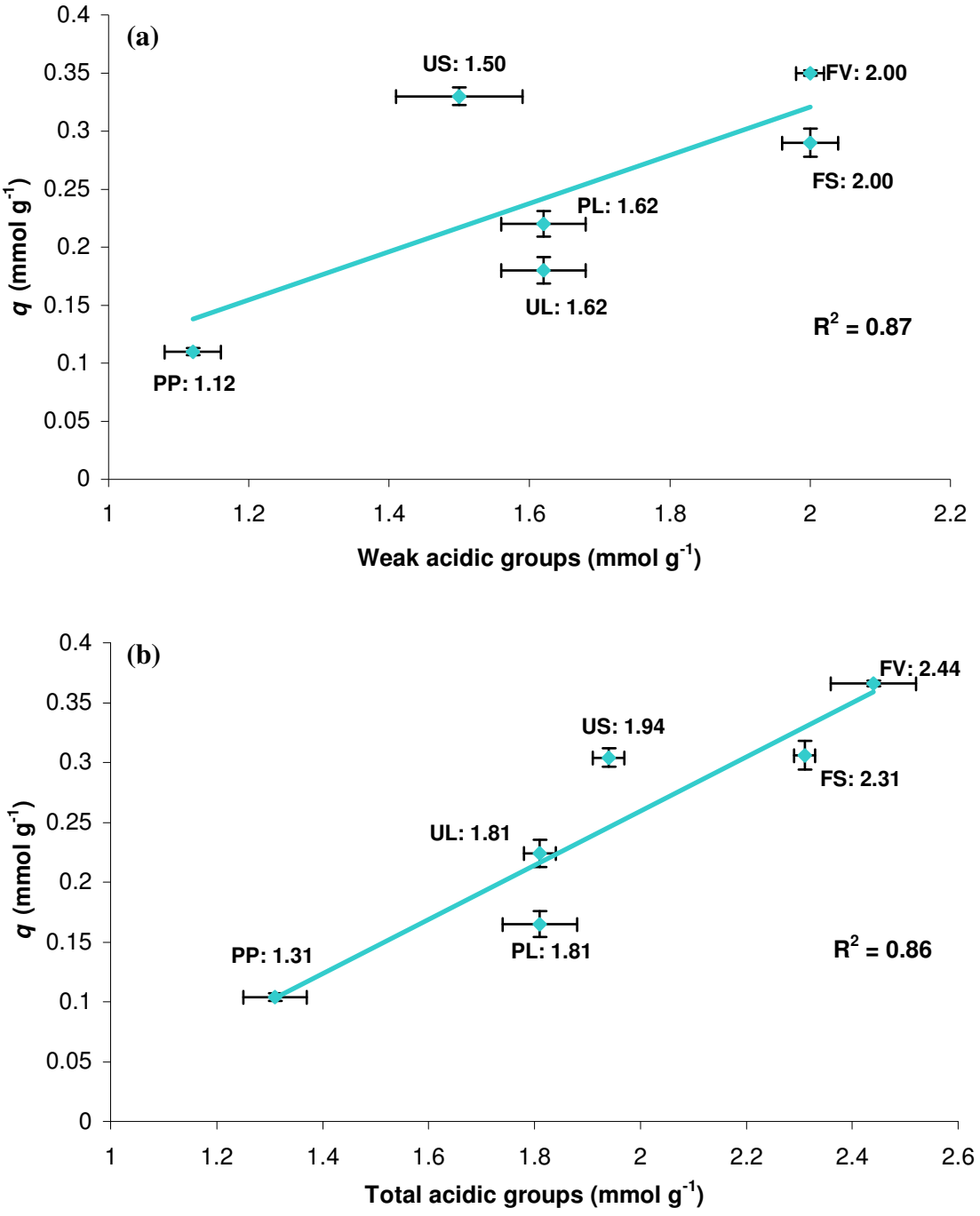

Figure 3.5 **Relationship between Cu (II) bound at equilibrium and (a) weak acidic groups and (b) total acidic groups. (FS: *Fucus spiralis*, FV: *Fucus vesiculosus*, PP: *Palmaria palmata*, PL: *Polysiphonia lanosa*, UL: *Ulva lactuca*, US: *Ulva* spp.). Errors bars are calculated based on triplicate runs with 95% Confidence Intervals. Initial Cu (II) ion concentration = 50mg L^{-1}, Biomass concentration = 2mg mL^{-1}, pH = 5.**

Regression analysis of metal uptake on acidic groups was carried out for both weak and total acidities using SPSS 14.0 Statistical Software with Equation 3.6 (a) and (b) obtained.

$$\text{Metal uptake} = -0.244 + 0.594 \text{ (weak acidic groups)} \quad \textbf{(Equation 3.6 a)}$$

$$\text{Metal uptake} = -0.193 + 0.226 \text{ (total acidic groups)} \quad \textbf{(Equation 3.6 b)}$$

Correlation between the maximum Cu (II) sorbed and the total number of acidic binding sites available on the seaweed surface was found ($r^2 = 0.86$) with an r^2 value of 0.87 when the weak acidic groups alone were considered. The standard *t*-test on the coefficient of acidic groups had P values of 0.006 and 0.007 respectively for weak and total acidities. This implies that it is highly unlikely that the true coefficient is zero. Therefore, it appears that metal uptake is almost certainly positively related to the number of sites. The *t*-test takes into account the sample size (n=6). Thus, even allowing for the small sample size, the relationship seems to be established.

Various authors have reported an ion-exchange mechanism for divalent cation binding to seaweeds [40-42]. For example, Kuyucak and Volesky [43] reported an enhanced release of ions (Ca^{2+}, K^{+}, Mg^{2+}, Na^{+}) from the alga *Ascophyllum nodosum* when reacted with a cobalt bearing aqueous solution rather than cobalt-free solution. Davis *et al*. [25] reported that, in cases where the non-treated marine alga *Sargassum* was reacted with a heavy metal solution, a pH increase and the release of light metal ions was observed. This also was explained in terms of ion-exchange, whereby the observed release of light metals balanced the uptake of protons and heavy metals.

In this study, the relationship between Cu^{2+} bound by the six seaweeds and the corresponding Ca^{2+} released at a was examined at various pH values. Figure 3.6 illustrates the Ca^{2+} released into solution upon Cu^{2+} binding to the six seaweeds.

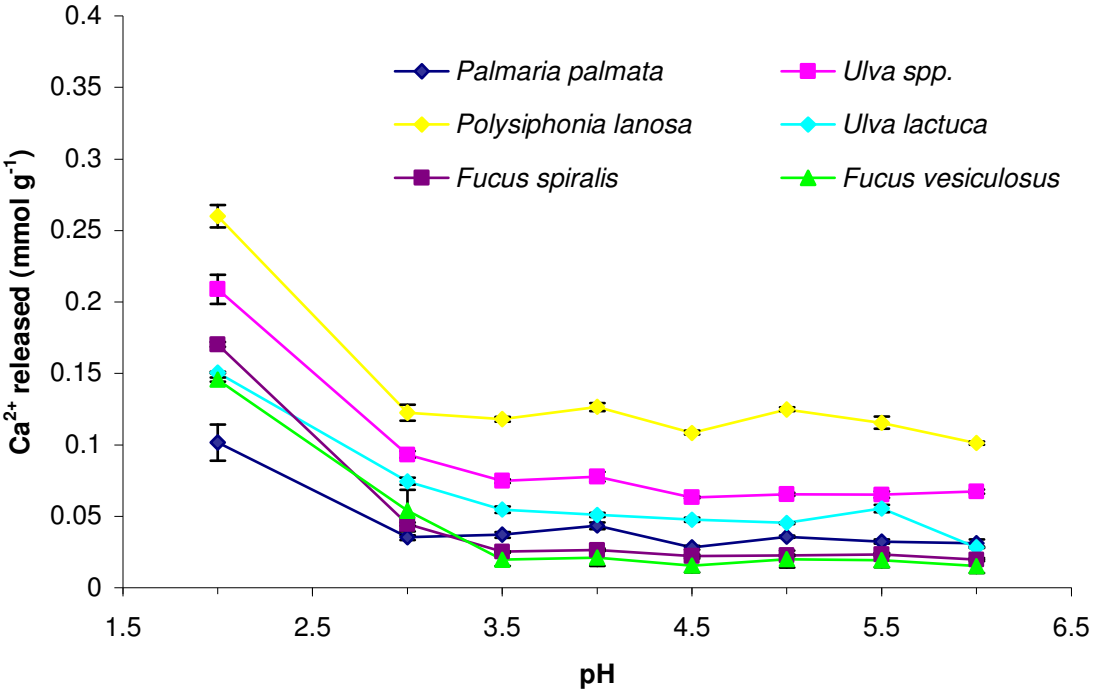

Figure 3.6 **Calcium release upon Cu (II) binding to six seaweeds. Errors bars are calculated based on triplicate runs with 95% Confidence Intervals. Initial Cu (II) concentration = 50mg L^{-1}, concentration of biomass= 2mg mL^{-1}.**

It is clearly seen from Figure 3.6 that calcium was released into solution from the biomass upon binding of Cu (II). As pH increased, calcium release decreased due to reduced numbers of protons in the metal solution. Table 3.3 compares the Ca (II) released and Cu (II) bound for the red seaweed *Palmaria palmata*.

Table 3.3 Calcium released from *Palmaria palmata* upon Cu (II) binding. Concentration of biomass = 2mg mL^{-1}, Initial Cu (II) concentration= 50 mg L^{-1}. Errors bars are calculated based on triplicate runs with 95% Confidence Intervals.

pH	Ca (II) released (mmol g^{-1})	Cu (II) bound (mmol g^{-1})
2	0.269 ± 0.007	0.063 ± 0.004
3	0.123 ± 0.005	0.074 ± 0.001
3.5	0.118 ± 0.001	0.079 ± 0.001
4	0.126 ± 0.003	0.104 ± 0.001
4.5	0.108 ± 0.001	0.084 ± 0.001
5	0.124 ± 0.002	0.091 ± 0.002
5.5	0.115 ± 0.004	0.097 ± 0.001
6	0.107 ± 0.001	0.101 ± 0.001

There is a discrepancy between the amounts of Ca (II) released and Cu (II) bound, the magnitude of which decreases with increasing pH. At low pH, a large amount of calcium is released but relatively lower amounts of copper are bound. This is due to the fact that, at low pH values, there is an abundance of protons in solution and metal cations must compete with these protons for binding sites on the biomass. As the pH increases, the number of protons in solution decreases and a general increase in the amount of Cu (II) bound is observed. Similar trends were observed for all seaweeds. The replacement of bound calcium with protons and Cu (II) ions therefore supports the theory of an ion-exchange mechanism for divalent metals.

3.3.1.2 Cr (III) and Cr (VI)

Figure 3.7 (a) and (b) illustrates the relationship between Cr (III) and Cr (VI) uptake and solution pH for the six seaweed species under investigation.

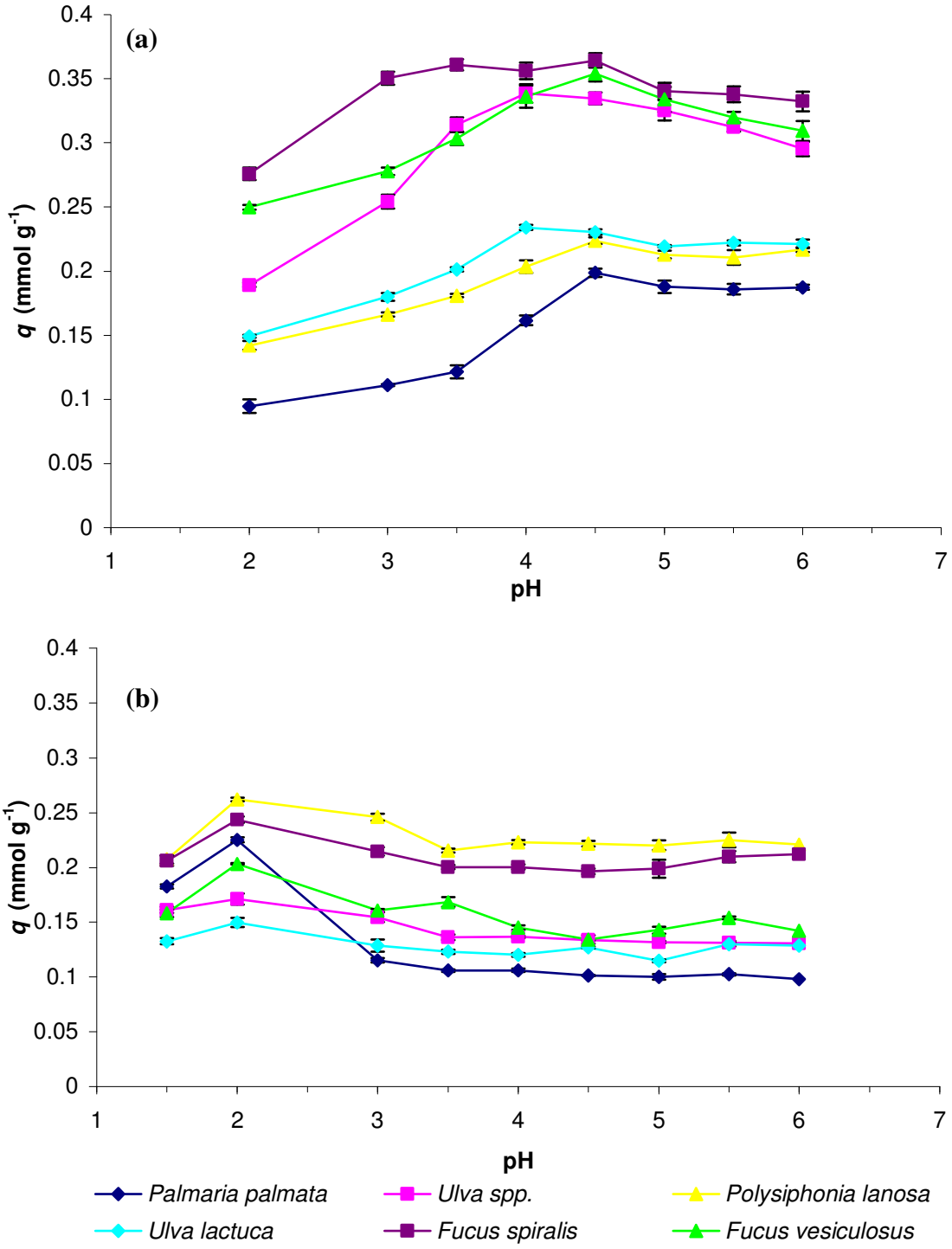

Figure 3.7 **Optimum pH determination for (a) Cr (III) and (b) Cr (VI) sorption. Initial Cu (II) ion concentration = 50mg L^{-1}, concentration of biomass = 2mg mL^{-1}, Equilibration Time = 360 minutes. Error bars are calculated based on triplicate runs with 95% Confidence Intervals.**

The pH dependence seen in Figure 3.7 has also been observed by various authors [14,23,36].

At pH 2, a decreased (relative to the higher experimental pH values) but not negligible Cr (III) uptake was observed for all seaweeds. In fact the amount of Cr (III) bound by *Fucus spiralis* at pH 2 is almost three times greater than the amount of Cu (II) bound by the same seaweed at that pH (Figure 3.4). For all species, Cr (III) uptake at pH 2 was greater than that observed for Cu (II). This is because sulphonate groups are dissociated at this pH and it has previously been postulated by Figueira *et al*. [2] that seaweed sulphonate groups are primarily responsible for the uptake of trivalent metal cations.

At pH values greater than pH 3.5, the biomass surface is more negatively charged due the dissociation of the sulphonate and carboxyl groups. This negative charge at increased pH means that while anionic chromate species are repelled by the biomass surface leading to decreased metal uptake, cationic Cr (III) experiences an attraction to the surface resulting in increased metal binding. However, the effect of biomass surface proteins on metal binding cannot be ignored as these proteins contain both amino and carboxyl groups. At low pH values, the amino groups are protonated thus making the surface more positive, and hence creating an electrostatic attraction between the anionic metal species such as those of Cr (VI) and the positively charged surface, while at higher pH values the carboxyl groups are dissociated making the surface more negative. For all seaweeds, an increase in pH resulted in an increase in Cr (III) uptake up to pH 4.5. However, a slight drop off in binding was observed above this pH. On the other hand, an increase in pH resulted in a general decrease in Cr (VI) uptake.

The optimum pH for Cr (III) sorption in this study was chosen as pH 4.5. At this pH, maximum metal uptake was achieved and metal precipitation was avoided. Yun *et al*. [44] showed that, at pH values greater than 5, chromium begins to precipitate as Cr $(OH)_3$.

Figure 3.8 illustrates chromium speciation depending on the solution pH as predicted from data by Haug and Smidsrød [45].

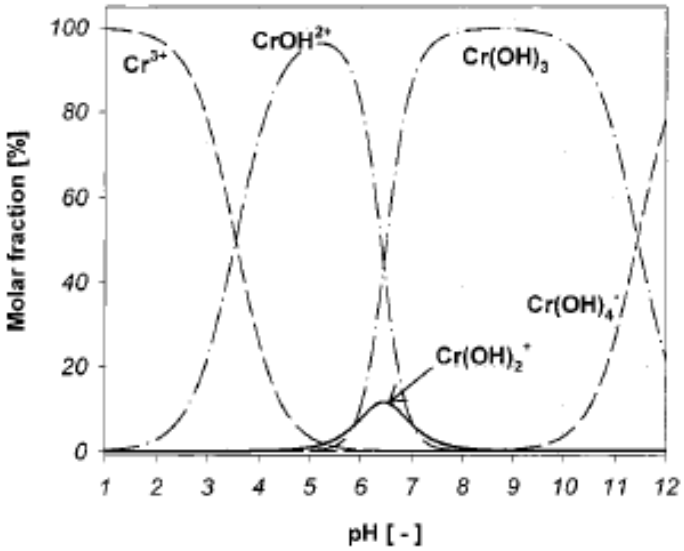

Figure 3.8 Chromium speciation depending on solution pH [44]. The curves were produced using the thermodynamic data reported in the literature [45].

In the pH range 1-5, Cr^{3+} and $CrOH^{2+}$ are the major species with $Cr(OH)_2^+$ found to be negligible [45].

In the experimental pH range (2-6), the speciation of chromium is expressed by Equation 3.7 [44]:

$$Cr^{3+} + H_2O \leftrightarrow CrOH^{2+} + H^+ \qquad \textbf{(Equation 3.7)}$$

$$K_s = \frac{[CrOH^{2+}][H^+]}{[Cr^{3+}]} = 10^{-3.55} \qquad \textbf{(Equation 3.8)}$$

Yun *et al*. [44] subsequently showed that at lower pH values (<3.5), $CrOH^{2+}$ binding remained at a level lower than that of Cr^{3+}. However, $CrOH^{2+}$ binding gradually increased with increasing pH, eventually exceeding the level of Cr^{3+} binding at pH > 4.5. The same authors [44] also determined from binding constants that the affinity of Cr^{3+} to the binding sites was likely to be much larger than that of $CrOH^{2+}$. This is possibly why a drop off in binding was observed above pH 4.5 in Figure 3.7 (a).

From Figure 3.7 (b), the optimum pH for Cr (VI) sorption was pH 2 with reduced uptake observed at pH values above and below this point. As solution pH increases, so too does the negative charge on the biomass. This increased negative charge repulses the anionic chromate species thus resulting in decreased Cr (VI) uptake at higher pH values.

According to the aquatic chemistry of chromium [46], Cr (VI) behaves as an oxy-anion in aqueous solution [47]. Therefore, it cannot be precipitated and also it may not bind to negatively charged common functional groups of biomass surfaces such as carboxyls, because of the respective charge repulsion.

Aqueous Cr (VI) may exist as five species in this system: H_2CrO_4, $HCrO_4^-$, CrO_4^{2-}, $Cr_2O_7^{2-}$ and $HCr_2O_7^-$ [48]. At lower pH values (pH 1-1.5), H_2CrO_4 is the dominant species. However, between pH 2 and 4, most Cr (VI) exists as $HCrO_4^-$ and $Cr_2O_7^{2-}$ [49,50] with their distribution dependent on the total Cr (VI) concentration in solution.

With the exception of the red seaweeds, the maximum equilibrium Cr (VI) uptake was lower than that of Cr (III). At pH 2, *Polysiphonia lanosa* showed the highest Cr (VI) uptake showing increased performance relative to its Cr (III) uptake. However, Cr (VI) binding was reduced by approximately 40-50% compared with Cr (III) binding for the green and brown seaweeds. At all pH values, the red seaweed *Polysiphonia lanosa* showed superior Cr (VI) uptake capacity over the other seaweeds studied.

This improved sorption performance of red seaweeds for hexavalent chromium has been observed by various authors [48,51,52]. Lee *et al*. [52] also suggested that red seaweeds have more cationic sites than brown seaweeds and thus have a relatively low affinity for

positively charged ions such as Cu^{2+} and Cr^{3+}. Instead, these cationic sites have a greater affinity for anionic species such as chromate thus resulting in increased anion uptake for red seaweeds.

The relationship between maximum chromium bound at equilibrium and quantity of acidic binding sites is illustrated in Fig. 3.9. Each point on the x-axis represents the total number of acidic binding sites (mmol g^{-1} biomass) as determined from potentiometric titration (Chapter 2).

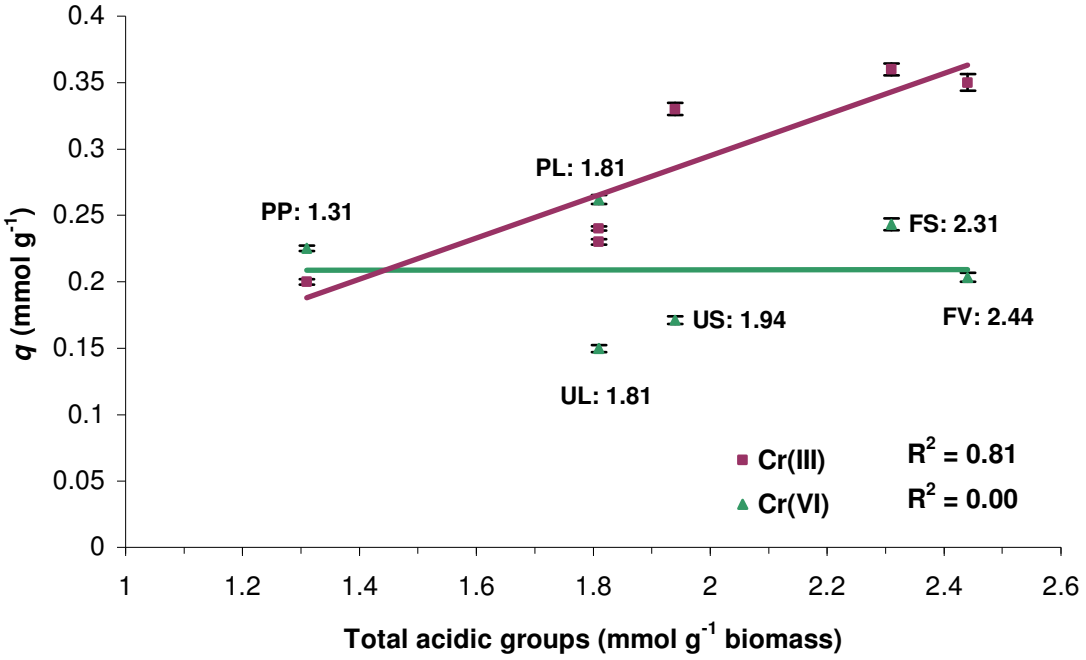

Figure 3.9 Relationship between maximum chromium bound at equilibrium and the total number of acidic groups. Errors bars are calculated based on triplicate runs with 95% Confidence Intervals. Initial metal concentration = 50 mg L^{-1}, concentration of biomass = 2 mg mL^{-1}, pH = 4.5 for Cr (III) and pH = 2 for Cr (VI).

Regression analyses of chromium uptake on total acidic groups were carried out as for Cu (II). Some correlation between the maximum Cr (III) sorbed at equilibrium and the total acidic binding sites was found (r^2 = 0.81). The standard *t*-test on the coefficient of total acidic groups had a P value of 0.01, indicating that it is highly unlikely that the true coefficient is zero. Therefore, it appears that, similarly to Cu (II), Cr (III) uptake is almost

certainly positively related to the total acidic groups. The *t*-test takes into account the sample size and thus, even allowing for the small sample size (n = 6 in this case), the relationship seems to be established.

However, for Cr (VI), the r^2 value was zero, indicating that there was no correlation between the maximum Cr (VI) bound at equilibrium and the total number of acidic groups on the seaweed. The standard *t*-test on the coefficient of total acidic groups had a P value of 0.99 indicating that it is almost certain that the true coefficient is zero and that Cr (VI) uptake by the seaweeds in question has no relationship to the number of acidic sites. The disparity in results indicates that, as expected, Cr (III) and Cr (VI) are bound to seaweed biomass by different mechanisms.

3.3.2 Determination of Equilibrium Binding Time

Equilibrium experiments were carried out at the optimum pH values (as determined in Section 3.3.1.1 and 3.3.1.2), where the maximum uptake capacity was achieved and metal precipitation was avoided. Figure 3.10 shows the results of the kinetic experiments conducted in order to determine the equilibrium binding time required for Cu (II), Cr (III) and Cr (VI) binding.

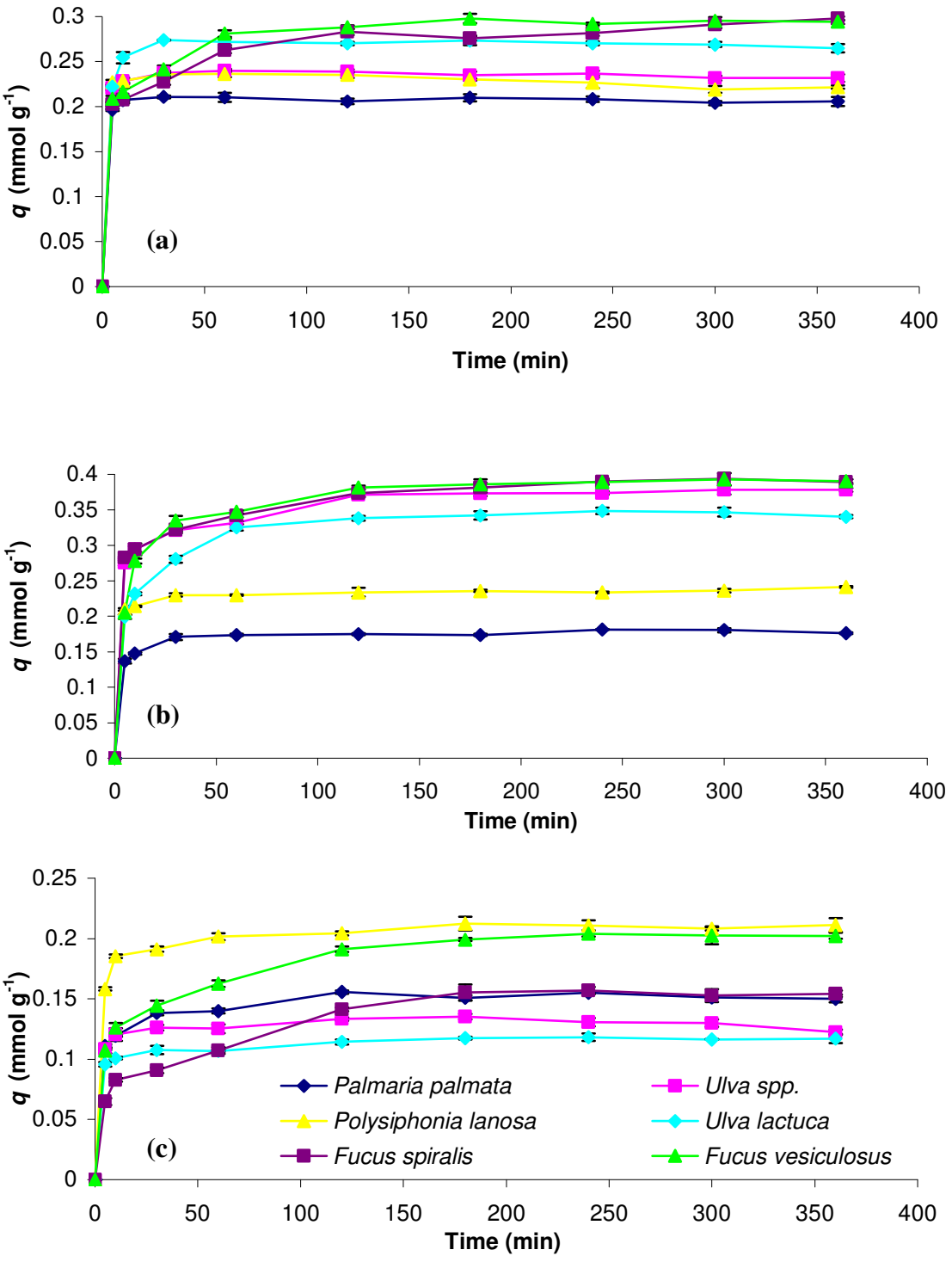

Figure 3.10 **Determination of equilibrium binding time for (a) Cu (II) (b) Cr (III) (c) Cr (VI) sorption. Errors bars are calculated based on triplicate runs with 95% Confidence Intervals. Initial metal ion concentration= 50mg L^{-1}, Biomass concentration= 2mg mL^{-1}, pH= (a) 5 (b) 4.5 (c) 2.**

Similar dynamic behaviour was observed for metal binding to the seaweeds with rapid initial sorption followed by a long period of much slower uptake. The equilibrium time needed for the different biomass-metal systems ranged from approximately 10 to 180 minutes with Cr (VI) binding requiring greater equilibrium times than either Cu (II) or Cr (III). This increased binding time for anionic Cr (VI) over cationic Cu (II) and Cr (III) therefore points to potential differences in binding mechanism between these metal ions.

Therefore, in subsequent experiments 4 hours was deemed more than sufficient to establish equilibrium. Table 3.4 summarises the equilibrium time required for metal uptake by the various seaweeds.

Table 3.4 Time required for sorption equilibrium in metal-biomass systems. Initial metal ion concentration = 50mg L^{-1}, biomass concentration =2mg mL^{-1}, pH=5, 4.5 and 2 for Cu (II), Cr (III) and Cr (VI) respectively.

	Equilibrium Time (min)		
	Cu (II)	**Cr (III)**	**Cr (VI)**
Fucus spiralis	60	120	180
Fucus vesiculosus	60	120	180
Ulva spp.	30	120	120
Ulva lactuca	30	60	120
Palmaria palmata	10	30	120
Polysiphonia lanosa	30	30	180

Various authors have also observed binding behaviour similar to that observed in this study. Khoo *et al.* [53] reported this two-stage behaviour for gold biosorption by immobilised biomass while Chen *et al.* [54] encountered the same patterns for conventional sorbents.

Rapid uptake of nickel by the alga *Chlorella vulgaris* within the first 10 minutes of contact has been reported by Aksu *et al.* [55] with equilibrium established in 30–60

minutes. In process applications, this rapid initial sorption is advantageous, since shorter contact time is required and allows for smaller equipment which in turn is beneficial for the operating cost of the process [16].

In their study on lead binding to modified *Laminaria japonica*, Luo *et al.* [23] proposed that the equilibrium behaviour observed could be due to the fact that, initially , all sites on the sorbent were vacant and the solute concentration was high. After that initial period, only a very small metal increase was observed possibly because there are a reduced number of active sites on the biomass. In other words, the initial time stages represent an increased concentration gradient between the sorbate in solution and sorbate on the biosorbent surface [32] which is reduced as time increases thus leading to a decrease in sorption rate at the later stages.

Increased equilibrium times for Cr (VI) sorption were also observed by Agarwal *et al*. [1] who reported times of 120, 150 and 180 min respectively for walnut shells, almond shells and tamarind seeds.

An issue relating to the dynamics of metal binding to seaweeds is whether or not the time taken to reach equilibrium is linked to the physical structure of the seaweed in terms of the number of acidic binding sites. Regression analysis was used to determine the relationship between the total number of acidic binding sites and equilibrium time required for the various metal ions. Figure 3.11 illustrates the relationship between the equilibrium binding time and the total number of acidic binding sites for Cu (II) binding.

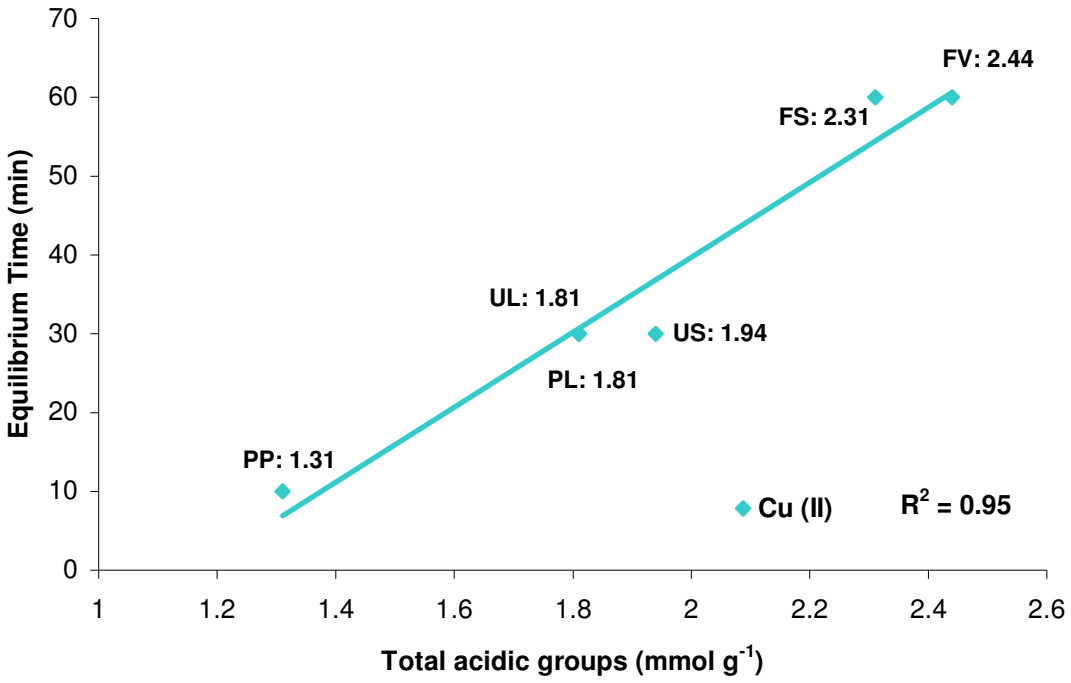

Figure 3.11 Relationship between equilibrium Cu (II) binding time and total acidic groups. Errors bars are calculated based on triplicate runs with 95% Confidence Intervals. Initial metal concentration = 50 mg L^{-1}, biomass concentration = 2 mg mL^{-1}, pH =5.

Results from this study indicated that there was strong correlation (r^2 = 0.95, P < 0.005) between the total number of acidic binding sites and the time taken to reach sorption equilibrium. The large number of binding sites in the brown seaweeds means that once initial sorption has taken place there may potentially be some steric hindrance of the surface functionalities resulting in the longer time required to reach sorption equilibrium.

Figure 3.12 illustrates the relationship between the equilibrium binding time and the number of acidic binding sites for Cr (III) and Cr (VI) binding.

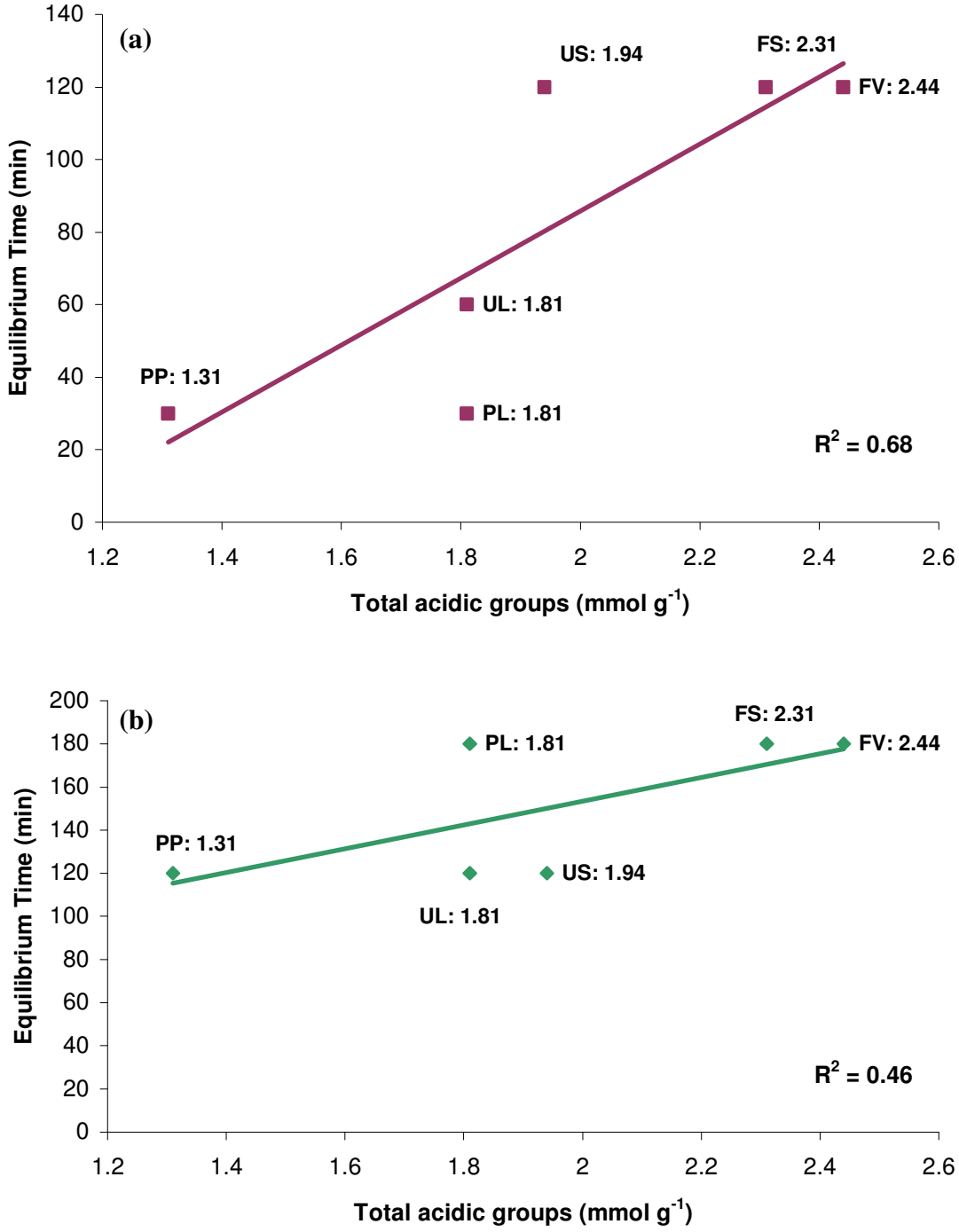

Figure 3.12 **Relationship between equilibrium (a) Cr (III) and (b) Cr (VI) equilibrium binding time and total acidic groups. Errors bars are calculated based on triplicate runs with 95% Confidence Intervals. Initial metal concentration = 50 mg L^{-1}, biomass concentration = 2 mg mL^{-1}, pH =4.5 and pH =2 for Cr (III) and Cr (VI) respectively.**

For both oxidation states some correlation was apparent between the number of binding sites and the time taken to reach equilibrium. For Cr (III) the r^2 value was 0.68 (P = 0.043) while an r^2 value of 0.46 (P = 0.059) was found for Cr (VI). The low P values (P < 0.06) found in both cases therefore indicate that is very likely that the true coefficient is not zero and that equilibrium binding time, for both Cr(III) and Cr(VI), is somewhat positively related to the total acidic groups on the biomass.

Correlation between binding sites and equilibrium time for Cr(VI) supports the binding mechanism as proposed by Park *et al*. [56] who showed that reduction of Cr (VI) by the biomass ultimately results in the formation of Cr (III) which possibly affects further Cr (VI) reduction and increases the equilibrium time required.

If anionic Cr (VI) were simply bound by cationic groups on the surface, then there should be no relationship between the number of anionic binding sites and the time required to reach equilibrium. This finding also supports their theory that once Cr (VI) has been reduced to Cr (III), the reduced species can then be bound by chromium-binding groups on the biomass.

The reduction mechanism for Cr (VI) binding differs from the ion exchange mechanism previously encountered for cation binding [25,57] and this disparity is evident in the equilibrium binding behaviour of the seaweeds and metals.

3.3.3 Effect of Ionic Strength

The effects of ionic strength on Cu (II), Cr (III) and Cr (VI) binding to the seaweeds in this study were examined. Figure 3.13 illustrates the effect of ionic strength on Cu (II) binding.

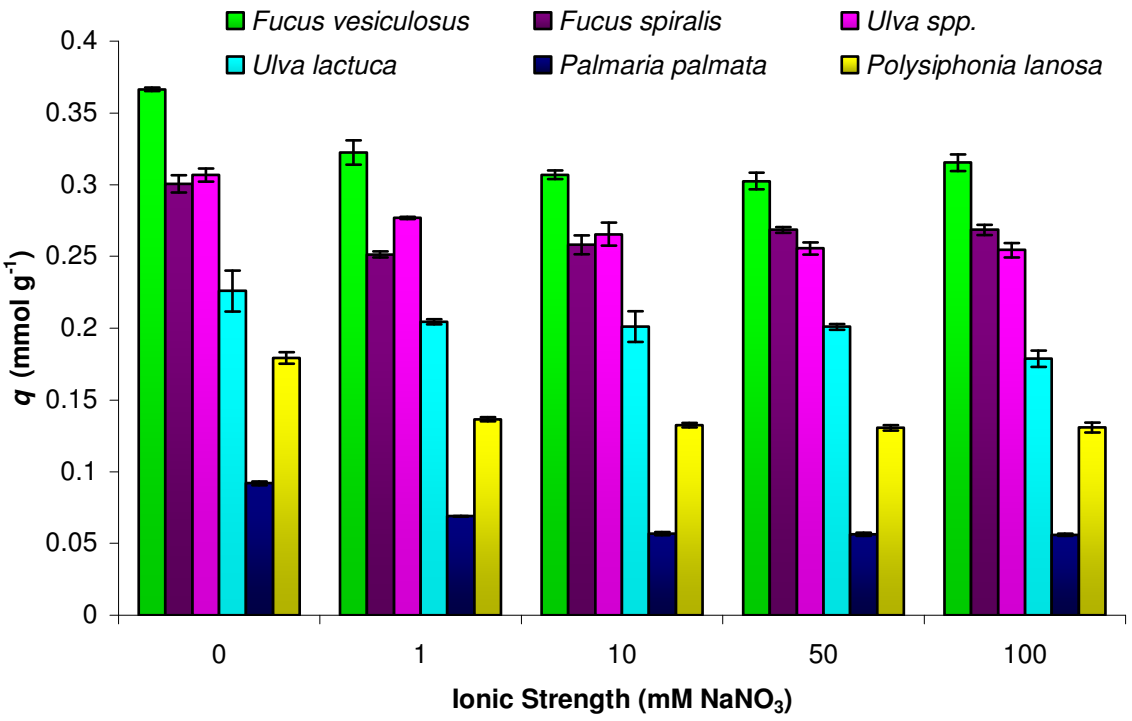

Figure 3.13 Effect of ionic strength on Cu (II) binding. Errors bars are calculated based on triplicate runs with 95% Confidence Intervals. Initial metal concentration = 50 mg L^{-1}, biomass concentration = 2 mg mL^{-1}, pH =5.

From Figure 3.13, it is seen that binding of Cu (II) was significantly reduced with increasing ionic strength. This is in agreement with the work of Tsui *et al*. [37] who found that binding of divalent metals (Cd (II), Co(II) ,Cu (II), Pb (II), Mn (II) ,Ni (II), Ag (II) and Zn (II)) to *Sargassum hemiphyllum* was reduced at high ionic strength. The effect of increasing ionic strength on Cr (III) and Cr (VI) binding is illustrated in Figure 3.14.

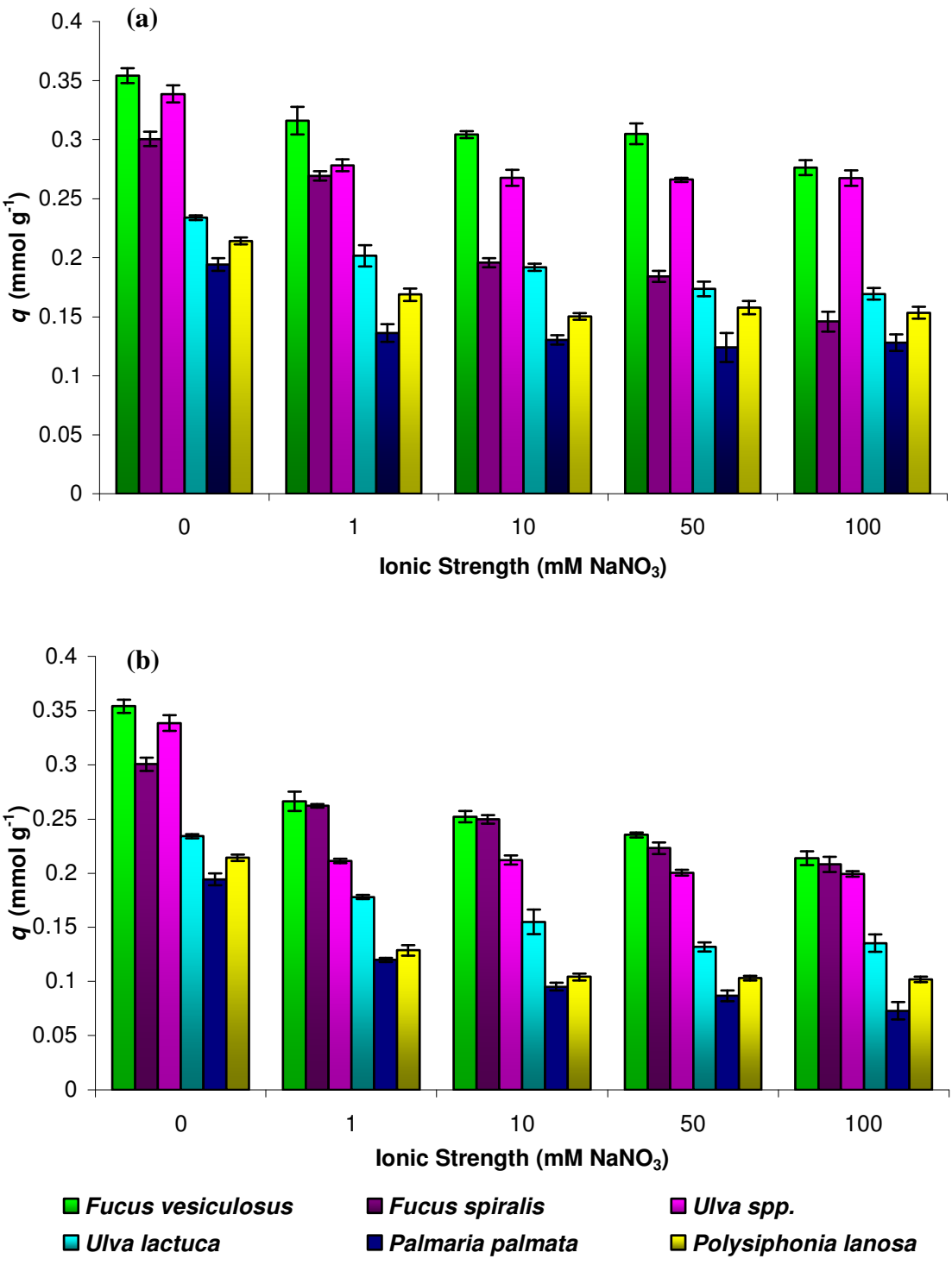

Figure 3.14 **Effect of ionic strength on Cr (III) and Cr (VI) binding. Errors bars are calculated based on triplicate runs with 95% Confidence Intervals. Initial metal concentration = 50 mg L^{-1}, biomass concentration = 2 mg mL^{-1}, pH =4.5 and 2 for Cr (III) and Cr (VI) respectively.**

Stumm and Morgan [58] reported that, because sodium is a typical hard ion, it will not be bound covalently and therefore does not compete directly with the covalent binding of heavy metals by the biosorbent. The effect of ionic strength can instead be explained as the result of competition of Na (I) with the heavy metals for electrostatic binding to the biomass [17,59]. Even heavy metals that form complexes are partially bound through electrostatic attraction and thus increased ionic strength will have some influence on their binding behaviour. Since deprotonated free carboxyl or sulphonate groups are negatively charged, they will electrostatically attract any cation [17], be it sodium, copper or any other heavy metal cation.

In the present study, increased ionic strength ($NaNO_3$) resulted in decreased metal binding for all metals under investigation, thus interfering with the electrostatic component of binding. According to the HSAB theory [60], hard ions such as Cr (III) and Cr (VI) bind mainly through electrostatic interactions as opposed to mostly covalent interactions for Cu (II). As a result it would be expected that increased ionic strength would have a greater impact on Cr (III) and Cr (VI) binding than on Cu (II) binding.

Table 3.4 summarises the relative percentage decreases in metal binding at increased ionic strength for the three metals. Average results from triplicate analyses are shown but error bars have been omitted for ease of interpretation.

Table 3.4 Changes in metal uptake capacity between at increased ionic strength. Initial metal concentration = 50 mg L^{-1}, biomass concentration = 2 mg mL^{-1}, pH=5, 4.5 and 2 for Cu (II), Cr (III) and Cr (VI) respectively. Average results from triplicate analyses are shown.

	Decrease in metal binding (%)					
	Cu (II)		Cr (III)		Cr (VI)	
	1 mM	100 mM	1 mM	100 mM	1 mM	100 mM
Fucus vesiculosus	12	14	11	22	25	40
Fucus spiralis	11	16	13	23	13	33
Ulva lactuca	9	17	13	26	26	43
***Ulva* spp.**	10	16	18	19	36	42
Palmaria palmata	24	29	28	41	42	63
Polysiphonia lanosa	23	27	19	38	42	52

In general, the decrease in metal uptake was lower for Cu (II) than for either Cr (III) or Cr (VI). This finding agrees with HSAB theory in that, if Cu (II) binds by mostly covalent interactions, the effect of increased ionic strength should have a lesser effect on metal uptake than ions that are primarily electrostatically bound such as Cr (III) and Cr (VI). However, because of the decrease in metal binding observed, the existence of some electrostatic binding for Cu (II) is also suggested.

Increases in ionic strength also increase the concentration of competitive anions in solution [56] which had an appreciable effect on Cr (VI) binding, again pointing to the significance of electrostatic binding of this ion. Work by Aksu and Balibek [61] on *Rhizopus arrhizus* produced similar results in that increasing ionic strength resulted in a decrease in Cr (VI) binding to the biomass.

For Cu (II), it is seen that there is little difference between the percentage decrease at medium (1mM $NaNO_3$) and high (100mM $NaNO_3$), thus possibly indicating near maximal interaction of Na^+ at a concentration of 1mM $NaNO_3$. However, for Cr (III) and Cr (VI), large differences in metal uptake were observed between medium and high ionic

strength, again showing that increased ionic strength has a greater effect on the electrostatic binding of these hard metals.

From Table 3.4, it is seen that, in general, increased ionic strength had the greatest effect on metal binding to the red seaweeds. This result may relate to the work of Lee *et al*. [52], where it was postulated that, because of their increased Cr (VI) uptake relative to the brown and green seaweeds, the red seaweeds may have more cationic sites on their surface. If this is the case, the presence of additional anions (NO_3^-) at increased ionic strength may result in increased competition between NO_3^- ions and Cr (VI) for cationic sites on the biomass.

3.3.4 Adsorption Isotherms

3.3.4.1 Experimental Isotherms

Data for the Langmuir and Freundlich isotherm models are obtained from experimental isotherm plots of metal uptake (***q***) against residual metal concentration (C_f). These raw data plots for Cu (II), Cr (III) and Cr (VI) are illustrated in Figures 3.15 and 3.16.

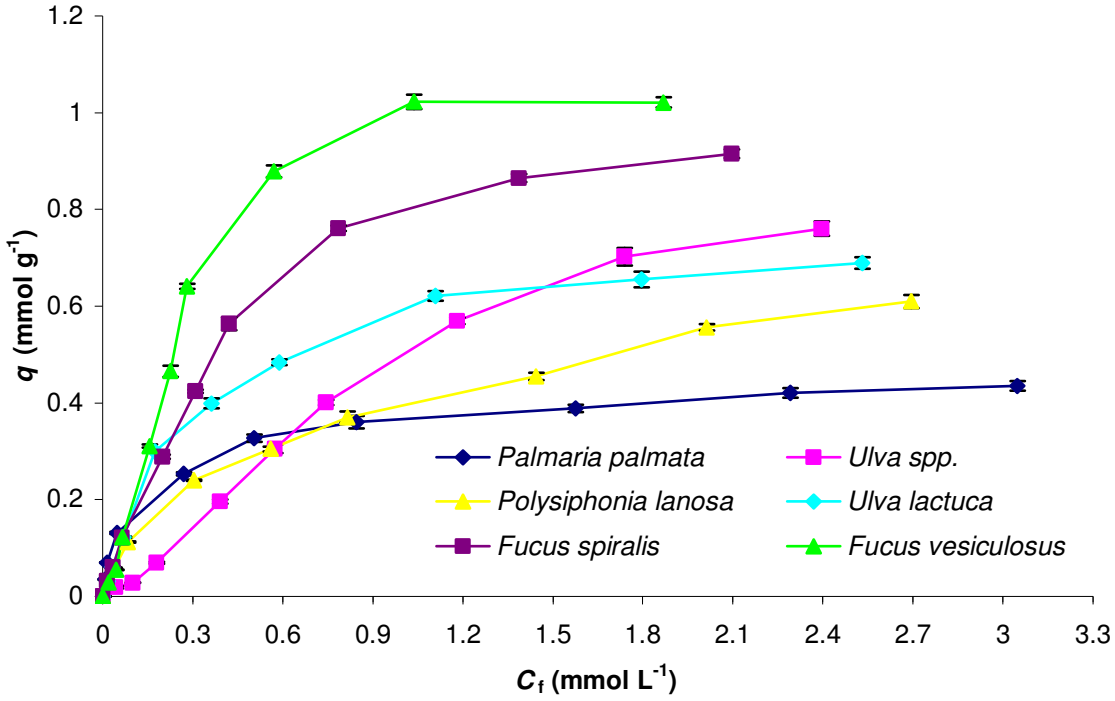

Figure 3.15 Experimental isotherm data of Cu (II) sorption for all seaweed species. Concentration of biomass=2mg mL^{-1}, pH=5, Equilibration time= 240 min. Error bars are calculated based on triplicate runs with 95% Confidence Intervals.

At increased residual concentrations (> 1.8 mmol L^{-1}), experimental data shows that *Fucus vesiculosus* had the largest equilibrium metal uptake (***q***), while below a residual concentration of approximately 0.10 mmol L^{-1}, *Palmaria palmata* displayed the largest equilibrium uptake of the seaweeds. The implications of these findings are later discussed in relation to the isotherm models.

Figure 3.16 (a) and (b) shows the experimental isotherm plots for respective Cr (III) and Cr (VI) uptake by the six seaweeds.

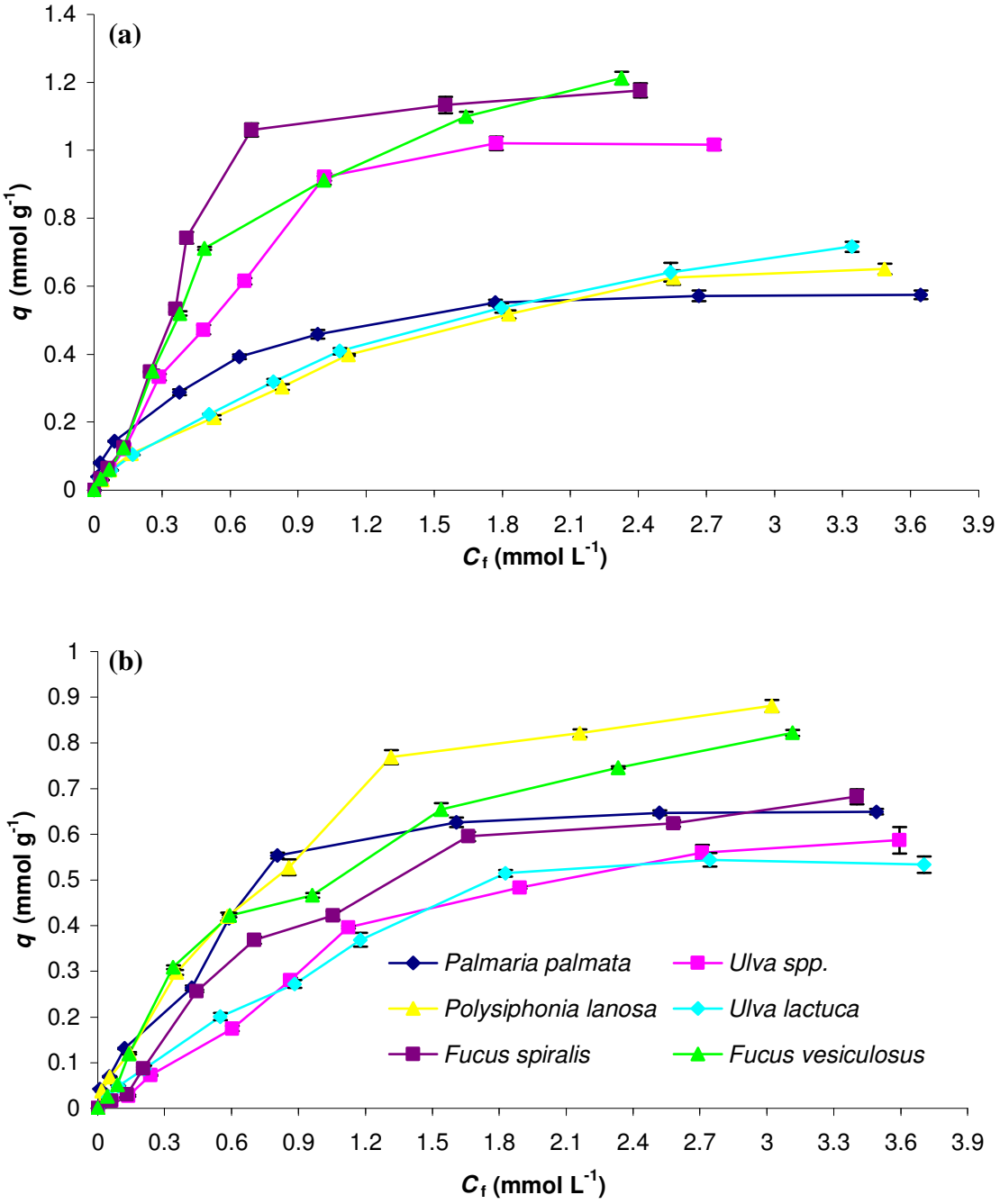

Figure 3.16 Experimental isotherm data for (a) Cr (III) & (b) Cr (VI) sorption Biomass concentration= 2mg mL^{-1}, pH=4.5 and pH 2 respectively, Equilibration time 240 min. Error bars are calculated based on triplicate runs with 95% Confidence Intervals.

Similarly, to Cu (II) binding, at high residual Cr (III) concentrations (> 2.1 mmol L^{-1}), *Fucus vesiculosus* displayed the highest ***q*** value. On the other hand, below residual concentrations of 0.15 mmol L^{-1} Cr (III), *Palmaria palmata* had the largest ***q*** value.

By contrast to Cu (II) and Cr (III), it was *Polysiphonia lanosa* that revealed the largest equilibrium Cr (VI) uptake (***q***) at high residual metal concentrations (> 2.7 mmol L^{-1}). Again, it was *Palmaria palmata* that displayed the largest uptake at low residual concentrations (<0.15 mmol L^{-1}). However, this seaweed also displayed the largest uptake at a residual concentration of 0.75 mmol L^{-1}.

Before carrying out isotherm analysis, another quantity known as the removal efficiency may be calculated. The removal efficiency (RE) of the seaweed on the metal in solution may be determined according to Equation 3.9 [37].

$$RE = \frac{(C_i - C_f)}{C_i} X \quad 100\% \qquad \textbf{(Equation 3.9)}$$

Where $\boldsymbol{C_i}$ and $\boldsymbol{C_f}$ are the initial and equilibrium metal solution concentrations (mmol L^{-1}).

Removal efficiencies (RE) were calculated using experimental isotherm data from Figures 3.15 and 3.16. However, while these plots show metal uptake at various residual concentrations, RE curves predict removal efficiency at a variety of initial metal concentrations.

Figure 3.17 (a) illustrates the RE curves obtained for Cu (II) removal with curve fitting to the red seaweeds shown in Figure 3.17 (b).

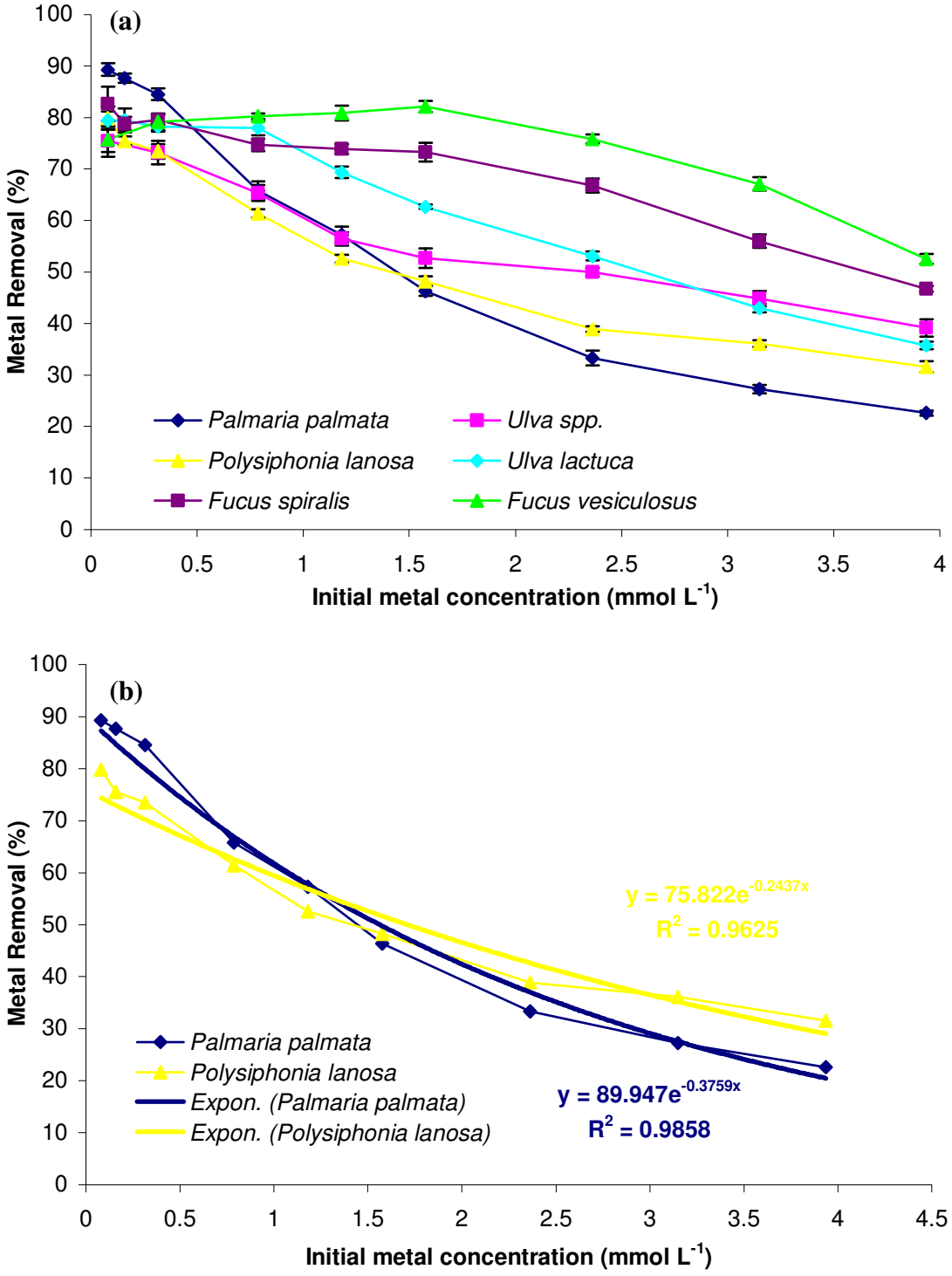

Figure 3.17 **(a) Cu (II) removal efficiency curves (b) Exponential curve fitting to Cu (II) RE data for the red seaweeds. Biomass concentration= 2 mg mL^{-1}, pH= 5. Average values from triplicate analyses are shown. Error bars calculated to 95% Confidence Intervals.**

From Figure 3.17a, it is clearly seen that an increase in the metal/biomass ratio caused a decrease in removal efficiency. As C_i increased, the removal efficiency decreased exponentially (r^2 ranging from 0.62 to 0.99) with the red seaweeds found to best fit the exponential curve. The negative decay constant in the exponential decay equation (Figure 3.17b) represents the magnitude of decrease in removal efficiency with the initial metal concentration. Similar type plots were obtained for Cr (III) and Cr (VI) binding.

Table 3.5 summarises the removal efficiency of the various seaweed metal combinations at their highest and lowest initial metal concentrations.

Table 3.5 Removal efficiency for Cu (II), Cr (III) and Cr (VI) binding to six seaweeds. Error bars are calculated based on triplicate analyses with 95% Confidence Intervals.

	Cu (II) (%)		**Cr (III) (%)**		**Cr (VI) (%)**	
	***C*i (mmol L^{-1})**		***C*i (mmol L^{-1})**		***C*i (mmol L^{-1})**	
	0.08	**3.93**	**0.09**	**3.84**	**0.09**	**3.84**
Fucus vesiculosus	76 ± 3	53 ± 1	74 ± 1	50 ± 2	76 ± 3	39 ± 1
Fucus spiralis	83 ± 3	47 ± 1	70 ± 3	43 ± 2	56 ± 3	35 ± 1
Ulva lactuca	79 ± 2	36 ± 1	73 ± 1	30 ± 1	50 ± 3	23 ± 1
***Ulva* spp.**	75 ± 3	39 ± 2	71 ± 1	43 ± 2	45 ± 1	25 ± 1
Palmaria palmata	89 ± 1	22 ± 1	87 ± 1	24 ± 1	91 ± 2	28 ± 1
Polysiphonia lanosa	79 ± 2	31 ± 1	63 ± 2	27 ± 1	81 ± 2	37 ± 2

From Table 3, it is clear that, at low initial metal concentrations (0.08-0.09 mmol L^{-1}), *Palmaria palmata* displayed the greatest removal efficiency for all three metals. However, as expected, its removal efficiency at higher metal concentrations was significantly decreased.

The brown seaweeds revealed the greatest removal efficiency at high initial metal concentrations (3.93 and 3.84 mmol L^{-1}) for Cu (II) and Cr (III) binding. However, for Cr

(VI) binding, the removal efficiency of *Fucus vesiculosus* and *Polysiphonia lanosa* were identical (within experimental error).

The results obtained in the removal efficiency plots may be explained by an increase in the number of metal ions competing for the available binding sites in the biomass at higher concentration levels. The relative reduction in cation removal efficiency at high ***C*i** values correlates with the quantity of acidic binding sites determined in potentiometric titration (Table 2.1), thus indicating that the availability of sites on the surface influences the removal efficiency e.g. *Fucus vesiculosus* was shown to have the highest number of acidic surface binding sites (2.44 ± 0.22 mmol g^{-1}), while *Palmaria palmata* had the least (1.31 ± 0.16 mmol g^{-1}). Their respective Cu (II) and Cr (III) removal efficiencies at high ***C*i** were 53% and 50% for *Fucus vesiculosus* and 22% and 24% for *Palmaria palmata*.

On the other hand, at low initial metal concentrations, the number of available binding sites on the biomass surface is high (relative to the metal concentration) and hence metal uptake was very efficient.

3.3.4.2 Adsorption Isotherm Models

For ease of manipulation, the q vs. C_f relationship was mathematically expressed by the linearised Langmuir and Freundlich models using data from experimental plots (Figures 3.15 and 3.16). Trendlines were fitted to the data using least squares regression.

3.3.4.2.1 Langmuir Isotherm

As previously discussed, the Langmuir Isotherm has traditionally been widely used to quantify and contrast the performance of different biosorbents [25]. This is due to the fact that it contains two parameters that are useful and easily interpretable [27]. The parameter q_{max} is the maximum metal uptake under the given conditions (mmol g^{-1}) and b is a coefficient related to the affinity between the sorbent and sorbate. These values may be determined by plotting experimental isotherm data.

Experimental isotherm data was plotted according to linear form of Langmuir Equation (Equation 3.2). Linearised Langmuir plots of Cu (II), Cr (III) and Cr (VI) binding to the seaweeds are given in Figure 3.18.

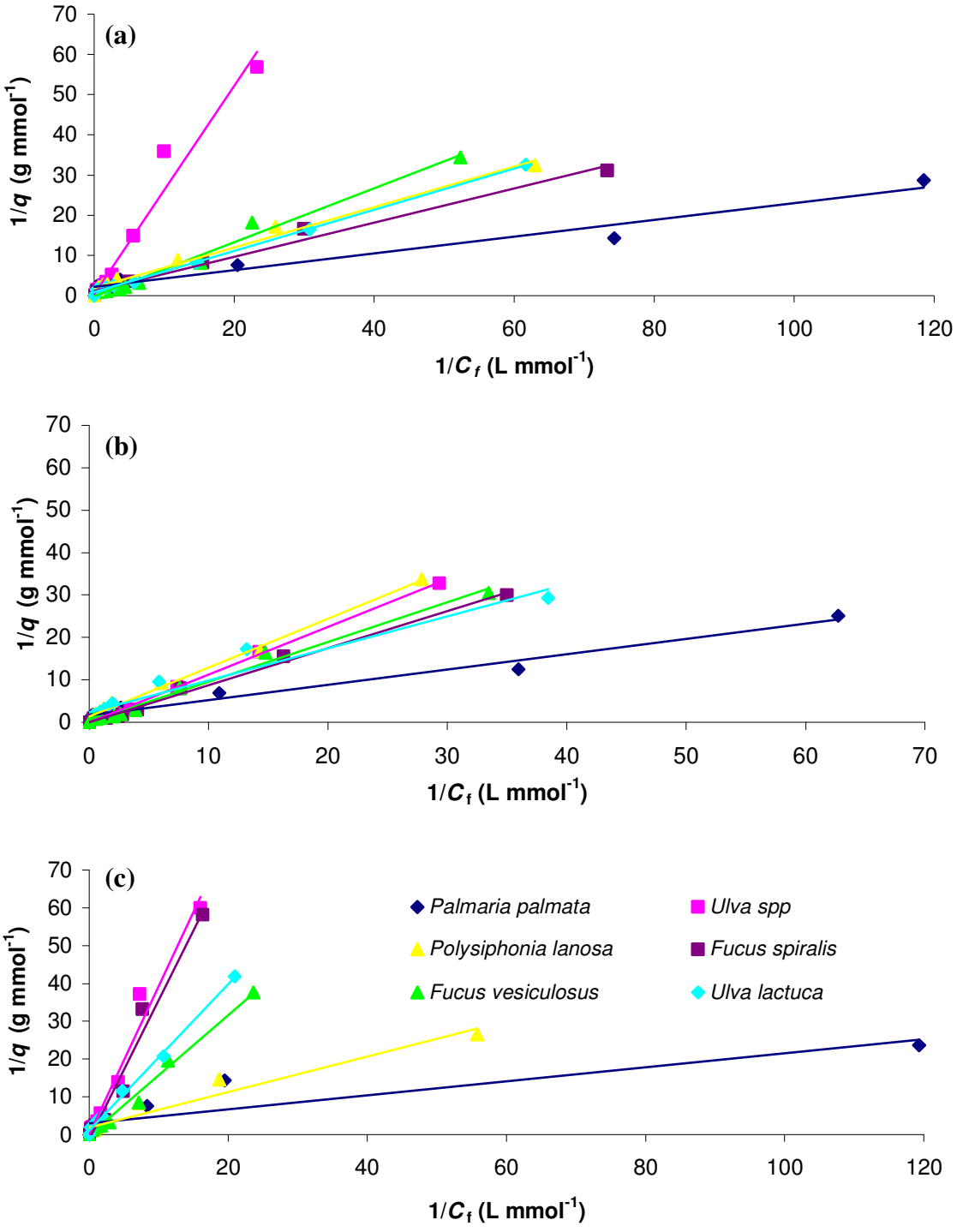

Figure 3.18 **Linearised Langmuir plots of (a) Cu (II) (b) Cr (III) (c) Cr (VI) binding based on experimental isotherm data. Average results from triplicate analyses are shown. Error bars have been omitted for clarity.**

From Equation 3.2, it is seen that a plot of $\mathbf{1/q}$ vs. $\mathbf{1/C_f}$ results in a straight line with a slope of ($\mathbf{1/(b.q_{max})}$) and with an intercept of ($\mathbf{1/q_{max}}$). The values of $\boldsymbol{q_{max}}$ and $\boldsymbol{b}$ estimated from the linearised Langmuir equation are summarised in Table 3.6.

Table 3.6 Langmuir parameters for metal biosorption on six seaweed species.

	q_{max} (mmol g^{-1})	b (L $mmol^{-1}$)	r^2
Cu (II)			
Fucus vesiculosus	1.02 ± 0.10	5.45 ± 0.33	0.98
Fucus spiralis	0.91 ± 0.06	4.58 ± 0.28	0.98
Ulva lactuca	0.69 ± 0.08	2.85 ± 0.19	0.99
Ulva spp.	0.74 ± 0.09	2.52 ± 0.15	0.96
Palmaria palmata	0.43 ± 0.04	11.2 ± 0.53	0.97
Polysiphonia lanosa	0.61 ± 0.05	5.57 ± 0.26	0.99
Cr (III)			
Fucus vesiculosus	1.21 ± 0.12	1.88 ± 0.20	0.98
Fucus spiralis	1.17 ± 0.09	1.77 ± 0.13	0.99
Ulva lactuca	0.71 ± 0.04	1.98 ± 0.19	0.94
Ulva spp.	1.02 ± 0.10	1.38 ± 0.12	0.99
Palmaria palmata	0.57 ± 0.03	4.94 ± 0.34	0.98
Polysiphonia lanosa	0.65 ± 0.03	1.34 ± 0.11	0.99
Cr (VI)			
Fucus vesiculosus	0.82 ± 0.04	1.76 ± 0.16	0.98
Fucus spiralis	0.68 ± 0.05	1.47 ± 0.15	0.97
Ulva lactuca	0.53 ± 0.07	1.97 ± 0.19	0.99
Ulva spp.	0.58 ± 0.07	1.20 ± 0.12	0.97
Palmaria palmata	0.65 ± 0.09	8.64 ± 0.31	0.86
Polysiphonia lanosa	0.88 ± 0.11	2.44 ± 0.23	0.94

The Langmuir parameters provide useful information regarding the equilibrium sorption process behaviour in terms of uptake capacity and affinity.

From Table 3.6, it is seen that q_{max} values for Cu (II) decreased in the order: brown> green > red. This finding is consistent with the work of various authors on the uptake of divalent metal cations [14,20,29]. For example, Jalali *et al*. [20] found that brown seaweeds outperformed the green and red seaweeds in the uptake of lead while Sheng *et al*. [14] reported the same trends for copper, cadmium and nickel uptake by various seaweeds.

Palmaria palmata also exhibited the highest b value (11.2 L $mmol^{-1}$) of all the seaweeds examined for Cu (II) binding, but had a maximum capacity of less than half of *Fucus vesiculosus*.

Davis *et al*. [62] showed that a high value of the Langmuir parameter b indicates a steep desirable beginning of the isotherm which reflects high affinity of the biosorbent for the sorbate while Ghimire *et al*. [63] also showed that the better biosorbents were indicated by higher values of the isotherm slope.

As previously shown, high b values relate to metal sorption at low residual metal concentrations. It was clearly seen in the experimental Cu (II) isotherm (Figure 3.15) that *Palmaria palmata* outperforms *Fucus vesiculosus* when the residual concentration is less than 0.15 mmol L^{-1} but has a lower overall maximum capacity. *Palmaria palmata* is therefore more efficient for processing dilute metal solutions compared to *Fucus vesiculosus*. However, this is not apparent if the q_{max} values alone are compared.

Similarly to Cu (II) binding, the q_{max} values obtained for Cr (III) uptake decreased in the order: brown > green > red with *Fucus vesiculosus* having the largest uptake capacity. Again, *Palmaria palmata* had the largest b values thus indicating its high affinity for the metal at low concentrations.

The q_{max} values obtained for cation binding in this study were comparable to those reported in the literature for other marine algae [15,64-66].

Yu *et al.* [67] investigated a group of nine marine algae and found that their q_{max} values were in the range 1.09-1.26 mmol g^{-1} for Cu (II) sorption with corresponding b values in the range 6.1-15.5 L $mmol^{-1}$. Davis *et al.* [62] also reported that six different species of *Sargassum* biomass exhibited q_{max} values in the range 0.8 to 0.93 mmol g^{-1} for Cu (II) with b values in the range 4.16 to 9.16 L $mmol^{-1}$. These values are of the same magnitude as those obtained for Cu (II) binding in this study.

Sheng *et al.* [14] reported a q_{max} value of 0.75 mmol g^{-1} for Cu (II) binding to the green seaweed *Ulva lactuca*. This corresponds well with the q_{max} value of 0.69 ± 0.08 mmol g^{-1} found for the same seaweed in this study.

In the same study [14], the red seaweed *Gracilaria* sp. revealed a q_{max} value of 0.59 mmol g^{-1} which was comparable with the value obtained here for *Polysiphonia lanosa* (0.61± 0.05 mmol g^{-1}) but was increased relative to *Palmaria palmata* (0.43 ± 0.04 mmol g^{-1}).

The b values obtained by Sheng *et al.* [14] for Cu (II) binding *Padina* sp. and *Sargassum* sp. (8.39 and 8.78 L $mmol^{-1}$) were higher than those found for the brown seaweeds in this study (4.58 ± 0.28 and 5.45 ± 0.33 for *Fucus vesiculosus* and *Fucus spiralis* respectively). However, similarly to the present study, these authors showed that b values for Cu (II) binding to the seaweeds decreased in the order: red > brown > green. Again, this indicates that the red seaweeds have a high affinity for metals in the low residual concentration range.

Several authors have reported the relatively lower Cu (II) uptake by various fungi [68,69] with lower values of q_{max} and b obtained than for macroalgae. Pagnanelli *et al.* [70] also reported that bacteria showed a lower biosorption capability than macroalgae for the removal of Cu (II).

Bishnoi *et al*. [71] carried out isotherm analysis of Cr (III) biosorption by *Spirogyra*. Langmuir analysis revealed q_{max} and b values of 28.16 mg g^{-1} and 0.034 L mg^{-1} respectively (0.54 mmol g^{-1} and 1.77 L $mmol^{-1}$). While the q_{max} value is of a similar magnitude to that obtained for *Palmaria palmata* (0.57 ± 0.03 mmol g^{-1}), the affinity constant, b, was significantly higher (4.94 ± 0.34 L $mmol^{-1}$) than that of *Spirogyra*.

In their comparative study on brown seaweed, Tsui *et al*. [37] found q_{max} values of 1.11 mmol g^{-1} and 1.39 mmol g^{-1} for Cu (II) and Cr (III) binding to *Sargassum hemiphyllum* respectively. These values were comparable to those found for the brown seaweeds in the present study which also revealed higher q_{max} values for Cr (III) than for Cu (II) e.g. for Cu (II) binding to *Fucus vesiculosus* q_{max} was 1.02 ± 0.10 mmol g^{-1} while for Cr (III) binding the value was 1.21 ± 0.12 mmol g^{-1}.

The corresponding b values were 6.93 L $mmol^{-1}$ for Cu (II) sorption and 10.9 for Cr (III) sorption [14]. The values obtained for Cu (II) were comparable to those obtained in this study (5.45 ± 0.33 and 4.58 ± 0.28 L $mmol^{-1}$ for *Fucus vesiculosus* and *Fucus spiralis* respectively). However, the Cr (III) values reported by these authors were much larger than those in this study (1.88 ± 0.20 and 1.77 ± 0.13L $mmol^{-1}$ for *Fucus vesiculosus* and *Fucus spiralis* respectively).

In contrast to cation binding, isotherm analysis of Cr (VI) binding to the six seaweeds revealed that the red seaweed *Polysiphonia lanosa* had the greatest q_{max} value (0.88 ± 0.11 mmol g^{-1}), closely followed by *Fucus vesiculosus* (0.82 ± 0.04 mmol g^{-1}). The seaweed with the lowest uptake capacity in this case was *Ulva lactuca* with a q_{max} value of 0.53 ± 0.07 mmol g^{-1}.

Similarly to Cu (II) and Cr (III), the Langmuir affinity parameter, b, was highest for *Palmaria palmata* (8.64 ± 0.31 L $mmol^{-1}$) followed by *Polysiphonia lanosa* (2.44 ± 0.23 L $mmol^{-1}$). Therefore, it is shown that *Palmaria palmata* has high affinity for both cations and anions at low residual concentrations.

Less information was found for Langmuir analysis of Cr (VI) than had been found for Cu (II) and Cr (III). Park *et al*. [72] applied Langmuir isotherm analysis to their data for Cr (VI) binding to *Ecklonia* biomass. The q_{max} and b values (at pH 2) were 74.2 mg g^{-1} and 0.0045 L mg^{-1} respectively. Converting these to mmol g^{-1} for comparison purposes, the values correspond to 1.42 mmol g^{-1} and 0.234 L $mmol^{-1}$ respectively.

Comparing these values to those obtained for the brown seaweeds in this study, it is seen that q_{max} values in this study were significantly lower than for *Ecklonia* sp. (0.82 ± 0.04 and 0.68 ± 0.05 mmol g^{-1} for *Fucus vesiculosus* and *Fucus spiralis* respectively). However, significantly larger b values were obtained for *Fucus vesiculosus* and *Fucus spiralis* in the present study (1.76 ± 0.16 and 1.47 ± 0.15 L $mmol^{-1}$ respectively). This implies that although the brown seaweeds in this study had lower overall capacities than *Ecklonia* sp., their affinity for Cr (VI) was much greater.

From the Langmuir parameters determined, the "best" seaweed for Cr (VI) biosorption is the red seaweed *Polysiphonia lanosa* as it possessed both large q_{max} and b values relative to the other seaweeds.

For Cu (II) and Cr (III), determination of the "best" seaweed for metal biosorption is dependent on its intended application. For high concentration applications, *Fucus vesiculosus* is most suitable as it reveals a high q_{max} for both Cu (II) and Cr (III). However, for low residual concentrations, *Palmaria palmata* is most suitable owing to its large b values.

Maximum metal binding in Table 3.6 is somewhat lower than the number of total sites (Table 2.1) which indicates some degree of multidentism in binding. The maximum Cu (II) sorption capacities for the various seaweeds correspond to approximately one half of the number of equivalent weak acidic groups as determined by potentiometric titration.

From Table 2.1, it was seen that *Fucus vesiculosus* and *Fucus spiralis* each contain 2.00 mmol g^{-1} of carboxyl groups. Since it is thought that carboxyl groups are primarily responsible for metal sorption in brown seaweeds and that it requires 2 carboxyl groups to co-ordinate one divalent metal ion [73], then the q_{max} values of 1.02 and 0.91 mmol g^{-1} obtained for *Fucus vesiculosus* and *Fucus spiralis* are in agreement with titration values. Similar findings were reported by Davis *et al*. [62] and Fourest and Volesky [73].

The values obtained for the remaining seaweeds are slightly less than 50% of the number of weak acidic groups determined. This decreased binding may be due to inaccessibility of the groups once initial binding has taken place. Figure 3.19 illustrates the relationship between the Langmuir q_{max} values and the total number of acidic groups as determined by potentiometric titration in Chapter 2.

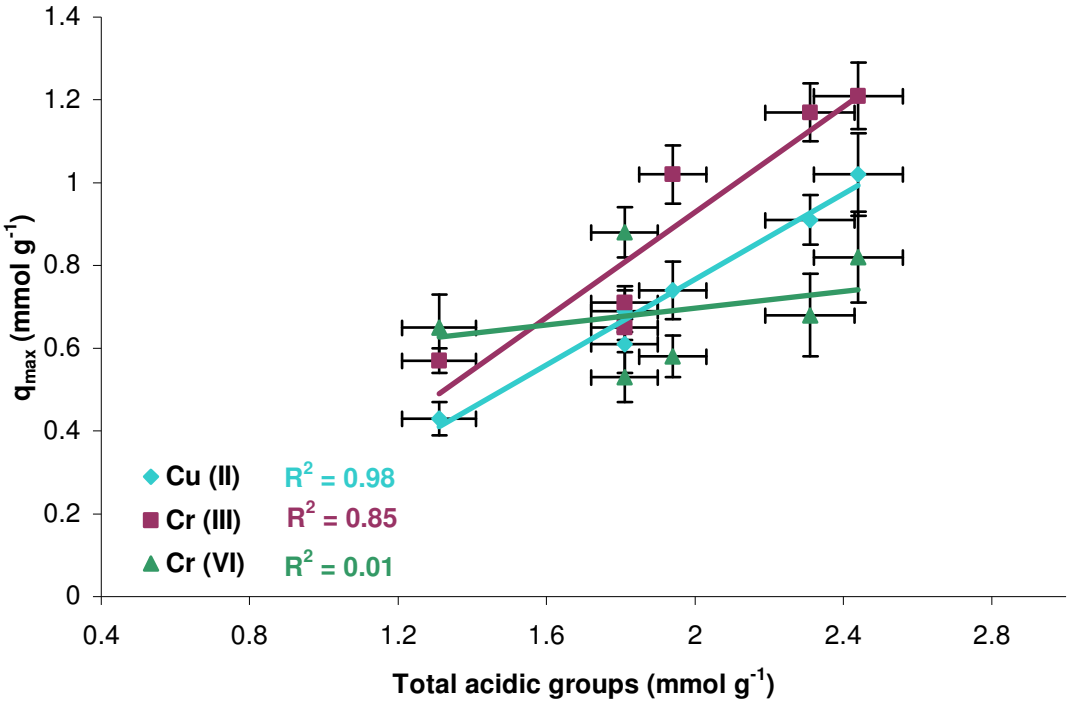

Figure 3.19 Relationship between the q_{max} of the various seaweeds and the total acidic groups on the biomass surface. Error bars are calculated based on triplicate analyses with 95% Confidence Intervals.

Results in Figure 3.19 show that there are high degrees of correlation between the q_{max} values and the total acidic sites for Cu (II) and Cr (III) binding (r^2= 0.98 for Cu (II) and 0.85 for Cr (III), P=0.00). However, no correlation was observed for Cr (VI) binding thus pointing to the differences in binding mechanism of cations and anions to seaweed biomass.

3.3.4.2.2 Freundlich Isotherm

The Freundlich isotherm has been widely used to fit experimental biosorption data [22,24,74,75]. It has been shown that high values of ***k*** (sorption capacity) and ***n*** (sorption intensity) indicate a high affinity for the biomass [35].

Experimental isotherm data was plotted according to linear form of Freundlich Equation (Equation 3.4). Linearised Freundlich plots of Cu (II), Cr (III) and Cr (VI) binding to the seaweeds are given in Figure 3.20.

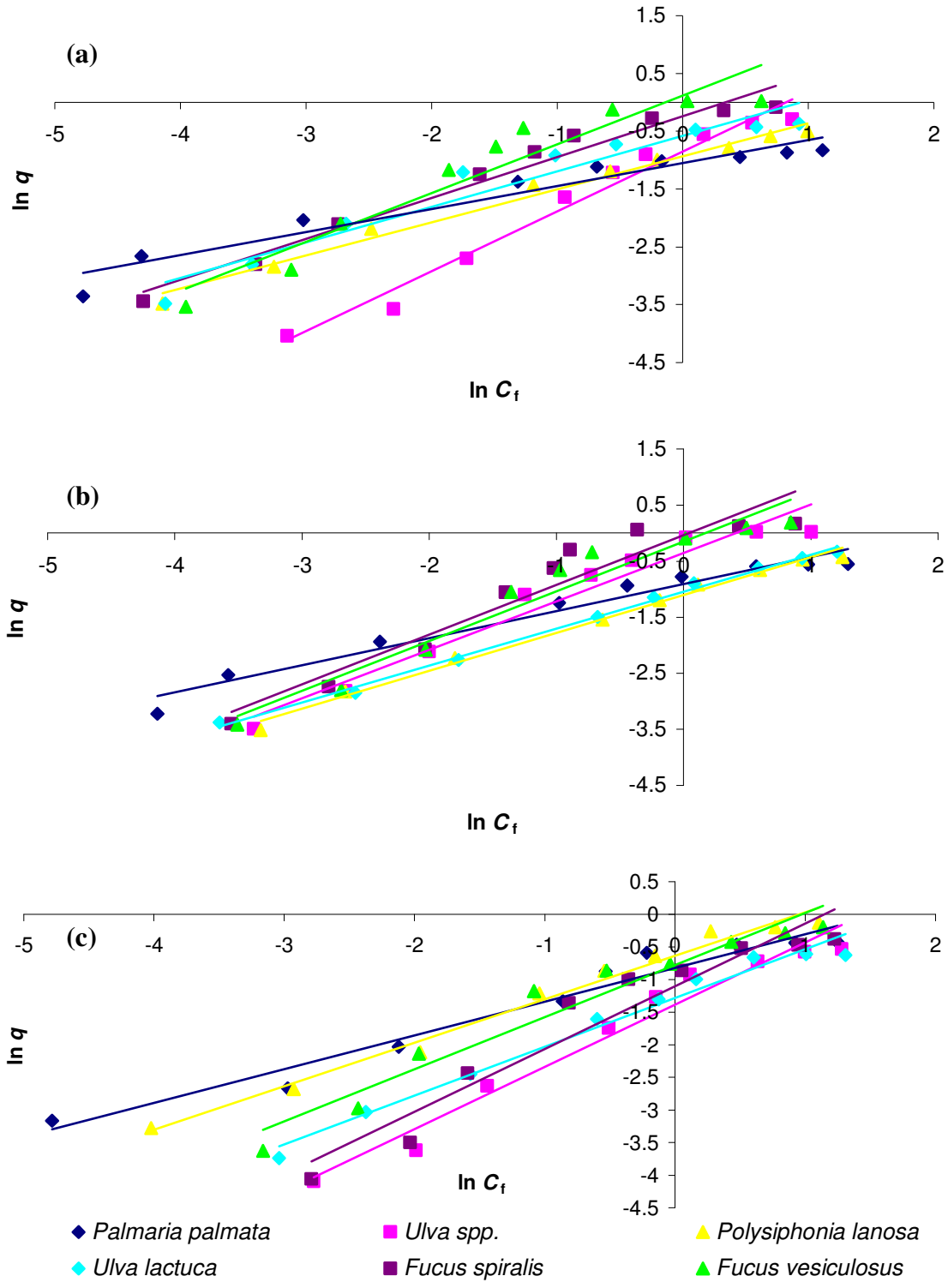

Figure 3.20 **Linearised Freundlich plots of (a) Cu (II) (b) Cr (III) (c) Cr (VI) binding. Average results from triplicate analyses are shown. Error bars have been omitted for clarity.**

From Equation 3.4, it is seen that a plot of **ln** q versus **ln** C_f results in a straight line with a slope of (1/n) and intercept of ln k. The values of k and n estimated from the linearised Freundlich equation are summarised in Table 3.7.

Table 3.7 Freundlich parameters for metal biosorption on six seaweed species.

	k (mmol g^{-1})	n	r^2
Cu (II)			
Fucus vesiculosus	1.13 ± 0.11	1.18 ± 0.15	0.91
Fucus spiralis	0.79 ± 0.09	1.41 ± 0.11	0.96
Ulva lactuca	0.56 ± 0.03	0.76 ± 0.09	0.93
Ulva spp.	0.62 ± 0.04	0.96 ± 0.20	0.97
Palmaria palmata	0.35 ± 0.02	2.51 ± 0.17	0.94
Polysiphonia lanosa	0.49 ± 0.03	1.74 ± 0.11	0.98
Cr (III)			
Fucus vesiculosus	0.86 ± 0.09	1.13 ± 0.11	0.94
Fucus spiralis	0.96 ± 0.13	1.12 ± 0.10	0.91
Ulva lactuca	0.40 ± 0.04	1.51 ± 0.14	0.99
Ulva spp.	0.70 ± 0.07	1.15 ± 0.12	0.95
Palmaria palmata	0.33 ± 0.04	2.07 ± 0.16	0.96
Polysiphonia lanosa	0.37 ± 0.03	1.47 ± 0.13	0.99
Cr (VI)			
Fucus vesiculosus	0.45 ± 0.03	1.25 ± 0.10	0.94
Fucus spiralis	0.33 ± 0.01	1.03 ± 0.09	0.92
Ulva lactuca	0.25 ± 0.02	1.33 ± 0.11	0.97
Ulva spp.	0.27 ± 0.02	1.05 ± 0.07	0.96
Palmaria palmata	0.43 ± 0.03	1.93 ± 0.12	0.95
Polysiphonia lanosa	0.53 ± 0.05	1.49 ± 0.14	0.98

In a general way, the Langmuir and Freundlich isotherms yield similar type information regarding the biosorption process. For example, q_{max} in the Langmuir isotherm is comparable to k in the Freundlich isotherm as both provide information on the metal uptake capacity of the biosorbent. Similarly, the parameters b and n represent similar quantities with each describing the affinity/ sorption intensity of the sorbent for the metal. Therefore, it may be possible to discuss any trends observed between the isotherms.

Similarly to the Langmuir trends observed for Cu (II), in the Freundlich isotherm *Fucus vesiculosus* again had the highest sorption capacity (1.13 mmol g^{-1}) but relatively low sorption intensity (1.18) while *Palmaria palmata* had the lowest sorption capacity (0.35 mmol g^{-1}) but the largest sorption intensity (2.51) of the seaweeds studied.

Freundlich Cu (II) sorption capacity (k) decreased in the order: brown > green > red which was in agreement with the findings for the Langmuir isotherm. Sorption intensity (n) decreased in the order red > brown > green which was also in agreement with Langmuir trends.

Lodeiro *et al*. [16] analysed Cd (II) and Pb (II) removal by *Cystoseira baccata* using the Freundlich isotherm. For Cd (II) k and n values were 0.67 ± 0.02 mmol g^{-1} and 3.1 ± 0.3 respectively while for Pb (II) the k value was 0.74 ± 0.06 mmol g^{-1} with an n value of 6 ± 1. While it is difficult to make a comparison between metals, the k values obtained by these authors for two divalent metals are of the same magnitude as those values obtained in this study. Increased sorption intensity was observed by these authors thus indicating that Cd (II) and Pb (II) are more strongly bound than Cu (II) to algal biomass. This agrees with the metal affinity sequence proposed for fucoidan by Paskins Hurlburt *et al*. [76] in which the order of affinity of these metals is: Pb (II) > Cd (II) > Cu (II).

The Freundlich parameters for Cr (III) sorption show that *Fucus spiralis* has the highest sorption capacity (0.96 ± 0.13 mmol g^{-1}). On the other hand, *Palmaria palmata* had the lowest sorption capacity (0.33 ± 0.04 mmol g^{-1}) but the highest sorption intensity (2.07 ±

0.16) of the seaweeds studied. Cr (III) sorption capacities decreased in the order: brown > green > red while sorption intensity decreased in the order: red > green > brown. It therefore appeared that there was an almost inverse relationship between the ***k*** and ***n*** values for Cr (III) binding in that seaweeds with higher sorption capacities displayed lower sorption intensity for the metal.

The Freundlich Isotherm predicts that binding strength decreases with the increasing degree of site occupation [25]. Therefore, those seaweeds with a greater number of binding sites may show a decrease in overall binding strength simply due to their quantity of binding sites. As a result of its lower number of binding sites (Table 2.1), *Palmaria palmata* displayed lower cation uptake with possible increased binding strength/affinity for the metals.

Bishnoi *et al*. [71] found that for Cr (III) sorption by *Spirogyra*, the Freundlich constant ***k*** was 10.51 mg g^{-1} (0.202 mmol g^{-1}) with an ***n*** value of 3.57. The reduced sorption capacity of *Spirogyra* relative to the seaweeds in this study illustrates that they are more suitable biosorbents than *Spirogyra* for Cr (III) removal at higher residual concentrations. However, the ***n*** value reported for *Spirogyra* above is significantly higher than those found for Cr (III) in this study, thus implying an increased binding affinity of Cr (III) to *Spirogyra* relative to the six seaweeds under investigation.

In the case of Cr (VI) binding, *Polysiphonia lanosa* showed the greatest sorption capacity (0.53 ± 0.05 mmol g^{-1}) as well as a high sorption intensity value (1.49 ± 0.14), second only to that of *Palmaria palmata* (1.93 ± 0.12). This is in contrast to the Freundlich results for Cu (II) and Cr (III) binding where the red seaweeds showed lower relative ***k*** values. On the other hand, this finding is in agreement with the results obtained using the Langmuir isotherm. Thus, high values of ***k*** and ***n*** for *Polysiphonia lanosa* and *Palmaria palmata* in the Freundlich isotherm show easy uptake of Cr (VI) with high sorption capacity.

3.3.4.2.3 Summary of Langmuir and Freundlich Isotherms

The adsorption isotherms obtained for metal ions by the various seaweeds obeyed to a satisfactory extent both the Freundlich and Langmuir predictions within the metal concentration range studied (5–250 mg L^{-1}). High correlation coefficients (Tables 3.6 and 3.7) illustrated the applicability of both models for describing sorption equilibrium. This observation may imply that monolayer biosorption, as well as heterogeneous surface conditions could co-exist under the applied experimental conditions and therefore both Freundlich and Langmuir isotherms can be used to model the experimental biosorption data for these six seaweeds.

A comparison of the order of species predicted by both the Langmuir and Freundlich models is given in Table 3.8.

Table 3.8 Comparison of the species order of uptake and affinity predicted by both isotherm models. Data is summarised from Table 3.6 (Langmuir) and Table 3.7 (Freundlich).

	Langmuir		Freundlich	
Cu (II)	q_{max}	FV >FS >US > UL > PL > PP	***k***	FV > FS > US > UL > PL > PP
	b	PP > PL > FV > FS > UL > US	***n***	PP > PL > FS > FV > US > UL
Cr (III)	q_{max}	FV > FS >US > UL > PL > PP	***k***	FS > FV > US > UL > PL > PP
	b	PP > UL > FV > FS > US > PL	***n***	PP > UL > PL > US > FV = FS
Cr (VI)	q_{max}	PL > FV > FS > PP > US > UL	***k***	PL > FV > PP> FS > US > UL
	b	PP > PL > UL > FV > FS > US	***n***	PP > PL > UL > FV > US > FS

Note: **FV:** ***Fucus vesiculosus*****; FS:** ***Fucus spiralis*****; UL:** ***Ulva lactuca*****; US:** ***Ulva*** **spp.; PP:** ***Palmaria palmata*****; PL:** ***Polysiphonia lanosa*****.**

Both models predicted high cation uptake for the brown seaweeds but reduced cation uptake for the red seaweeds.

For all metals, *Palmaria palmata* had the highest affinity / sorption intensity of the seaweeds studied making it an extremely promising biosorbent for the removal of both cations and anions when present at low residual concentrations. On the other hand the brown seaweeds displayed lower affinities for the biomass, highlighting the fact that although their overall cation binding capacity is large, their low affinity means that they may not be applicable for low residual metal concentrations.

Both the Langmuir and Freundlich Isotherms illustrated that careful consideration of both the seaweed's overall capacity and binding affinity are required when identifying the "best" seaweed for metal biosorption.

3.3.5 Competition between metal ions

In the competitive metal sorption experiments (adapted from a procedure by Chen and Yang [36]), the simultaneous uptake of Cu (II) and Cr (III) was demonstrated.

The influence of competitive ions on metal binding is dependent on the binding strength of the metal ions onto the sorbent. Both Cu (II) and Cr (III) displayed differing Langmuir ***b*** values (Table 3.6) and Freundlich ***n*** values (Table 3.7) for the various seaweeds and therefore, differences in binding behaviour in a competitive situation were expected.

An experimental pH of 4.5 was selected for the study, because in earlier pH experiments (Section 3.3.1.1) there was little difference between Cu (II) uptake at pH 4.5 and pH 5. However, at pH values > pH 5 Cr (III) begins to precipitate as the hydroxide $Cr(OH)_3$ thus adding an error to results (Section 3.3.1.2).

Figure 3.21 illustrates the simultaneous uptake of Cu (II) and Cr (III) onto *Fucus vesiculosus*.

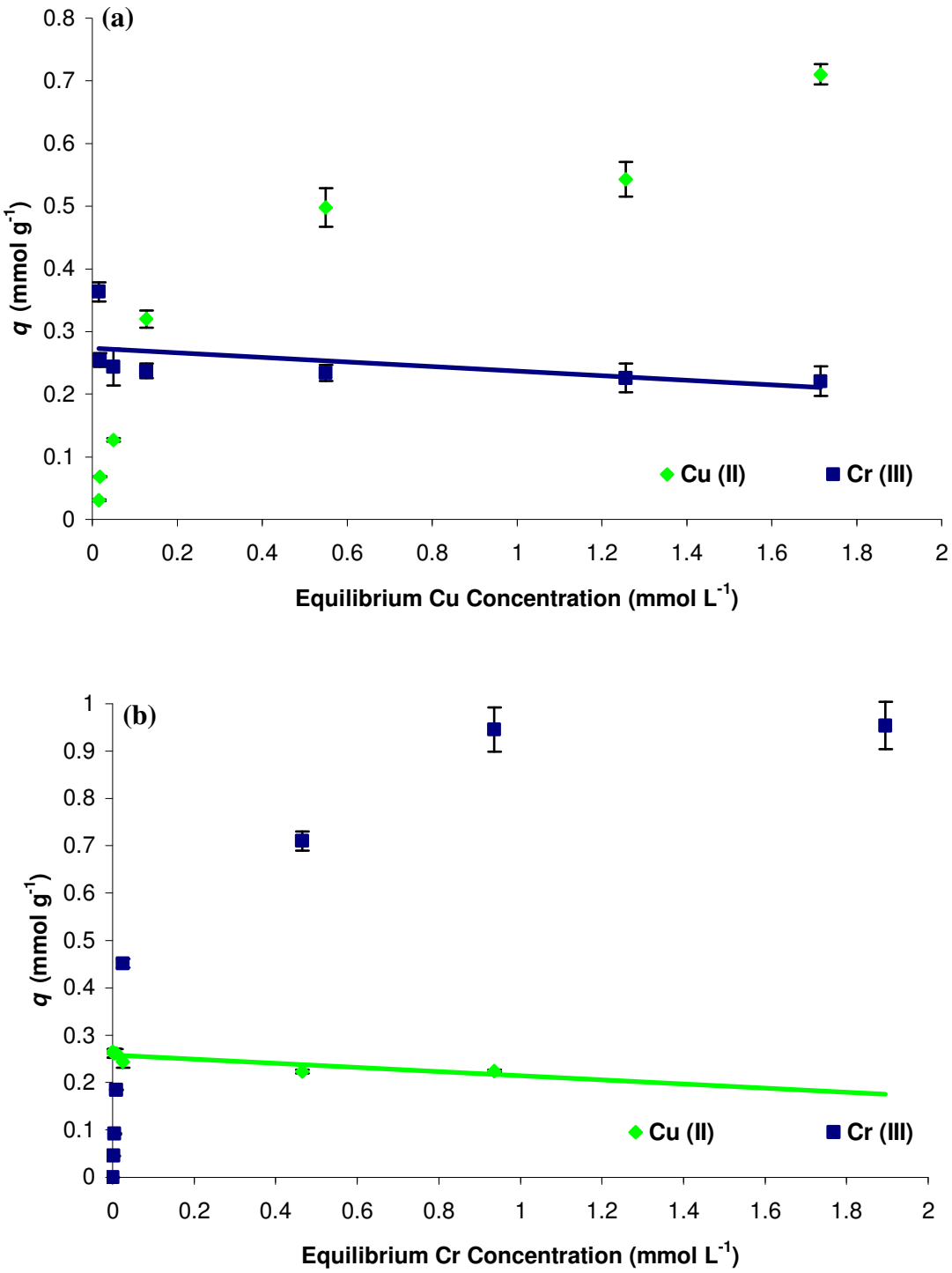

Figure 3.21 **Simultaneous biosorption of Cu (II) and Cr (III) onto *Fucus vesiculosus* under conditions of (a) Constant Cr (III) and (b) Constant Cu (II) (each at 40 mg L^{-1}). Biomass concentration = 2 mg mL^{-1}, pH= 4.5. Error bars are based on triplicate analyses with 95% Confidence Intervals.**

As expected, the presence of competitive ions in the system had a depressive effect on both Cu (II) and Cr (III) binding. In a single ion system with an initial Cu (II) concentration of 3.14 mmol L^{-1}, the Cu (II) uptake was 0.88 mmol g^{-1} (Figure 3.15). However, in the presence of Cr (III), this was reduced to 0.71 mmol g^{-1}, corresponding to a 19% decrease in binding. Similarly, for Cr (III) in a single ion system (with initial Cr (III) concentration of 2.88 mmol L^{-1}, Figure 3.16), metal uptake was 1.01 mmol g^{-1} which was reduced to 0.90 mmol g^{-1} in a competitive situation (11% decrease).

It is seen that as the initial Cu (II) concentration increased (Figure 3.21a), there was a 39 % decrease in the quantity of Cr (III) sorbed by the biomass, from 0.36 to 0.22 mmol g^{-1}. This is to be expected as the Langmuir affinity constant ***b*** was much greater for Cu (II) than for Cr (III) (5.45 ± 0.33 and 1.88 ± 0.20 L $mmol^{-1}$ respectively). Although Freundlich ***n*** values for Cu (II) and Cr (III) were much closer (1.18 ± 0.15 for Cu (II) and 1.13 ± 0.11 for Cr (III)), the value for Cu (II) was marginally higher.

Under conditions of constant Cu (II) in Figure 3.22b, it was seen that an increase in Cr (III) concentration resulted in a 15 % decrease in the amount of Cu (II) sorbed by the seaweed (0.26 to 0.22 mmol g^{-1}). This implies that the competitive effect from Cu (II) is more significant than that from Cr (III) i.e. that Cu (II) is more strongly bound to *Fucus vesiculosus* than is Cr (III). Further analysis on the remaining seaweeds shall be carried out in the future.

3.4 Conclusions

Some conclusions drawn from work in this chapter are as follows:

The biosorption process was pH dependent, with increased cation binding and decreased anion binding observed with increasing pH.

Strong correlation was found between equilibrium Cu (II) uptake and the quantity of acidic sites on the seaweed surface. Some correlation was found for Cr (III) binding but none was observed for Cr (VI).

An ion-exchange mechanism involving calcium was observed for Cu (II) binding to the seaweeds.

Binding of anionic Cr (VI) to the seaweeds required prolonged equilibrium times relative to the binding of cationic Cu (II) and Cr (III). This may be due to a surface reduction mechanism during Cr (VI) binding to the seaweeds. For all metals, some correlation between the quantity of surface acidic sites and the time required to reach equilibrium was observed.

Increased ionic strength resulted in decreases in metal binding for Cu (II), Cr (III) and Cr (VI), the effects of which were more significant for the latter two. Ionic strength effects for Cu (II) revealed some electrostatic interaction with the biomass in addition to complex formation.

Removal efficiency studies revealed that at low initial metal concentrations, *Palmaria palmata* was the most efficient seaweed for removal of metal ions. However, at high initial metal concentrations, *Fucus vesiculosus* exhibited superior biosorption performance.

Langmuir and Freundlich Isotherm analysis revealed that, in general, *Fucus vesiculosus* displayed the greatest uptake capacity for Cu (II) and Cr (III). However, Freundlich analysis of Cr (III) binding showed that the capacity of *Fucus spiralis* was greater. The increased sorption capacity of *Fucus vesiculosus* was in agreement with potentiometric titration results (Chapter 2). In addition to this, both models predicted high anion uptake for *Polysiphonia lanosa*.

In all cases *Palmaria palmata* had the highest affinity/ sorption intensity for the metal ions under investigation making it an extremely promising biosorbent for the removal of both cations and anions when present at low residual concentrations. On the other hand, the high capacities of *Fucus vesiculosus* and *Polysiphonia lanosa* for cation and anion removal respectively, point to their suitability as biosorbents when the residual metal concentration is large.

Strong correlation was found between the maximum metal uptake (as predicted by the Langmuir Isotherm) and the total number of acidic surface binding sites for Cu (II) and Cr (III). By contrast, no correlation was found for Cr (VI) binding thus pointing to differences in the binding mechanism of cations and anions.

Competitive binding studies indicated a depressive effect on Cu (II) and Cr (III) binding in a competitive situation with the competitive effect from Cu (II) being more significant on Cr (III) binding than vice versa. This was in agreement with Langmuir isotherm data which showed that the ***b*** values of *Fucus vesiculosus* for Cu (II) and Cr (III) were 5.45 ± 0.33 and 1.88 ± 0.20 L $mmol^{-1}$ respectively.

3.5 References

[1] Agarwal, G. S., Bhuptawat, H. K. and Chaudhari, S. *Bioresource Technology*, **97**, 949-956 (2006).

[2] Figueira, M. M., Volesky, B. and Mathieu, H. J. *Environmental Science & Technology*, **33**, 1840-1846 (1999).

[3] Chen, J. P., Hong, L. A., Wu, S. N. and Wang, L. *Langmuir*, **18**, 9413-9421 (2002).

[4] Matheickal, J. T. and Yu, Q. M. *Bioresource Technology*, **69**, 223-229 (1999).

[5] Luef, E., Prey, T. and Kubicek, C. P. *Applied Microbiology and Biotechnology*, **34**, 688-692 (1991).

[6] Kratochvil, D. and Volesky, B. *Trends in Biotechnology*, **16**, 291-300 (1998).

[7] Benguella, B. and Benaissa, H. *Water Research*, **36**, 2463-2474 (2002).

[8] Becker, T., Schlaak, M. and Strasdeit, H. *Reactive and Functional Polymers*, **44**, 289-298 (2000).

[9] Vasudevan, P., Padmavathy, V. and Dhingra, S. C. *Bioresource Technology*, **89**, 281-287 (2003).

[10] Vazquez, G., Gonzalez-Alvarez, J., Freire, S., Lopez-Lorenzo, M. and Antorrena, G. *Bioresource Technology*, **82**, 247-251 (2002).

[11] Hanzlik, J., Jehlicka, J., Sebek, O., Weishauptova, Z. and Machovic, V. *Water Research*, **38**, 2178-2184 (2004).

[12] Leyva-Ramos, R., Rangel-Mendez, J. R., Mendoza-Barron, J., Fuentes-Rubio, L. and Guerrero-Coronado, R. M. *Water Science and Technology*, **35**, 205-211 (1997).

[13] Lodeiro, P., Cordero, B., Grille, Z., Herrero, R. and De Vicente, M. E. S. *Biotechnology and Bioengineering*, **88**, 237-247 (2004).

[14] Sheng, P. X., Ting, Y. P., Chen, J. P. and Hong, L. *Journal of Colloid and Interface Science*, **275**, 131-141 (2004).

[15] Cruz, C. C. V., da Costa, A. C., Henriques, C. A. and Luna, A. S. *Bioresource Technology*, **91**, 249-257 (2004).

[16] Lodeiro, P., Barriada, J. L., Herrero, R. and De Vicente, M. E. S. *Environmental Pollution*, **142**, 264-273 (2006).

[17] Schiewer, S. and Wong, M. H. *Chemosphere*, **41**, 271-282 (2000).

[18] Herrero, R., Cordero, B., Lodeiro, P., Rey-Castro, C. and Sastre de Vicente, M. E. *Marine Chemistry*, **99**, 106-116 (2006).

[19] Yu, Q., Matheickal, J. T., Yin, P. and Kaewsarn, P. *Water Research*, **33**, 1534-1541 (1999).

[20] Jalali, R., Ghafourian, H., Asef, Y., Davarpanah, S. J. and Sepehr, S. *Journal of Hazardous Materials*, **92**, 253-262 (2002).

[21] Oguz, E. *Colloids and Surfaces A: Physicochemical and Engineering Aspects*, **252**, 121-128 (2005).

[22] Hanif, M. A, Nadeem, R., Bhatti, H. N., Ahmad, N. R. and Ansari, T. M. *Journal of Hazardous Materials*, **139**, 345-355 (2007).

[23] Luo, F., Liu, Y., Li, X., Xuan, Z. and Ma, J. *Chemosphere*, **64**, 1122-1127 (2006).

[24] Bai, R. S. and Abraham, T. E. *Water Research*, **36**, 1224-1236 (2002).

[25] Davis, T. A., Volesky, B. and Mucci, A. *Water Research*, **37**, 4311-4330 (2003).

[26] Langmuir, I. *Journal of the American Chemical Society*, **40**, 1361-1403 (1918).

[27] Volesky, B., Equilibrium Biosorption Performance, In: Sorption and Biosorption, BV-Sorbex, Inc., St.Lambert, Quebec, 103-116 (2004).

[28] Ho, Y. S., Huang, C. T. and Huang, H. W. *Process Biochemistry*, **37**, 1421-1430 (2002).

[29] Hashim, M. A. and Chu, K. H. *Chemical Engineering Journal*, **97**, 249-255 (2004).

[30] Tsezos, M. *Hydrometallurgy*, **59**, 241-243 (2001).

[31] Volesky, B., Weber, J. and Park, J. M. *Water Research*, **37**, 297-306 (2003).

[32] Senthilkumar, R., Vijayaraghavan, K., Thilakavathi, M., Iyer, P. V. R. and Velan, M. *Journal of Hazardous Materials*, **136**, 791-799 (2006).

[33] Freundlich, H. *Z Phys Chem*, **57**, 385-470 (1907).

[34] Cossich, E. S., Tavares, C. R. G. and Ravagnani, T. M. K. *Electronic Journal of Biotechnology*, **5**, 133-140 (2002).

[35] Abu Al Rub, F. A., El-Naas, M. H., Benyahia, F. and Ashour, I. *Process Biochemistry*, **39**, 1767-1773 (2004).

[36] Chen, J. P. and Yang, L. *Langmuir*, **22**, 8906-8914 (2006).

[37] Tsui, M. T. K., Cheung, K. C., Tam, N. F. Y. and Wong, M. H. *Chemosphere*, **65**, 51-57 (2006).

[38] Dodson, J. R. and Aronson, J. M. *Botanica Marina*, **21**, 241-246 (1978).

[39] Hayden, H. S., Blomster, J., Maggs, C. A., Silva, P. C., Stanhope, M. J. and Waaland, J. R. *European Journal of Phycology*, **38**, 277-294 (2003).

[40] Schiewer, S. and Volesky, B. *Environmental Science & Technology*, **31**, 2478-2485 (1997).

[41] Lee, H. S. and Volesky, B. *Water Research*, **31**, 3082-3088 (1997).

[42] Myklesta, S. *Journal of Applied Chemistry of the Ussr*, **18**, 30-37 (1968).

[43] Kuyucak, N. and Volesky, B. *Biotechnology and Bioengineering*, **33**, 809-814 (1989).

[44] Yun, Y. S., Park, D., Park, J. M. and Volesky, B. *Environmental Science & Technology*, **35**, 4353-4358 (2001).

[45] Haug, A. and Smidsrod, O. *Acta Chemica Scandinavica*, **24**, 843-847 (1970).

[46] Gupta, V. K., Shrivastava, A. K. and Jain, Neeraj. *Water Research*, **35**, 4079-4085 (2001).

[47] Bajpai, J., Shrivastava, Ruma and Bajpai, A. K. *Colloids and Surfaces A: Physicochemical and Engineering Aspects*, **236**, 81-90 (2004).

[48] Cabatingan, L. K., Agapay, R. C., Rakels, J. L. L., Ottens, M. and van der Wielen, L. A. M. *Industrial & Engineering Chemistry Research*, **40**, 2302-2309 (2001).

[49] Park, D., Yun, Y. S., Ahn, C. K. and Park, J. M. *Chemosphere*, **66**, 939-946 (2007).

[50] Cainelli, G. and Cardillo, G., Chromium Oxidations in Organic Chemistry, Springer-Verlag, Berlin, 1-7 (1994).

[51] Nourbakhsh, M., Sag, Y., Ozer, D., Aksu, Z., Kutsal, T. and Caglar, A. *Process Biochemistry*, **29**, 1-5 (1994).

[52] Lee, D. C., Park, C. J., Yang, J. E., Jeong, Y. H. and Rhee, H. I. *Applied Microbiology and Biotechnology*, **54**, 445-448 (2000).

[53] Khoo, K. M. and Ting, Y. P. *Biochemical Engineering Journal*, **8**, 51-59 (2001).

[54] Chen, J. P. and Lin, M. *Water Research*, **35**, 2385-2394 (2001).

[55] Aksu, Z. *Process Biochemistry*, **38**, 89-99 (2002).

[56] Park, D., Yun, Y. S., Jo, J. H. and Park, J. M. *Journal of Microbiology and Biotechnology*, **15**, 780-786 (2005).

[57] Fuks, L., Filipiuk, D. and Majdan, M. *Journal of Molecular Structure*, **792-793**, 104-109 (2006).

[58] Stumm, W. and Morgan, J. J., Aquatic Chemistry, Wiley Interscience, New York, 3-32 (1996).

[59] Lee, M. Y., Hong, K. J., Shin-Ya, Y. and Kajuchi, T. *Journal of Applied Polymer Science*, **96**, 44-50 (2005).

[60] Williams, D. R., The Metals of Life: The Solution Chemistry of Metal Ions in Biological Systems, Van Nostrand Reinhold, London (1971).

[61] Aksu, Z. and Balibek, E. *Journal of Hazardous Materials*, **145**, 210-220 (25-6-2007).

[62] Davis, T. A., Volesky, B. and Vieira, R. H. S. F. *Water Research*, **34**, 4270-4278 (2000).

[63] Ghimire, K. N., Inoue, K., Ohto, K. and Hayashida, T. *Bioresource Technology*, **In Press, Corrected Proof**, (2007).

[64] Holan, Z. R. and Volesky, B. *Biotechnology and Bioengineering*, **43**, 1001-1009 (1994).

[65] Lodeiro, P., Cordero, B., Barriada, J. L., Herrero, R. and Sastre de Vicente, M. E. *Bioresource Technology*, **96**, 1796-1803 (2005).

[66] Matheickal, J. T. and Yu, Q. *Water Science and Technology*, **34**, 1-7 (1996).

[67] Yu, Q., Matheickal, J. T., Yin, P. and Kaewsarn, P. *Water Research*, **33**, 1534-1537 (1999).

[68] Fourest, E, Canal, C. and Roux, J. C. *Fems Microbiology Reviews*, **14**, 325-332 (1994).

[69] Puranik, P. R., Modak, J. M. and Paknikar, K. M. *Hydrometallurgy*, **52**, 189-197 (1999).

[70] Pagnanelli, F., Trifoni, M., Beolchini, F., Esposito, A., Toro, L. and Veglio, F. *Process Biochemistry*, **37**, 115-124 (2001).

[71] Bishnoi, N. R., Kumar, R., Kumar, S. and Rani, S. *Journal of Hazardous Materials*, **145**, 142-147 (2007).

[72] Park, D., Yun, Y. S., Yim, K. H. and Park, J. M. *Bioresource Technology*, **97**, 1592-1598 (2006).

[73] Fourest, E. and Volesky, B. *Environmental Science & Technology*, **30**, 277-282 (1996).

[74] Koelmans, A. A., Gillissen, F. and Lijklema, L. *Water Research*, **30**, 853-864 (1996).

[75] Akar, T. and Tunali, S. *Bioresource Technology*, **97**, 1780-1787 (2006).

[76] Paskins-Hurlburt, A. J., Tanaka, Y. and Skoryna, S. C. *Botanica Marina*, **19**, 59-60 (1976).

Chapter 4
FTIR Analysis of the Seaweed

4.1 Introduction

Work in Chapter 2 characterised the seaweeds in terms of the quantity of acidic binding sites and surface area. Results from Chapter 3 built on these initial findings by identifying the parameters affecting metal biosorption as well as determining the relationship between metal uptake, quantity of binding sites and specific surface a. Once these parameters were identified, the next step was to determine the seaweed functional groups responsible for metal binding. Fourier Transform Infrared (FTIR) Spectroscopy has been widely used to determine the interactions of functional groups on the seaweed surface with metal ions [1-3] and in this chapter it is used to investigate both the functionalities involved in metal binding and the time scale of metal binding with these functionalities.

4.1.1 Fourier Transform Infrared Spectroscopy

The infrared region of the electromagnetic spectrum includes radiation with wavenumbers ranging from approximately 12,800 to 10 cm^{-1}. This is divided into near-, mid- and far infrared with wavenumbers 12800-4000 cm^{-1}, 4000-200 cm^{-1} and 200-10 cm^{-1} respectively [4]. The range used in seaweed surface analysis is the mid infrared range. Infrared spectra arise from various changes in energy brought about by transitions of molecules from one vibrational or rotational energy state to another. The energy at which any peak in a spectrum appears corresponds to the frequency of a vibration of a particular part of a sample molecule [5].

Vibrational energy levels are quantised, and for most molecules the energy differences between quantum states correspond to the mid-infrared region. Relatively discrete closely spaced lines are normally observed for the infrared spectrum of a gas, while broadened vibrational peaks are noted for solid and liquid samples [6]. Vibrations can involve either a change in bond length (stretching) or bond angle (bending). In this work, only bond stretching shall be discussed. Bond stretching may be simplified into two types as illustrated in Figure 4.1.

Symmetric stretch **Asymmetric stretch**

Figure 4.1 Stretching modes resulting from infrared excitation.

A molecule can only absorb radiation when the incoming infrared radiation is of the same frequency as one of the fundamental modes of vibration of the molecule. This means that the vibrational motion of a small part of the molecule is increased while the rest of the molecule is left unaffected [5]. Larger complex molecules may contain several types of atoms/bonds giving rise to a multitude of possible vibrations and interactions thus making spectral interpretation of these compounds more difficult.

4.1.2 Attenuated Total Reflectance FTIR (ATR FTIR)

In this study, Attenuated Total Reflectance (ATR) FTIR techniques shall be used for the analysis of the seaweed samples.

ATR relies upon total internal reflection within a crystal [7]. Internal reflection occurs when light enters a solid at or above its critical angle (θ) causing reflections at the internal surface to return inside the crystal (Figure 4.2). At the points of reflection, radiation penetrates the surface of any substance in good optical contact with the surface. The penetrating radiation is called the evanescent wave and ***n*** is the refractive index of the substance or ATR crystal. If a substance in contact with the crystal absorbs IR radiation, an IR spectrum of the substance can be obtained.

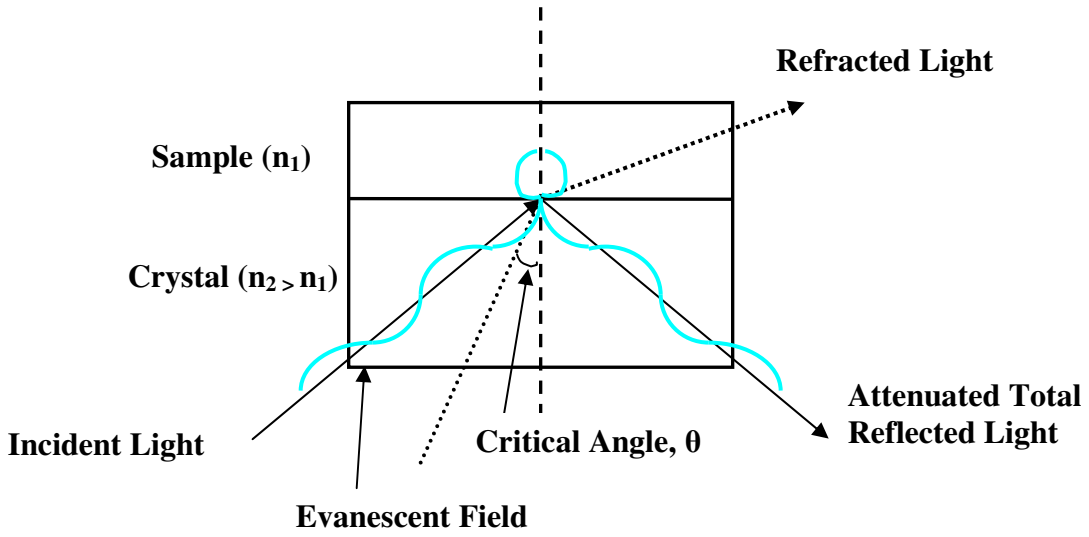

Figure 4.2 Sample Analysis by Attenuated Total Reflectance Spectroscopy [8].

Traditionally, when carrying out seaweed analysis, authors have favoured the use of KBr methods, either using diffuse reflectance [2,9] or by incorporating the sample into a KBr pellet [3,10]. Therefore, validation of this new method was required to ensure that there were no significant differences between the methods. The advantages of using an ATR method over diffuse reflectance are the ease of sample preparation, its non-destructive nature, the small sample quantities required as well as increased sensitivity due to a lack of dilution.

Using ATR techniques the sample may be placed directly onto the crystal. Since the ATR effect only takes place very close to the surface of the crystal, intimate contact between the diamond and the sample must take place. This is achieved by the use of a micrometer screw press with 815 lbs of pressure available to keep the sample in optical contact with the diamond. Reproducible sampling is also achieved by application of the same amount of pressure to each sample using the press.

4.1.3 FTIR Analysis of Seaweeds

FTIR spectroscopy has been frequently used to detect vibrational frequency changes in seaweeds [1,2,10,11]. It has been shown that the IR spectra of seaweeds are relatively complex reflecting the complex nature of the biomass surface [1].

FTIR analysis offers excellent information on the nature of the bonds present on the seaweed surface and allows identification of different functional groups on the cell surface which are capable of interacting with metal ions [3]. Changes in band frequency can also be used to estimate the relative importance of the various surface functionalities in metal sorption.

It has previously been shown that numerous chemical groups may be responsible for the biosorption of metals by macroalgae. These include carboxyl, sulphonate, hydroxyl and amino groups [12]. The relative importance of these groups in metal binding may depend on factors such as the quantity of sites, their accessibility, chemical state and affinity between site and metal.

Table 4.1 summarises some of the commonly observed stretching frequencies encountered in the FTIR spectra of seaweeds. Assignment of peaks to specific functional groups is based on the work of Clothup *et al*. [13].

Table 4.1 Commonly observed stretching frequencies in seaweed FTIR spectra [13].

Wavenumber (cm^{-1})	Assignment
3200-3500	Bonded –OH, -NH stretching
2920	Asymmetric stretch of aliphatic chains (-CH)
2854	Symmetric stretch of aliphatic chains (-CH)
1740	Free C=O stretch of COOH
1630	Asymmetric C=O (COOH)
1530	-NH stretch
1450	Symmetric C=O (COOH)
1371	Asymmetric $-SO_3$ stretching
1237	C-O stretch of COOH
1160	Symmetric $-SO_3$ stretching
1117	C-O (ether)
1033	C-O (alcohol)
817	S=O stretch

The frequencies between 3200 and 3500 cm^{-1} may contain stretching of both amino ($-NH_2$) and alcoholic groups (-OH) [13], but because bands in this region are usually broad in seaweed spectra, it is difficult to assign the centre of the peak. As a result, sharper peaks in the fingerprint region (~1500-400 cm^{-1}) are more useful for identifying the functionalities involved in metal binding in seaweeds.

Figueira *et al.* [10] demonstrated that it was possible to identify two absorbance peaks in the seaweed spectra which are characteristic of coordination compounds between carboxyl groups and the ions used. The distance between these two peaks ($\Delta\nu$) is related to the relative symmetry of the carboxyl group and reflects the nature of the coordination compound [10]. The lower the $\Delta\nu$ value, the more symmetrical is the carboxyl group.

The bands at ~1744 and at 1237 cm^{-1} correspond to the stretching vibrations of the carbonyl double bond ($\nu_{C=O}$) and the carbon-oxygen single bond (ν_{C-O}) respectively [13] indicating typical carboxylic absorption. Figure 4.3 illustrates the typical structure of a carboxyl group with its characteristic stretches.

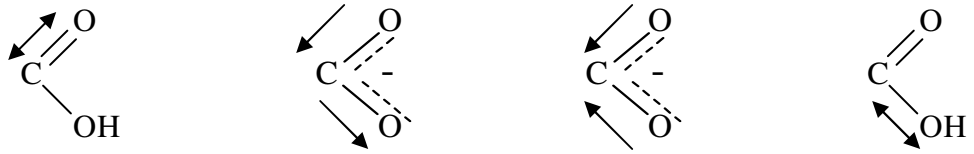

Figure 4.3 Characteristic stretches of carboxyl groups.

After metal ions are bound to the biosorbents, the carbonyl double bond stretching band exhibits a clear shift to a lower wavenumber, while the carbon-oxygen single bond stretch increases in wavenumber [14].

Nakamoto [15] showed that increases in the wavenumber of the C-O band (1237 cm^{-1}) usually indicates complexation of the C-O oxygen. This corresponds to metal complexation to C=O and C-O bonds. The various types of complexation that can occur between metal cations and carboxyl groups in seaweed biosorbents are summarised in Figure 4.4.

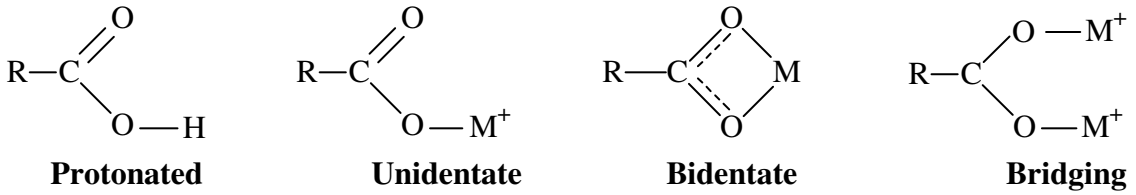

Figure 4.4 Types of complexation that can occur between metal cations and biosorbent carboxyl groups [14].

Nakamoto [15] showed that protonated compounds exhibited the highest Δν values, followed by unidentate complexes. It was also shown that bridging complexes displayed higher Δν values compared to chelating complexes [15]. Therefore Δν values decrease in the order: protonated > unidentate > bridging > bidentate.

Results from previous chapters indicated that carboxyl groups were important in metal binding to the seaweeds. Therefore, the FTIR behaviour of these groups after metal binding is investigated in detail. The contributions of other surface functionalities such as amino and sulphonate groups are also discussed in detail.

4.1.4 Objectives of the Research

The main objectives of the work in this chapter were:

- To identify the functional groups responsible for heavy metal binding to the selected seaweeds.
- To identify the percentage ionic binding for each seaweed-metal combination.
- To elucidate any differences between binding of various chromium oxidation states.
- To identify the timescale of Cu (II) binding to the seaweeds and hence attempt to assess the relative importance of the surface functionalities in binding.

4.2 Experimental

4.2.1 Materials and Methods

4.2.1.1 Chemicals

- Sodium Hydroxide (solid) - Ridel de Haën, Germany.
- Hydrochloric Acid (37%) - LabScan Ltd., Dublin, Ireland.
- Analytical grade metal solutions (1000mg L^{-1}) of Na (I), Cu (II), Cr (III) and Cr (VI) - Sigma-Aldrich Ltd. Dublin, Ireland.
- Alginic acid (from brown algae) - Sigma-Aldrich Ltd., Dublin, Ireland.
- KBr (spectroscopic grade) - Sigma-Aldrich Ltd., Dublin, Ireland.

4.2.1.2 Instrumentation

Sample spectra were obtained using a Digilab Scimitar Series infrared spectrometer (Figure 4.5a) employing a MIRacle™ Single Reflection HATR accessory (Figure 4.5b) with up to 815 lbs of pressure available to keep the sample in optical contact with the diamond. Data was processed using Bio-Rad Win-IR Pro 3.1 software.

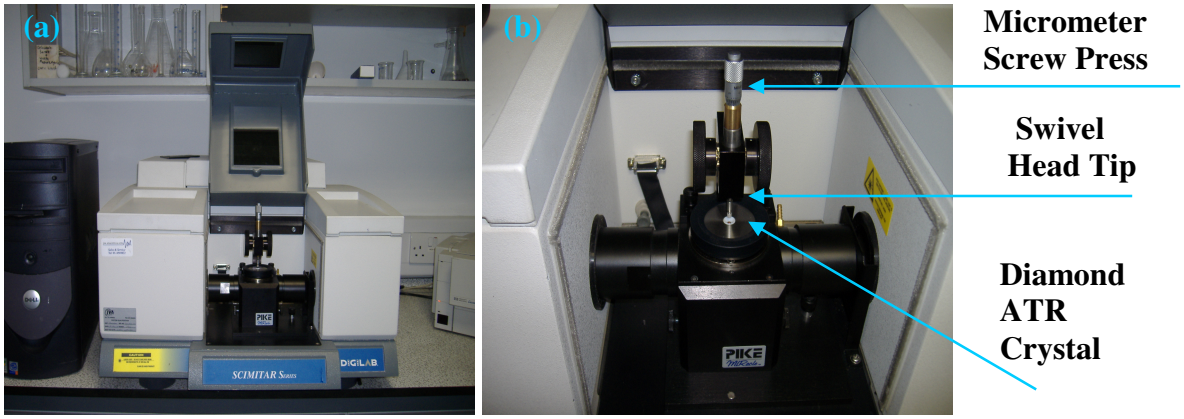

Figure 4.5 (a) Digilab Scimitar Series Infrared Spectrometer (b) MIRacle™ Single Reflection HATR accessory.

Spectra were recorded using a DTGS detector in the wavenumber range 4000-700cm^{-1} at a resolution of 2. The average number of scans was 40.

4.2.1.3 Validation of ATR Methods

Alginic acid was chosen as the reference material in order to validate the method. 10mg of alginic acid (Sigma-Aldrich) was mixed with 100mg of spectroscopic grade KBr (Sigma-Aldrich) and analysed by diffuse reflectance. An alginic acid sample was subsequently analysed using the single reflection ATR accessory with the parameters as previously specified in Section 4.2.1.2. Experiments were carried out in triplicate.

4.2.1.3.1 Analysis of metal alginate complexes

In order to determine the interactions of pure alginic acid with the metals under investigation, 100mg of alginic acid was contacted with 50mL of a 200 μg L^{-1} metal solution at pH 5 for Cu (II), pH 4.5 for Cr (III) and pH 2 for Cr (VI) (as determined in Chapter 3). Exposure to 200 μg L^{-1} Ca (II) and Na (I) solutions was also carried out at pH 5. The flasks were shaken for 4h at 200rpm and room temperature (21±1°C). The samples were then filtered under vacuum and washed thoroughly with distilled water. The metal-loaded alginic acid was then oven-dried at 60°C for 24h and subsequently analysed. Experiments were carried out in triplicate.

4.2.1.4 FTIR Analysis of Seaweeds

4.2.1.4.1 Metal Exposure

Protonated biomass (See Section 2.1), in a size range of 500-850μm and at a concentration of 2mg mL^{-1} was exposed to 200 μg L^{-1} Na (I), Cu (II), Cr (III) and Cr (VI) solutions. The flasks were shaken for 4h at 200 rpm and room temperature (21 ± 1°C) with the pH maintained at pH 5 for Cu (II), pH 4.5 for Cr (III) and pH 2 for Cr (VI) (as determined in Chapter 3). After exposure, the biomass was filtered under vacuum and oven-dried at 60°C for 24h. Samples were subsequently analysed by FTIR using the parameters specified in Section 4.2.1.2. Triplicate analysis was carried out on all samples.

4.2.1.4.2 Time Course Cu (II) Exposure

Protonated biomass (See Section 2.2.2.1.) at a concentration of 2mg mL^{-1} was exposed to a 200 μg L^{-1} Cu (II) solution. The flasks were shaken at 200 rpm and room temperature (21±1°C) with the pH maintained at pH 5. Samples were withdrawn at various time intervals; t = 5, 10, 30, 60, 120 and 240 min and were subsequently filtered under vacuum. The samples were then oven-dried at 60°C for 24h and analysed via ATR FTIR in order to establish the relative importance of the various functionalities in Cu (II) binding. Triplicate analysis was carried out on all samples

4.3 Results and Discussion

4.3.1 Validation of ATR Methods

As previously stated, alginic acid was used as a reference material. This material was chosen because the main stretching bands of alginic acid have been previously published by various authors [1,16]. These bands were obtained using Diffuse Reflectance FTIR. Figure 4.6 shows the alginic acid spectra obtained in this study using both (a) ATR and (b) diffuse reflectance methods.

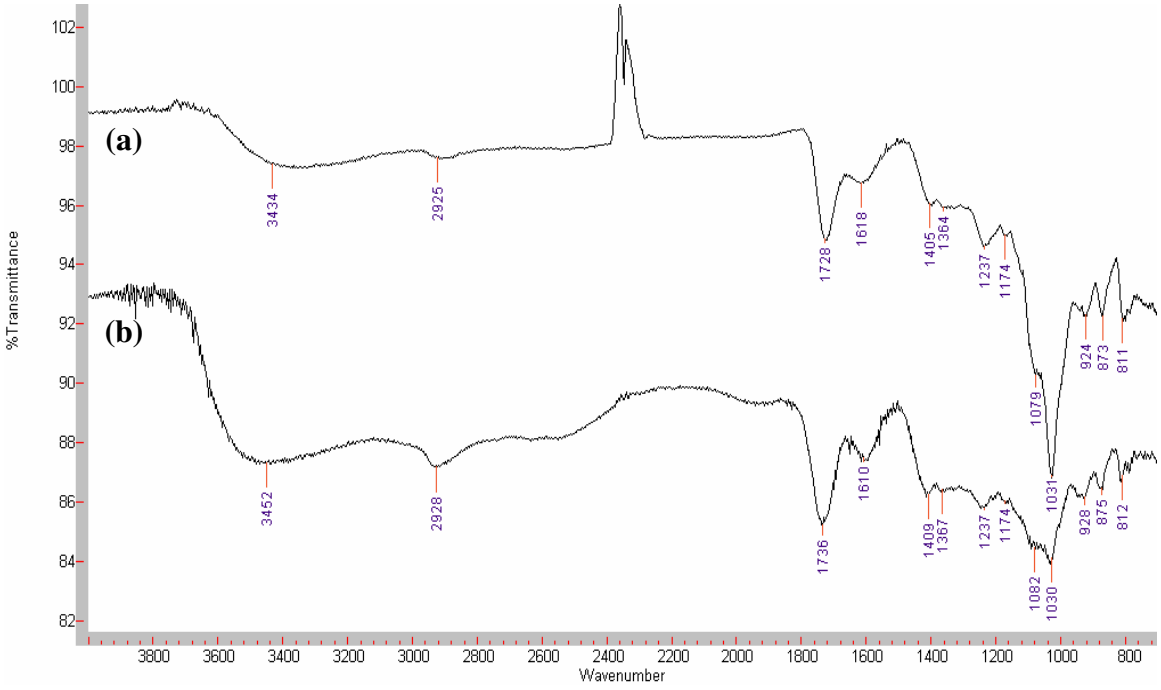

Figure 4.6 FTIR spectra of Alginic Acid obtained by (a) ATR and (b) Diffuse Reflectance Methods. (Number of scans= 40, Resolution= 2). Sample spectra from triplicate analysis are shown.

Table 4.2 compares the frequencies obtained by Filipiuk *et al.* [16] for alginic acid to those obtained experimentally using Diffuse Reflectance and ATR techniques.

Table 4.2 Wavenumbers observed by Filipiuk *et al.* [16] for alginic acid compared to those observed in this study. Spectra were obtained from an average of 40 scans at a resolution of 2. Average experimental data from triplicate analyses are shown.

Alginic acid (ATR) (cm^{-1})	Alginic acid (Diffuse Reflectance) (cm^{-1})	Alginic Acid [16] (cm^{-1})
3434	3452	3482[a]
2925	2928	2926 [a]
1728	1736	1737 [a]
1618	1610	1620 [a]
1405	1409	1461 [a]
1364	1367	**Not specified**
1237	1237	1248 [a]
1174	1174	**Not specified**
1079	1082	1091 [a]
1026	1030	1033 [a]
924	928	**Not specified**
873	875	875 [a]
811	812	812 [a]

[a] Number of replicates not specified.

Although differences in result data were observed between the ATR and Diffuse Reflectance spectra of alginic acid, the individual bands and their related functionalities could be easily identified. Differences in the intensity of the ATR spectrum (Figure 4.3) were also observed. However, the intensity of the ATR spectrum is related to the penetration depth of the evanescent wave in the sample and this depth is dependent on the refractive index of the diamond and the sample, and also on the wavenumber [5]. The change in penetration depth over the spectrum results in the discrepancies seen between transmission and ATR spectra and does not infer that there are differences in the number or types of bands observed. The comparable results obtained between techniques coupled with the reduced noise in the ATR spectrum and repeatability between samples

(Variation in wavenumbers between analysis was between ± 1 cm^{-1}), pointed to the suitability of the Diamond ATR method for sample analysis.

4.3.1.1 Analysis of metal alginate complexes

The presence of multiple pK_a values in the carboxyl region of the potentiometric titration curves (Chapter 2) indicated that different types of carboxyl groups i.e. those having different orientations, may have been present on the seaweed surface. The most well documented example of this is the difference in carboxyl orientation in mannuronic and guluronic acid residues in alginic acid (Figure 1.5).

According to *Chen et al*. [9] the possible metal coordination sites on alginic acid in brown seaweeds include hydroxyl, carboxyl and ether groups. These groups are illustrated in Figure 4.7, where G and M represent guluronic and mannuronic acid respectively.

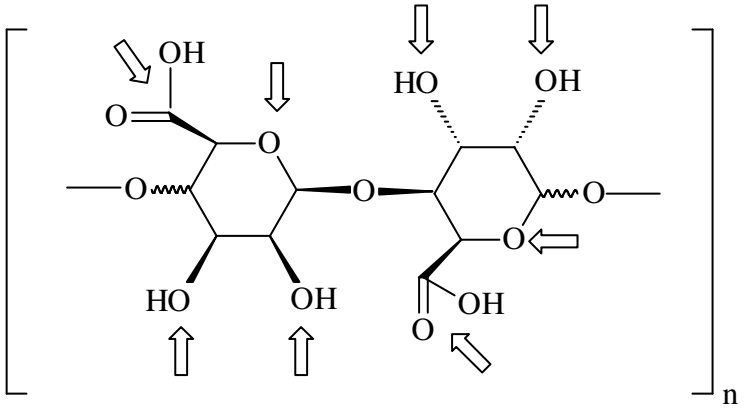

Figure 4.7 Possible sites of interaction for metal ions on alginic acid [16].

From Figure 4.4 it was seen that carboxyl groups can coordinate cations in a variety of different ways and that this difference in coordination leads to variation in Δν values for the carboxyl stretching frequencies [15,17,18]. By monitoring the Δν values of metal-alginate compounds an indication of the type of carboxyl-metal coordination is given. The bands obtained for the pure alginate species may then be used in conjunction with

those proposed by Clothup *et al*. [13] to investigate the influence of metal binding on band behaviour in the selected seaweeds.

The carboxyl stretches found for the metal-alginate complexes in the present study have been summarised in Table 4.3, where ν is the wavenumber of the carboxyl bands C=O and C-O and Δν is the difference (in wavenumber) between these two bands.

Table 4.3 Carboxyl stretching frequencies for the metal-alginate complexes. Average results from triplicate analyses are presented.

Material	Wavenumber (cm^{-1})		
	$\nu_{C=O}$	ν_{C-O}	$\Delta\nu$ ($\nu_{C=O} - \nu_{C-O}$)
Alginic Acid	1728	1237	491
Na-Alginate	1632	1402	230
Ca-Alginate	1634	1412	222
Cu (II)-Alginate	1630	1412	223
Cr (III)-Alginate	1627	1408	219
Cr (VI)-Alginate	1631	1412	219

It is clearly seen that Δν for pure alginic acid was much larger than that observed for the metal loaded alginates. It can be observed that Δν decreased in the order: Alginic acid > Na-alginate> Ca-alginate ≈ Cu (II)-alginate > Cr (III)-alginate = Cr (VI)-alginate. The data obtained with pure alginic acid showed that heavy metal complexation i.e. with Cu (II), Cr (III) and Cr (VI) tends to increase the symmetry of the carboxyl groups compared to sodium ionisation because the lower the Δν, the more symmetrical is the carboxyl group [15].

In seaweed-metal binding, one functional group can participate in different binding mechanisms e.g. carboxyl groups can engage both in complexation and electrostatic attraction of metal cations. Consequently, several mechanisms often act in combination [19].

Because carboxyl groups play an important role in metal binding, the percentage of ionic binding (PIB) was calculated by *Chen et al.* [9]. The percentage of ionic binding can be defined as:

$$PIB = \frac{\nu_{COOH} - \nu_{COOM}}{\nu_{COOH} - \nu_{COONa}} \qquad \textbf{(Equation 4.1)}$$

Where,

ν is the frequency of the asymmetric vibration of the carboxyl group and ν_{COOM} describes the asymmetric vibration for the investigated transition metal complex. The denominator is the FTIR frequency shift of the asymmetric C=O vibration from covalent bonding in carboxylic acid to ionic bonding in sodium carboxylate. The numerator meanwhile is the frequency shift of the same vibration when a particular metal is bound.

Table 4.4 summarises the percentage of ionic binding for the various heavy metal-alginate complexes in this work. Values are calculated from Equation 4.1 using data in Table 4.3.

Table 4.4 Percentage of ionic binding for metal-alginate complexes. Average data from triplicate analyses are shown.

PIB (%)[a]			
Ca (II)	**Cu (II)**	**Cr (III)**	**Cr (VI)**
98 ± 2	102 ± 2	105 ± 2	101 ± 2

[a] **Carboxyl stretching frequencies obtained from Table 4.3**

In the case of Cu (II), Cr (III) and Cr (VI), the PIB values are greater than 100 %. PIB values for these metals were the same (within error). The values obtained in this study are of a similar magnitude to those obtained by Chen *et al.* [9] in their study of an alginate-based ion-exchange resin. These authors reported PIB values of 89, 111 and 102 % for Ca (II), Pb (II) and Cu (II) respectively.

According to Chen *et al*. [9], PIB values >100 % can be interpreted as a decrease in electron density at the carboxyl group as a result of electron delocalisation. The electron delocalisation could be attributed to polarisation or electronic feedback bonding between the metal ion and the carboxyl bond. In general, it has been shown that electron delocalisation effects are beneficial to metal-carboxyl binding [9].

4.3.2 Seaweeds under investigation

In their work on cobalt biosorption by seaweeds, Kuyucak and Volesky [20] used what was termed "free" biosorbent. It was later discovered that the biosorbent was loaded with alkali and alkaline earth ions (Na^{+}, K^{+}, Mg^{2+} and Ca^{2+}) initially present in seawater and a true indication of band shifting upon metal binding could not be obtained [1]. In raw seaweeds, high concentrations of calcium and magnesium bind to the seaweed polymers thus creating a net of cross-linking [21]. Changes in seaweed structure following metal binding are investigated in Chapters 5 and 7.

As previously discussed, assignment of bands is based on the work of Clothup *et al.* [13] and is supported by the work of various authors on seaweed biomass [1,10,14] and alginic acid [16,22].

In all cases protonated biomass was used as the biosorbent control in order to ensure that the correct estimation of band shifting behaviour was obtained for each seaweed-metal combination. Seaweed spectra in this study are well matched with those observed in the literature [2,14].

FTIR data presented in this study are more robust than those which have been found in the literature as all spectra are supported by triplicate analyses. In all cases excellent wavenumber repeatability was observed between replicate scans with any differences being one wavenumber or less. As the resolution of the instrument was fixed at 2 cm^{-1}, wavenumber changes greater than this value are considered to be valid.

4.3.2.1 *Fucus vesiculosus*

The FTIR spectra of protonated, Cu (II)-, Cr (III)- and Cr (VI)-loaded *Fucus vesiculosus* are shown in Figure 4.8 with carboxyl stretching frequencies summarised in Table 4.5.

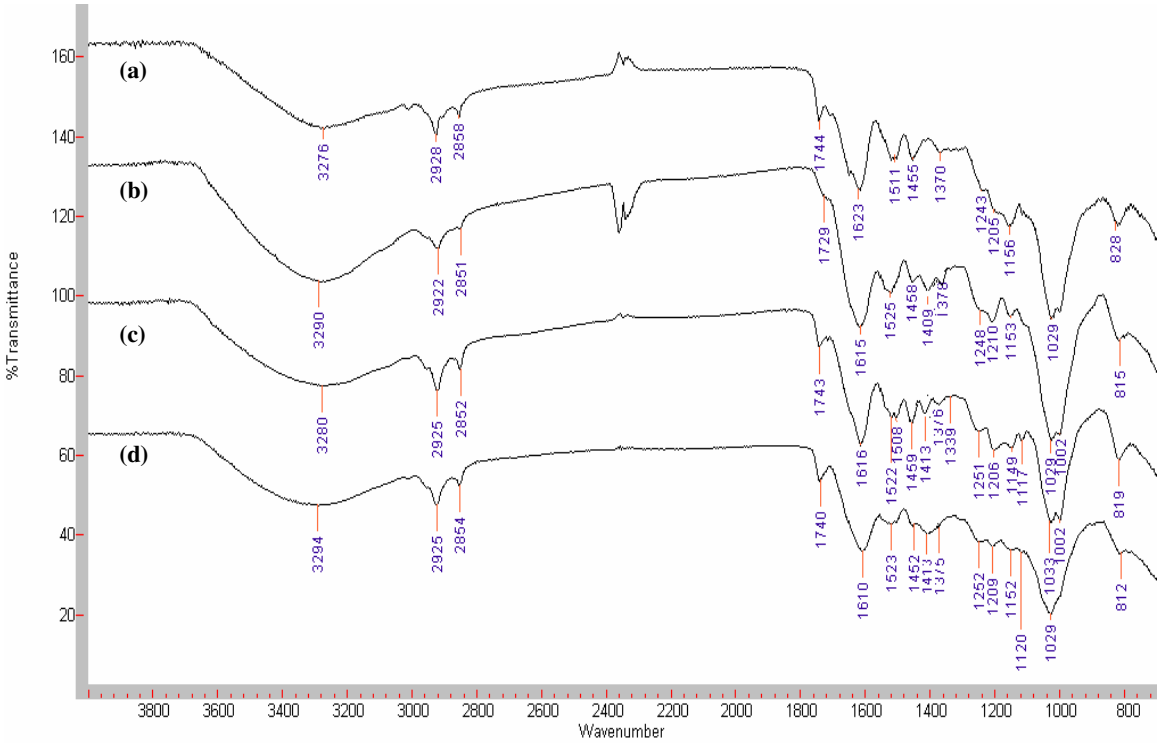

Figure 4.8 **FTIR Spectra of *Fucus vesiculosus* (a) Protonated (b) Cu (II)-loaded (c) Cr (III)-loaded (d) Cr (VI)-loaded. Number of scans= 40, Resolution= 2. Average spectra from triplicate analyses are shown.**

Table 4.5 **Carboxyl stretching frequencies for protonated and metal-loaded *Fucus vesiculosus*. Average data from triplicate analyses are presented.**

Material	Wavenumber (cm^{-1})		
	$\nu_{C=O}$	ν_{C-O}	$\Delta\nu$ ($\nu_{C=O}$ - ν_{C-O})
Protonated	1744	1205	539
Cu (II)	1613	1409	204
Cr (III)	1616	1413	203
Cr (VI)	1610	1413	197

It is clearly seen that the protonated biosorbent has much larger values Δν than the metal loaded biosorbents. After metal binding, the spectra exhibited clear shifts of C=O stretching to lower frequencies and increases in the C-O stretching frequency which is typical for complexation of the carbonyl group with the metal [15]. The reduced distance (smaller Δν) between bands after binding is due to higher symmetry in the cell wall matrix as a result of complexation with the metal ion [3].

Δν values decreased in the order: Protonated >> (Cu (II)-loaded ≈ Cr (III)-loaded) > Cr (VI)-loaded. The Δν values in the range 204-197 cm^{-1} indicated that bidentate complexation between metals and carboxyl groups had taken place. Nara *et al.* [23] predicted that a general decrease in the Δν values with decreased cationic radius may be connected with an increase of the symmetry and equalisation of bond lengths in the carboxylate group of the investigated species. The ionic radii of Ca (II), Cu (II) and Cr (III) are 1.14, 0.71 and 0.63 Å respectively [24].

The FTIR bands of the remaining seaweed functionalities are summarised in Table 4.6.

Table 4.6. FTIR band shifting behaviour for protonated and metal-loaded *Fucus vesiculosus*. Average data from triplicate analyses are presented.

Band	Wavenumber (cm^{-1})			
	Protonated	**Cu (II)-loaded**	**Cr (III)-loaded**	**Cr (VI)-loaded**
-NH	1511	1525	1522 (1508)	1523
$-SO_{3\ asymm}$	1370	1378	1376	1375
$-SO_{3\ symm}$	1156	1153	1149	1152
C-O (ether)	*	*	1117	1120
C-O (alcohol)	1029	1029	1028 (1001)	1029
S=O	828	815	819	812

***- band not observed**

Band shifting of the –NH stretch in Table 4.6 was of a similar magnitude for all metals thus indicating significant amino group involvement in binding to *Fucus vesiculosus*.

For sulphonate groups, no significant differences were observed between metals but an indication of their involvement in metal binding was given from slight increases in the asymmetric $–SO_3$ stretch. Nakamoto [15] showed that coordination through sulphur will shift $–SO_3$ stretching bands to higher frequencies. Binding to sulphonate groups was also indicated by a change in frequency of the S=O band from 828 cm^{-1} to lower wavenumbers after metal binding.

The infrared frequency at 1029 cm^{-1} is associated with the stretching of alcoholic groups [13]. It has been shown that changes in the C-O (alcohol) band with accompanying formation of a C-O ether band at ~1111 cm^{-1} may be due to complexation of the metal between adjacent ether groups [9]. In the case of *Fucus vesiculosus*, no interaction between the alcohol groups and metal ions was apparent but exposure to Cr (III) and Cr (VI) brought about formation of small ether peaks indicating possible ether group interaction.

4.3.2.2 *Fucus spiralis*

The FTIR spectra of protonated, Cu (II)-, Cr (III)- and Cr (VI)-loaded *Fucus spiralis* are shown in Figure 4.9 with carboxyl stretching frequencies summarised in Table 4.7.

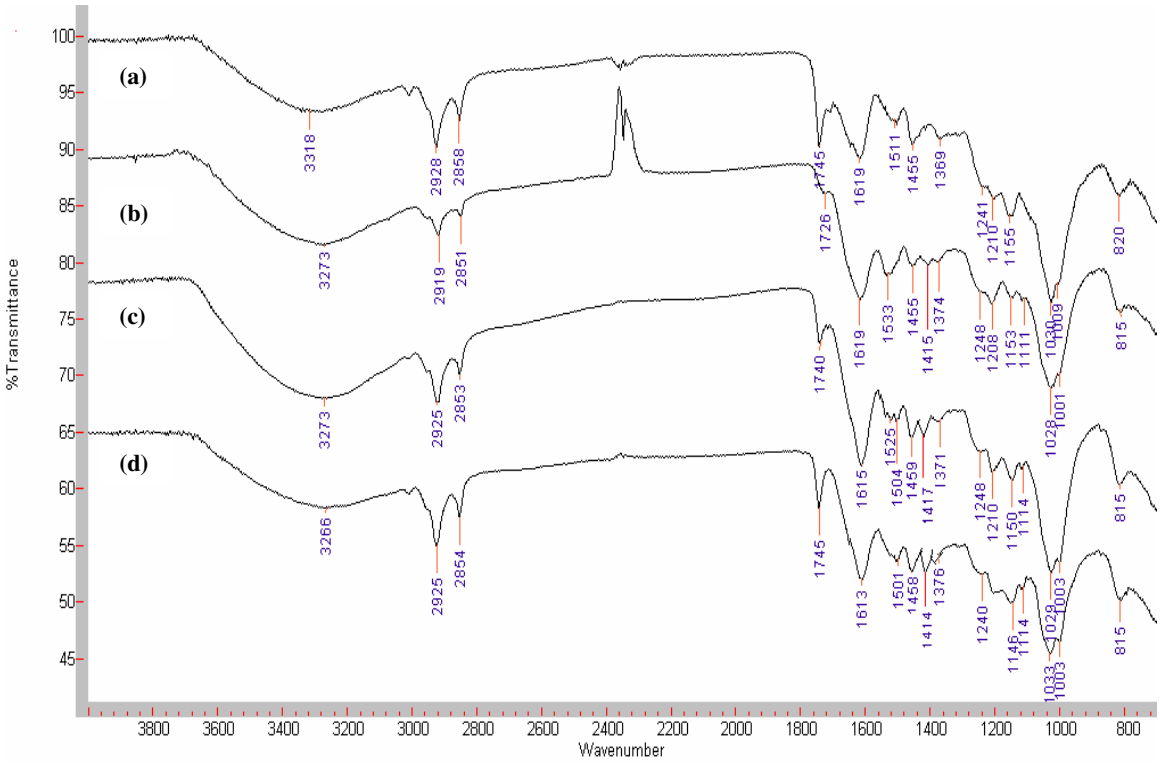

Figure 4.9 **FTIR Spectra of *Fucus spiralis* (a) Protonated (b) Cu (II)-loaded (c) Cr (III)-loaded (d) Cr (VI)-loaded. Number of scans= 40, Resolution = 2. Sample spectra from triplicate analyses are shown.**

Table 4.7 **Carboxyl stretching frequencies for protonated and metal-loaded *Fucus spiralis*. Average data from triplicate analyses are presented.**

Material	Wavenumber (cm^{-1})		
	$\nu_{C=O}$	ν_{C-O}	$\Delta\nu$ ($\nu_{C=O}$ - ν_{C-O})
Protonated	1745	1210	535
Cu (II)	1619	1415	204
Cr (III)	1615	1417	198
Cr (VI)	1615	1414	201

In the case of *Fucus spiralis*, Δν values decreased in the order: Protonated >> Cu (II)-loaded > Cr (VI)-loaded > Cr (III)-loaded. Similarly to *Fucus vesiculosus* the protonated seaweed exhibited a much larger Δν value than the metal-bound seaweeds with bidentate complexation illustrated by Δν values in the range of 198-204 cm^{-1}.

The FTIR bands of the remaining seaweed functionalities are summarised in Table 4.8.

Table 4.8 FTIR band shifting behaviour for protonated and metal-loaded *Fucus spiralis*. Average data from triplicate analyses are presented.

Band	Wavenumber (cm^{-1})			
	Protonated	**Cu (II)-loaded**	**Cr (III)-loaded**	**Cr (VI)-loaded**
-NH	1511	1533	1504	1501
$-SO_{3\ asymm}$	1369	1374	1371	1376
$-SO_{3\ symm}$	1155	1153	1150	1145
C-O (ether)	*	1111	1114	1114
C-O (alcohol)	1033	1028	1029	1033
	1009	1001	1003	1003
S=O	820	815	815	815

***- band not observed**

The predominant interactions in *Fucus spiralis* were again due to carboxyl and amino groups. Significant increases were observed in the –NH stretch for Cu (II) while a decrease in this band was seen for Cr (III) and Cr (VI). The direction of these band shifts based on metal binding requires further investigation (See Section 4.3.2.3 for comparison with *Ulva lactuca*).

The spectra also showed sulphonate group interaction with an increase in frequency of the asymmetric $–SO_3$ bands as well as minor participation of the C-O (alcohol) groups for Cu (II) and Cr (III).

Cu (II) and Cr (III) binding revealed possible complexation biomass ether groups due to the change in wavenumber and shape of the C-O (alcohol) band and accompanying formation of an ether peak at 1111 and 1114 cm^{-1} respectively [9]. Cr (VI) showed no movement of the alcohol peak but did show new band formation at 1114 cm^{-1} perhaps indicating some minimal ether interaction.

In their work on *Sargassum fluitans*, Fourest and Volesky [1] noted that the peak corresponding to complexation of carbonyl groups ($C=O_{asymm}$ at ~1630 cm^{-1}) was still present in the protonated biomass spectrum despite extensive acid washing. This was in addition to the free C=O band at ~ 1740 cm^{-1}. They suggested that these ligands might form internal complexes with other electrophilic groups in the biomass thus accounting for their presence in the protonated spectra. Similar results were found for all seaweeds in this study with both carboxyl bands present in the protonated seaweed spectra.

On the other hand, results for metal-loaded alginic acid [1] showed that when the material was exposed to lower concentrations of cadmium (0.8 mmol g^{-1}) the free C=O stretch was still observed in the spectrum. This indicated that not all of the free carboxyl groups were bound to the metal. However, when the biomass was exposed to a much higher metal concentration (2.8 mmol g^{-1} Cd), this peak disappeared completely indicating that free carboxyl groups had interacted with the metal.

In the present work, the spectra of *Fucus spiralis* and *Fucus vesiculosus* showed the presence of the free C=O peak even after metal binding. However, this peak was shifted to lower wavenumbers thus indicating that while the metal was bound to a proportion of the carboxyl groups, some free carboxyl groups still remained on the biomass surface. This was as expected, given that the metal concentrations to which the seaweeds were exposed were relatively low. As a result we can assume that not all of the potential binding sites were occupied by metal ions.

Another observation for the brown seaweeds was that, in the Cr (VI)-loaded spectra, the free C=O band appears to be much more intense than in the Cu (II) and Cr (III)-loaded spectra. Yang and Chen [25] postulated that, when the seaweed is exposed to $K_2Cr_2O_7$

solution at pH 2 (as was the case in this study), C=O groups could be formed as a result of oxidation of the biomass secondary alcohol groups by Cr (VI) in acidic solution. Thus, this may account for the increased peak size observed relative to the other metal-loaded samples.

4.3.2.3 *Ulva lactuca*

The FTIR spectra of protonated, Cu (II)-, Cr (III)- and Cr (VI)-loaded *Ulva lactuca* are shown in Figure 4.10 with carboxyl stretching frequencies summarised in Table 4.9.

Figure 4.10 FTIR Spectra of *Ulva lactuca* (a) Protonated (b) Cu (II)-loaded (c) Cr (III)-loaded (d) Cr (VI)-loaded. Number of scans= 40, Resolution= 2. Sample spectra from triplicate analyses are shown.

Table 4.9. Carboxyl stretching frequencies for protonated and metal-loaded *Ulva lactuca*. Average data from triplicate analyses are presented.

Material	Wavenumber (cm^{-1})		
	$\nu_{C=O}$	ν_{C-O}	$\Delta\nu$ ($\nu_{C=O}$ - ν_{C-O})
Protonated	1723	1200	523
Cu (II)	1630	1409	221
Cr (III)	1627	1413	214
Cr (VI)	1631	1409	222

Significant changes were observed between the protonated and metal-loaded seaweed spectra of *Ulva lactuca* with chromium binding (both Cr (III) and Cr (VI)) having an apparently greater influence on the seaweed than Cu (II) binding.

For *Ulva lactuca*, carboxyl Δν values decreased in the order: Protonated >> (Cr (VI)-loaded ≈ Cu (II)-loaded) > Cr (III)-loaded. Bidentate complexation is again seen with Δν values for metal loaded seaweeds (214-222 cm^{-1}) being significantly lower than those of the protonated seaweed.

The FTIR bands of the remaining seaweed functionalities are summarised in Table 4.10.

Table 4.10 FTIR band shifting behaviour for protonated and metal-loaded *Ulva lactuca*. Average data from triplicate analyses are presented.

Band	Wavenumber (cm^{-1})			
	Protonated	**Cu (II)-loaded**	**Cr (III)-loaded**	**Cr (VI)-loaded**
-NH	1533	1525	1543	1542
$-SO_{3\ asymm}$	1381	1339	*	*
$-SO_{3\ symm}$	1157	1156	1149	1152
C-O (alcohol)	1026	1023	1019	1024
		984 (sh)	987	990
S=O	*	842	841	845

*** - band not observed**

It was seen from Figure 4.10 that while Cu (II) binding brought about a decrease in wavenumber for the –NH stretching band, Cr (III) and Cr (VI) binding caused an increase in wavenumber of the band and a significant reduction in peak size. However, the direction of these band shifts was in direct contrast to that observed in *Fucus spiralis*, where Cu (II) exposure caused an increase in the wavenumber of the –NH stretch and Cr (III) and Cr (III) binding caused a decrease. It therefore appears that metal interaction

with certain functional groups depends on both the metal and the seaweed involved and indicates that further study of these shifts is required.

Similarly to the brown seaweeds, sulphonate groups appeared to play a role in metal binding to *Ulva lactuca*. A large decrease in wavenumber of the asymmetric $–SO_3$ band was apparent for Cu (II) with the band disappearing completely on Cr (III) and Cr (VI) binding (Table 4.10). In contrast to the browns, the S=O band was absent from the protonated spectrum of *Ulva lactuca* but, in metal loaded samples was shifted to higher wavenumbers (841-845 cm^{-1}) than had been seen in the brown seaweeds (812-828 cm^{-1}).

Involvement of biomass alcohol groups was also seen in Figure 4.11 with minor decreases observed for the C-O (alcohol) band. Changes in peak shape were also apparent with the formation of a shoulder at 984 cm^{-1} in the Cu (II)-loaded sample and the appearance of a minor band at 987 and 990 cm^{-1} respectively for Cr (III) and Cr (VI)-loaded samples.

4.3.2.4 *Ulva* spp.

The FTIR spectra of protonated, Cu (II)-, Cr (III)- and Cr (VI)-loaded *Ulva* spp. are shown in Figure 4.11.

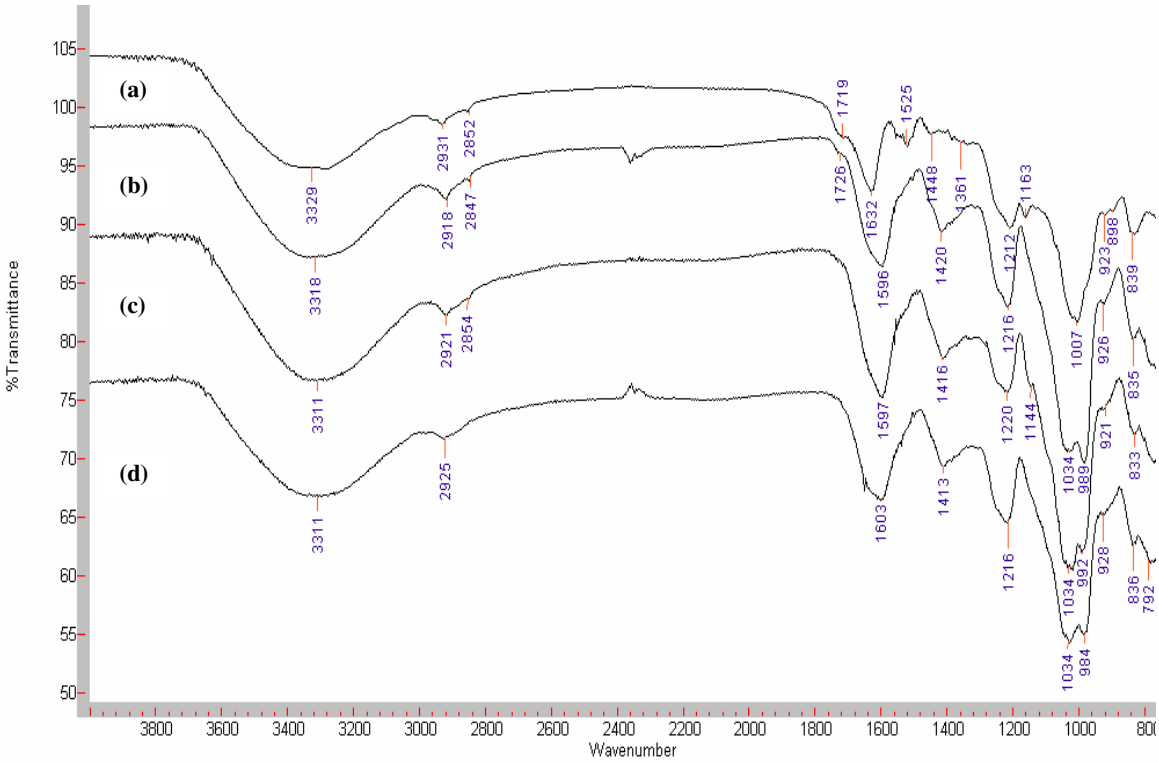

Figure 4.11 FTIR Spectra of *Ulva* spp. (a) Protonated (b) Cu (II)-loaded (c) Cr (III)-loaded (d) Cr (VI)-loaded. Number of scans= 40, Resolution= 2. Sample spectra from triplicate analyses are shown.

Similarly to *Ulva lactuca*, the spectra of metal-loaded *Ulva* spp. revealed significant differences to the raw with much simplified spectra observed after metal binding. The carboxyl stretching frequencies observed in Figure 4.11 obtained are summarised in Table 4.11.

Table 4.11 Carboxyl stretching frequencies for protonated and metal-loaded *Ulva* spp. Average data from triplicate analyses are presented.

Material	Wavenumber (cm^{-1})		
	$\nu_{C=O}$	ν_{C-O}	$\Delta\nu$ ($\nu_{C=O} - \nu_{C-O}$)
Protonated	1719	1212	507
Cu (II)	1596	1420	176
Cr (III)	1597	1416	181
Cr (VI)	1603	1413	190

From Figure 4.11 and Table 4.11, it is seen that metal binding brought about significant changes in the carboxyl groups in *Ulva* spp. These changes included large decreases in the frequency of the asymmetric stretching band (1632-1597 cm^{-1}) and the disappearance of the symmetric stretching band at 1448 cm^{-1}.

Although the $\Delta\nu$ values for *Ulva* spp. are lower than those observed for the brown seaweeds and *Ulva lactuca*, the magnitude of the values (176-190 cm^{-1}) nevertheless points to bidentate complexation with carboxyl ligands in the seaweed. Similarly to the other seaweeds, metal complexed species showed significantly reduced $\Delta\nu$ values in comparison to the protonated species with carboxyl $\Delta\nu$ values decreasing in the order: Cr (VI)-loaded > Cr (III)-loaded > Cu (II)-loaded.

The FTIR bands of the remaining seaweed functionalities are summarised in Table 4.12.

Table 4.12 FTIR band shifting behaviour for protonated and metal-loaded *Ulva* spp. Average data from triplicate analyses are presented.

Band	Wavenumber (cm^{-1})			
	Raw	Cu (II)-loaded	Cr (III)-loaded	Cr (VI)-loaded
-NH	1525	*	*	*
$-SO_{3\ asymm}$	1361	*	*	*
$-SO_{3\ symm}$	1163	*	*	*
C-O (alcohol)	1007	1034	1034	1034
		989	992	984
S=O	839	835	833	836

***- band not observed**

Carboxyl interaction with metal ions has previously been shown in Table 4.11.

Disappearance of the –NH stretching band after exposure to metal solutions also indicated significant involvement of biomass amino groups in metal binding to *Ulva* spp.

The disappearance of the $–SO_3$ bands after metal binding indicates sulphonate group binding to the three metal ions. In contrast to *Ulva lactuca* the S=O band of *Ulva* spp. is present in the protonated spectrum with bands in the metal loaded spectra present at lower wavenumbers in this case (833-836 cm^{-1} for *Ulva* spp. as opposed to 841-845 cm^{-1} for *Ulva lactuca*).

A greater degree of band shifting for *Ulva lactuca* and *Ulva* spp. indicates that sulphonate groups perhaps play a more significant role in metal binding in green seaweeds than in brown seaweeds. As well as this, sulphonate groups show greater interaction with metal ions in *Ulva* spp. over *Ulva lactuca*. This however, may be due to their relative quantities in the biomass as determined by potentiometric titration in Chapter 2 (0.44 mmol g^{-1} for *Ulva* spp. and 0.19 mmol g^{-1} for *Ulva lactuca*).

Large wavenumber increases in the C-O (alcohol) band as well as evidence of the original peak splitting into two peaks, indicate significant participation of alcohol/hydroxyl functionalities in metal binding. This is in contrast to the brown seaweeds as well as *Ulva lactuca* where biomass alcohol groups appeared to play minimal roles in binding at the experimental metal concentration.

4.3.2.5 *Palmaria palmata*

The FTIR spectra of protonated, Cu (II)-, Cr (III)- and Cr (VI)-loaded *Palmaria palmata* are shown in Figure 4.12 with carboxyl stretching bands summarised in Table 4.13.

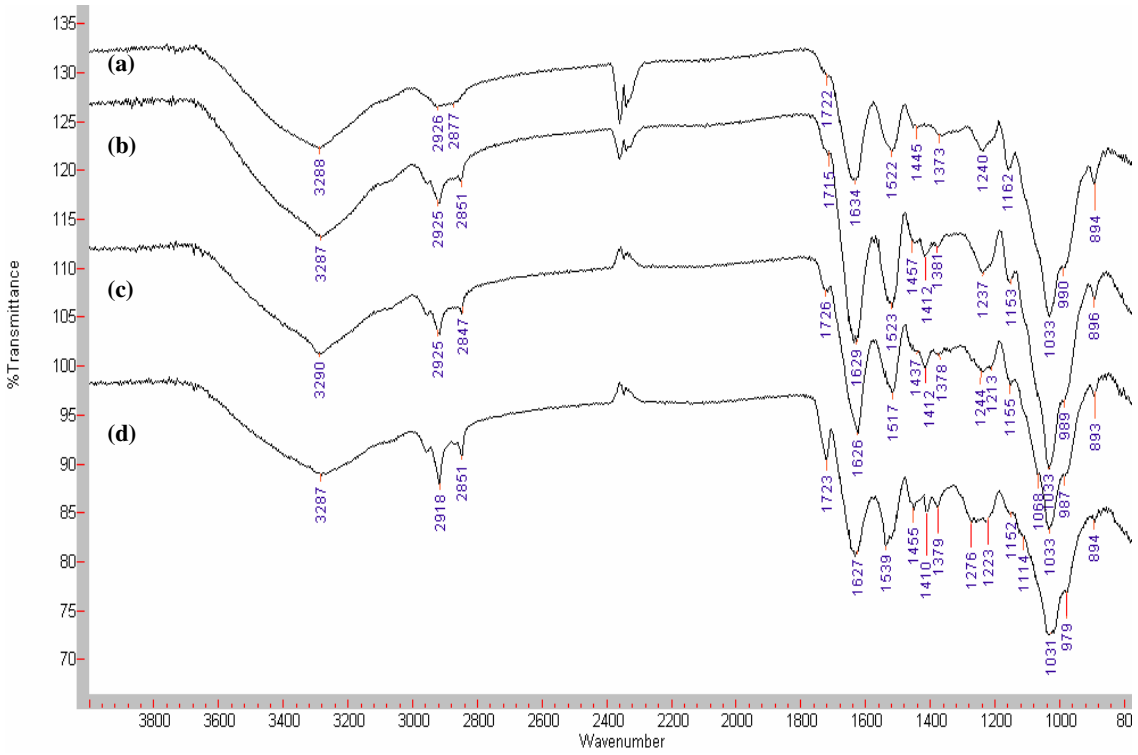

Figure 4.12 FTIR Spectra of *Palmaria palmata* (a) Protonated (b) Cu (II)-loaded (c) Cr (III)-loaded (d) Cr (VI)-loaded. Number of scans= 40, Resolution= 2. Sample spectra from triplicate analyses are shown.

Table 4.13 Carboxyl stretching frequencies for protonated and metal-loaded *Palmaria palmata*. Average data from triplicate analyses are presented.

Material	Wavenumber (cm^{-1})		
	$\nu_{C=O}$	ν_{C-O}	$\Delta\nu$ ($\nu_{C=O}$ - ν_{C-O})
Protonated	1722	1240	482
Cu (II)	1629	1412	217
Cr (III)	1626	1412	214
Cr (VI)	1627	1410	217

As previously found, Δν values for the metal loaded seaweeds were much lower than observed for the protonated seaweed. The Δν values decreased in the order: Cu (II) = Cr (VI) > Cr (III) in the range 217-214 cm^{-1}. Again, these values indicate bidentate complexation with carboxyl ligands in *Palmaria palmata*. Similarly to the brown seaweeds, the free C=O band in the Cr (VI) loaded spectrum was much larger than in the Cu (II) or Cr (III)-loaded spectra. Again, this may be due to oxidation of secondary alcohols to C=O groups by Cr (VI) in acidic conditions contributing to this band [25].

The FTIR bands of the remaining seaweed functionalities are summarised in Table 4.14.

Table 4.14 FTIR band shifting behaviour for protonated and metal-loaded *Palmaria palmata*. Average data from triplicate analyses are presented.

Band	Wavenumber (cm^{-1})			
	Raw	**Cu (II)-loaded**	**Cr (III)-loaded**	**Cr (VI)-loaded**
-NH	1522	1523	1517	1539
$-SO_{3\ asymm}$	1373	1381	1378	1379
$-SO_{3\ symm}$	1162	1153	1153	1152
C-O (alcohol)	1033	1033	1033	1031
	990 (sh)	989 (sh)	897 (sh)	979 (sh)

***- band not observed**

In contrast to the other seaweeds in this study, no evidence of amino group participation was observed for Cu (II) binding to *Palmaria palmata*. On the other hand, differences in band shifting behaviour between the chromium oxidation states were observed with Cr (III) causing a decrease in wavenumber of the –NH stretch and Cr (VI) causing an increase. Thus, possible differences in chromium binding mechanism to amino groups are highlighted.

Also, there was no detectable involvement of biomass hydroxyl groups in metal binding to *Palmaria palmata*. This is in contrast to the green seaweeds where hydroxyl group interactions were significant in metal binding.

4.3.2.6 *Polysiphonia lanosa*

The FTIR spectra of protonated, Cu (II)-, Cr (III)- and Cr (VI)-loaded *Polysiphonia lanosa* are shown in Figure 4.13 with carboxyl stretching bands summarised in Table 4.15.

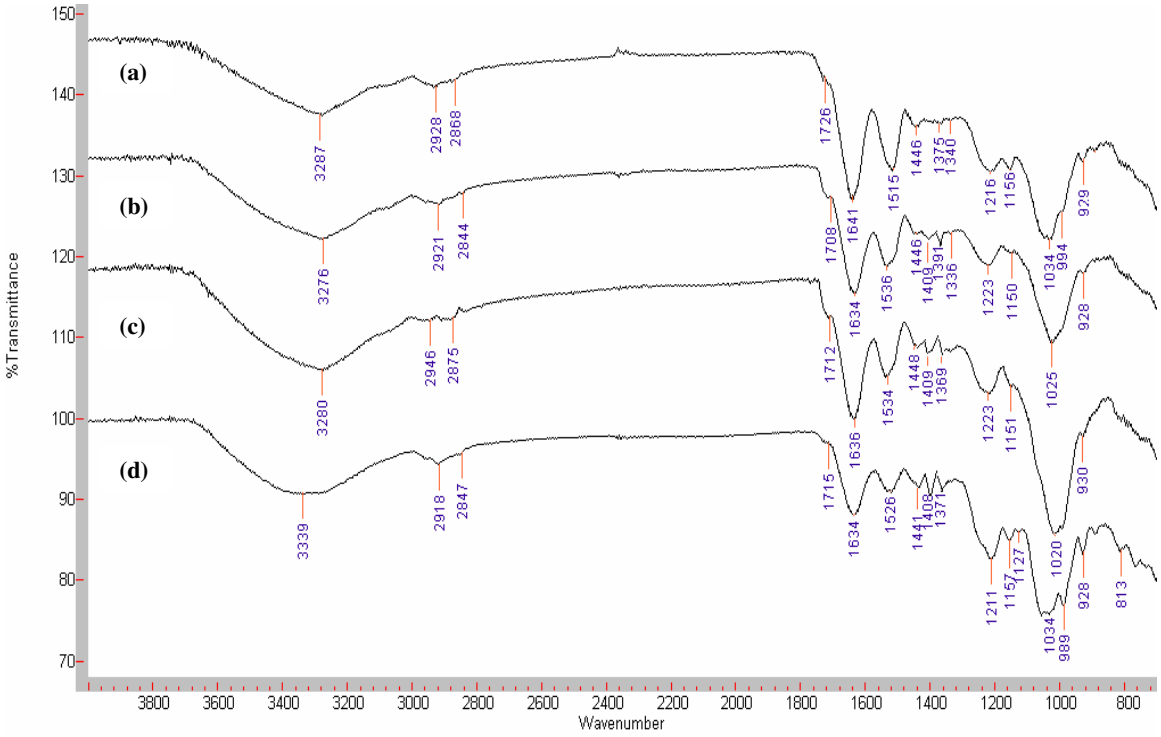

Figure 4.13 FTIR Spectra of *Polysiphonia lanosa* (a) Protonated (b) Cu (II)-loaded (c) Cr (III)-loaded (d) Cr (VI)-loaded. Number of scans= 40, Resolution= 2. Sample spectra from triplicate analyses are shown.

Table 4.15 Carboxyl stretching frequencies for protonated and metal-loaded *Polysiphonia lanosa*. Average data from triplicate analyses are presented.

Material	Wavenumber (cm^{-1})		
	$\nu_{C=O}$	ν_{C-O}	$\Delta\nu$ ($\nu_{C=O}$ - ν_{C-O})
Protonated	1726	1216	506
Cu (II)	1634	1409	225
Cr (III)	1636	1409	227
Cr (VI)	1634	1408	226

When compared with previous seaweed-metal combinations, the Δν values observed were generally higher for *Polysiphonia lanosa*. The Δν values for the heavy metal loaded seaweeds were within a 2 cm^{-1} range and as the instrument resolution was fixed at 2, there was no significant difference between the values. The FTIR bands of the remaining seaweed functionalities are summarised in Table 4.16.

Table 4.16 FTIR band shifting behaviour for protonated and metal-loaded *Polysiphonia lanosa*. Average data from triplicate analyses are presented.

Band	Wavenumber (cm^{-1})			
	Raw	**Cu (II)-loaded**	**Cr (III)-loaded**	**Cr (VI)-loaded**
-NH	1515	1536	1534	1526
$-SO_{3\ asymm}$	1375	1391	1378	1371
$-SO_{3\ symm}$	1156	1150	1151	1157
C-O (ether)	*	*	*	1127
C-O (alcohol)	1034	1025	1020	1034

***- band not observed**

In contrast to *Palmaria palmata*, Cu (II) binding to *Polysiphonia lanosa* showed significant involvement of biomass amino groups. Changes in the –NH stretching band pointed to amino group participation for all metals. However, similarly to *Palmaria palmata*, movement of the –NH stretch was significantly different for both chromium oxidation states. Although exposure caused an increase in wavenumber in both cases, a difference of 8 cm^{-1} was observed between them.

The appearance of a small C-O (ether) band at 1127 cm^{-1} accompanied by a change in shape of the C-O (alcohol) band points to possible ether group involvement in Cr (VI) binding. However, this was not apparent for Cu (II) and Cr (III) binding. On the other hand large wavenumber changes were observed in the C-O (alcohol) band for Cu (II) and Cr (III) binding where none is observed for Cr (VI).

4.3.2.7 Summary of band behaviour for the seaweeds under investigation

Metal binding to carboxyl groups was significant in all seaweed-metal combinations. In all cases, the Δν values suggested bidentate coordination between metal ions and carboxyl groups. Nakamoto [15] suggested that the structure of the metal bound by carboxyl ligands in a bidentate form would be as follows:

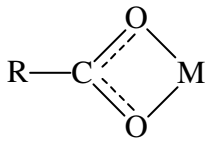

Figure 4.14 Carboxyl bound metal in chelating / bidentate form [15].

A plot of wavenumber change against seaweed species is given in Figure 4.15, thus facilitating a comparison between the effects of (1) metal ion and (2) seaweed type on Δν.

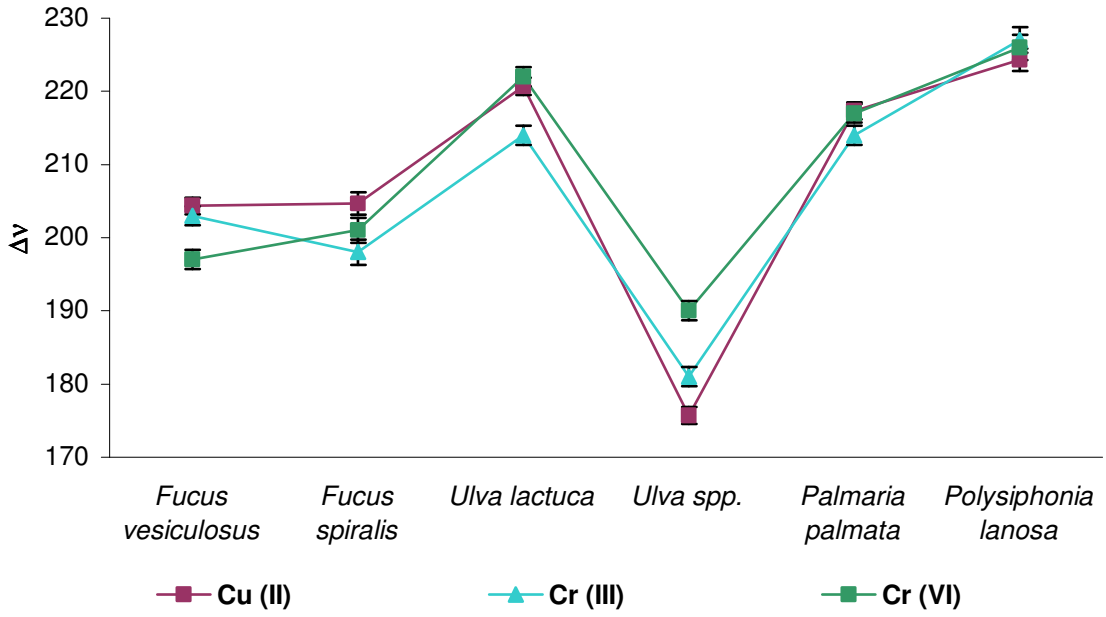

Figure 4.15 Plot of Δν ($\nu_{C=O}$ - ν_{C-O}) versus species. Average values from triplicate analyses are shown.

From Figure 4.15 it is seen that Δν values generally decreased in the order: *Polysiphonia lanosa*> *Ulva lactuca*> *Palmaria palmata*> *Fucus spiralis* ≈ *Fucus vesiculosus* > *Ulva* spp. thus implying that band shifts for each metal are not constant between species. Therefore, this indicates that the carboxyl Δν values observed depend both on the seaweed species and metal under investigation.

Amino groups contributed to metal binding in all cases except for Cu (II) binding to *Palmaria palmata*. While binding of Cu (II), Cr (III) and Cr (VI) brought about similar changes in carboxyl groups, in a number of cases, variations in –NH band shifting behaviour were observed between the metals. The three metals had a similar effect in *Fucus vesiculosus*, while in *Fucus spiralis* Cu (II) increased the wavenumber of the –NH stretch, Cr (III) and Cr (VI) caused a decrease in wavenumber.

In the green seaweed *Ulva* spp., metal binding resulted in the disappearance of the –NH stretching band thus indicating significant involvement in binding. However, Cu (II) binding to *Ulva lactuca* (in contrast to *Fucus spiralis*) resulted in a decrease in wavenumber of the band with Cr (III) and Cr (VI) increasing the wavenumber. Further investigation into the direction of band shifting is required.

Unlike the brown and green seaweeds, differences in binding between Cr (III) and Cr (VI) were also observed for the red seaweeds. In *Palmaria palmata*, Cr (III) binding decreased the wavenumber of the –NH stretch while Cr (VI) brought about an increase in wavenumber. For *Polysiphonia lanosa*, the direction of the band shift was the same for both Cr (III) and Cr (VI) but a wavenumber difference of 8 cm^{-1} was observed between them. Although preliminary, these findings require further investigation in order to ascertain whether there is a disparity in the mechanism of Cr (VI) binding to the red seaweeds compared to the brown and green seaweeds which might perhaps relate to increased numbers of cationic sites reported for red seaweeds [26] or the extent of protonation of the biomass amino groups at the experimental pH values [27].

Sulphonate participation in metal binding was observed in all cases with their contribution being most significant in the green seaweeds.
Ether interactions again varied between species and metals. Their contribution was apparent for all metals in *Fucus spiralis*, but only for Cr (III) and Cr (VI) in *Fucus vesiculosus*. No contribution to binding was found for the green seaweeds or *Palmaria palmata* while ether binding was apparent only for Cr (VI) to *Polysiphonia lanosa*.

Biomass hydroxyl (alcohol) interactions were generally less significant than those of amino, carboxyl and sulphonate groups. No hydroxyl group interaction was found for *Fucus vesiculosus* or *Palmaria palmata*; some interaction was found for *Fucus spiralis* *Ulva lactuca* and *Polysiphonia lanosa* while the contribution of hydroxyl functionalities was significant for metal binding to *Ulva* spp. In the case of *Polysiphonia lanosa*, differences between chromium oxidation states were observed for hydroxyl binding.

4.3.2.8 Percentage Ionic Binding of the Seaweeds

In order to calculate the percentage ionic binding for each seaweed-metal combination using Equation 4.1 [9], it is necessary to use the stretching frequencies observed for sodium-loaded seaweeds as a means of comparison. The carboxyl stretching frequencies observed for the sodium-bound seaweeds in this work are given in Table 4.17.

Table 4.17 Carboxyl stretches observed for sodium-bound seaweeds. Average data from triplicate analyses are presented.

	$\nu_{C=O}$	ν_{C-O}	$\Delta\nu$ ($\nu_{C=O}$ - ν_{C-O})
Fucus vesiculosus	1645	1417	228
Fucus spiralis	1625	1412	213
Ulva lactuca	1639	1412	227
***Ulva* spp.**	1631	1400	231
Palmaria palmata	1634	1403	231
Polysiphonia lanosa	1642	1402	234

All $\Delta\nu$ values for the sodium-loaded seaweeds were greater than those observed for the heavy metal-loaded species. This implies that sodium ionisation of seaweeds has a less stabilising effect on carboxyl groups than metal complexation [15].

Similarly to the metal-alginate species in Table 4.4, percentage ionic binding (PIB) values for the six seaweeds were calculated according to Equation 4.1. $\Delta\nu$ values for the carboxyl groups of the various seaweed species were obtained from Tables 4.5, 4.7, 4.9, 4.11, 4.13 and 4.15.

Calculated PIB values are summarised in Table 4.18.

Table 4.18 Percentage ionic binding for the selected seaweed species. Average data from triplicate analyses are presented.

	PIB (%)		
	Cu (II)	**Cr (III)**	**Cr (VI)**
Fucus vesiculosus	132	129	135
Fucus spiralis	105	105	105
Ulva lactuca	110	114	109
***Ulva* spp.**	139	138	132
Palmaria palmata	106	109	108
Polysiphonia lanosa	102	109	109

All seaweed-metal combinations in Table 4.18 were shown to have PIB values greater than 1 with *Ulva* spp. having elevated values relative to the other seaweeds. In general PIB decreased in the order: *Ulva* spp > *Fucus vesiculosus* > *Ulva lactuca* > *Palmaria palmata* > *Polysiphonia lanosa* > *Fucus spiralis*. As previously discussed in Section 4.3.1.1, this increased PIB (>100 %) can be interpreted as a decrease in electron density at the carboxyl group (as a result of electron delocalisation to the metal) which has a stabilising effect on the carboxyl groups.

In section 4.3.1.1, it was seen that carboxyl groups could engage in both complexation and electrostatic attraction of metal ions [19]. In general, results in this work indicated that those seaweeds with the highest PIB values had lower $\Delta\nu$ values (Figure 4.15). This indicates that there possibly is some complementary relationship between ionic binding and coordination to biomass carboxyl groups.

4.3.3 FTIR Time Course Analysis- Cu (II) binding

Results in previous sections have indicated that many of the same functional groups are responsible for Cu (II) binding to red, green and brown seaweeds. However, the relative contribution of these groups can vary not only between seaweed types but also within species. To investigate the relative effect of each of these functionalities, FTIR time-course analyses were carried out. Estimation of the time scale of interaction for the various functionalities has not previously been encountered in the literature, thus illustrating the novelty of the time-course study

FTIR time-course experiments identified the time scale of interaction of these functionalities with Cu (II) over a 4 h period. Time course analysis has taken the ATR FTIR technique as validated in Section 4.3.1 and has refined it in an attempt to align FTIR behaviour with equilibrium studies in Chapter 3.

Figure 4.17 illustrates the FTIR stretches observed for *Fucus vesiculosus* exposed to 200 μg L^{-1} Cu (II) over a 4h period.

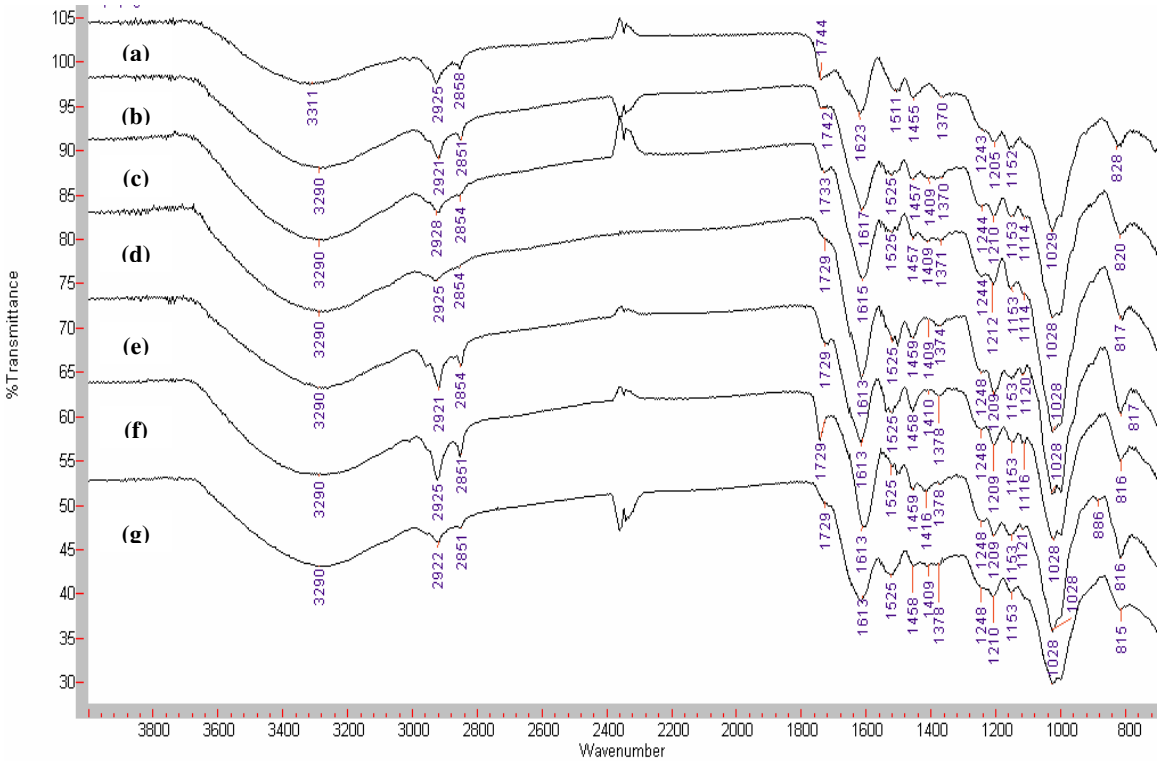

Figure 4.17 FTIR spectra of protonated *Fucus vesiculosus* exposed to Cu (II) at t= (a) 0 (b) 5 (c) 10 (d) 30 (e) 60 (f) 120 and (g) 240 minutes. Number of scans= 40, Resolution= 2. Sample spectra from triplicate analyses are shown.

Tables 4.19- 4.21 give a summary of the stretching bands obtained for the brown, green and red seaweeds over a 4h period. Discussion of band shifting has been restricted to those functionalities which played a major role in binding, namely carboxyl, amino and sulphonate.

Table 4.19 **FTIR stretching frequencies observed for *Fucus vesiculosus* and *Fucus spiralis* Cu (II) time course experiment. Initial metal concentration = 200µg L^{-1}, Number of scans= 40, Resolution= 2. Average data from triplicate analyses is shown.**

	Time (min)						
	0	**5**	**10**	**30**	**60**	**120**	**240**
Fucus vesiculosus	Wavenumber (cm^{-1})						
Free C=O	1744	1742	1733	**1729**	1729	1729	1729
C=O $_{asymm}$	1623	1617	1615	**1613**	1613	1613	1613
-NH stretch	1511	**1525**	1525	1525	1525	1525	1525
-SO_3 $_{asymm}$	1370	1370	1370	1374	**1378**	1378	1378
C-O (COOH)	1205	**1409**	1409	1409	1409	1409	1409
-SO_3 $_{sym}$	1152	1153	1153	1154	1153	1153	1153
Fucus spiralis							
Free C=O	1740	1740	1740	1740	**1726**	1726	1726
C=O $_{asymm}$	1619	1605	1614	1616	**1619**	1619	1619
-NH stretch	1511	1532	**1533**	1533	1533	1533	1533
-SO_3 $_{asymm}$	1369	1374	1374	1374	1374	1374	1374
C-O (COOH)	1210	**1416**	1416	1415	1415	1415	1415
-SO_3 $_{sym}$	1155	**1154**	1154	1153	1153	1153	1153

Changes are initially seen in both carboxyl and amino groups for both *Fucus vesiculosus* and *Fucus spiralis*. Immediate shifting of the asymmetric –SO_3 band was seen for *Fucus spiralis* but this band did not shift until 30 minutes in *Fucus vesiculosus* possibly indicating that sulphonate groups play a more dominant role in Cu (II) binding to *Fucus spiralis* than *Fucus vesiculosus*.

Table 4.20 FTIR stretching frequencies observed for *Ulva lactuca* and *Ulva* spp. Cu (II) time course experiment. Initial metal concentration = 200µg L^{-1}, Number of scans= 40, Resolution= 2. Average data from triplicate analyses is shown.

	Time (min)						
	0	**5**	**10**	**30**	**60**	**120**	**240**
Ulva lactuca							
			Wavenumber (cm^{-1})				
Free C=O	1723	1720	**1720**	1719	1719	1719	1719
C=O $_{asymm}$	1636	1632	1632	**1630**	1630	1630	1630
-NH stretch	1533	**1525**	1525	1525	1525	1525	1525
-SO_3 $_{asymm}$	1381	**1338**	1339	1339	1339	1339	1339
C-O (COOH)	1200	**1409**	1409	1409	1409	1409	1409
-SO_3 $_{sym}$	1157	**1156**	1157	1157	1156	1156	1156
***Ulva* spp.**							
Free C=O	1719	1722	1724	**1726**	1726	1726	1726
C=O $_{asymm}$	1632	**1597**	1596	1596	1596	1596	1596
-NH stretch	1525	1521	*	*	*	*	*
-SO_3 $_{asymm}$	1361	1344	1340	**1337**	*	*	*
C-O (COOH)	1212	1416	1423	**1420**	1420	1420	1420
-SO_3 $_{sym}$	1163	*	*	*	*	*	*

***- not observed**

Carboxyl, amino and sulphonate groups all exhibited shifts within the first 5 minutes of exposure to the Cu (II) solution in both *Ulva lactuca* and *Ulva* spp. with equilibrium reached within 30 minutes for both seaweeds.

Table 4.21 FTIR stretching frequencies observed for *Palmaria palmata* and *Polysiphonia lanosa* Cu (II) time course experiment. Initial metal concentration = 200µg L^{-1}, Number of scans= 40, Resolution= 2. Average data from triplicate analyses is shown.

	Time (min)						
	0	**5**	**10**	**30**	**60**	**120**	**240**
Palmaria palmata							
			Wavenumber (cm^{-1})				
Free C=O	1722	1718	**1715**	1715	1715	1715	1715
C=O $_{asymm}$	1634	1630	**1629**	1629	1629	1629	1629
-NH stretch	**1522**	1522	1523	1523	1523	1523	1523
-SO_3 $_{asymm}$	1373	1377	**1381**	1381	1381	1381	1381
C-O (COOH)	1240	**1412**	1412	1412	1412	1412	1412
-SO_3 $_{sym}$	1162	1160	**1153**	1153	1153	1153	1153
Polysiphonia lanosa							
Free C=O	**1722**	1722	1722	1722	1722	1722	1722
C=O $_{asymm}$	1641	1639	1636	**1634**	1634	1634	1634
-NH stretch	1515	1528	1530	**1536**	1536	1536	1536
-SO_3 $_{asymm}$	1375	1388	**1391**	1391	1391	1391	1391
C-O (COOH)	1216	1412	**1409**	1409	1409	1409	1409
-SO_3 $_{sym}$	1156	1154	1153	**1150**	1150	1150	1150

Both seaweeds showed initial carboxyl band shifting accompanied by sulphonate group interaction with significant shifting of the –NH stretch in *Polysiphonia lanosa* observed after 5 minutes. No significant band movement was apparent after 10 minutes in *Palmaria palmata* and after 30 minutes in *Polysiphonia lanosa*.

For all seaweeds, the results of the FTIR time-courses were in agreement with the equilibrium behaviour observed i.e. once equilibrium had been achieved, no further band

shifting was observed in the FTIR spectra. This is as expected, as correlation between the number of acidic binding sites and the time required to reach equilibrium was previously found.

The Freundlich Isotherm [28] predicted that stronger binding sites are occupied first and that binding strength decreases with increasing degree of site occupation. Therefore, from time course analysis, it is possible to crudely estimate the relative contribution of the three main functional groups to Cu (II) binding to seaweeds. Table 4.22 gives a summary of the results obtained.

Table 4.22 Estimated relative Cu (II) binding strengths of seaweed surface functionalities based on time course analysis.

Seaweed	Relative Contribution
Fucus vesiculosus	Carboxyl ≅ Amino >Sulphonate
Fucus spiralis	Carboxyl ≅ Amino ≅ Sulphonate
Ulva lactuca	Carboxyl ≅ Amino ≅ Sulphonate
***Ulva* spp.**	Carboxyl ≅ Amino ≅ Sulphonate
Palmaria palmata	Carboxyl ≅ Sulphonate
Polysiphonia lanosa	Carboxyl ≅ Amino ≅ Sulphonate

In all cases it is seen that carboxyl and sulphonate groups play a role in Cu (II) binding to seaweeds. Time course analysis predicts that these groups are of more or less equal affinity except in the case of *Fucus vesiculosus* where carboxyl groups show increased affinity relative to sulphonate groups. The importance of amino groups is also clear with these groups having a comparable contribution to that of carboxyl groups in five of the six seaweeds.

This study, although preliminary in nature points to differences in binding affinity of the various functional groups for Cu (II) and indicates the feasibility of further studies which may be carried out on the relationship between seaweed composition and FTIR behaviour

at a variety of metal concentrations. Further investigation into whether this preferential interaction with carboxyl and amino groups may be due to the relative numbers of these groups in the biomass or due to increased binding strength of these groups is required. Time-course studies on Cr (III) and Cr (VI) binding shall also be carried out.

4.4 Conclusions

Heavy metal binding to carboxyl groups in alginic acid was via bidentate complexation, thus increasing the symmetry of the carboxyl groups.

Percentage Ionic Binding was greater than 100% for metal alginate complexes in this study as a result of electron delocalisation effects which are beneficial to metal-carboxyl binding

Metal binding to seaweed carboxyl groups was via bidentate complex formation in all seaweed-metal combinations.

Metal binding brought about increased symmetry to the carboxyl groups with lower $\Delta\nu$ values obtained for metal-loaded biomass over protonated biomass.

The main groups responsible for metal binding were carboxyl, amino and sulphonate to varying degrees with some hydroxyl and ether interaction in a number of cases.

Differences in Cr (III) and Cr (VI) behaviour in *Palmaria palmata* and *Polysiphonia lanosa* indicate some mechanistic differences in chromium binding to red seaweed species.

PIB values for the seaweeds were greater than 100 % in all cases with *Ulva* spp. having the largest values.

Novel analysis on the timescale of Cu (II) binding to the seaweeds was in agreement with equilibrium experiments conducted in Chapter 3. Once sorption equilibrium had been reached, no further band movement was observed in the FTIR spectra.

Timescale experiments revealed that band movement ceased after 10 min of exposure in *Palmaria palmata* and 60min in *Fucus vesiculosus*.

The results in this chapter illustrate the significance of the metal ions on surface functional groups. The impacts of these ions on surface morphology as well as further investigations into binding mechanism are carried out in Chapter 5.

4.5 References

[1] Fourest, E. and Volesky, B. *Environmental Science & Technology*, **30**, 277-282 (1996).

[2] Sheng, P. X., Ting, Y. P., Chen, J. P. and Hong, L. *Journal of Colloid and Interface Science*, **275**, 131-141 (2004).

[3] Raize, O., Argaman, Y. and Yannai, S. *Biotechnology and Bioengineering*, **87**, 451-458 (2004).

[4] Stuart, B., George, B. and McIntyre, B., Introduction, In: Modern Infrared Spectroscopy, John Wiley & Sons, Chichester, UK, 1-18 (1996).

[5] Chalmers, J. M. and Griffiths, P. R., Handbook of Vibrational Spectroscopy, Theory and Instrumentation, Wiley, Chichester, 1-240 (2002).

[6] Stuart, B., George, B. and McIntyre, B., Instrumentation, In: Modern Infrared Spectroscopy, John Wiley & Sons, Chichester, UK, 32-54 (1996).

[7] MIRacle Single Reflection HATR Installation and User Guide, Pike Technologies Inc, Madison, WI, 16-21 (2006).

[8] Pons, M. N., Le Bonte, S. and Potier, O. *Journal of Biotechnology*, **113**, 211-230 (2004).

[9] Chen, J. P., Hong, L. A., Wu, S. N. and Wang, L. *Langmuir*, **18**, 9413-9421 (2002).

[10] Figueira, M. M., Volesky, B. and Mathieu, H. J. *Environmental Science & Technology*, **33**, 1840-1846 (1999).

[11] Park, D., Yun, Y. S., Cho, H. Y. and Park, J. M. *Industrial & Engineering Chemistry Research*, **43**, 8226-8232 (2004).

[12] Smith, R. W. and Lacher, C. *Minerals Engineering*, **15**, 187-191 (2002).

[13] Clothup, N. B., Daly, L. H. and Wiberley, S. E., Introduction to Infrared and Raman Spectroscopy, 3rd Edition, Academic Press, London (1990).

[14] Chen, J. P. and Yang, L. *Langmuir*, **22**, 8906-8914 (2006).

[15] Nakamoto, K., Applications in Coordination Chemistry, In: Infrared and Raman Spectra of Inorganic and Coordination Compounds, John Wiley and Sons, New York, 57-62 (1997).

[16] Filipiuk, D., Fuks, L. and Majdan, M. *Journal of Molecular Structure*, **744**, 705-709 (2005).

[17] Deacon, G. B. and Phillips, R. J. *Coordination Chemistry Reviews*, **33**, 227-250 (1980).

[18] Choudhury, Ch. R., Datta, A., Gramlich, V., Hossain, G. M. G., Malik, K. M. A and Mitra, S. *Inorganic Chemistry Communication*, 790 (2003).

[19] Volesky, B., Weber, J. and Park, J. M. *Water Research*, **37**, 297-306 (2003).

[20] Kuyucak, N. and Volesky, B. *Biotechnology and Bioengineering*, **33**, 809-814 (1989).

[21] Percival, E. G. V. and McDowell, R. H., Chemistry and Enzymology of Marine Algal Polysaccharides, Academic Press, London, UK, 99-126 (1967).

[22] Fuks, L., Filipiuk, D. and Majdan, M. *Journal of Molecular Structure*, **792-793**, 104-109 (2006).

[23] Nara, M., Torii, H. and Tasumi, M. *Journal of Physical Chemistry*, **100**, 19812 (1997).

[24] Cotton, F. A., Wilkinson, G., Murillo, C. A. and Bochmann, M., Basic Inorganic Chemistry, John Wiley & Sons Inc., New York, 815-817 (1999).

[25] Yang, L. and Chen, J. P. *Bioresource Technology*, **In Press, Corrected Proof**, (2007).

[26] Jalali, R., Ghafourian, H., Asef, Y., Davarpanah, S. J. and Sepehr, S. *Journal of Hazardous Materials*, **92**, 253-262 (2002).

[27] Park, D., Yun, Y. S. and Park, J. M. *Chemosphere*, **60**, 1356-1364 (2005).

[28] Freundlich, H. *Z Phys Chem*, **57**, 385-470 (1907).

Chapter 5
SEM/EDX and XPS Analysis of the Seaweed

5.1 Introduction

FTIR analysis in Chapter 4 gave an indication of the functional groups responsible for metal binding, while the calcium release study (Chapter 3) indicated that ion-exchange played a significant role in Cu (II) binding to the seaweeds. Work in this chapter consolidates the results obtained previously as it identifies changes in surface structures and functionalities following metal binding as well as further investigating the mechanisms of cation and anion binding to the selected seaweeds.

The novelty of approach in this work is illustrated in the combined use of SEM/EDX and XPS analysis as supporting techniques for elucidation of binding mechanisms. An introduction into the use of SEM/EDX and XPS techniques is given below.

5.1.1 Scanning Electron Microscopy with Energy Dispersive X-ray (EDX) Analysis

In SEM, the surface of a solid sample is scanned in a raster pattern with a beam of energetic electrons. Several types of signals are produced from the surface in this process, including backscattered, secondary and Auger electrons; X-ray fluorescence photons; and other photons of various energies [1]. The two most common are (1) backscattered and (2) secondary electrons which serve as the basis for SEM. An image is obtained by measuring the intensity of the secondary electrons generated where the beam intercepts the sample surface. A schematic diagram of the Scanning Electron Microscope is given in Figure 5.1.

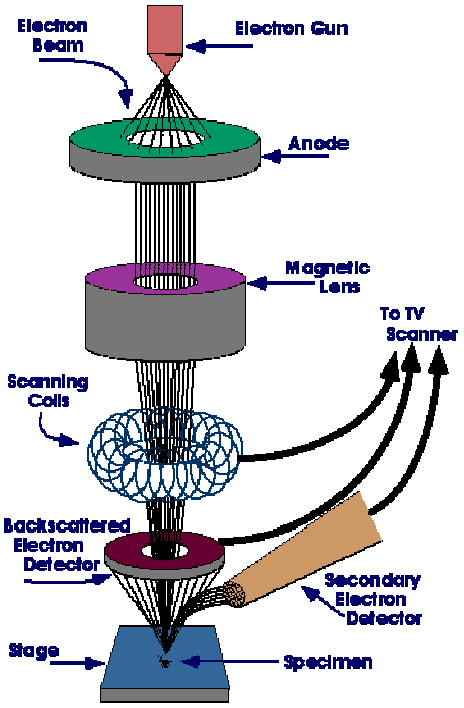

Figure 5.1 Schematic diagram of a Scanning Electron Microscope [2].

In this study, SEM allows examination of the topography of the seaweed surface and identification of any morphological changes which might take place in the seaweed after metal exposure.

An EDX instrument can be attached to an SEM to provide supplementary information. As the SEM electron beam strikes the sample surface X-rays are produced. An X-ray photon impinging on the surface of the EDX detector produces electron hole pairs which are detected as a single pulse by the liquid nitrogen cooled preamplifier. The pulse energy is determined by the X-ray energy which in turn is determined by the element being examined [1]. The EDX analyser produces a spectrum of the elements present in targeted areas of the sample allowing detectable elements to be quantified or mapped.

5.1.1.1 SEM/EDX in Seaweed Analysis

Scanning Electron Microscopy can be used to visualise the surface morphology of the seaweeds before and after metal binding, allowing for direct observation of any changes.

Raize *et al.* [3] studied the effects of metal binding to *Sargassum vulgaris* using combined SEM and EDX techniques. SEM analysis revealed that there were significant morphological changes, including shrinking and layer sticking, in the seaweed after metal binding.

Figueira *et al.* [4] also studied the effects of iron binding in *Sargassum* biomass in a similar manner. In all cases, the use of raw biomass was favoured rather than protonated biomass. This is because raw seaweed biomass contains ions commonly present in seawater such as K^+, Ca^{2+}, Mg^{2+}, Na^+ and these ions can be detected in the EDX spectra. In protonated biomass, these ions are, to a large extent, replaced by H^+ ions and these cannot be detected via EDX. Monitoring the presence of these alkali and alkaline earth metals may aid deduction of mechanism. For example, if these ions are present in the raw seaweed spectrum and absent in the metal loaded spectrum then this may indicate that the metal is bound via an ion-exchange mechanism and that the ions initially present on the cell wall have been replaced with metal ions. Qualitative EDX can achieve limits of detection of 100 mg L^{-1} in favourable cases [5].

5.1.2 X-ray Photoelectron Spectroscopy (XPS)

X-ray photoelectron spectroscopy (XPS) is a widely used method for surface analysis of materials, due to its sensitivity and chemical specificity [6]. XPS involves irradiating a sample under vacuum with mono-energetic X-rays. The electrons produced are then analysed according to energy. Since only electrons emitted from atoms near the surface escape without losing energy, this technique is surface sensitive. Figure 5.2 illustrates the basic components of a monochromatic XPS system [7].

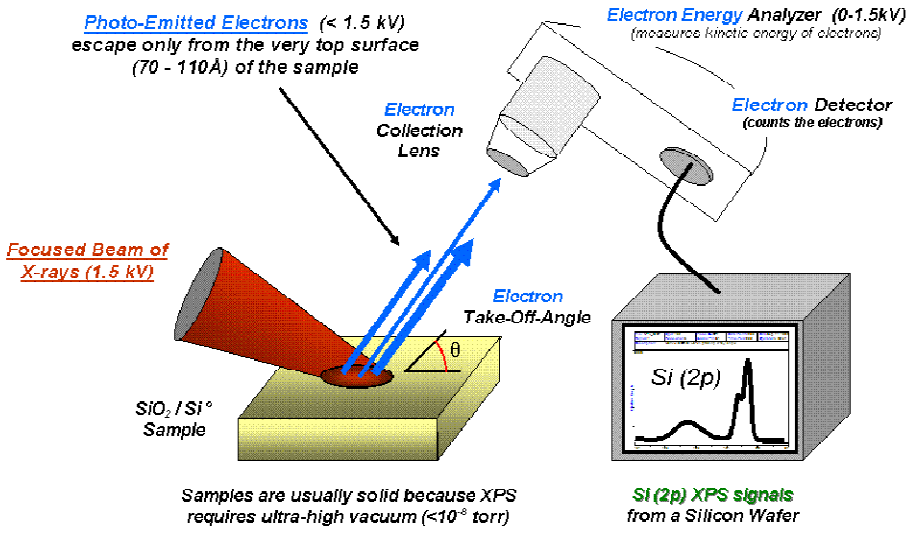

Figure 5.2 Basic components of a monochromatic XPS system [7].

Because each element has a unique set of binding energies for electrons, XPS can be used to identify and determine the concentration of the elements on the surface [1]. It is a non-destructive technique that allows quantitative elemental surface analysis, chemical state surface analysis, and determination of the molecular environment and/or oxidation state of metals. High performance XPS instruments can detect all elements with the exception of hydrogen and helium. A detailed description of this technique and its interpretation was reported by Briggs [8]. Limits of detection in XPS are in the region of 0.1–1.0 atomic percentage (%), where 0.1% equals 1 part per thousand or 1000 parts per million [7].

5.1.2.1 XPS in Seaweed Analysis

From the XPS spectra, the elements present and their chemical state (valence) can be determined. Subtle changes in peak positions and shape can yield important information on changes in surface chemistry, giving XPS the ability to determine the elemental composition on the surface of materials.

XPS analysis has been used by various authors [3,4,9] for the characterisation of functional groups involved in metal binding to seaweed biomass. It provides information about the elemental and chemical composition of a surface and may be used to determine

the interactions between the organic functional groups within the biomass and metals adsorbed.

Through the use of the various elemental spectra and analysis of the seaweed's elemental composition before and after metal binding, an attempt to characterise the binding can be made. Binding of metals ions on biomaterials having different functional groups depends on ionic properties such as electronegativity, ionisation potential, ionic radius and the redox potential of these metals as well as the composition of the biomass surface [10].

Figueira *et al*. [4] used both FTIR and XPS techniques for studying the mechanism of iron binding to seaweed biomass. Instrumental analysis revealed the chelating character of iron complexation to carboxyl and sulphur groups. Ashkenazy *et al*. [9] used the same techniques for investigating the mechanism of lead biosorption by acid-washed biomass of the yeast *Saccharomyces uvarum*. FTIR analysis showed changes in the carboxyl groups while the XPS analysis showed changes in the concentration of oxygen and nitrogen in the sample. Thus, it was concluded that lead uptake occurred mainly through binding to carboxyl groups as well as nitrogen-containing groups.

Raize *et al*. [3] also used XPS to study binding of cadmium, nickel and lead to the brown seaweed *Sargassum vulgaris*. They found that heavy metal uptake was accompanied by changes in sulphur, nitrogen, oxygen and carbon binding. Significant decreases were also observed for the calcium and magnesium concentrations, which indicated the existence of both chelation and ion-exchange mechanisms.

5.1.3 Objectives of the Research

The main objectives of the work in this chapter are:

- To evaluate the surface morphology of the seaweeds and any changes that may occur after metal binding.
- To identify the elemental composition of the seaweed surface before and after metal binding by both EDX and XPS analysis and hence identify the predominant functionalities in binding.
- To investigate the predominant mechanisms of binding for cations and anions.

5.2 Experimental

5.2.1 Materials and Methods

5.2.1.1 Chemicals

- Sodium Hydroxide (solid) - Ridel de Haën, Germany.
- Hydrochloric Acid (37%) - LabScan Ltd., Dublin, Ireland.
- Analytical grade metal solutions of Cu (II), Cr (III) and Cr (VI) - Sigma-Aldrich Ltd., Dublin, Ireland.

5.2.1.2 Instrumentation

- **Sputter Coater (SEM)** - Unit PS3 Agar Aids for Electron Microscopy.
- Hitachi S4000 SEM/EDX System (Figure 5.3a).
- Kratos AXIS 165 X-ray photoelectron spectrometer. (Figure 5.3b).

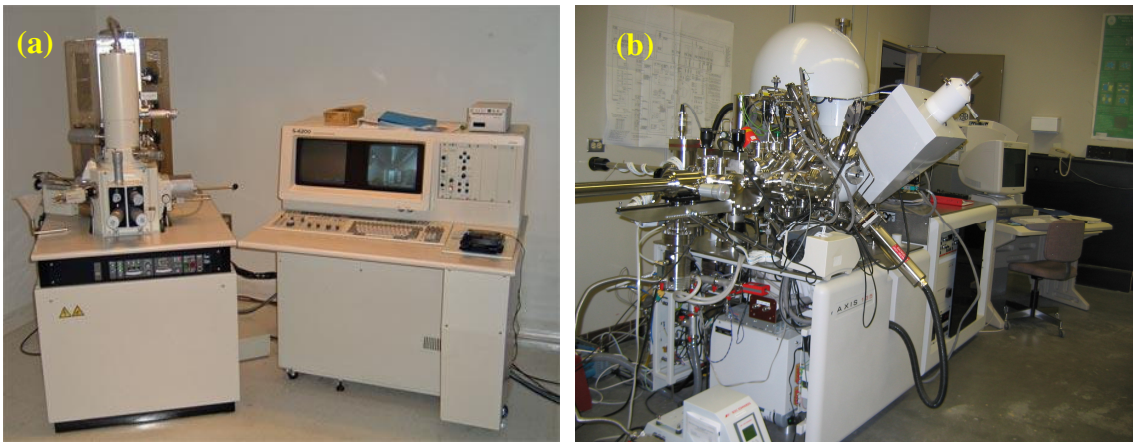

Figure 5.3 (a) Hitachi S4000 SEM System (b) Kratos AXIS 165 X-ray photoelectron spectrometer.

SEM/EDX analysis was carried out in the Tyndall National Institute, Cork as funded under the National Access Programme (NAP), while XPS analysis was carried out in the Materials and Surface Science Institute (MSSI) in the University of Limerick.

5.2.1.3 Exposure to Metal Solutions

Intact raw seaweed samples were oven dried at 60°C for 24h and subsequently exposed to solutions containing 2000mg L^{-1} of each of the metals under investigation, Cu (II), Cr

(III) and Cr (VI). The use of elevated metal concentrations (relative to previous experiments) ensured detection by EDX and XPS techniques.

The biomass was added at a concentration of 2mg mL^{-1} to each solution. The flasks were agitated at 200 rpm and room temperature (21 ± 1°C) for 6h. The solution pH was maintained at pH 5 for Cu (II), pH 4.5 for Cr (III) and pH 2 for Cr (VI). The biomass was then filtered under vacuum and washed thoroughly with distilled water. Samples were dried at 60°C for 24h and stored in airtight polyethylene bags until required.

5.2.2 SEM/EDX

Dehydrated raw and metal exposed seaweed samples were attached to 10 mm diameter metal mounts using carbon tape and sputter coated with gold under vacuum in an argon atmosphere. The coated samples were subsequently analysed using SEM/EDX with a voltage of ~10keV.

5.2.3 XPS

Dehydrated samples were attached to the sample holder using a layer of adhesive tape. The dehydrated raw and metal loaded seaweed samples were examined in high (20eV pass energy) and low resolution (160eV pass energy). High and low resolutions are also referred to as narrow and survey scans respectively. A vacuum of at least 10^{-9} Torr was maintained for all analyses. The instrument was calibrated using an Au $4f_{7/2}$ peak binding energy of 84eV. The binding energies for the XPS spectra were referenced to the hydrocarbon component of the spectrum at 284.8 eV [11]. The XPS spectra were fitted using Gaussian-Lorentzian peak shapes and Shirley's baseline correction function was subtracted [8]. The thickness of the analysed layer was 50-100 Å. For better counting statistics, spectra were taken over multiple sweeps. The resultant spectrum is an averaged sum of the spectra taken during these multiple scans.

5.3 Results and Discussion

5.3.1 SEM Analysis

All SEM micrographs are given at a magnification of 1000X. Results at a higher magnification of 6000X were also obtained, but the focussed beam at higher magnification caused thermal degradation of the samples. Therefore, in all subsequent cases, 1000X was chosen as a suitable magnification. Micrographs shown are representative of those taken over the entire sample surface.

5.3.1.1 Brown seaweeds

The SEM micrographs obtained for raw and metal loaded *Fucus vesiculosus* are shown in Figure 5.4 while those of *Fucus spiralis* are shown in Figure 5.5.

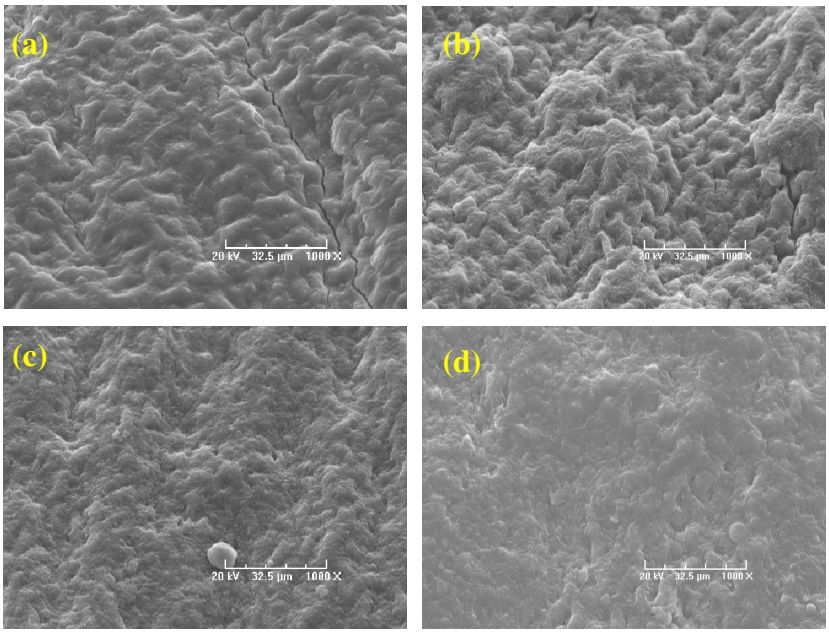

Figure 5.4 SEM micrographs of *Fucus vesiculosus* (a) Raw (b) Cu (II)-loaded (c) Cr (III)-loaded (d) Cr (VI)-loaded. Magnification = 1000X.

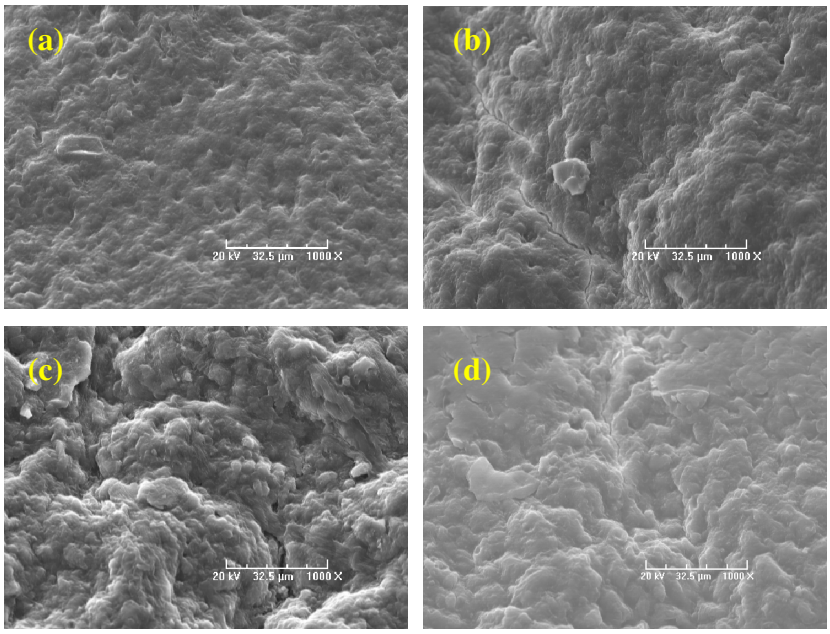

Figure 5.5 SEM micrographs of *Fucus spiralis* (a) Raw (b) Cu (II)-loaded (c) Cr (III)-loaded (d) Cr (VI)-loaded. Magnification = 1000X.

Figures 5.4 and 5.5 reveal some morphological differences between the raw and metal-loaded seaweeds. In both cases, the raw seaweed surface appears smoother than that in the metal-loaded samples with some surface shrinking after metal binding also apparent. The microstructures present in some micrographs (Cr (III)-loaded *Fucus vesiculosus* and raw and Cu (II)-loaded *Fucus spiralis*) may be due to calcium or other crystalloid deposition.

Although the surface appears rougher in the metal loaded seaweeds, it is generally quite difficult to discern the morphological changes in the brown seaweeds in this study. Therefore, comments on any variations between the effects of cation and anion binding are not valid in these cases. Certainly in the case of the brown seaweeds, the qualitative nature of SEM means that little meaningful information on the seaweed surface can be obtained. As a result, a more quantitative estimation of the surface morphology by techniques such as Scanning Force Microscopy would be desirable (See Chapter 7).

The elemental composition of the seaweed surface was simultaneously measured by EDX. The EDX spectra of raw and metal-loaded *Fucus vesiculosus* are shown in Figure 5.6.

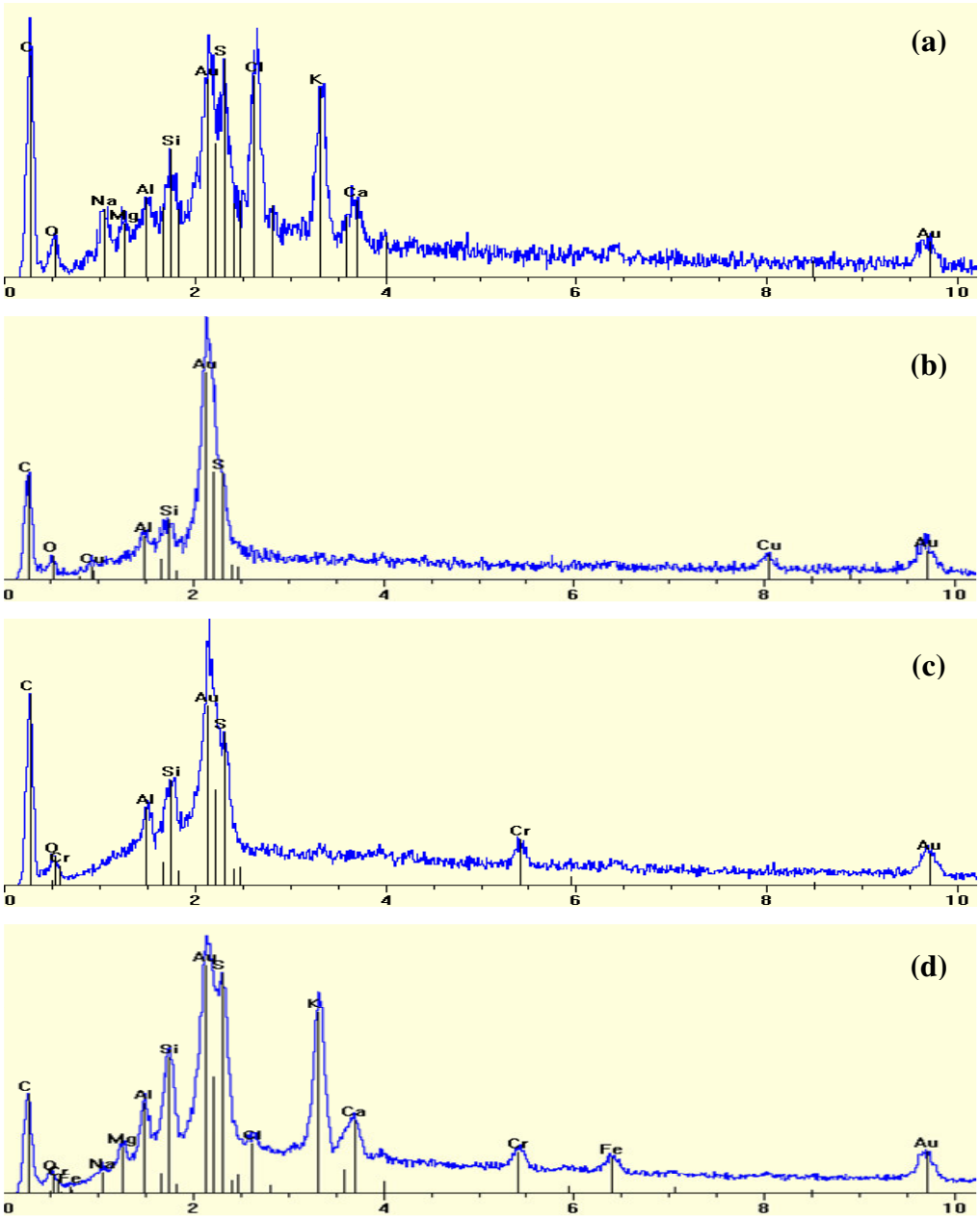

Figure 5.6 EDX spectra of (a) Raw (b) Cu (II)-loaded (c) Cr (III)-loaded (d) Cr (VI)-loaded *Fucus vesiculosus*. Magnification: 1000X.

EDX analysis of the five remaining seaweeds yielded similar spectra to that of *Fucus vesiculosus*. The peaks present in each of the spectra have been summarised in Tables 5.1-5.3.

Table 5.1 Elemental peaks in the EDX spectra of *Fucus vesiculosus* and *Fucus spiralis*.

	Raw	Cu (II)-loaded	Cr (III)-loaded	Cr (VI)-loaded
Fucus vesiculosus				
	Carbon	Carbon	Carbon	Carbon
	Oxygen	Oxygen	Oxygen	Oxygen
	*	**Copper**	**Chromium**	**Chromium**
	Sodium	*	*	Sodium
	Magnesium	*	*	Magnesium
	Sulphur	Sulphur	Sulphur	Sulphur
	Potassium	*	*	Potassium
	Calcium	*	*	Calcium
	*	*	*	Iron
Fucus spiralis				
	Carbon	Carbon	Carbon	Carbon
	Oxygen	Oxygen	Oxygen	Oxygen
	*	**Copper**	**Chromium**	**Chromium**
	Sodium	*	*	Sodium
	Magnesium	*	*	Magnesium
	Sulphur	Sulphur	Sulphur	Sulphur
	Potassium	*	*	Potassium
	Calcium	*	*	Calcium

* Band not observed

Some of the peaks from the EDX spectra in Figure 5.6 and Table 5.1 are not necessarily related to the sample surface. For example Au peaks in EDX spectra originate from the gold sputter coating on the samples while the Al peak that is sometimes detected comes from the sample holder. On the other hand, the iron present in the Cr (VI) spectrum of *Fucus vesiculosus* may be due to some surface contamination of the seaweed from the sampling site.

From Table 5.1 it is seen that binding behaviour was identical for both brown seaweeds.

The raw seaweed spectra had a greater number of peaks than those observed after cation exposure. This is due to the alkali and alkaline earth metals (Na^+, K^+, Ca^{2+} and Mg^{2+}) from seawater being present in the raw biomass.

The Cu (II) and Cr (III) loaded spectra of the brown seaweeds revealed the disappearance of alkali and alkaline earth metal peaks. The disappearance of these metals after cation binding indicates the existence of an ion-exchange mechanism. As this technique has been used only qualitatively and the scale used for the EDX spectra is arbitrary, unless a peak disappears after metal binding, it is difficult to evaluate changes in peak size or intensity. Therefore, even though FTIR analysis indicates the involvement of sulphur and oxygen containing functionalities for Cu (II), Cr (III) and Cr (VI), it is not possible to evaluate metal interactions with these elements due to the existence of these peaks after metal binding.

Cr (VI)-loaded spectra showed the present of all ions initially found on the seaweed surface indicating that ion-exchange did not appear to be the dominant binding mechanism for hexavalent chromium to these seaweeds. The mechanism of Cr (VI) binding was thus investigated using XPS analysis (Section 5.3.2).

The oxidation states of bound chromium in Cr (III) and Cr (VI)-loaded samples could not be differentiated using EDX analysis and therefore, positive identification of the presence of chromium on the seaweed surface was all that was possible in these cases.

5.3.1.2 Green seaweeds

In contrast to the brown seaweeds, significant morphological differences between the raw and metal-loaded seaweeds were apparent in the green species. Figure 5.7 shows the SEM micrographs obtained for *Ulva lactuca*.

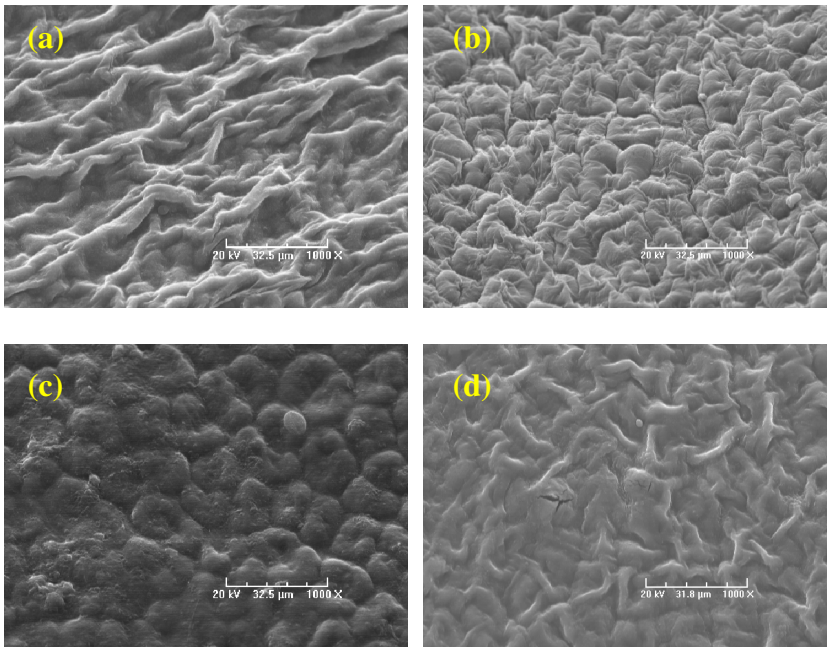

Figure 5.7 SEM micrographs of *Ulva lactuca* (a) Raw (b) Cu (II)-loaded (c) Cr (III)-loaded (d) Cr (VI)-loaded. Magnification: 1000X.

The raw seaweed (a) shows evidence of fold structures arranged in quite a regular pattern on the surface while these are not present in the Cu (II) or Cr (III)-loaded images. However, the Cr (VI)-loaded surface is more similar to the raw seaweed in terms of morphology than to either of the other metal-loaded seaweeds perhaps indicating variations in cation and anion binding mechanisms.

After cation loading in (b) and (c), large visible morphological changes are apparent with the formation of mound-like structures seen in these micrographs. These results are in agreement with the work of Chen *et al.* [12] who observed a change in surface morphology of a Ca-alginate based resin after Ca^{2+} ions were replaced with Cu^{2+} ions. In that case, an apparently smoother surface was observed for the Cu (II)-loaded biomass

and it was postulated that this morphological change was related to the metal's ionic radius and coordination sphere.

It has been shown that Cu^{2+} offers a smaller coordination sphere than Ca^{2+} since Cu^{2+} has a smaller ionic radius than Ca^{2+} (0.71 Å for Cu^{2+} as opposed to 1.14 Å for Ca^{2+} {Cotton, 1999 399 /id}). Therefore, the coordination sphere of Cu^{2+} would incorporate a smaller number of hydroxyl and carboxyl groups than that of Ca^{2+} [12] and as a result the polymer chains become less twisted or folded in the Cu^{2+} bound matrix.

This appears to be the case for both the Cu (II) and Cr (III)-loaded seaweed leading to the visible morphological differences in SEM micrographs. The ionic radius of Cr^{3+}, at 0.63 Å {Cotton, 1999 399 /id} is again significantly smaller than that of Ca^{2+} and it would be expected that effects similar to Cu (II) binding may take place. Qualitative estimates of the Cr (III) loaded seaweed indicate a flattening of the surface relative to even the Cu (II) loaded seaweed. Again, this possibly relates to the smaller coordination sphere of Cr^{3+} relative to Cu^{2+}. Confirmation of these measurements could be obtained by the use of a quantitative technique such as scanning force microscopy.

The ionic radius of Cr (VI) was shown to be 0.58 Å [14]. The ridge structures originally present in the raw seaweed are still visible in the Cr (VI)-loaded seaweed (d) albeit to a lesser extent indicating that some changes in surface structure have taken place after Cr (VI) binding.

Similarly to *Ulva lactuca*, significant differences in surface morphology are observed between raw and metal-loaded samples of *Ulva* spp. (Figure 5.8).

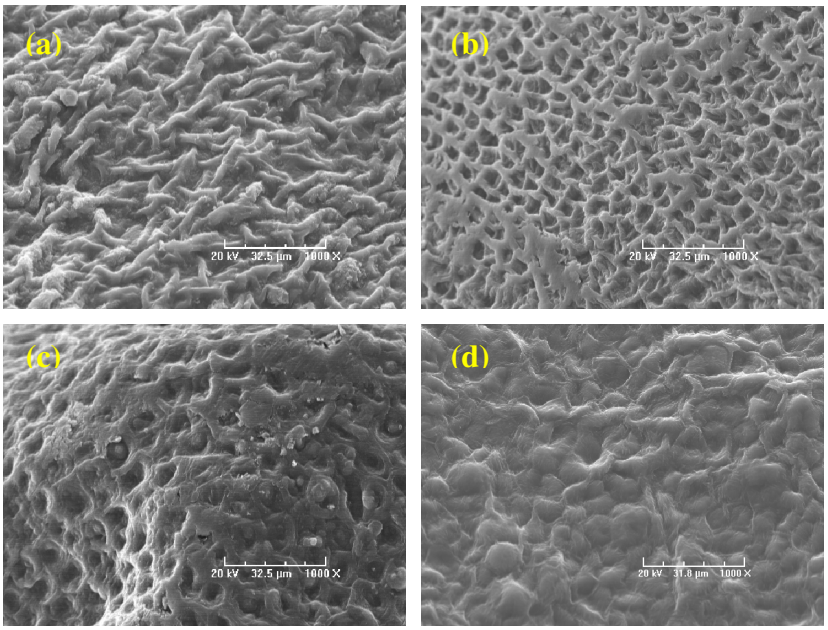

Figure 5.8 SEM micrographs of *Ulva* spp. (a) Raw (b) Cu (II)-loaded (c) Cr (III)-loaded (d) Cr (VI)-loaded. Magnification: 1000X.

Raw *Ulva* spp. (a) contains chain structures similar to those observed for raw *Ulva lactuca*. However, in *Ulva* spp. these chains appear to be smaller in size and are arranged in a more random pattern than in *Ulva lactuca*. SEM images of the Cu (II) and Cr (III) samples (b) and (c) reveal honeycomb-like structures which may indicate significant changes in the surface structure. These changes may again be related to differences in the ionic radii of the ions resulting in differences in coordination spheres. Differences between the structure observed in cation-loaded *Ulva lactuca* and cation-loaded *Ulva* spp. indicate that metal binding behaviour is different for different species in the same genus. This is most likely due to surface compositional differences between the seaweeds.

Cr (VI)-loaded *Ulva* spp. does show differences in morphology to the raw seaweed as well as to the other metal loaded samples. Some ridge structures are still present, but the seaweed surface appears to be smoother than that observed for the raw seaweed. Again, this points to differences between cation and anion binding to seaweeds.

The presence of the ridge structures in the raw green seaweeds compares favourably with specific surface area values in Chapter 2 as *Ulva lactuca* and *Ulva* spp. were shown to have increased specific surface areas relative to the brown seaweeds. Table 5.2 summarises the significant peaks observed in the EDX spectra of the raw and metal loaded green seaweeds.

Table 5.2 Elemental peaks in the EDX spectra of *Ulva lactuca* and *Ulva* spp.

	Raw	**Cu (II)-loaded**	**Cr (III)-loaded**	**Cr (VI)-loaded**
Ulva lactuca				
	Carbon	Carbon	Carbon	Carbon
	Oxygen	Oxygen	Oxygen	Oxygen
	*	**Copper**	**Chromium**	**Chromium**
	Sodium	*	*	Sodium
	Magnesium	*	*	Magnesium
	Sulphur	Sulphur	Sulphur	Sulphur
	Calcium	*	*	Calcium
***Ulva* spp.**				
	Carbon	Carbon	Carbon	Carbon
	Oxygen	Oxygen	Oxygen	Oxygen
	*	**Copper**	**Chromium**	**Chromium**
	Sodium	*	*	Sodium
	Magnesium	*	*	Magnesium
	Sulphur	Sulphur	Sulphur	Sulphur
	Calcium	*	*	Calcium

* Band not observed

Metal binding was identical for both green species with the alkali and alkaline earth metals disappearing upon Cu (II) and Cr (III) binding. This indicated that, similarly to the brown seaweeds, an ion-exchange mechanism is significant in cation binding to green seaweeds. However, in contrast to the brown seaweeds, potassium was absent from the raw seaweeds and no traces of iron were found on the seaweed surface.

Again, the Cr (VI)-loaded spectrum showed no discernable change in the elemental composition of the sample.

5.3.1.3 Red Seaweeds

Figures 5.9 and 5.10 illustrate the SEM micrographs of raw and metal-loaded *Palmaria palmata* and *Polysiphonia lanosa* respectively.

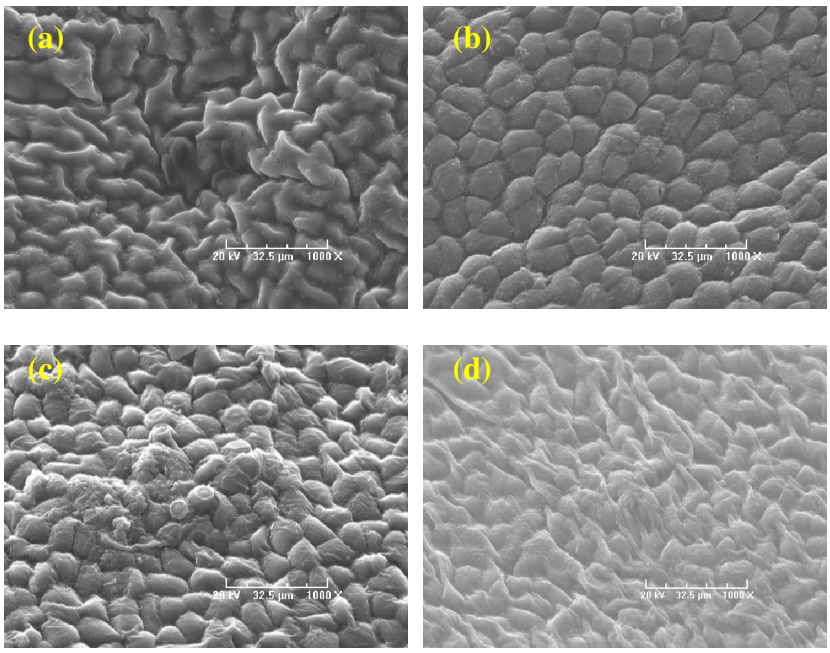

Figure 5.9 SEM micrographs of *Palmaria palmata* (a) Raw (b) Cu (II)-loaded (c) Cr (III)-loaded (d) Cr (VI)-loaded. Magnification: 1000X.

The raw seaweed (a) contains some fold structures similar to those observed in the green seaweeds but in *Palmaria palmata* these structures are fewer and less pronounced giving the surface a "folded" appearance. The Cu (II) and Cr (III) micrographs displayed similar characteristic patterns with an apparently smoother surface than for the raw seaweed. Similarly to *Ulva lactuca*, the cation loaded seaweeds reveal the formation of mound-like structures indicating changes in surface folding. Again, it is fair to postulate that the changes in surface morphology are related to changes in the polymer chains after cation binding. However, in order to obtain a more quantitative estimate of this, another technique such as scanning force microscopy is required.

The SEM micrograph of Cr (VI)-loaded *Palmaria palmata* shows some small changes in surface morphology which are quite distinct from cation loaded samples. In contrast to

the cation-loaded seaweeds, Cr (VI) - binding to *Palmaria palmata* appears to increase the surface roughness by precipitating the formation of ridge structures on the seaweed surface.

Figure 5.10 illustrates the SEM micrographs obtained for raw and metal-loaded *Polysiphonia lanosa*.

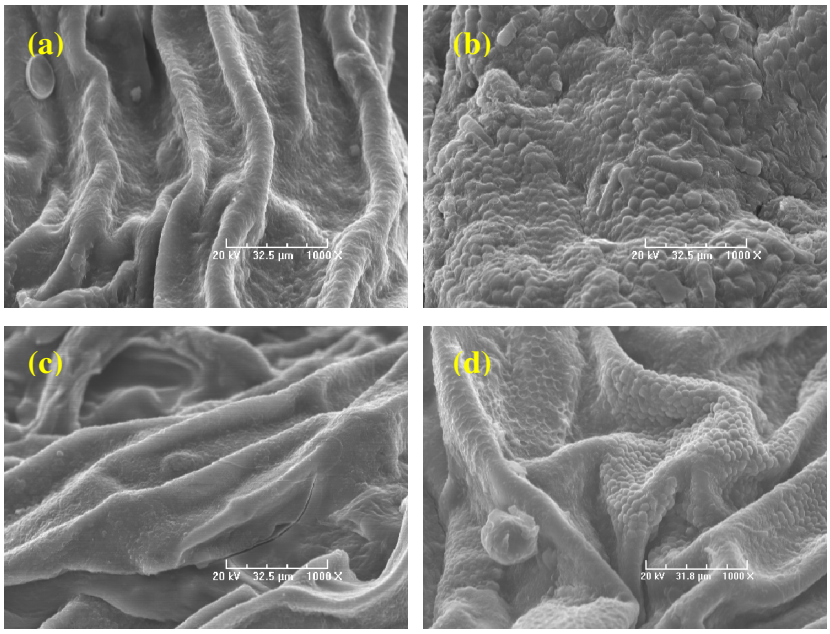

Figure 5.10 SEM micrographs of *Polysiphonia lanosa* (a) Raw (b) Cu (II)-loaded (c) Cr (III)-loaded (d) Cr (VI)-loaded. Magnification: 1000X.

Similarly to the green seaweeds, SEM micrographs of *Polysiphonia lanosa* revealed the presence of folds on the seaweed surface. Again, this correlates with the increased specific surface area found in Chapter 2 for *Polysiphonia lanosa*.

The Cu (II)-loaded sample shows a significant change in morphology to the raw, Cr (III) and Cr (VI) images. The Cu (II)-loaded micrograph reveals a much flatter surface morphology with no evidence of the fold-like structures observed in the raw or chromium loaded seaweed surface. As previously discussed, if an ion-exchange mechanism is operating for Cu (II) uptake, Cu^{2+} ions may replace Ca^{2+} ions initially present in the cell

wall, thus incorporating smaller numbers of hydroxyl and carboxyl groups into its coordination sphere. Therefore, the polymer chains are less twisted in the Cu (II)-loaded seaweed possibly accounting for the change in surface morphology observed in the SEM micrograph. However, this does not appear to agree with the results obtained for Cr (III)

Similarly to *Palmaria palmata*, Cr (VI) binding to *Polysiphonia lanosa* appears to bring about an increase in surface roughness compared to the raw seaweed by altering the surface folding of polymer chains. This result is in contrast to those obtained for the green seaweeds and requires further investigation by SFM.

Table 5.3 summarises the significant peaks observed in the EDX spectra of raw and metal loaded red seaweeds.

Table 5.3 Elemental peaks in the EDX spectra of *Palmaria palmata* and *Polysiphonia lanosa*

	Raw	**Cu (II)-loaded**	**Cr (III)-loaded**	**Cr (VI)-loaded**
Palmaria palmata				
	Carbon	Carbon	Carbon	Carbon
	Oxygen	Oxygen	Oxygen	Oxygen
	*	**Copper**	**Chromium**	**Chromium**
	Sulphur	*	Sulphur	Sulphur
	Potassium	*	*	Potassium
	Calcium	*	*	Calcium
Polysiphonia lanosa				
	Carbon	Carbon	Carbon	Carbon
	Oxygen	Oxygen	Oxygen	Oxygen
	*	**Copper**	**Chromium**	**Chromium**
	Sulphur	*	Sulphur	Sulphur
	Potassium	*	*	Potassium
	Calcium	*	*	Calcium

* Band not observed

Sodium and magnesium were absent from the raw seaweeds. In contrast to the brown and green seaweed species, Cu (II) binding to both red seaweeds brought about the

disappearance of the sulphur peak in the EDX spectrum. This indicated significant interactions between Cu (II) ions and sulphur-containing groups (e.g. sulphonate) on the biomass surface. However, no change in the sulphur peak was evident for the Cr (III) or Cr (VI)-loaded samples. This is in agreement with FTIR results (Chapter 4) which showed that, at 200 μg L^{-1}, Cu (II) had a greater interaction with sulphonate groups in red seaweeds than Cr (III) or Cr (VI). As found with the brown and green species, cation loaded red seaweeds also showed the disappearance of potassium and calcium indicating the existence of an ion-exchange mechanism. On the other hand, no change in the elemental composition was seen for the Cr (VI)-loaded sample.

5.3.1.4 Overview of SEM/EDX results

When raw seaweed samples were exposed to metal solutions, metal cations may have replaced some Ca^{2+} and Mg^{2+} in the cell wall via an ion-exchange mechanism.

Raize *et al*. [3] proposed that replacement of these ions with metal cations altered the nature of the cross-linking due to stronger electrostatic and coordinative bonding between the metal and the negatively charged groups in the cell wall polymers.

This is supported by experimental data in this study where the disappearance of not only calcium and magnesium peaks, but also sodium and potassium peaks was observed in the cation-loaded EDX spectra. Thus, it appears that changes in the cross-linking behaviour, linked to the metal's coordination sphere, resulted in visible morphological changes in the seaweed surface.

5.3.2 XPS Analysis

While EDX results in this study offer a qualitative estimation of the elemental changes in the seaweed surface, XPS offers a more quantitative picture of these changes. XPS analysis may also act as verification for the results obtained in FTIR and EDX analysis as well as being a means of elucidating metal binding mechanisms in seaweeds.

5.3.2.1 Cu (II) Analysis

Ulva lactuca and *Polysiphonia lanosa* have been selected as example species for Cu (II) binding. Table 5.4 shows the changes in atomic concentrations of the various elements after Cu (II) binding. Only the elements of importance to binding are shown.

Table 5.4 XPS atomic concentration in *Ulva lactuca* and *Polysiphonia lanosa* before and after exposure to Cu (II) ions. Percentage changes in concentration between the raw and Cu (II)-loaded samples are given in parentheses.

Element	Atomic concentration (%)			
	Ulva lactuca		*Polysiphonia lanosa*	
	Raw	**Cu (II)**	**Raw**	**Cu (II)**
C	56.11	60.95 **(+ 9)**	59.18	63.45 **(+ 7)**
Ca	0.89	Not detected **(-100)**	0.57	0.02 **(- 96)**
K	Not detected	Not detected	0.35	Not detected **(-100)**
Mg	0.55	Not detected **(-100)**	Not detected	Not detected
N	2.01	3.18 **(+ 58)**	6.83	3.9 **(- 43)**
Na	1.55	Not detected **(- 100)**	Not detected	Not detected
O	29.02	24.52 **(-16)**	29.00	20.68 **(- 29)**
S	1.22	0.41 **(- 66)**	0.82	0.91 **(+ 11)**
Cu	Not detected	0.17	Not detected	0.12

XPS findings revealed that Cu (II) binding to these seaweeds is accompanied by changes in sulphur, nitrogen, oxygen and carbon binding indicating that Cu (II) ions interact with functional groups containing these elements. This is in agreement with FTIR analysis which revealed that amino, carboxyl, sulphonate and alcohol groups were involved in Cu (II) binding to both *Ulva lactuca* and *Polysiphonia lanosa*. The decrease in the concentrations of alkali and alkaline earth metals supports the theory of an ion-exchange mechanism, in addition to coordination with various functional groups on the biomass. This is in agreement with EDX and FTIR results previously obtained for Cu (II) binding to *Ulva lactuca* and *Polysiphonia lanosa*.

The fact that the decreases in oxygen concentration were larger than the quantity of Cu (II) bound to the seaweeds also indicates that there may be a degree of multidentism in metal binding with oxygen-containing functionalities. Again, this agrees with the bidentate complexation found for Cu (II) binding in the FTIR study (Chapter 4)

Potentiometric titrations revealed that *Ulva lactuca* and *Polysiphonia lanosa* contained the same quantity of acidic binding sites, both total (1.81 mmol g^{-1}) and weak (1.62 mmol g^{-1}). However, XPS analysis revealed that a greater quantity of Cu (II) was bound to *Ulva lactuca*. This is in agreement with isotherm analysis which showed that *Ulva lactuca* had a $\boldsymbol{q}_{\mathbf{max}}$ value of 0.69 mmol g^{-1} while that of *Polysiphonia lanosa* was marginally lower at 0.61 mmol g^{-1}.

Because carbon containing functionalities such as carboxyl groups have been shown to be important in Cu (II) binding to seaweeds, changes in the binding energy of the coordination carbon atom (C1*s*) in the biomass were studied. Figure 5.11 shows the C1s spectra obtained for raw and Cu (II)-loaded *Ulva lactuca* and *Polysiphonia lanosa*.

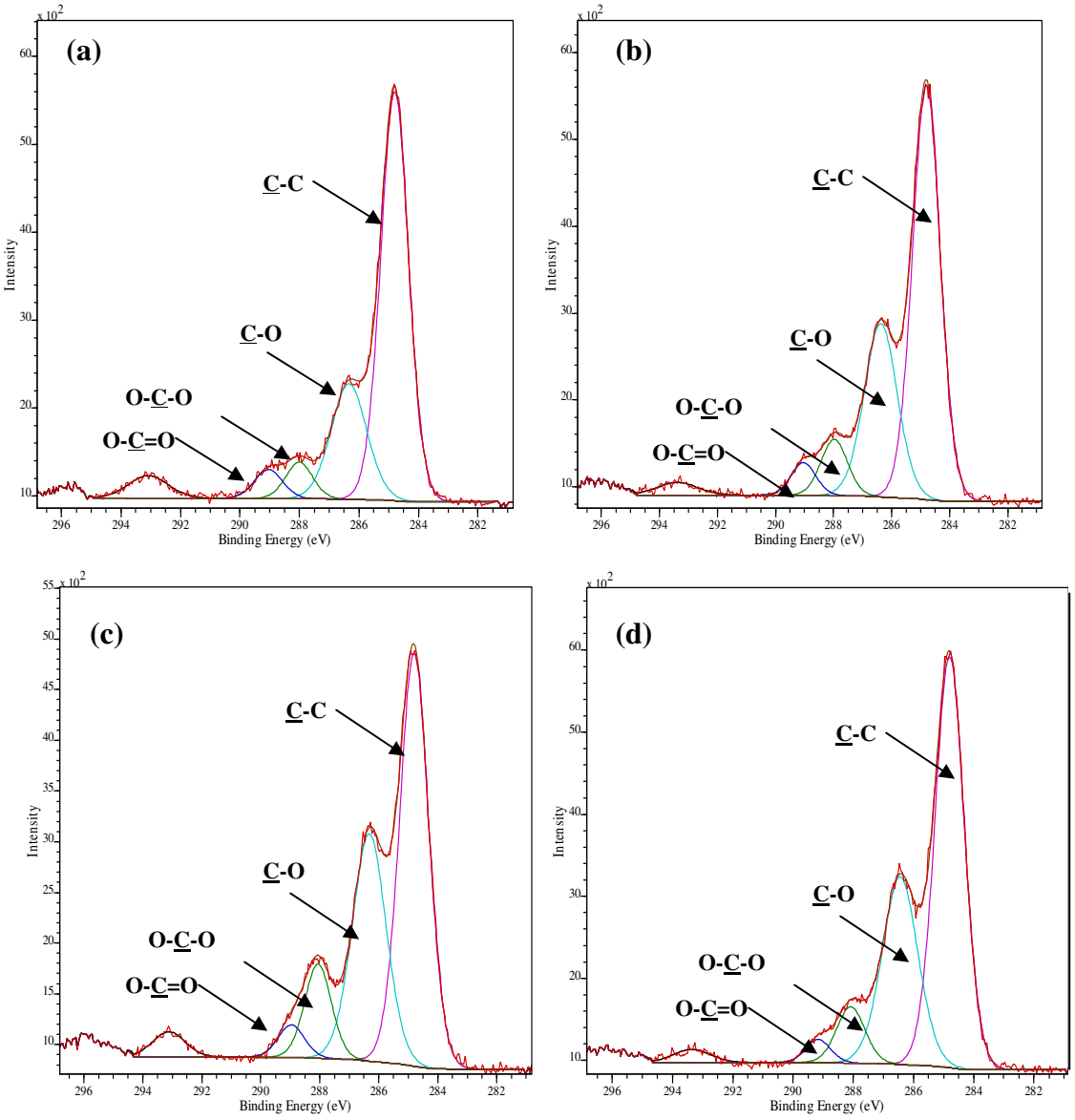

Figure 5.11 C1s spectra (a) Raw *Ulva lactuca* (b) Cu (II)-loaded *Ulva lactuca* (c) Raw *Polysiphonia lanosa* (d) Cu (II)-loaded *Polysiphonia lanosa*.

The arbitrary units on the y-axis describe the number of electrons arriving on the detector per unit time versus binding energy (BE) [8]. Chemical shifts were considered significant when they exceeded 0.5 eV.

Figure 5.11 shows that the carbon 1*s* spectra of both *Ulva lactuca* and *Polysiphonia lanosa* comprise four peaks of binding energies of 284.8 eV, 286.3 eV, 288.0 eV and 289.0 eV respectively. Peaks were identified via deconvolution.

The peak with a binding energy of 284.8 eV relates to hydrocarbon groups which are used for energy calibration [1]. The remaining peaks can be assigned to C-O, O-C-O and O=C-O which correspond to alcoholic, ether and carboxylate groups [15]. The variation in binding energies occurs because the carbon atoms in these three functional groups possess slightly different electron densities [16].

Table 5.5 summarises the carbon 1s binding energies and peak area ratios obtained for raw and Cu (II)-loaded *Ulva lactuca* and *Polysiphonia lanosa*. No significant changes (> 0.5eV) in carbon peak energies were observed after Cu (II) binding to these seaweeds.

Table 5.5 Carbon 1s binding energies and peak area ratios for *Ulva lactuca* and *Polysiphonia lanosa*.

Biomass	Assignment of C1s peak	Peak (eV)	Peak Area Ratio (%)	
			Raw	Cu (II)-loaded
Ulva lactuca	C-C	284.80	65.84	58.80
	C-O	286.34	23.80	29.34
	C-O-C	288.01	5.67	7.69
	O=C-O	289.04	4.68	4.15
Polysiphonia lanosa	C-C	284.80	51.97	57.57
	C-O	286.37	33.35	32.03
	C-O-C	287.98	10.93	7.65
	O=C-O	289.03	3.74	2.74

From Table 5.5 it is seen that the proportion of C-C groups decreases in *Ulva lactuca* after Cu (II) binding, possibly indicating some slight loss in organic content.

On the other hand, increases in the C-C content in *Polysiphonia lanosa* after Cu (II) binding may point to some surface contamination during the process [16].

The area distribution of the peaks implies that, excluding C-C groups, the alcohol groups are the most abundant in both *Ulva lactuca* and *Polysiphonia lanosa.*

The area of the carboxyl peak decreased after Cu (II) binding to *Ulva lactuca* (4.68 to 4.15%) and *Polysiphonia lanosa* (3.74 to 2.74%) indicating that the formation of carboxyl-metal complexes had taken place. In these complexes, the oxygen atom donates electrons to metal ions and thus the electron density at the adjacent carbon decreases [16]. This agrees with FTIR findings which showed carboxyl group interactions to be one of the most important in Cu (II) binding to these seaweeds.

For *Polysiphonia lanosa*, the area ratio of the ether carbon decreased after metal sorption. This is indicative of the formation of ether–metal complex species, in which the ether oxygen donates electrons to metal ions and therefore the electron density at the adjacent two carbon atoms decreases [17] causing an increase in binding energy. When coordination complexes are formed with metal ions, the ether group would undergo the largest change of the three functional groups [17]. The C-O-C angle of an ether group will expand to a certain extent upon coordination to a transition metal ion bringing about a change in binding energy. However, in contrast, an increase in the area ratio was seen for the ether peaks in *Ulva lactuca*.

Interactions with biomass ether groups were not apparent in the FTIR spectra for Cu (II) binding to either *Ulva lactuca* or *Polysiphonia lanosa*. However, this may have been due to the lower metal concentrations used in FTIR work.

After Cu (II) binding, an increase in peak area ratio was observed for the alcohol peak of *Ulva lactuca* (23.80 % to 29.34 %) while the peak area decreased slightly in *Polysiphonia lanosa* (33.35 % to 32.03 %). Changes in this peak implied that there was some interaction between the alcoholic groups and metal cations in both cases. This result is in agreement with FTIR findings for *Polysiphonia lanosa* which showed interactions between Cu (II) ions and alcohol groups on the surface. However, this is not the case for

Ulva lactuca. Again, low metal concentrations in FTIR may be responsible for this difference.

High resolution O, 1s XPS spectra of the raw and Cu (II)-loaded seaweeds were also obtained but peak deconvolution was not carried out.

Ulva lactuca exhibited a peak shift from 532 to 532.5 eV, while the shift observed for *Polysiphonia lanosa* was from 532 to 533eV. This indicated involvement of oxygen containing functionalities in Cu (II) binding and agrees with the results in Table 5.4 which showed that Cu (II) binding to *Polysiphonia lanosa* brought about a greater decrease in the oxygen concentration (29%) than *Ulva lactuca* (16%).

Therefore, to summarise the results obtained for Cu (II) binding to *Ulva lactuca* and *Polysiphonia lanosa*, it was seen that Cu (II) was coordinated to groups containing oxygen, sulphur and nitrogen and also took part in an ion-exchange mechanism with the alkali and alkaline earth metals in raw biomass.

5.3.2.2 Cr (VI) Analysis

Although it was possible to identify the presence of chromium on the seaweed surface using EDX analysis, it was not possible to determine the oxidation state in which the chromium was bound. On the other hand, XPS analysis can give an indication of the local oxidation states and chemical bonding environment of the material under investigation. Also, while EDX gave an indication of an ion-exchange mechanism for Cu (II) and Cr (III), it yielded little information on the Cr (VI) binding mechanism.

Therefore XPS was further used in this work to investigate the binding of Cr (VI) to the seaweeds under investigation and in particular to determine the oxidation state in which chromium was bound.

Studies by a number of authors have investigated hexavalent chromium binding to various biomass types [18-21]. While much of this work studied the kinetics and equilibrium behaviour of Cr (VI) binding [22-24], a number of authors have studied the potential of various biomasses including bacteria [25], microalgae [26] and macroalgae [27] to bio-reduce hexavalent chromium. Dambies *et al*. [28] also analysed Cr (VI) reduction by chitosan in various formats. It was shown that chitosan beads which had been cross-linked with glutaraldehye completely reduced Cr (VI) to Cr (III) while raw beads reduced only 60%.

Lytle *et al*. [29] reported that Cr(VI) taken from the fine lateral roots of wetland plants was rapidly reduced to Cr(III). Gardea- Torresdey *et al*. [30] reported that Cr(VI) could potentially bind to an oat byproduct, but could be easily reduced to Cr(III) by positively charged functional groups, and be subsequently bound by available carboxyl groups. Park *et al*. [31] also reported that Cr(VI) was completely reduced to Cr(III) by contact with the brown seaweed *Ecklonia* biomass below pH 5.

Three seaweeds, namely, *Fucus vesiculosus*, *Palmaria palmata* and *Ulva* spp. have been chosen as representative examples for discussion of Cr (VI) binding behaviour. The

atomic concentration of surface elements after Cr (VI) binding is given in Table 5.6. Results for the raw seaweeds from MSSI are awaited.

Table 5.6 XPS atomic concentration of the relevant elements in the seaweeds after Cr (VI) exposure.

	% Atomic Concentration		
	Fucus vesiculosus	***Palmaria palmata***	***Ulva spp.***
C 1s	75.75	63.71	60.18
N 1s	0.39	4.59	6.74
O 1s	22.15	29.77	32.05
S 2p	0.57	0.79	0.28
Cr 2p	1.13	1.14	0.76

Because, they did not show any participation in Cr (VI) binding in EDX spectra, the alkaline earth metals and alkali metals have been omitted from the discussion. The percentage atomic concentrations in Table 5.7 give an indication of the total chromium bound and not necessarily the oxidation state in which it was bound.

Results indicated that similar amounts of chromium were bound to both *Fucus vesiculosus* and *Palmaria palmata* (1.13 and 1.14% respectively) while a lower amount was bound to *Ulva* spp. (0.76%).

These results agree with earlier isotherm results which showed that *Fucus vesiculosus* and *Palmaria palmata* had similar q_{max} values (0.68 and 0.65 mmol g^{-1} respectively) for Cr (VI) sorption while *Ulva* spp had a q_{max} value of 0.58 mmol g^{-1}.

Figure 5.12 shows the C1s spectra obtained for Cr (VI)-loaded seaweeds while the corresponding peak area distributions of the raw and Cr (VI)-loaded seaweeds are summarised in Table 5.7.

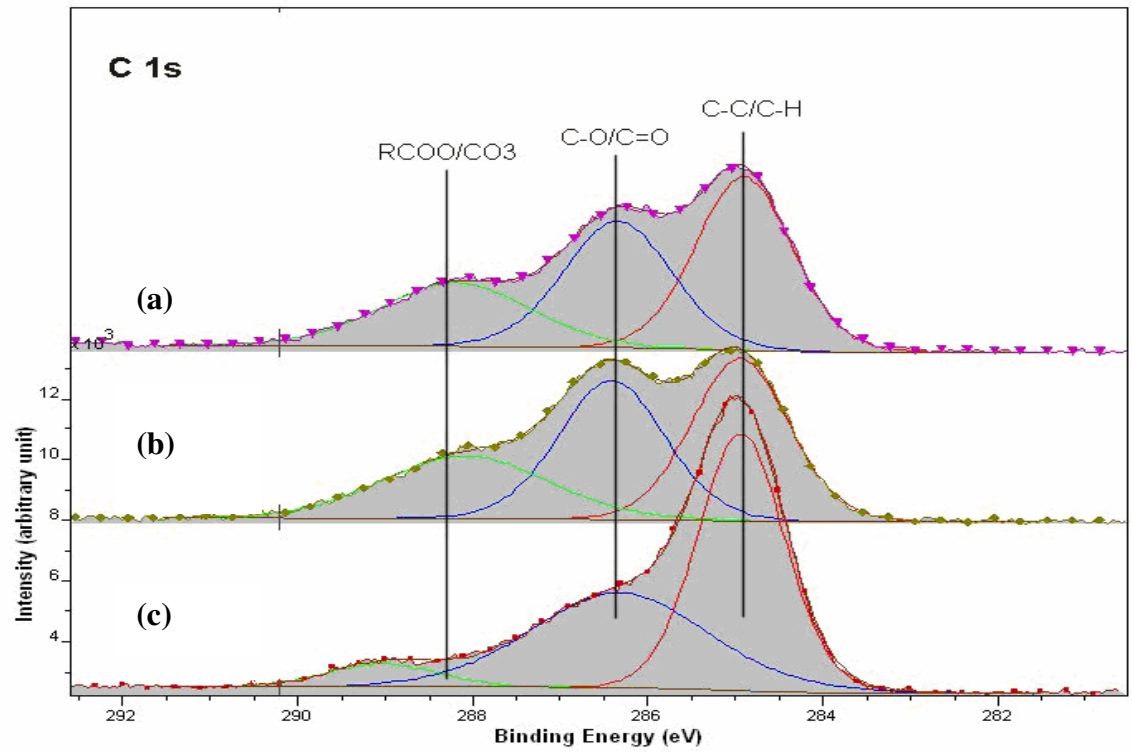

Figure 5.12 **C1s spectra of Cr (VI)-loaded (a) *Ulva* spp. (b) *Palmaria palmata* (c) *Fucus vesiculosus*.**

Table 5.7 **C1s binding energies and peak area ratios for Cr (VI)-loaded *Fucus vesiculosus*, *Palmaria palmata* and *Ulva* spp.**

	Position (eV)	**% Atomic Concentration**
Fucus vesiculosus		
C-C	284.93	53.60
C-O	286.33	40.36
R-COO	289.02	**6.05**
Palmaria palmata		
C-C	284.94	38.54
C-O	286.41	36.17
R-COO	288.09	**25.29**
Ulva spp.		
C-C	284.90	42.05
C-O	286.34	34.52
R-COO	288.20	**23.43**

From Figure 5.12, it is clear that the carboxyl peak in *Fucus vesiculosus* is shifted to a higher binding energy than the other seaweeds after Cr (VI) binding. This may be due to stronger interactions between the carboxyl groups and Cr (VI) in *Fucus vesiculosus* which decrease the electron density on the adjacent carbon atom thus raising the binding energy of the group.

The binding energy of the carboxyl groups in *Ulva* spp. is also marginally higher than that *Palmaria palmata* perhaps indicating that the shift in binding energy may be related to the quantity of carboxyl groups in the seaweed. From Table 2.1, *Fucus vesiculosus* contained 2.00 mmol g^{-1} carboxyl groups while *Ulva* spp. and *Palmaria palmata* contained 1.50 and 1.12 mmol g^{-1} respectively.

Although titrations show increased carboxyl content in the brown seaweeds, Table 5.8 reveals that the carboxyl content (in terms of area distribution) in Cr (VI)-loaded *Fucus vesiculosus* is significantly lower than that of either *Ulva* spp. or *Palmaria palmata*. This indicates that carboxyl groups play an extremely significant role in Cr (VI) binding to brown seaweeds and to a lesser extent in the green and red seaweeds.

Ether bands are not visible in the Cr (VI) loaded C1s spectra in Figure 5.12. Again, this may have been due to the formation of metal-ether complexes which raised the binding energy of these groups rendering the peaks indistinguishable from the carboxyl bands.

The chromium 2p spectra obtained for the Cr (VI)-loaded seaweeds is shown in Figure 5.13.

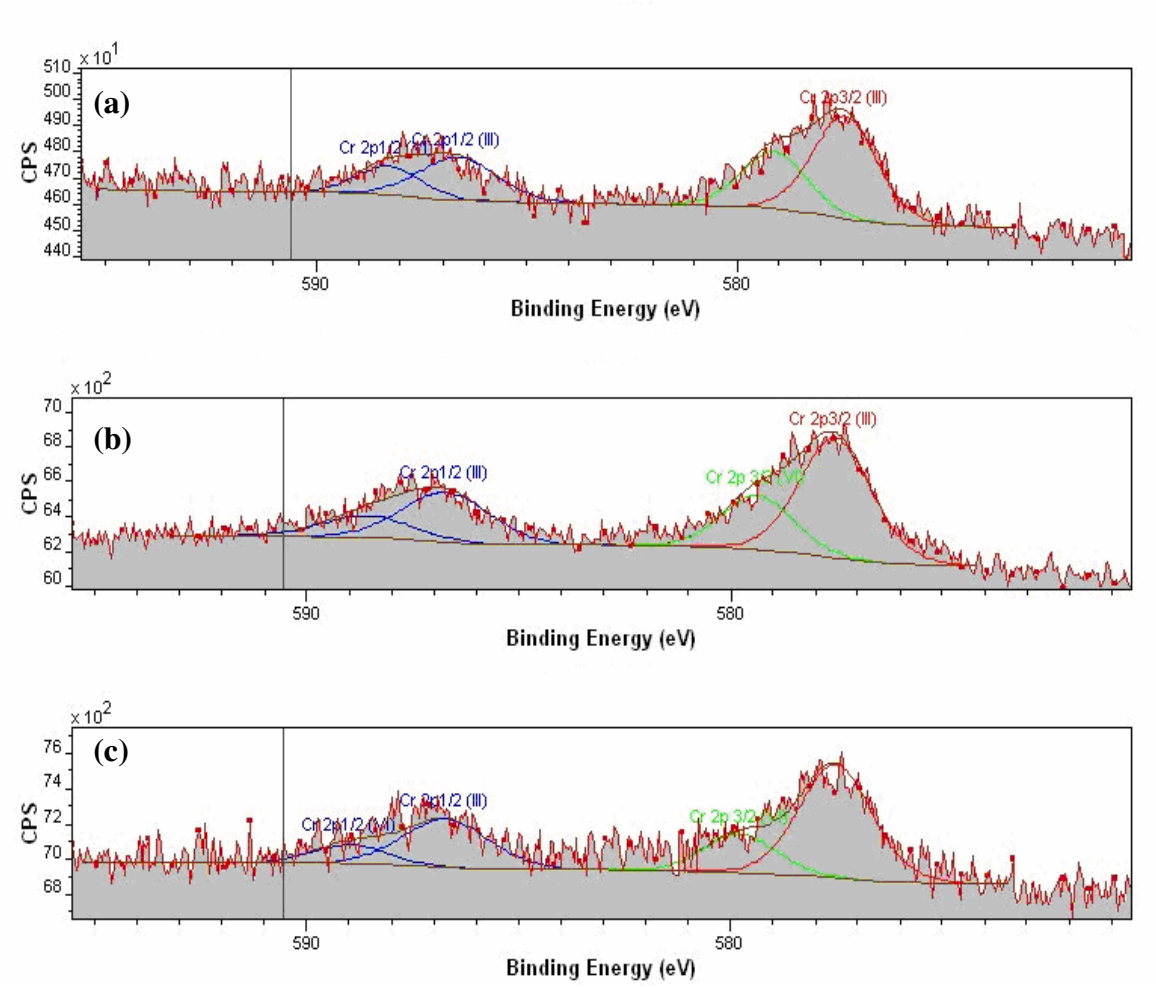

Figure 5.13 Cr 2p XPS spectra of (a) *Fucus vesiculosus* (b) *Palmaria palmata* (c) *Ulva* spp.

As previously seen in Table 5.7, high resolution spectra showed the presence of chromium on the biomass after metal loading. Dambies *et al*. [28] reported that the Cr 2p3/2 orbitals are assigned at 577.2 eV ($CrCl_3$) and 576.2–576.5 eV (Cr_2O_3) for Cr(III) compounds, while Cr(VI) forms are characterised by higher binding energies such as 578.1 eV (CrO_3) or 579.2 eV ($K_2Cr_2O_7$). Therefore, by comparing the peaks observed for each species, it is possible to establish whether chromium is bound to the biomass in trivalent or hexavalent form. Chromium binding data is summarised in Table 5.8.

Table 5.8 Cr 2p binding data from high resolution spectra of three seaweeds exposed to Cr (VI).

Sample	Name	Position (eV)	% Atomic Concentration	Cr (III) / Cr (VI) Ratio
Fucus vesiculosus	Cr 2p3/2 (III)	577.42	32.93	1.79
	Cr 2p1/2 (III)	586.62	31.28	
	Cr 2p 3/2 (VI)	579.11	18.36	
	Cr 2p1/2 (VI)	588.31	17.43	
Palmaria palmata	Cr 2p3/2 (III)	577.53	35.06	2.22
	Cr 2p1/2 (III)	586.73	33.90	
	Cr 2p 3/2 (VI)	579.37	15.78	
	Cr 2p1/2 (VI)	588.57	15.26	
***Ulva* spp.**	Cr 2p3/2 (III)	577.52	38.02	2.97
	Cr 2p1/2 (III)	586.72	36.77	
	Cr 2p 3/2 (VI)	579.77	12.82	
	Cr 2p1/2 (VI)	588.97	12.40	

For all seaweeds, significant bands were present at ~577 eV and ~586 eV. The former corresponds to Cr 2p3/2 orbitals, the latter to Cr 2p1/2 orbitals. Thus, the presence of Cr (III) was apparent in the Cr-laden biomass.

However, the presence of Cr (VI) was also detected on the biomass surface with peaks at 579.11 eV and 588.57 eV, corresponding respectively to Cr 2p3/2 and 2p1/2 orbitals. Despite the presence of noise peaks in the spectra a rough estimation of the ratio of Cr (III) to Cr (VI) on the biomass surface was obtained.

The presence of reduced chromium in all three seaweeds indicates that it is not simply brown seaweeds that posses the ability to reduce hexavalent chromium. The reduction capacity of brown seaweeds such as *Ecklonia* has been well documented by Park *et al.*

[31-33] but no work has been found on Cr (VI) reduction by red and green seaweeds. In all cases the presence of Cr (III) on the seaweed surface was much larger than that of Cr (VI) with *Ulva* spp. possessing almost three times the quantity of Cr (III) to Cr (VI). This indicated that significant bio-reduction had taken place in these seaweeds.

The magnitude of the Cr (III)/ Cr (VI) relationship decreased in the order: *Ulva* spp. > *Palmaria palmata* > *Fucus vesiculosus*. Both the biomass and metal concentrations (2 mg mL^{-1} and 2000mg L^{-1} respectively) were kept constant for all three seaweeds and therefore this implies that, of the three seaweeds studied, *Ulva* spp. had the greatest bio-reduction capacity for hexavalent chromium.

In their study of Cr (VI) biosorption onto *Sargassum* sp., Yang and Chen [34] showed that the raw seaweed reduced 48% of the Cr (VI) to Cr (III) at pH 1 and 77% of Cr (VI) at pH 2 (initial concentration =1mM). However, modification of the biomass with formaldehyde resulted in complete reduction of Cr (VI) to Cr (III) at pH 2. Therefore the reduction ability of the modified biosorbents in Chapter 6 should also be studied.

Results in the present study showed approximately 64 % reduction for *Fucus vesiculosus*, 69% for *Palmaria palmata* and 75% for *Ulva* spp. This indicated that the degree of reduction in this study was greater than that observed for the raw seaweed by Yang and Chen [34].

It is also important to note that the Cr (VI) concentration used in this study was significantly higher (approximately 30 times) than that used by Yang and Chen [34]. This indicates the potential of these three seaweeds to bring about significant reduction and detoxification of Cr (VI) at elevated metal levels.

5.4 Conclusions

SEM analysis of the red and green seaweeds, revealed significant changes in morphology occurred after cation binding to the seaweeds with apparent smoothing of the surface. However, changes in brown seaweed morphology were only slightly discernable and require further quantitative investigation.

While Cu (II) and Cr (III) binding generally brought about comparable changes in morphology, changes brought about by Cr (VI) binding were unique. This again highlights differences in cation and anion binding mechanism and warrants further study.

Changes in seaweed morphology were attributed to changes in the ionic radii and coordination spheres of the heavy metals under study.

EDX analysis revealed an ion-exchange mechanism for cation binding to all seaweeds but gave little information on anionic Cr (VI) binding. It also indicated that interactions with sulphur containing functionalities were of great importance in Cu (II) binding to red seaweeds.

Agreement was found between the EDX and XPS results as both confirmed the presence of an ion-exchange mechanism for Cu (II) binding to seaweeds. In addition, XPS analysis showed participation of oxygen, sulphur and nitrogen containing functionalities in metal complexation to *Ulva lactuca* and *Polysiphonia lanosa*. Therefore, it was concluded that, for Cu (II) binding to *Ulva lactuca* and *Polysiphonia lanosa*, an ion-exchange mechanism is accompanied by coordination to various functional groups on the biomass.

Surface reduction appeared to be the significant binding mechanism for Cr (VI) binding to *Fucus vesiculosus*, *Palmaria palmata* and *Ulva* spp. biomass, as Cr (VI) was reduced in large quantities to Cr (III) on contact with these seaweeds.

Ulva spp. was found to be the most efficient reducing agent for Cr (VI) with an almost 3:1 ratio of Cr (III): Cr (VI). This result is totally novel as the reduction ability of green seaweeds has not previously been found in the literature.

The work in this chapter has demonstrated the presence of ion-exchange and complexation mechanisms for Cu (II) and Cr (III) binding to the seaweeds as well as a reduction mechanism for Cr (VI). Results have verified those obtained by FTIR which indicated the involvement of oxygen, nitrogen and sulphur-containing functionalities in metal binding. While qualitative information regarding morphological changes has been obtained using SEM, a quantitative estimation of these changes is also required. Scanning force Microscopy was used in Chapter 7 to quantitatively describe the changes in seaweed surface morphology after metal binding.

5.5 References

[1] Surface Characterization by Spectroscopy and Microscopy, In: Principles of Instrumental Analysis, Skoog, D. A., Holler, F. J., and Nieman, T. A. (Ed.), Saunders College Publishing, 535-566 (1992).

[2] Purdue University Radiological and Environmental Management Facilities., http://www.purdue.edu/REM/rs/sem.htm, (2006).

[3] Raize, O., Argaman, Y. and Yannai, S. *Biotechnology and Bioengineering*, **87**, 451-458 (2004).

[4] Figueira, M. M., Volesky, B. and Mathieu, H. J. *Environmental Science & Technology*, **33**, 1840-1846 (1999).

[5] Goldstein, J. I., Newbury, D. E., Echlin, P., Joy, D. C., Romig Jr., A. D., Lyman, C. E., Fiori, C. and Lifshin, E., X-ray Spectral Measurement, In: Scanning Electron Microscopy and X-Ray Microanalysis, Plenum Press, 297-354 (2002).

[6] Mohan, S. V., Ramanaiah, S. V., Rajkumar, B. and Sarma, P. N. *Bioresource Technology*, **98**, 1006-1011 (2007).

[7] Crist, B. V., Wikipedia (http://en.wikipedia.org/wiki/X-ray_photoelectron_spectroscopy), (2006).

[8] Briggs, D., Applications of XPS in Polymer Technology, In: Practical Surface Analysis, Briggs, D. and Seah, M. P. (Ed.), 436-483 (1990).

[9] Ashkenazy, R, Gottlieb, L. and Yannai, S. *Biotechnology and Bioengineering*, **55**, 1-10 (1997).

[10] Allen, S. J. and Brown, P. A. *Journal of Chemical Technology and Biotechnology*, **62**, 17-24 (1995).

[11] www.nist.gov/srd/nist20.html., NIST XPS Database, (2007).

[12] Chen, J. P., Hong, L. A., Wu, S. N. and Wang, L. *Langmuir*, **18**, 9413-9421 (2002).

[13] Cotton, F. A., Wilkinson, G., Murillo, C. A. and Bochmann, M., Advanced Inorganic Chemistry, Sixth Edition, John Wiley & Sons Inc., New York (1999).

[14] Park, S. J. and Kim, Y. M. *Materials Science and Engineering A*, **391**, 121-123 (2005).

[15] Moulder, J. F., Stickle, W. F., Sobol, P. E. and Bomben, K. D., Handbook of X-ray Photoelectron Spectroscopy, Perkin–Elmer Corp., Minnesota (1992).

[16] Chen, J. P. and Yang, L. *Langmuir*, **22**, 8906-8914 (2006).

[17] Sheng, P. X., Ting, Y. P., Chen, J. P. and Hong, L. *Journal of Colloid and Interface Science*, **275**, 131-141 (2004).

[18] Cimino, G., Passerini, A. and Toscano, G. *Water Research*, **34**, 2955-2962 (2000).

[19] El-Sikaily, A., Nemr, A. El, Khaled, A. and Abdelwehab, O. *Journal of Hazardous Materials*, **In Press, Corrected Proof**, -113 (2007).

[20] Lee, D. C., Park, C. J., Yang, J. E., Jeong, Y. H. and Rhee, H. I. *Applied Microbiology and Biotechnology*, **54**, 445-448 (2000).

[21] Bosinco, S., Roussy, J., Guibal, E. and LeCloirec, P. *Environmental Technology*, **17**, 55-62 (1996).

[22] Agarwal, G. S., Bhuptawat, H. K. and Chaudhari, S. *Bioresource Technology*, **97**, 949-956 (2006).

[23] Khezami, L. and Capart, R. *Journal of Hazardous Materials*, **123**, 223-231 (2005).

[24] Loukidou, M. X., Zouboulis, A. I., Karapantsios, T. D. and Matis, K. A. *Colloids and Surfaces A: Physicochemical and Engineering Aspects*, **242**, 93-104 (2004).

[25] Chirwa, E. M. N. and Wang, Y. T. *Environmental Science and Technology*, **31**, 1446-1451 (1997).

[26] Han, X., Wong, Y. S., Wong, M. H. and Tam, Nora F. Y. *Journal of Hazardous Materials*, **146**, 65-72 (19-7-2007).

[27] Park, D., Yun, Y. S. and Park, J. M. *Environmental Science and Technology*, **38**, 4860-4864 (2004).

[28] Dambies, L., Guimon, C., Yiacoumi, S. and Guibal, E. *Colloids and Surfaces A: Physicochemical and Engineering Aspects*, **177**, 203-214 (2001).

[29] Lytle, C. M., Lytle, F. W., Yang, N., Qian, J. H., Hansen, D., Zayed, A. and Terry, N. *Environmental Science and Technology*, **32**, 3087-3093 (1998).

[30] Gardea-Torresdey, J. L., Tiemann, K. J., Armendariz, V., Bess-Oberto, L., Chianelli, R. R., Rios, J., Parsons, J. G. and Gamez, G. *Journal of Hazardous Materials*, **80**, 175-188 (2000).

[31] Park, D., Yun, Y. S. and Park, J. M. *Environmental Science & Technology*, **38**, 4860-4864 (2004).

[32] Park, D., Yun, Y. S., Yim, K. H. and Park, J. M. *Bioresource Technology*, **97**, 1592-1598 (2006).

[33] Park, D., Yun, Y. S., Jo, J. H. and Park, J. M. *Journal of Microbiology and Biotechnology*, **15**, 780-786 (2005).

[34] Yang, L. and Chen, J. P. *Bioresource Technology*, **In Press, Corrected Proof**, (2007).

Chapter 6
Chemical Modification

6.1 Introduction

Previous chapters have identified the metal binding capacities of the selected seaweeds as well as investigating the involvement of the various functional groups in binding. From Chapters 4 and 5, it was seen that carboxyl and amino groups played significant roles in metal binding. The work in this chapter illustrates the relative contribution of these groups in binding by modifying their availability. The use of chemical modification to alter the seaweeds' metal uptake as well as the effects of treatment on surface composition is investigated.

6.1.1 Rationale behind chemical modification

Various authors have used chemical modification to alter (and more importantly, enhance) the seaweeds' metal binding capacity. Park *et al*. [1] performed a variety of modifications on *Ecklonia* biomass, while Lodeiro *et al*. [2] carried out their study on the invasive macroalgae *Sargassum muticum*. These and other authors have used a variety of modification techniques including:

1. Acid washing which removes previously bound cations from the biomass thus "freeing" the available sites [3].
2. Alkali treatment which increases the negative charge on the biomass [4].
3. Treatment with organic solvents such as acetone which may remove protein and lipid fractions from the biomass [5].
4. Ca^{2+} solution treatment which may enhance ion-exchange by the biomass [6].
5. Treatment with chelating agents such as EDTA which may disrupt cellulose polymers [7].

Various authors have shown that carboxyl and amino functionalities are extremely important in metal binding to seaweeds [1,8,9]. As a result, modifications which enhance the quantity of either of these groups should bring about a corresponding increase in metal binding.

Jeon *et al*. [10] reported that carboxylated alginic acid prepared through the oxidation reaction with potassium permanganate had higher levels of metal uptake than the non-carboxylated species. This modification method increased the quantity of carboxyl groups on the alginic acid thus leading to enhanced uptake. Luo *et al*. [11] carried out similar modifications with *Laminaria japonica* with increased capacity for lead also reported.

In their study on Cr (VI) biosorption by chemically modified *Ecklonia* sp. [1], Park *et al.* found that amination of the carboxyl groups, using carbodiimide reagent increased the metal removal efficiency. They interpreted this enhancement of Cr (VI) removal as being due to the cell wall becoming enriched with amino groups. These in turn provided abundant positively charged sites at acidic pH for Cr (VI) complexation.

It is seen clearly that enhanced binding through the addition of functional groups is extremely desirable. However, in order to study the contribution of these groups to binding, modifications which block the interactions of these functionalities by reducing their ability to bind metals are also desirable. Modification of these groups and their subsequent binding behaviour may also act as a pointer to binding mechanism. Two of the most common methods of blocking these functionalities are methylation of amino groups [1,12,13] and esterification of carboxyl groups [5,14,15]

6.1.2 Amino Modification

Modification of biomass amino groups is typically carried out by contacting the raw biomass with formaldehyde (HCHO) and formic acid (HCOOH) for 6 h. This treatment is expected to result in methylation of the amino group [12]. The general reaction takes place according to Equation 6.1.

$$RCH_2NH_2 \xrightarrow{HCHO + HCOOH} RCH_2N(CH_3)_2 + CO_2 + H_2O \quad \textbf{(Equation 6.1)}$$

An alternative method for modification of the biomass amino groups is using sodium iodoacetate [16]. The biomass is shaken with 0.1M sodium iodoacetate, maintained at pH 8 for 6h, then washed and dried. This reagent typically attaches itself to and neutralises amino groups at low or neutral pH by introducing a carboxyl group as illustrated in Equation 6.2. However, the reagent may also bind to phenolic or hydroxyl groups at higher pH.

$$RNH_3^+ + ICH_2COO^- \longrightarrow RNH_2CH_2COO^- + HI \qquad \textbf{(Equation 6.2)}$$

Beveridge and Murray [17] observed that modification of amino and carboxyl groups resulted in a significant drop in copper biosorption by *Bacillus subtilis* while Kapoor and Viraraghavan [12] also showed that when the amino groups of *Aspergillus niger* were modified, biosorption of copper was reduced by significant amounts. The work of Park *et al*. [1] on chemically modified *Ecklonia* biomass also pointed to the importance of these groups in Cr (VI) binding.

6.1.3 Carboxyl Modification

Chemical modification of biomass carboxyl groups usually involves esterification of these groups by various methods [14,18]. If metal binding occurs through interaction with carboxyl groups, then chemical modification that reduces the availability of these groups should result in a marked reduction in metal binding.

It has been shown that treatment of the biomass with anhydrous methanol and a small amount of concentrated HCl causes esterification of the carboxyl groups present on the biomass [12]. The reaction takes place according to Equation 6.3.

$$RCOOH + CH_3OH \xrightarrow{H^+} RCOOCH_3 + H_2O \qquad \textbf{(Equation 6.3)}$$

Another method used for modification of carboxyl groups is the use of carbodiimide reagent [16]. In this procedure, ethylenediamine is added to an aqueous suspension of biomass, with sufficient 1-ethyl-3-(3-dimethyl aminopropyl) carbodiimide hydrochloride included to give a carbodiimide concentration of 0.2 M. The reaction mixture is then shaken for 6h at pH 4.75, subsequently washed and dried as appropriate. This reagent typically attaches and neutralises carboxyl groups by introducing an amino group [16] as illustrated in Equation 6.4.

$$RCOOH + NH_2CH_2CH_2NH_2 \xrightarrow{\text{Carbodiimide}} RCONHCH_2CH_2NH_2 + H_2O$$

(Equation 6.4)

While the use of carbodiimide reagents is beneficial because of its high degree of specificity and mild conditions, it is unattractive due to the high cost of reagents and equipment required to complete the modification [14]. Also, this method does not facilitate easy monitoring of the degree of modification. On the other hand, Gardea-Torresday *et al*. [14] showed that the use of acidic methanol to esterify carboxyl groups (Equation 6.1) is relatively inexpensive and facilitates convenient monitoring of the reaction.

6.1.4 Evaluating changes in biomass composition

Given that the seaweed biomass is subjected to somewhat harsh treatments in a number of cases, changes in biomass composition are expected. These changes may be investigated using FTIR spectroscopy. Results from Chapter 4 indicated there are numerous bands associated with seaweed surface functionalities. Therefore, changes in these bands after modification may give some indication of alterations taking place in the seaweed surface structure.

Various authors have used FTIR to examine structural changes in biosorbents after chemical modification e.g. Bai and Abraham [5] studied changes in the FTIR spectrum of *Rhizopus nigricans* after a number of chemical treatments, while Kapoor and

Viraraghavan investigated changes in *Aspergillus niger* biomass [12]. Yang and Chen [19] also used FTIR in their study of Cr (VI) binding to modified *Sargassum* sp.

The novelty of approach of the work in this chapter is clearly illustrated. A comprehensive overview of the effects of seven chemical modification techniques on six seaweeds for three heavy metals has been given. A study with this breadth has not been found in the literature, where studies typically comprise a number of modifications for one seaweed species and one metal ion [1,2] or one modification technique for a single species and two metal ions [9].

6.1.5 Objectives of the Research

The main objectives of the work in this chapter are:

- To compare a variety of chemical modification techniques and to investigate their effects on metal uptake by the seaweeds.
- To investigate the relative importance of carboxyl and amino functionalities in metal binding by blocking their interaction.
- To identify alterations in biomass composition after chemical modification and relate these to binding capacity.

6.2 Experimental

6.2.1 Materials and Methods

6.2.1.1 Chemicals

- Acetone (99.8% purity) - ROMIL Ltd., Cambridge, England.
- Sodium Chloride (solid) - Ridel de Haën, Germany.
- Na_2-EDTA (solid) - BDH Laboratory Supplies, England.
- Sodium Hydroxide (solid) - Ridel de Haën, Germany.
- Hydrochloric Acid (37%) - LabScan Ltd., Dublin, Ireland.
- $CaCl_2$- BDH Laboratory Supplies, England.
- Methanol (99% purity) - LabScan Ltd., Dublin, Ireland.
- Formaldehyde - Fisons Laboratory Reagents, Loughborough, England.
- Formic acid - BDH Laboratory Supplies, England.
- Analytical grade metal solutions (1000mg L^{-1}) of Cu (II), Cr (III) and Cr (VI) - Sigma-Aldrich Ltd., Dublin, Ireland.

6.2.1.2 Instrumentation

- Varian SpectrAA 600 Atomic Absorption Spectrophotometer.
- Digilab Scimitar Series Fourier Transform Infrared Spectrometer (operating conditions are specified in Chapter 4).

6.2.1.3 Treatment with acid, alkali, organic solvents and other chemicals

Approximately 5g of the raw biomass was separately mixed with 200mL each of 0.1M HCl, 0.1M NaOH, acetone, 0.1M $CaCl_2$ and 0.1M Na_2-EDTA for 6h at room temperature (21 ± 1°C) and 200rpm [20]. Each modified biomass was then filtered under vacuum and washed with distilled water until a constant conductance was obtained for the filtrate. The biomass was oven-dried for 24 hours at 60°C.

6.2.1.4 Methylation of biomass amino groups

Approximately 5g of the raw biomass was mixed with 100 mL of formaldehyde (HCHO) and 200 mL of formic acid (HCOOH), and the reaction mixture was shaken on a rotary

shaker for 6h at 200rpm with the temperature maintained at 21 ± 1°C. The biomass was subsequently filtered under vacuum and washed with distilled water until a constant conductance was obtained for the filtrate. The biomass was oven-dried for 24h at 60°C.

6.2.1.5 Esterification of biomass carboxyl groups

Approximately 5g of the raw biomass was suspended in 500mL of anhydrous methanol with 5mL of concentrated hydrochloric acid added to the suspension. The reaction mixture was shaken on a rotary shaker for 6h at room temperature (21 ± 1 °C) and 200rpm. The biomass was filtered under vacuum and washed with distilled water until a constant conductance was obtained for the filtrate. The biomass was oven-dried for 24h at 60°C.

6.2.1.6 Re-exposure to metal solutions

The metal uptake capacity of the chemically modified seaweeds was examined after exposure to metal solutions of 250mg L^{-1}. Based on earlier isotherm experiments (Chapter 3), it was expected that this concentration would result in close to maximum saturation levels of the respective metal uptakes. Approximately 100mg of modified biomass was dispersed in 50mL metal solution adjusted to the appropriate pH (pH 5 for Cu (II), pH 4.5 for Cr (III) and pH 2 for Cr (VI)). Samples were shaken for 4h at 200 rpm and room temperature (21 ± 1 °C). The biomass was filtered under vacuum, washed with distilled water until a constant conductance was obtained for the filtrate and oven-dried for 24h at 60°C.

6.2.1.7 FTIR analysis of chemically modified biomass

FTIR spectra of the raw and treated biomasses were taken in order to evaluate the effects of chemical treatment on biomass functional groups. Samples were analysed using the parameters specified in Chapter 4 (Section 4.2.1.2). Spectra were recorded in triplicate with sample spectra shown.

6.3 Results and Discussion

6.3.1. Mass losses

A major consideration in the treatment applied to seaweed biomass is that of the magnitude of mass loss after treatment. Obviously lower mass losses are desirable for scale-up operations. Table 6.1 summarises the percentage mass losses observed for the seaweeds after chemical treatment.

Table 6.1 Mass losses for six seaweeds after chemical treatment. Error bars are calculated based on triplicate analyses with 95% Confidence Intervals.

Seaweed	*Fucus vesiculosus*	*Fucus spiralis*	*Ulva lactuca*	*Ulva* spp.	*Palmaria palmata*	*Polysiphonia lanosa*
Treatment	**Mass loss (%)**					
HCl	49 ± 2	47 ± 3	45 ± 1	45 ± 2	45 ± 1	49 ± 2
NaOH	41 ± 3	45 ± 4	43 ± 2	41 ± 2	35 ± 3	56 ± 3
Acetone	21 ± 1	15 ± 1	32 ± 4	33 ± 3	24 ± 1	35 ± 2
$CaCl_2$	10 ± 3	19 ± 4	11 ± 3	21 ± 2	12 ± 1	11 ± 2
Na_2EDTA	29 ± 4	27 ± 2	34 ± 3	20 ± 2	23 ± 2	30 ± 3
Methylation	18 ± 3	14 ± 3	11 ± 1	10 ± 2	20 ± 3	30 ± 4
Esterification	19 ± 2	23 ± 4	39 ± 3	30 ± 5	21 ± 2	36 ± 2

It was found that all seaweeds exhibited mass losses after chemical treatment. Average mass losses were in the general order: HCl > NaOH > Esterification > Na_2-EDTA > Acetone > Methylation > $CaCl_2$. It therefore appears that acid and alkali treatments are the most aggressive towards these seaweeds while $CaCl_2$ is the least.

The raw biomass is stabilised with cations such as Na^+, K^+, Ca^{2+} and Mg^{2+} found in seawater [21]. As a result of acid treatment these ions that are bound to active sites are substituted by protons and thus large weight losses are observed when protonation is carried out.

The low mass losses observed with $CaCl_2$ may also point to its suitability as a desorption agent for regeneration of metal-loaded biomasses. Davis *et al*. [22] reported that a desorbing agent must be effective, non-damaging to the biomass, non-polluting and cheap. Vijayaraghavan *et al*. [23] compared the use of mineral acids and $CaCl_2$ for desorption of Co (II) and Ni (II) from *Sargassum wightii*. It was found that mineral acids released 100% of the bound metal but that the biomass became fragile after acid exposure. On the other hand, $CaCl_2$ released almost 99% of the metal with no significant mass losses [23]. The results in this study agree with the above findings with large mass losses for HCl treatment (45-49%) and smaller losses for $CaCl_2$ treatment (10-21%).

6.3.2 Seaweed metal uptake after chemical modification

Metal uptake capacities for the raw biomass were obtained from experimental isotherm plots in Chapter 3. The metal uptake capacities of the modified seaweeds are shown in Figures 6.1 and 6.2

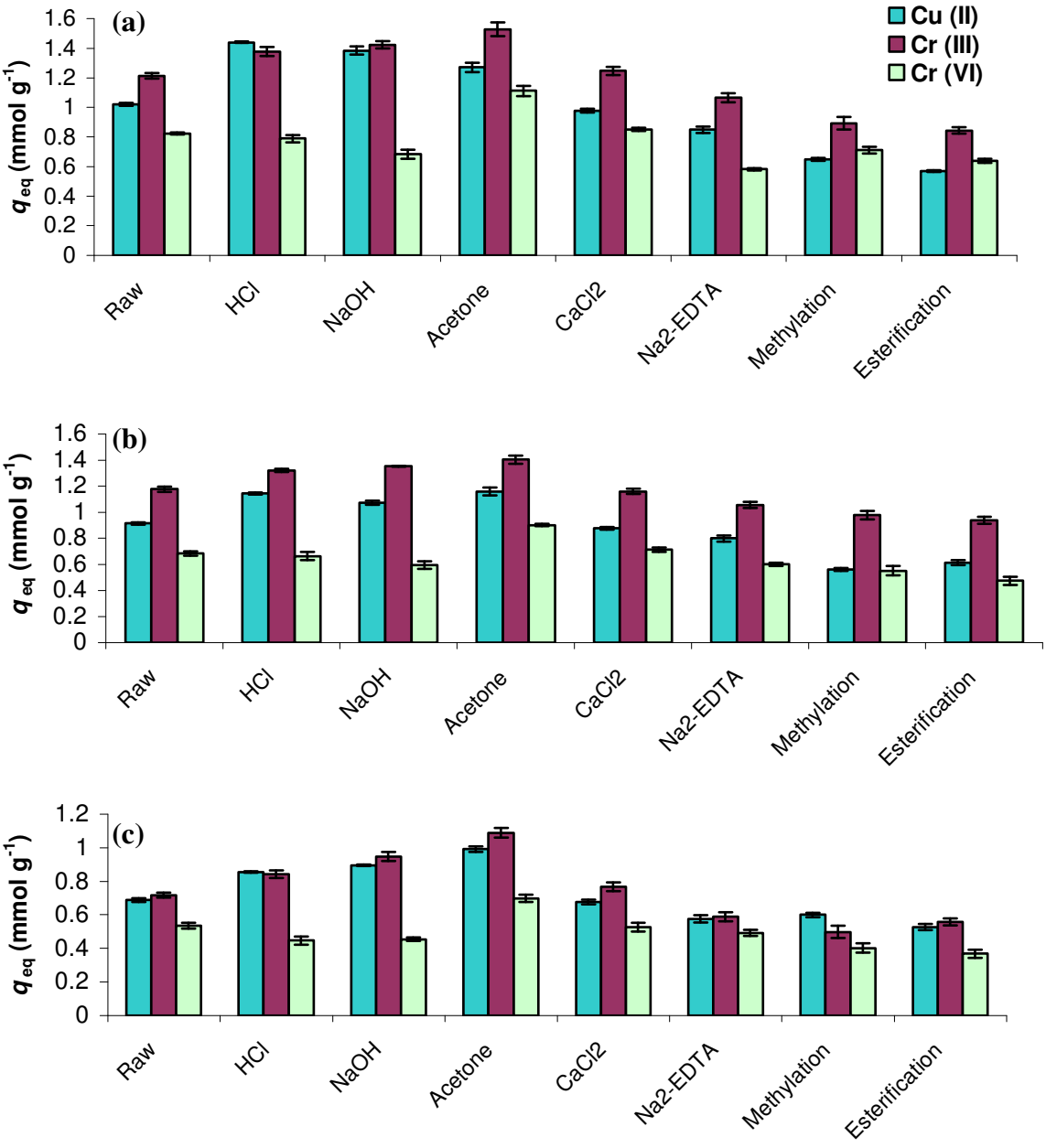

Figure 6.1 **Metal uptake before and after chemical treatment for (a) *Fucus vesiculosus* (b) *Fucus spiralis* (c) *Ulva lactuca*. Error bars are calculated based on triplicate analyses with 95% Confidence Intervals.**

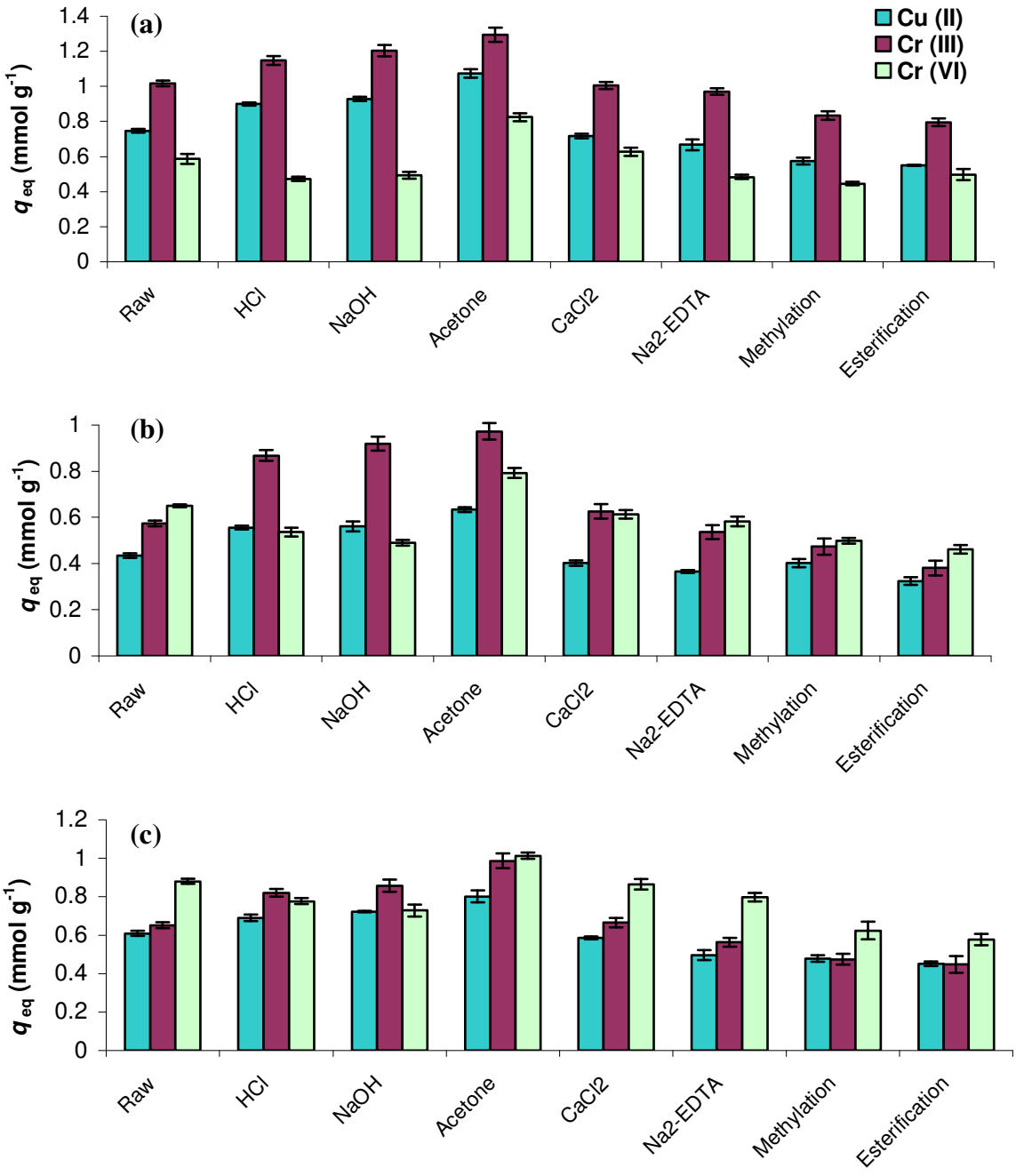

Figure 6.2 **Metal uptake before and after chemical treatment for (a) *Ulva* spp. (b) *Palmaria palmata* (c) *Polysiphonia lanosa*. Error bars are calculated based on triplicate analyses with 95% Confidence Intervals.**

6.3.2.1 Acid treatment (HCl)

Various authors have shown that acid treatment is generally used for cleaning the cell wall and replacing the natural mixture of ionic species bound on the cell wall with protons [7,24].

As seen from mass loss data, acid washing is one of the most aggressive pre-treatments for the stability of the biomass structure. This is because a substantial portion of soluble biomass material, smaller organic molecules and ions are released upon acidification [5]. It is known that concentrated HCl can rupture the structure of polymer chains and destroy their hydrogen bonding capacity by hydrolysis. As a result repeated exposure of the biomass to a strongly acidic environment could lead to a reduction in the metal binding sites on the biomass [25].

Table 6.2 summarises the percentage changes in metal uptake observed for the seaweeds after acid treatment. Average data from Figures 6.1 and 6.2 are presented.

Table 6.2 Percentage changes in biomass metal uptake capacity after acid treatment. Errors are calculated based on triplicate analyses with 95% Confidence Intervals.

	% Change in binding capacity		
	Cu (II)	**Cr (III)**	**Cr (VI)**
Fucus vesiculosus	+ 41 (± 3)	+ 13 (± 3)	- 4 (±1)
Fucus spiralis	+ 25 (± 1)	+ 13 (± 2)	- 3 (± 1)
Ulva lactuca	+ 24 (± 3)	+ 17 (± 1)	- 16 (± 3)
***Ulva* spp.**	+ 20 (± 1)	+14 (± 3)	-19 (± 2)
Palmaria palmata	+ 27 (± 1)	+ 51 (± 2)	-17 (± 3)
Polysiphonia lanosa	+ 13 (± 2)	+26 (± 2)	-13 (± 2)

From Table 6.2 it is clearly seen that, in all cases, acid treatment brought about an increase in binding of cationic Cu (II) and Cr (III) but a decreased capacity for anionic Cr (VI). For the brown and green seaweeds, a greater increase was seen for Cu (II) over Cr

(III) while the converse was true for the red seaweeds. For Cr (VI), the magnitude of the decrease was greater for the green and red seaweeds.

These trends may be due to a number of factors:

1. As raw biomass is stabilised with alkali and alkaline earth metal ions, heavy metal ions must compete with these ions for binding sites, and therefore not all the binding sites will be occupied by the heavy metal [26]. Acid treatment removes these previously sorbed cations from biomass binding sites, thus making the sites available for subsequent metal binding.
2. Acidic pre-treatment may also have caused some hydrolysis of functional groups and generated more anionic sites for metal sorption [27] thus enhancing cation uptake.
3. Reduction in the positive charge on the cell surface [13] may also have increased the sorption capacity of the biomass for metal cations and correspondingly decreased anion uptake.

6.3.2.2 Alkali treatment (NaOH)

Yan and Viraraghavan [28] reported that alkali pretreatment is an effective method to improve the metal biosorption capacity of dead biomass. It was shown that alkali treatment could destroy autolytic enzymes causing putrefaction of biomass, remove lipids and proteins that mask binding sites and could also release certain biopolymers from the cell wall that have a high affinity towards heavy metal ions.

The various interpretations in relation to alkali treatment are that it exposes certain chemical groups on the biomass which leads to enhanced binding of metal cations and also that it may remove extraneous materials from the cell surface that might otherwise interfere with metal ion binding [1].

Alkali treatment has been shown to be quite aggressive to biomass stability with large mass losses observed (Table 6.1). Generally, alkali-treatment is known to cause breakage of cellulose polymers, thus hindering the operational stability of the biomass [7]. Treatment with higher alkali concentrations can also cause disintegration of the biomass.

Table 6.3 summarises the percentage changes in metal uptake observed for the seaweeds after alkali treatment. Average data from Figures 6.1 and 6.2 are presented.

Table 6.3 Percentage changes in biomass metal uptake capacity after alkali treatment. Errors are calculated based on triplicate analyses with 95% Confidence Intervals.

	% Change in binding capacity		
	Cu (II)	**Cr (III)**	**Cr (VI)**
Fucus vesiculosus	+ 35 (± 3)	+ 17 (± 2)	- 17 (± 3)
Fucus spiralis	+ 17 (± 2)	+ 15 (± 1)	- 13 (± 3)
Ulva lactuca	+29 (± 1)	+32 (± 3)	-15 (± 1)
***Ulva* spp.**	+ 25 (± 1)	+ 18 (± 3)	-16 (± 2)
Palmaria palmata	+ 28 (± 2)	+ 59 (± 3)	-22 (± 1)
Polysiphonia lanosa	+ 18 (± 1)	+ 37 (± 3)	-17 (± 3)

In this case, treatment of the biomass with 0.1M alkali (NaOH) brought about increases in cation binding and decreases in anion binding. These trends were observed for all seaweeds under investigation.

Various authors have observed similar favourable effects for cation binding after alkali treatment. Ashkenazy *et al*. [29] reported enhanced binding of Pb (II) by *Saccharomyces uvarum* biomass after boiling with NaOH while Mehta and Gaur [26] also found that alkali treatment increased the Cu (II) sorption capacity of *Chlorella vulgaris*. Lodeiro *et al*. [2] also reported a 32 % increase in Cd (II) binding after alkali treatment which compares favourably with a number of results in Table 6.3.

Park *et al*. [1] reported a 14% decrease in Cr (VI) biosorption by *Ecklonia* sp. (brown) after modification with NaOH. The values obtained in the present study for Cr (VI) were of similar magnitude to this.

As seen in the XPS results in Chapter 5, their results also showed that hexavalent chromium was reduced to trivalent chromium on contact with the seaweed surface. The increased negative charge on the biomass would lead to a greater repulsion between the negatively charged surface and the anionic Cr (VI) species thus reducing the quantity of metal bound.

6.3.2.3 Treatment with Acetone

Table 6.4 summarises the percentage changes in metal uptake observed for the seaweeds after acetone treatment. Average data from Figures 6.1 and 6.2 are presented.

Table 6.4 Percentage changes in biomass metal uptake capacity after acetone treatment. Errors are calculated based on triplicate analyses with 95% Confidence Intervals.

	% Change in binding capacity		
	Cu (II)	**Cr (III)**	**Cr (VI)**
Fucus vesiculosus	+ 24 (± 3)	+ 25 (± 4)	+35 (± 5)
Fucus spiralis	+ 27 (±2)	+ 19 (± 4)	+32 (±3)
Ulva lactuca	+ 44 (± 2)	+ 52 (± 3)	+ 30 (± 2)
***Ulva* spp.**	+ 43 (± 4)	+ 27 (± 2)	+ 40 (± 4)
Palmaria palmata	+ 45 (± 3)	+ 69 (± 4)	+22 (± 1)
Polysiphonia lanosa	+ 31 (± 3)	+ 51 (± 4)	+ 15 (± 2)

Treatment of the biomasses with the organic solvent acetone resulted in favourable effects for both cations and anions with an increase in metal binding observed in all

cases. This is in contrast to the acid and alkali treatments which brought about increases in cation binding only.

Ashkenazy *et al*. [29] found that treatment of yeast biomass with acetone removed the protein and lipid fractions of the biomass surface, thus exposing more metal binding sites and improving Pb (II) uptake by the biomass. Increases in cation binding after acetone modification have also been reported by Lodeiro *et al*. [2] who found a 35 % increase in Cd (II) binding after modification.

Acetone treatment has also been reported to enhance anion binding. Bai and Abraham [5] Have reported an increase in Cr (VI) binding to *Rhizopus nigricans* as did Park *et al*. [1] for Cr (VI) binding to *Ecklonia* sp. The results obtained in this study are in agreement the above findings for both cation and anion binding.

However, in contrast to the results obtained in this work, Kapoor and Viraraghavan [12] found that for *Aspergillus niger*, treatment with acetone caused slight decreases in the biosorption of lead, cadmium and copper. They suggested that this decrease may have been due to structural changes that may have occurred when the biomass was subjected to harsh conditions during lipid extraction.

6.3.2.4 Treatment with $CaCl_2$

Table 6.5 summarises the percentage changes observed in metal uptake for the seaweeds after $CaCl_2$ treatment. Average data from Figures 6.1 and 6.2 are presented.

Table 6.5 Percentage changes in biomass metal uptake capacity after $CaCl_2$ treatment. Errors are calculated based on triplicate analyses with 95% Confidence Intervals.

	% Change in binding capacity		
	Cu (II)	**Cr (III)**	**Cr (VI)**
Fucus vesiculosus	- 4 (± 1)	+ 3 (± 1)	+ 3 (± 1)
Fucus spiralis	- 3 (± 1)	- 2 (± 1)	+ 4 (± 1)
Ulva lactuca	- 2 (± 1)	+ 7 (± 2)	- 2 (± 1)
***Ulva* spp.**	- 4 (± 2)	- 1 (± 1)	+ 7 (± 2)
Palmaria palmata	- 8 (± 1)	+ 9 (± 3)	-6 (± 2)
Polysiphonia lanosa	- 4 (± 1)	+ 2 (± 1)	- 4 (± 2)

Pre-washing of the biomass with 0.1M $CaCl_2$ only slightly affected metal uptake by the seaweeds studied with both minor increases and decreases in binding capacity observed. Generally $CaCl_2$ treatment resulted in minor decreases in Cu (II) binding, with both increases and decreases observed for Cr (III) and Cr (VI) binding.

Akhthar *et al*. [30] found that heavy metal biosorption by dead fungal biomass was significantly improved by calcium and/or magnesium saturation of the biomass while Park *et al*. [1] showed enhanced Cr (VI) sorption by *Ecklonia* biomass after treatment with $CaCl_2$. The latter postulated that this enhancement of binding may have been due to cleaning of the biomass surface by calcium ions which may have been easily replaced with reduced Cr during Cr (VI) biosorption. However, no such trends were found in this study.

6.3.2.5 Treatment with Na_2-EDTA

Table 6.6 summarises the percentage changes in metal uptake observed for the seaweeds after Na_2-EDTA treatment. Average data from Figures 6.1 and 6.2 are presented.

Table 6.6 Percentage changes in biomass metal uptake capacity after Na_2-EDTA treatment. Errors are calculated based on triplicate analyses with 95% Confidence Intervals.

	% Change in binding capacity		
	Cu (II)	**Cr (III)**	**Cr (VI)**
Fucus vesiculosus	- 16 (± 2)	- 12 (± 3)	- 29 (± 3)
Fucus spiralis	- 13 (± 2)	- 10 (± 2)	- 11 (± 1)
Ulva lactuca	- 16 (± 2)	- 17 (± 3)	- 7 (± 2)
***Ulva* spp.**	- 10 (± 3)	- 4 (± 2)	-17 (± 1)
Palmaria palmata	-15 (± 1)	- 6 (± 3)	- 10 (± 2)
Polysiphonia lanosa	- 19 (± 3)	- 13 (± 2)	- 9 (± 2)

From Table 6.6, it is clearly seen that treatment of the biomasses with the chelating agent Na_2-EDTA brought about decreases in binding for all seaweed-metal combinations.

It is known that treatment with strong chelating agents may cause breakage of the cellulose polymers of the seaweed biomass [7]. Park *et al*. [1] found that treatment by 1M Na_2-EDTA caused serious degradation of the biomass cell walls, resulting in complete solubilisation of the biomass. In this study, treatment with 0.1 M Na_2-EDTA caused some degradation of the biomass cell wall polymers (mass losses 20-34%) thus reducing its metal uptake capacity for both cationic and anionic species.

6.3.2.6 Methylation of amino groups

Equation 6.3 illustrated that treatment with formaldehyde and formic acid brings about methylation of the amino groups present on the biomass surface [12]. The effects of methylation on the seaweeds metal binding capacity are discussed below.

Table 6.7 summarises the percentage changes observed for the seaweeds after methylation of the biomass amino groups. Average data from Figures 6.1 and 6.2 are presented.

Table 6.7 Percentage changes in biomass metal uptake capacity after methylation of the amino groups. Errors are calculated based on triplicate analyses with 95% Confidence Intervals.

	% Change in binding capacity		
	Cu (II)	**Cr (III)**	**Cr (VI)**
Fucus vesiculosus	- 36 (± 1)	-26 (± 4)	-13 (± 2)
Fucus spiralis	- 38 (± 3)	- 17 (± 2)	- 19 (± 2)
Ulva lactuca	-13 (± 1)	- 30 (± 3)	- 23 (± 3)
***Ulva* spp.**	- 22 (± 2)	- 17 (± 2)	- 23 (± 3)
Palmaria palmata	- 8 (± 2)	- 17 (± 4)	- 23 (± 1)
Polysiphonia lanosa	-21 (± 2)	-27 (± 3)	-29 (± 5)

6.3.2.6.1 Cu (II)

All seaweeds showed reduced Cu (II) binding after methylation of biomass amino groups. The brown seaweeds showed the largest decline in binding with 36 and 38 % decreases in binding observed for *Fucus vesiculosus* and *Fucus spiralis* respectively. These results are in agreement with FTIR results (Chapter 4) which show the involvement of amino groups in Cu (II) binding to the brown seaweeds.

The percentage decreases observed for the remaining seaweeds were much lower; Cu (II) binding to *Ulva* spp. and *Polysiphonia lanosa* decreased by 22 and 21 % respectively with *Ulva lactuca* dropping by 13%. Meanwhile Cu (II) binding to *Palmaria palmata* decreased by only 8%, indicating that biomass amino groups had a less significant role to play in Cu (II) binding to *Palmaria palmata* than to the other seaweeds. Again, this result agrees with FTIR results (Chapter 4) which show no detectable movement of the –NH stretch in *Palmaria palmata* after exposure to Cu (II) solution.

6.3.2.6.2 Cr (III)

Following methylation of the amino groups, *Ulva lactuca* exhibited the largest decrease in Cr (III) binding (30%), followed by *Polysiphonia lanosa* and *Fucus vesiculosus* with respective 27 and 26% decreases. A 17 % decrease in binding was observed for the remaining seaweeds; *Fucus spiralis*, *Ulva* spp. and *Palmaria palmata*. FTIR data (Chapter 4) indicated that amino groups played a significant role in Cr (III) binding to *Ulva lactuca*. Therefore, it is expected that blocking of these groups would result in a significant reduction in Cr (III) binding to the seaweed. Similar trends in FTIR data were shown for *Fucus vesiculosus* and *Polysiphonia lanosa*.

6.3.2.6.3 Cr (VI)

Cr (VI) binding experiments are carried out at pH 2 where it has been shown that amino group methylation reduces the number of positively charged sites on the biomass surface.

As previously seen, at low pH, protonation of functional groups (e.g. carboxyl and amino) gives the biomass an overall positive charge. The seaweed is then able to adsorb negatively charged metal ions such as anionic chromate [31]. However, if amino groups have been methylated, they will no longer become protonated in the low pH range and as a result will not be available to bind Cr (VI). This is apparent as reduced Cr (VI) binding was observed for all seaweeds.

Polysiphonia lanosa showed the greatest decrease in Cr (VI) binding after methylation of the amino groups (29 %). FTIR studies showed large differences in the –NH stretching band before and after Cr (VI) exposure pointing to significant amino group participation in Cr (VI) binding to this seaweed. *Ulva lactuca*, *Ulva* spp. and *Palmaria palmata* each displayed a decrease in binding of 23 % while the decreases for *Fucus vesiculosus* and *Fucus spiralis* were 13 and 19 % respectively.

The results therefore indicate that amino groups play a significant role in Cr (VI) binding to red seaweeds followed by green and then brown seaweeds.

6.3.2.7 Esterification of carboxyl group

The metal binding ability of carboxyl groups should be significantly reduced as a result of esterification. Gardea-Torresdey *et al*. [14] showed that while carboxyl oxygen atoms of esters are known to coordinate to metal ions, the interaction between the oxygen and metal is much weaker than that observed with carboxyl oxygen. Since it is thought that the biosorption performance of seaweeds is related to the abundance of carboxyl groups, it would be expected that esterification of these groups would result in significant changes in the seaweeds' metal binding capacity. FTIR analysis (Chapter 4) showed carboxyl group interaction for all seaweed-metal combinations. Therefore, metal binding should be affected in all cases.

Table 6.8 summarises the percentage changes observed for the seaweeds after esterification of biomass carboxyl groups. Average data from Figures 6.1 and 6.2 are presented.

Table 6.8 Percentage changes in biomass metal uptake capacity after esterification of carboxyl groups. Errors are calculated based on triplicate analyses with 95% Confidence Intervals.

	% Change in binding capacity		
	Cu (II)	**Cr (III)**	**Cr (VI)**
Fucus vesiculosus	- 44 (± 3)	- 31 (± 2)	- 22 (± 2)
Fucus spiralis	- 32 (± 2)	- 19 (± 3)	- 30 (± 3)
Ulva lactuca	- 23 (± 2)	- 22 (± 3)	- 31 (± 3)
***Ulva* spp.**	- 25 (± 1)	- 21 (± 2)	- 15 (± 3)
Palmaria palmata	- 25 (± 2)	- 33 (± 3)	- 28 (± 2)
Polysiphonia lanosa	- 25 (± 1)	- 31 (± 4)	- 34 (± 3)

6.3.2.7.1 Cu (II)

All seaweeds showed a reduction in Cu (II) binding capacity. Large decreases in Cu (II) binding were observed for the brown seaweeds with decreases of 44 and 32 % observed

for *Fucus vesiculosus* and *Fucus spiralis* respectively. This is in agreement with metal-loaded titrations (Chapter 2) and FTIR results (Chapter 4) which showed significant involvement of brown seaweed carboxyl groups in Cu (II) binding. Metal binding to *Ulva* spp., *Palmaria palmata* and *Polysiphonia lanosa* decreased by 25 % with *Ulva lactuca* showing a reduction of 23 %.

6.3.2.7.2 Cr (III)

Decreases in Cr (III) binding were observed for all seaweeds after esterification. *Palmaria palmata* displayed the largest decrease (33%) followed by *Polysiphonia lanosa* and *Fucus vesiculosus*, each showing a decrease of 31% in Cr (III) binding. Similar values were observed for the remaining seaweeds, with Cr (III) binding *Fucus spiralis*, *Ulva lactuca* and *Ulva* spp. decreasing by 19, 22 and 21 % respectively. These results agree with FTIR findings which showed participation of carboxyl groups to varying degrees in Cr (III) binding.

6.3.2.7.3 Cr (VI)

Park *et al*. [1] observed that esterification of biomass carboxyl groups decreased Cr (VI) uptake by reducing the amount of positively charged sites for Cr (VI) complexation at acidic pH values.

Carboxyl modification in this study did in fact bring about a decrease in Cr (VI) binding in all seaweeds, which was in agreement with the work of Park *et al*. as mentioned above [1]. The greatest reduction in binding was for *Polysiphonia lanosa* (34%) which was closely followed by *Ulva lactuca*, *Fucus spiralis* and *Palmaria palmata* with reductions in binding of 31, 30 and 28% respectively while *Fucus vesiculosus* and *Ulva* spp. had decreases of 22 and 15%.

The decrease in metal binding for all seaweed-metal combinations clearly illustrates the importance of carboxyl ligand binding in seaweeds. The variation in results in this study showed that the relative importance of carboxyl group participation varies between

seaweeds and also between the various seaweed-metal combinations. This theory is supported by FTIR data in Chapter 4.

EDX results in Chapter 5 pointed to the existence of an ion-exchange mechanism for Cu (II) and Cr (III) binding to seaweeds. This was later confirmed using XPS analysis which also pointed to the involvement of oxygen- and nitrogen-containing functionalities in cation binding. While EDX results did not suggest a binding mechanism for Cr (VI), XPS analysis (Chapter 5) has shown that hexavalent chromium may be reduced to trivalent chromium by brown, green and red seaweeds. FTIR analysis and chemical modification have also pointed to the importance of carboxyl and amino groups in Cr (VI) binding. Therefore, the results obtained in this study are in agreement with the Cr (VI) binding mechanism proposed by Park *et al*. [1] for brown seaweed biomass (Figure 6.3).

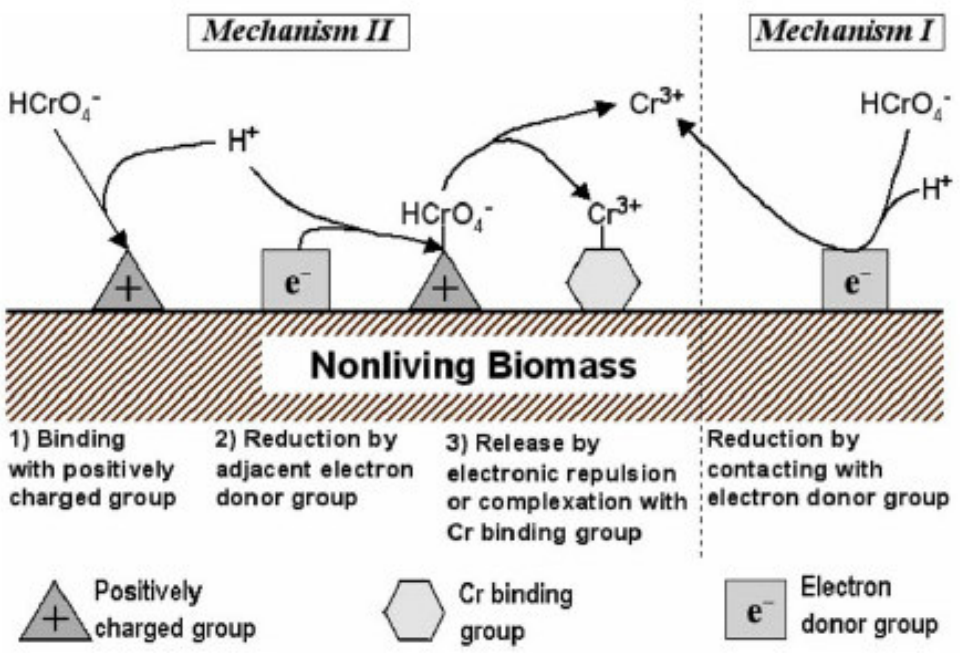

Figure 6.3 Proposed mechanism of Cr (VI) biosorption by dead seaweed biomass [1].

The mechanisms in Figure 6.3 are explained as [1]:

Mechanism I - Direct reduction

Here, Cr (VI) is directly reduced to Cr (III) in the aqueous phase by direct contact with the electron-donor groups in the biomass i.e. groups having lower reduction potentials than that of Cr (VI) (+1.3V).

Mechanism II - Indirect reduction

Indirect reduction consists of three steps as detailed in Figure 6.3. Amino and carboxyl groups take part in step (1) of this mechanism. As the pH of the aqueous phase is lowered (to pH 2 in this case), the larger number of hydrogen ions can easily co-ordinate with the amino and carboxyl groups on the biomass surface thus making the surface more positive and better able to attract the anionic chromate species.

Low pH also enhances the reduction reaction in mechanisms I and II, since protons take part in this reaction.

6.3.2.7.4 Comparison of the effects of amino and carboxyl blocking

For all seaweeds, blocking of the amino and carboxyl groups by functional group modification resulted in a decrease of the seaweeds' metal uptake capacity. This is as expected as FTIR work pointed to their significant involvement in metal binding. The importance of these groups was shown to vary between seaweed type and metal. Based on the results in Table 6.7 and 6.8 some general conclusions can be drawn about the effect of functional group blocking. For ease of comparison, the information contained in these tables (this time expressed in mmol g^{-1}) has been summarised in Table 6.9.

Table 6.9 Decreases observed in maximum metal uptake capacity after functional group modification. Errors (shown in parentheses) are calculated based on triplicate analyses with 95% Confidence Intervals.

	Decreased Metal Uptake Capacity (mmol g^{-1})					
	Cu (II)		Cr (III)		Cr (VI)	
	NH_2 [a]	COOH [b]	NH_2 [a]	COOH [b]	NH_2 [a]	COOH [b]
Fucus vesiculosus	**0.37**	**0.38**	**0.33**	**0.37**	**0.12**	**0.19**
	(0.01)	(0.01)	(0.04)	(0.02)	(0.01)	(0.02)
Fucus spiralis	**0.30**	**0.34**	**0.19**	**0.23**	**0.12**	**0.19**
	(0.01)	(0.02)	(0.03)	(0.02)	(0.04)	(0.03)
Ulva lactuca	**0.09**	**0.17**	**0.15**	**0.21**	**0.13**	**0.17**
	(0.01)	(0.02)	(0.03)	(0.02)	(0.03)	(0.02)
***Ulva* spp.**	**0.16**	**0.19**	**0.19**	**0.23**	**0.15**	**0.18**
	(0.02)	(0.01)	(0.02)	(0.02)	(0.01)	(0.03)
Palmaria palmata	**0.03**	**0.11**	**0.09**	**0.19**	**0.15**	**0.19**
	(0.01)	(0.01)	(0.03)	(0.03)	(0.01)	(0.02)
Polysiphonia	**0.14**	**0.16**	**0.17**	**0.21**	**0.27**	**0.31**
lanosa	(0.02)	(0.01)	(0.02)	(0.04)	(0.04)	(0.03)

[a] Methylation of amino groups [b] Esterification of carboxyl groups.

In general, it was shown that esterification of biomass carboxyl groups caused a larger decrease in metal binding than methylation of amino groups. However, when errors are considered, it is seen that, in some cases, error bars overlapped for amino and carboxyl blocking, thus making the contribution from the amino and carboxyl groups approximately equal e.g. *Polysiphonia lanosa* and *Ulva* spp. binding to all metals.

Results indicated that the relative importance of carboxyl groups in Cu (II) and Cr (III) binding follows the order: brown > green > red, while, Cr (VI) follows the order: red > brown > green.

The relative importance of amino groups in Cu (II) and Cr (III) binding followed the order: brown > green > red while Cr (VI) order was: red > green > brown.
Together, modification of amino and carboxyl groups had the largest effect on Cu (II) binding to brown and green seaweeds with lesser effects observed for Cr (III) and Cr (VI) binding. However, in the case of the red seaweeds, modification of these groups had the greatest influence on Cr (VI) binding with Cu (II) and Cr (III) binding being more or less equal.

6.3.3 Titration of Esterified Seaweeds

Many authors have pointed to the significance of carboxyl groups in metal binding to seaweeds. Therefore, it is important to investigate the relationship between the degree of carboxyl blocking and the decrease in metal uptake.

Fourest and Volesky [15] carried out potentiometric titrations on chemically modified biomass in order to establish the extent of the chemical modification after treatment with methanolic HCl.

Figure 6.4 compares the first derivative plots obtained from potentiometric titration data for raw and esterified *Fucus vesiculosus*, *Ulva* spp. and *Polysiphonia lanosa*. The quantity of acidic groups determined by titration are summarised in Table 6.10.

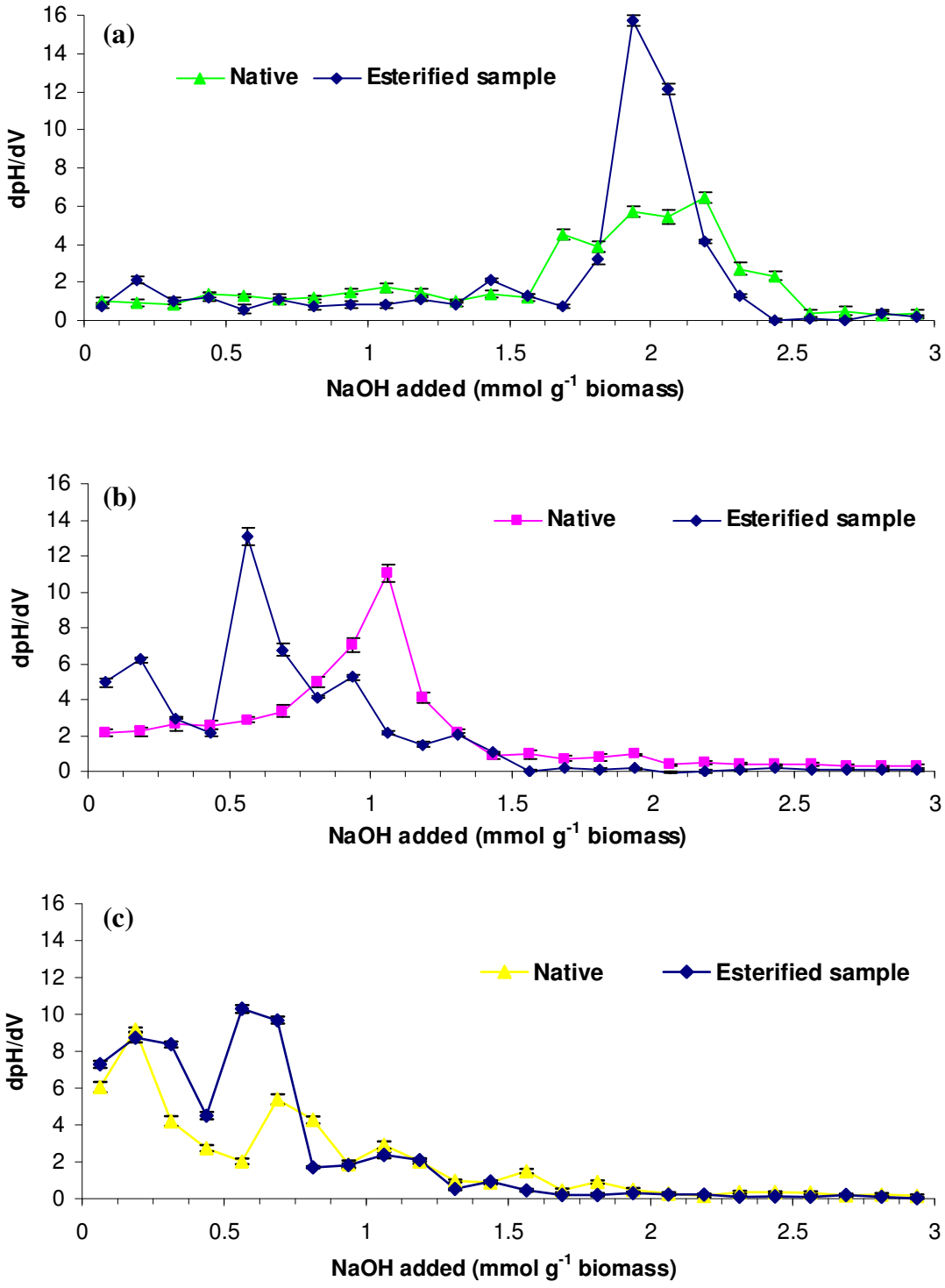

Figure 6.4 **First derivative potentiometric titration curves for (a) *Fucus vesiculosus* (b) *Ulva* spp. (c) *Polysiphonia lanosa*. Error bars are calculated based on triplicate analyses with 95% Confidence Intervals.**

Table 6.10 Surface acidic groups of esterified seaweed biomass as determined via potentiometric titration. Error bars are calculated based on triplicate analyses with 95% Confidence Intervals.

	Acidic Groups (mmol g^{-1})		
	Total	**Strong**	**Weak**
Fucus vesiculosus			
Native	2.44 ± 0.22[a]	0.44 ± 0.16[a]	2.00 ± 0.20[a]
Esterified	1.94 ± 0.21	0.19 ± 0.07	1.73 ± 0.14
***Ulva* spp.**			
Native	1.94 ± 0.13[a]	0.44 ± 0.11[a]	1.50 ± 0.22[a]
Esterified	1.31 ± 0.13	0.19 ± 0.09	1.12 ± 0.11
Polysiphonia lanosa			
Native	1.81 ± 0.16[a]	0.19 ± 0.06[a]	1.62 ± 0.11[a]
Esterified	1.44 ± 0.09	0.19 ± 0.08	1.25 ± 0.08

[a] **Titration data obtained from Table 2.2**

Loss of complexity in the carboxyl region of the plots in Figure 6.4 as well as decreases in the quantity of weak acidic functionalities indicates blocking of carboxyl groups had taken place after esterification.

In Chapter 3 (Figure 3.18), Cu (II) binding showed very strong correlation (r^2= 0.98) between metal uptake and the quantity of acidic groups on the biomass surface. Therefore, only decreases in the binding of this metal shall be considered. The decrease in total acidic groups was 0.50, 0.63 and 0.37 mmol g^{-1} for *Fucus vesiculosus*, *Ulva* spp. and *Polysiphonia lanosa* respectively of which 0.27, 0.38 and 0.37 mmol g^{-1} were attributed to carboxyl groups.

Since two carboxyl groups are necessary for chelation of one divalent metal cation [15] (Cu (II) in this case), it was anticipated that if the quantity of carboxyl groups decreased by 0.27 mmol g^{-1} as in *Fucus vesiculosus*, then the decrease in Cu (II) binding should be approximately 0.14 mmol g^{-1}. Similarly for *Ulva* spp. and *Polysiphonia lanosa*, the

magnitude of the expected decrease in Cu (II) binding would be 0.19 and 0.18 mmol g^{-1} respectively.

Good correlation between the degree of carboxyl blocking and the decrease in Cu (II) binding was found for *Ulva* spp. and *Polysiphonia lanosa* with decreases in binding of 0.19 and 0.16 mmol g^{-1} respectively. However, as already shown in Table 6.2, the decrease in Cu (II) binding to *Fucus vesiculosus* was in fact 0.38 mmol g^{-1} instead of approximately 0.14 mmol g^{-1}. Therefore, the decrease in binding must be related to inhibition of some other functionality as well as carboxyl esterification.

Although Jansen and Jang [32] used HCl in absolute methanol to esterify carboxyl groups from galacturonic acid and polyuronides, it was Kantor and Schubert [33] who described that desulphonation reactions may accompany these reactions. This desulphonation is shown by decreases in the quantity of strong acidic groups with a reduction of 0.25 mmol g^{-1} observed for *Fucus vesiculosus* and *Ulva* spp. These reactions may also account for some of the decreased metal binding in esterified samples. No change in the quantity of strong acidic groups was observed for *Polysiphonia lanosa*.

FTIR analysis of esterified *Fucus vesiculosus* (Section 6.3.7) reveals band shifts in both carboxyl and sulphonate functionalities after esterification indicating that changes had taken place in these groups.

6.3.4 FTIR Analysis of Treated Biomass

In order to discuss the trends in FTIR band shifting after chemical treatment, *Fucus vesiculosus* has been selected as a representative example. Figure 6.5 illustrates the FTIR spectra obtained for raw and chemically modified *Fucus vesiculosus*.

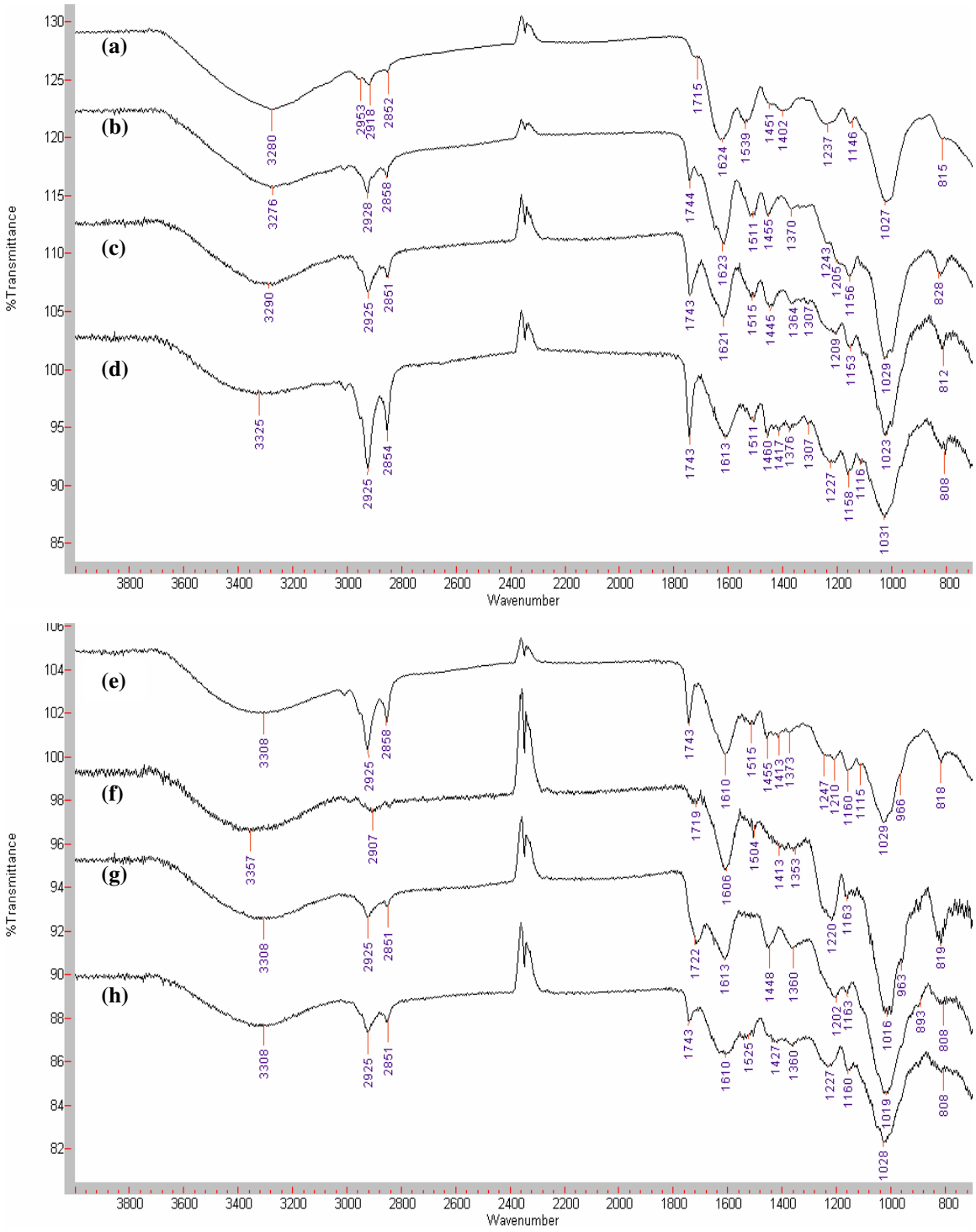

Figure 6.5 **FTIR spectra of *Fucus vesiculosus* before and after chemical modification (a) Raw (b) Acid treated (c) Alkali treated (d) Acetone washed (e) $CaCl_2$ washed (f) Na_2-EDTA washed (g) Methylation of amino groups (h) Esterification of carboxyl groups. Number of scans= 40, Resolution= 2. Sample spectra from triplicate analyses are shown.**

Table 6.11 summarises the carboxyl bands obtained for *Fucus vesiculosus* while the bands observed for the remaining functionalities are given in Table 6.12.

Table 6.11 Carboxyl bands observed for *Fucus vesiculosus* before and after chemical treatment. Number of scans= 40, Resolution= 2. Average data from triplicate runs are shown.

	Raw	Acid	Alkali	Acetone	$CaCl_2$	EDTA	NH_2[a]	COOH[b]
Assignment								
Free C=O	1715	1744	1743	1743	1743	1719	1722	1743
C=O $_{asymm}$	1629	1620	1621	1613	1610	1606	1613	1610
C=O $_{symm}$	1434	1457	1445	1460	1455	*	1448	1427
C-O	1402	1205	1209	1417	1413	1413	1202	1227
(COOH)			1243[1]					

[a] **Methylation of amino groups** [b] **Esterification of carboxyl groups** [1] **Peak shoulder**

Table 6.12 FTIR band shifting behaviour for raw and chemically treated *Fucus vesiculosus*.

	Raw	Acid	Alkali	Acetone	$CaCl_2$	EDTA	NH_2[a]	COOH[b]
Assignment								
-NH	1539	1517	1515	1511	1515	1504	*	1525
$SO_{3\ asymm}$	*	1371	1364	1376	1373	1353	1360	1360
$SO_{3\ symm}$	1153	1156	1153	1158	1160	1163	1163	1160
C-O (ether)	*	*	*	1116	1115	*	*	*
C-O (alc)	1027	1026	1023	1031	1029	1016	1019	1028

[a] **Methylation of amino groups** [b] **Esterification of carboxyl groups**

FTIR discussions for the modified biomasses are speculative in nature being based only on preliminary results for *Fucus vesiculosus*. However, further analysis is required in order to obtain a more conclusive indication of the changes in biomass structure after chemical treatment.

6.3.4.1 Acid Treatment

FTIR work in Chapter 4 used protonated biomass as the biosorbent control. As previously discussed, this is because raw biomass contains ions such as Na^+, K^+, Mg^{2+} and Ca^{2+}, which are naturally present in seawater making it unsuitable to use as a baseline. As seen in Figure 6.5 there are significant differences between the raw and protonated spectra of *Fucus vesiculosus* in terms of the wavenumber of various bands. Major changes in carboxyl bands (Both C=O and C-O stretches) are observed in Table 6.12 with changes also observed for sulphonate and amino groups in Table 6.13. These differences are observed because of replacement of the alkali and alkaline earth metal ions with H^+ ions during protonation. This replacement of ions results in wavenumber changes in the same way changes are observed when heavy metal ions bind to the protonated seaweed.

6.3.4.2 Alkali Treatment

Treatment with NaOH had comparable effects to HCl in terms of the spectrum obtained with similar band shifts being obtained in many cases. Both spectra showed similar wavenumbers for the (1) Free C=O stretch (2) asymmetric C=O stretch (3) the carboxyl C-O stretch and (4) the –NH stretching band. This perhaps indicates that in terms of their FTIR spectra, washing the biomass with sodium hydroxide has similar effect to protonation in "cleaning" the biomass surface. This is in contrast to the specific surface area measurements which saw a decrease in area after acid treatment but an increase following alkali treatment. This finding warrants further study.

6.3.4.3 Treatment with Acetone

The position of the free C=O stretch in acetone treated *Fucus vesiculosus* was identical to that obtained in the alkali treated biomass. However, differences in both the asymmetric and symmetric carboxyl stretches (1613 and 1460 cm^{-1} respectively) were observed with the carboxyl C-O stretch being closer in wavenumber to that of the acid treated biomass but significantly different to the alkali-treated biomass. In general, large changes in carboxyl group stretches were found after treatment with acetone.

A large wavenumber shift was observed for the –NH stretch with some movement of the C-O alcohol band also seen. As previously seen, treatment with acetone removes some protein and lipid fractions of the biomass surface. These groups contain $–NH_2$, -COOH and –OH functionalities and so changes in these groups would be expected in the FTIR spectra. The appearance of an ether band at 1116 cm^{-1} was also noted. Therefore, the spectra reveal changes in the composition of the seaweed surface after modification with acetone.

6.3.4.4 Treatment with $CaCl_2$

Based on metal uptake and surface area results, it was not expected that washing the biomass with $CaCl_2$ would have any great influence on the FTIR spectrum. The presence of naturally occurring Ca^{2+} on the raw seaweed surface also led to this assumption.

In fact, treatment with $CaCl_2$ brought about significant changes in the carboxyl stretching bands in comparison to the raw seaweed. These changes were apparent for the free, asymmetric and symmetric carboxyl stretches as well as the carboxyl C-O stretch (Table 6.11). These changes are due to the replacement of existing bound species e.g. Na^+, K^+ or Mg^{2+} by Ca^{2+} ions which changes the symmetry of the carboxyl group thus resulting in the wavenumber shifts observed.

Changes in sulphonate and amino groups were also apparent after biomass washing with the –NH shift from 1539 to 1511 cm^{-1} being more significant. The appearance of an ether band at 1115 cm^{-1} indicated changes in these groups after $CaCl_2$ washing.

6.3.4.5 Treatment with Na_2- EDTA

Treatment with Na_2- EDTA resulted in large changes in the FTIR spectra. Similarly to previous treatments, Na_2- EDTA caused shifts in the free and asymmetric carboxyl bands. However, unlike other treatments the symmetric carboxyl band was no longer visible after exposure. A large wavenumber change (1539 to 1504 cm^{-1}) and decrease in intensity was observed for the –NH stretch with almost complete disappearance of the

band after Na_2- EDTA washing. Significant changes were also observed for biomass sulphonate and alcohol groups. Changes in the FTIR spectra agree with the work of Park *et al*. [1] who reported that strong chelating agents may damage biomass cell wall and cause disintegration of the biomass. Perhaps if a more concentrated solution had been used complete disappearance of these bands would be observed.

6.3.4.6 Methylation of amino groups

Methylation of the amino groups of *Fucus vesiculosus* resulted in changes in biomass carboxyl groups with wavenumber decrease for the free C=O stretch and the asymmetric C=O stretch as well as a major decrease in the carboxyl C-O stretch. Some changes in biomass sulphonate groups had taken place with a significant wavenumber decrease for the C-O (alcohol) band.

The disappearance of the –NH stretching band (present in the raw spectrum at 1539 cm^{-1}) suggests that significant changes had taken place in the biomass amino groups in accordance with Equation 6.3.

The free amino groups initially present on the biomass surface have the structure R-NH_2 but after methylation they present an R-$N(CH_3)_2$ structure. Since the band at 1539 cm^{-1} relates to –NH stretching in the biomass, the disappearance of this band after methylation is as expected since the -NH_2 species has been replaced by -$N(CH_3)_2$. Therefore, the disappearance of this band proves that methylation of the amino groups has taken place. This also corresponds with the decrease in metal binding observed after blocking of these groups.

6.3.4.7 Esterification of carboxyl groups

Given that the aim of this modification technique is to alter biomass carboxyl groups, it would be expected that significant band shifts would be observed for these groups. Kapoor and Viraraghavan [12] postulated that formation of the ester should result in either a decrease or disappearance of the free carboxyl band. In the case of *Fucus*

vesiculosus, the free C=O band was still visible but a decrease in intensity was observed. The wavenumber of the band increased 1715 cm^{-1} to 1743 cm^{-1} pointing to possible formation of the ester.

Significant changes occurred for the both asymmetric C=O stretch (1629 to 1610 cm^{-1}) and the symmetric stretch (1434 to 1427cm^{-1}) while a large decrease in the wavenumber of the C-O (COOH) stretch was observed from 1402 cm^{-1} to 1227 cm^{-1}. This implied that the ester had been formed with the -C-OH of the biomass carboxyl groups replaced by a –C-OCH_3 (according to Equation 6.3).

Large wavenumber changes were also observed for the amino and sulphonate groups which may have been due to the presence of HCl in the reaction mixture.

6.4 Conclusions

Pre-treatment with acetone (0.1M) was the most effective modification method investigated as it yielded biomasses with enhanced capacity for both cations and anions.

Chemical modification of the biomass amino and carboxyl groups resulted in decreased ability of the seaweeds to bind both cations and anions illustrating the importance of these functionalities in metal binding to seaweeds. These results confirm the results previously identified by potentiometric titration, FTIR and XPS analysis.

Some correlation was found between the degree of carboxyl group blocking and the decrease in Cu (II) binding to *Fucus vesiculosus* and good correlation for *Ulva* spp. and *Polysiphonia lanosa*. This indicates that while carboxyl groups are important for metal binding, they are not the only functional group with a role to play.

FTIR analysis confirmed the change in biomass surface composition after chemical modification.

Work in previous chapters has identified the seaweeds with the greatest metal uptake capacity as well as the functional groups responsible for binding (Chapters 2-4). EDX and XPS analyses (Chapter 5) have pointed to the metal binding mechanisms while chemical modification techniques have identified the most suitable treatment in terms of binding capacity enhancement (Chapter 6).

While SEM analysis in Chapter 5 has revealed a qualitative estimate of the changes in seaweed surface morphology, Chapter 7 investigates and quantifies these changes on a μm level using a novel scanning force microscopy protocol.

6.5 References

[1] Park, D., Yun, Y. S. and Park, J. M. *Chemosphere*, **60**, 1356-1364 (2005).

[2] Lodeiro, P., Cordero, B., Grille, Z., Herrero, R. and De Vicente, M. E. S. *Biotechnology and Bioengineering*, **88**, 237-247 (2004).

[3] Yang, J. and Volesky, B. *Environmental Science and Technology*, **33**, 751-757 (1999).

[4] Gürisik, E., Arica, M. Y., Bejtas, S. and Genc, O. *Engineering in Life Sciences*, **4**, 86-89 (2004).

[5] Bai, R. S. and Abraham, T. E. *Water Research*, **36**, 1224-1236 (2002).

[6] Kratochvil, D., Pimentel, P. and Volesky, B. *Environmental Science & Technology*, **32**, 2693-2698 (1998).

[7] Davis, T. A., Volesky, B. and Mucci, A. *Water Research*, **37**, 4311-4330 (2003).

[8] Sheng, P. X., Ting, Y. P., Chen, J. P. and Hong, L. *Journal of Colloid and Interface Science*, **275**, 131-141 (2004).

[9] Chen, J. P. and Yang, L. *Langmuir*, **22**, 8906-8914 (2006).

[10] Jeon, C., Park, J. Y. and Yoo, Y. J. *Water Research*, **36**, 1814-1824 (2002).

[11] Luo, F., Liu, Y., Li, X., Xuan, Z. and Ma, J. *Chemosphere*, **64**, 1122-1127 (2006).

[12] Kapoor, A. and Viraraghavan, T. *Bioresource Technology*, **61**, 221-227 (1997).

[13] Beveridge, T. J., Williams, F. M. R. and Koval, J. J. *Canadian Journal of Microbiology*, **24**, 1439-1451 (1978).

[14] Gardea-Torresdey, J. L., Becker-Hapak, M. K., Hosea, J. M. and Darnall, D. W. *Environmental Science & Technology*, **24**, 1372-1378 (1990).

[15] Fourest, E. and Volesky, B. *Environmental Science & Technology*, **30**, 277-282 (1996).

[16] Brady, D. and Duncan, J. R. *Enzyme and Microbial Technology*, **16**, 633-638 (1994).

[17] Beveridge, T. J. and Murray, R. G. *Journal of Bacteriology*, **141**, 876-887 (1980).

[18] Brady, D., Stoll, A. and Duncan, J. R. *Environmental Technology*, **15**, 429-438 (1994).

[19] Yang, L. and Chen, J. P. *Bioresource Technology*, **In Press, Corrected Proof**, (2007).

[20] Figueira, M. M., Volesky, B., Ciminelli, V. S. T. and Roddick, F. A. *Water Research*, **34**, 196-204 (2000).

[21] Crist, R. H., Oberholser, K., Mcgarrity, J., Crist, D. R., Johnson, J. K. and Brittsan, J. M. *Environmental Science & Technology*, **26**, 496-502 (1992).

[22] Davis, T. A., Volesky, B. and Vieira, R. H. S. F. *Water Research*, **34**, 4270-4278 (2000).

[23] Vijayaraghavan, K., Jegan, J., Palanivelu, K. and Velan, M. *Separation and Purification Technology*, **44**, 53-59 (2005).

[24] Yun, Y. S., Park, D., Park, J. M. and Volesky, B. *Environmental Science & Technology*, **35**, 4353-4358 (2001).

[25] Chu, K. H., Hashim, M. A., Phang, S. M. and Samuel, V. B. *Water Science and Technology*, **35**, 115-122 (1997).

[26] Mehta, S. K. and Gaur, J. P. *Ecological Engineering*, **18**, 1-13 (2001).

[27] Fourest, E. and Roux, J. C. *Applied Microbiology and Biotechnology*, **37**, 399-403 (1992).

[28] Yan, G. and Viraraghavan, T. *Bioresource Technology*, **78**, 243-249 (2001).

[29] Ashkenazy, R, Gottlieb, L. and Yannai, S. *Biotechnology and Bioengineering*, **55**, 1-10 (1997).

[30] Akthar, N. Md., Sastry, K. S. and Mohan, P. M. *Biometals*, **9**, 21-28 (1995).

[31] Niu, H. and Volesky, B. *Hydrometallurgy*, **71**, 209-215 (2003).

[32] Jansen, E. F. and Jang, R. *Journal of the American Chemical Society*, **68**, 1475-1477 (1946).

[33] Kantor, T. G. and Schubert, M. *Journal of the American Chemical Society*, **79**, 152-153 (1957).

Chapter 7 Development of a Scanning Force Microscopy Protocol for Seaweed Analysis

7.1 Introduction

Results to date have described the functionalities involved in metal binding as well as qualitatively investigating the substantial changes in surface morphology brought about by this binding. The work in this chapter involves the development of a preliminary scanning force microscopy protocol for seaweed analysis and presentation of some of the initial results obtained. The use of this protocol allows the analysis of changes in the seaweeds by measuring parameters such as the surface roughness and height which may be compared with the qualitative images obtained by scanning electron microscopy.

The use of scanning force microscopy to measure such changes in seaweed surface morphology has not previously been presented in the literature.

7.1.1 Scanning Probe Microscopy

As discussed in Chapter 1, a scanning probe microscope (SPM) is comprised of a sensing probe, piezoelectric ceramics for positioning the probe, an electronic control unit, and a computer for controlling the scan parameters as well as generating and presenting images [1]. The sensors available for scanning probe microscopy i.e. the force sensor and the tunneling sensor are introduced in Section 1.5.5. Seaweed analysis in this work has been carried out using the force sensor and its related technique; scanning force microscopy.

Scanning force microscopy (SFM) allows scanning of non-conductive samples. In SFM, the interaction of interest takes place between a single atom at the apex of a tip and a single atom on the surface of the sample. As the tip and surface are atomically close to one another, the interaction between the two can be strong enough to deform the surface, the tip or both.

The SFM's scanning operation can be divided into two essential modes: contact and non-contact mode. These terms simply refer to whether or not the probe comes into contact with the sample surface.

In contact mode, the probe tip scans across the sample surface, coming into direct physical contact with the sample. As the probe tip scans, varying topographic features cause deflection of the tip and cantilever [1].

In non-contact operation, the cantilever is oscillated above the sample at its resonant frequency. In this mode, changes in force between the tip and sample are detected, even though they are not in contact. As the probe gets closer to the sample surface, the attractive force between the tip and the sample changes, thus modifying both the oscillation amplitude and phase of the vibrating cantilever. Either of these changes can be detected and used to track the surface and map topographic data.

7.1.2 SFM Analysis of Biological Materials

As outlined in Chapter 1, a wide range of biological materials from bio-molecules to entire cells have been imaged with SFM [2].

Biological samples can either be imaged in wet or dry environments. However, even for surfaces free of contamination, ambient humidity can cause capillary forces to act on the tip [3]. In order to eliminate these forces, the general preference is to image under liquid. The crucial issue then becomes one of sample preparation as it is necessary to immobilise the sample onto a suitable substrate without introducing imaging artifacts. Contact mode under liquid has successfully been used to image DNA molecules in propanol, water an aqueous buffers [4,5]. Imaging in aqueous buffer solutions has the advantage that the native structure of the biomolecules is preserved making it possible to study the course of biological interactions e.g. Drake *et al.* [6] used SFM to follow the formation of a polymerized fibrin network on a mica surface in real time by adding thrombin to a solution of fibrinogen.

7.1.3 Rationale behind the use of SFM for seaweed analysis

Although SEM analysis in Chapter 5 revealed substantial changes in seaweed surface morphology after metal binding, the information provided was qualitative in nature. Since a more quantitative estimation of the surface changes was required, scanning force microscopy (SFM) was selected as a suitable analysis technique.

Compared with Scanning Electron Microscope, SFM provides extraordinary topographic contrast, direct height measurements and unobstructed views of surface features as no coating (e.g. gold sputter) is necessary.

As previously discussed, a number of authors have used scanning force microscopy to investigate the native polysaccharide networks present in some seaweed polymers [3,7,8]. The results of their work are summarised in Chapter 1. It was found that an obstacle to imaging these polymers was the development of large adhesive forces which could "glue" the tip to the surface and as a result damage samples during scanning [8]. Adhesion may result from capillary condensation [9] or "debris" collected by the probe tip [10].

While Feng and Aldrich [11] previously used scanning force microscopy to analyse the surface of *Ecklonia maxima*, no quantitative data regarding the nature of the algal surface was given. Figure 7.1 illustrates the SFM topographic images obtained by these authors for the raw, $CaCl_2$ treated and metal desorbed seaweed.

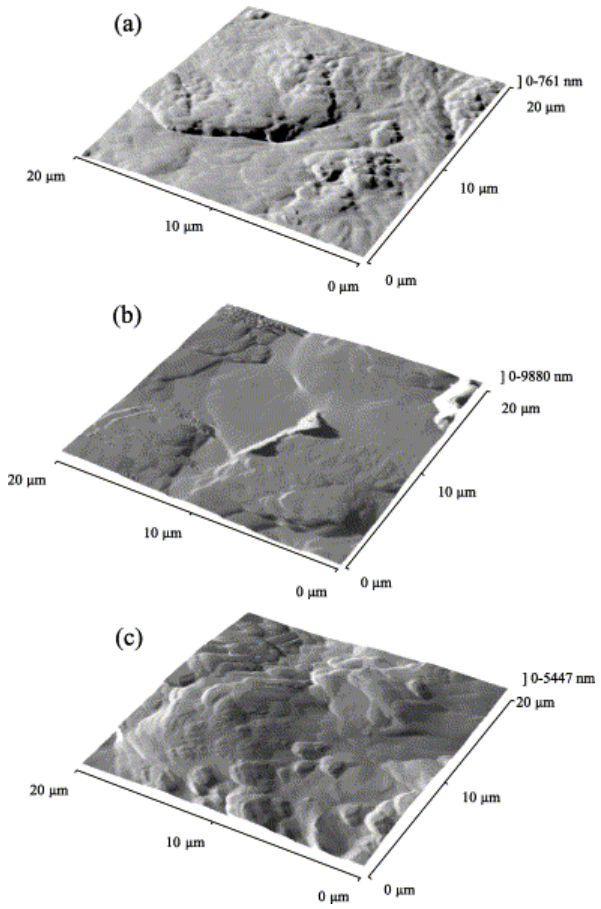

Fig 7.1 **SFM Topographic images for an 0.8 mm *Ecklonia maxima* particle showing (a) raw seaweed (b) 0.2M $CaCl_2$ treated (c) metal stripped seaweed [11]. Scan range= 20µm.**

From Figure 7.1, the authors observed that the surface of the $CaCl_2$-treated seaweed particle (b) was rough, while the surface of the regenerated seaweed particle (c) was comparatively flat. They postulated that this was due to the loss of alginate on the seaweed surface after regeneration leading to loss of sorption capacity. However, no quantifiable changes in the seaweed surface were identified by these authors.

In fact, no literature has been found in which SFM is used to quantify changes in seaweed surface morphology after heavy metal binding. In the present study, *Ulva lactuca* was chosen for analysis as it had showed significant morphological changes after Cu (II)

exposure (Chapter 5, Figure 5.7b). It is envisaged that the analysis protocol developed for *Ulva lactuca* will be applicable to the analysis of various other seaweed species.

7.1.4 Objectives of the Research

The main objectives of the work in this chapter were:

- To demonstrate the use of a novel Scanning Force Microscopy technique for seaweed surface analysis.
- To quantify changes in the surface morphology of *Ulva lactuca* after Cu (II) binding and correlate these with changes observed using Scanning Electron Microscopy.
- To potentially describe Cu (II) binding to *Ulva lactuca* on a μm scale.

7.2 Experimental

7.2.1 Chemicals

- 1000 mg L^{-1} Cu (II) AAS Standard- Sigma Aldrich (Ireland) Ltd.
- 0.1M NaOH
- 0.1M HCl

7.2.2 Instrumentation

- Explorer™ SPM Head with integral CCD (charge-coupling device) camera: ThermoMicroscope -VEECO
- TMX 1010 stage
- Electronic Control Unit- ECU-*Plus* ™
- Nano-k ™ vibration isolation table - minus k technology
- Optical Bench - THORLABS
- SPMLab 602 Image Processing Software
- B/W microscope monitor – Ikegami

7.2.3 Sample Preparation

Intact specimens of *Ulva lactuca* were thoroughly washed with Milli-Q distilled water in order to remove any adhering debris and residual salt from the seaweed surface. Samples were exposed to 50mL of Cu (II) at pH 5 at a biomass concentration of 2 mg mL^{-1}. Initial Cu (II) concentrations were: 1 ng L^{-1}, 1 μg L^{-1} and 50 μg L^{-1}. Samples were shaken for 4h at 200 rpm and room temperature (21 ± 1°C) and oven dried at 60°C for 24h. In order to minimise any debris on the seaweed surface the samples were subsequently blown with nitrogen (99.99% Purity) and then stored in sealed airtight containers until required.

7.2.4 Imaging samples with Scanning Force Microscopy

Seaweed samples (approximately 3 cm x 3 cm) were attached to magnetic sample holders using a thin layer of non-conductive glue. Special care was taken to ensure that samples

were completely flat so that no additional roughness was added to the measurement. Samples were also checked for the presence of air bubbles before analysis.

Samples were imaged in air using a piezoceramic tripod type dry scanner arrangement. Analysis was carried out in contact mode with non-conductive silicon nitride (Si_3N_4) pyramidal probes (200μm). Probes were integrated onto the end of a cantilever with a spring constant (K) in the region of 0.03 N m^{-1} - 0.6 N m^{-1}. Samples were scanned at a range of 50, 20, 10 and 5μm at a scan rate of 2 x (scan range).

7.3 Results and Discussion

From Chapter 1, it was seen that the cell wall matrix of Chlorophyta e.g. *Ulva lactuca* contains highly complex sulphated hetero-polysaccharides [12] as well as a high protein content (10-26%) [13]. The presence of these polysaccharides and proteins offers carboxyl, sulphonate and amino groups for metal binding. FTIR analysis (Chapter 4) showed that carboxyl, amino and sulphonate groups interacted with Cu (II), while XPS analysis (Chapter 5) illustrated an ion-exchange mechanism as well as interactions with oxygen, nitrogen and sulphur containing functionalities. This indicated that there were contributions from both seaweed polysaccharides and proteins, both of which are polymeric in nature.

50 µm scans were taken of the surface of the raw, 1 ng L^{-1}, 1 µg L^{-1} and 50 µg L^{-1} samples (Figures 7.2-7.5). Areas of light and dark in the image represent the peaks and troughs present on the seaweed surface.

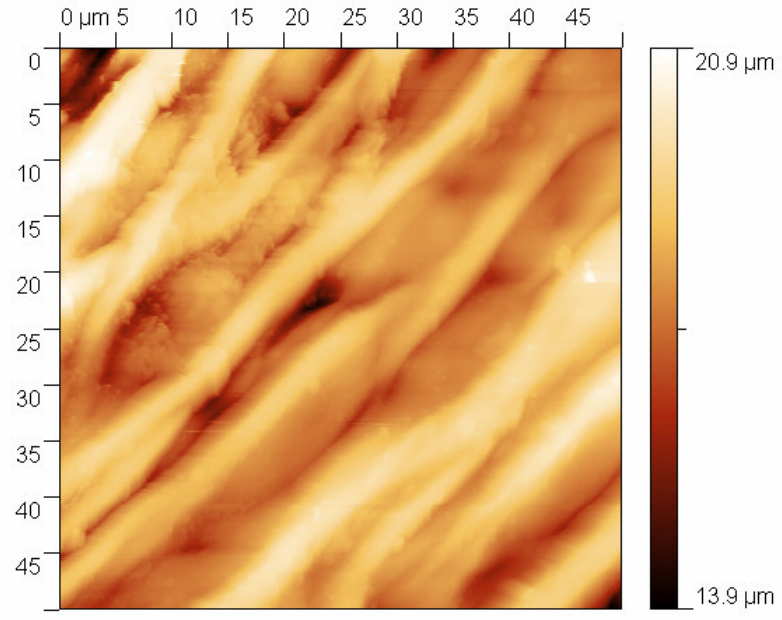

Figure 7.2 SFM image of raw *Ulva lactuca*. Scan range = 50 µm, scan rate = 100 µm s^{-1}. A representative image from triplicate analyses is presented.

Significant agreement was seen between the SEM micrographs (Figure 5.7a) and the images of raw *Ulva lactuca* obtained using scanning force microscopy. The series of parallel chains visible on the surface have an average width of 5 ± 1.5 µm (n=10). These chain structures are most likely due to interactions between adjacent polymer chains and metal cations naturally present in the seaweed e.g. Na^{+}, Ca^{2+} and Mg^{2+}. EDX analysis (Chapter 5) revealed the absence of K^{+} in raw *Ulva lactuca*.

Figure 7.3 illustrates a 3D projection of the seaweed surface in Figure 7.2.

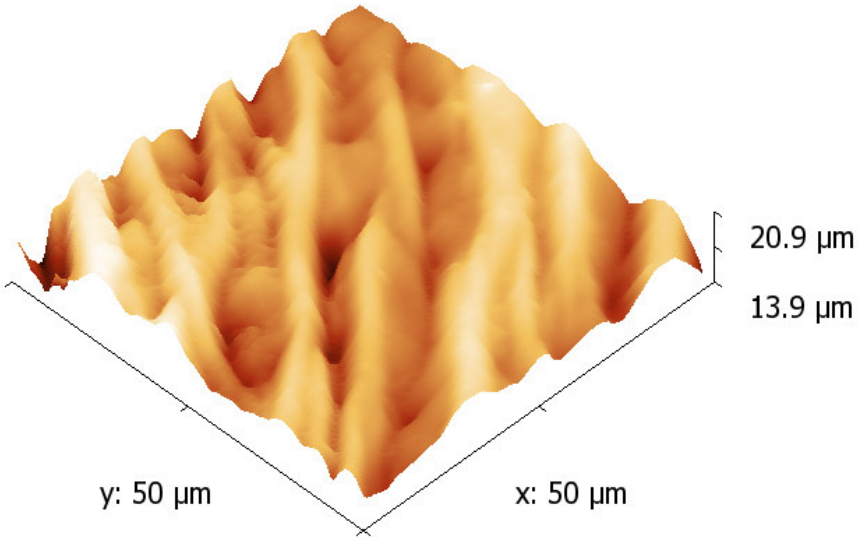

Figure 7.3 3D projection of the surface of raw *Ulva lactuca* obtained in Figure 7.2. Scan range = 50 µm, scan rate = 100 µm s^{-1}.

Figure 7.4 (a) and (b) respectively illustrate the SFM images obtained for *Ulva lactuca* after exposure to 1 ng L^{-1} Cu (II) and the 3D projection of the seaweed surface.

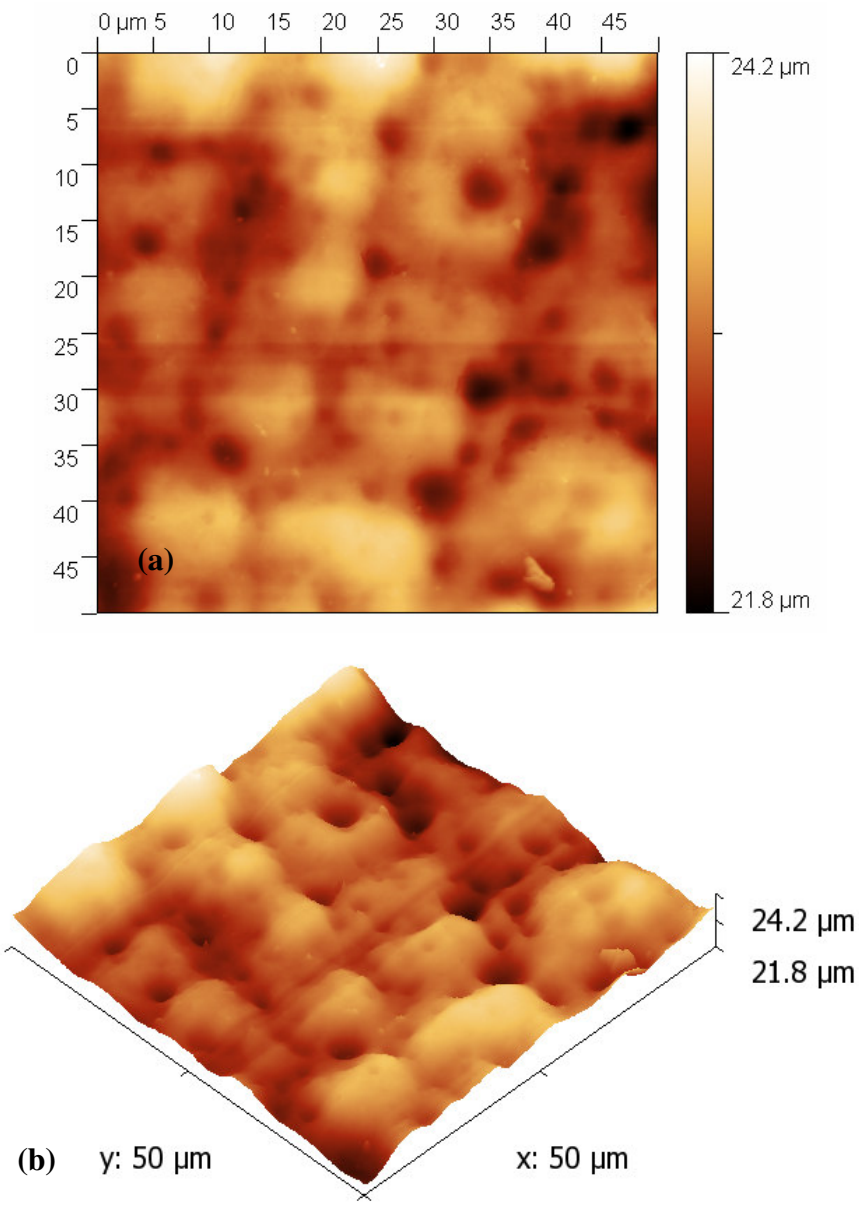

Figure 7.4 **(a) SFM image of *Ulva lactuca* exposed to 1 ng L^{-1} Cu (II). Scan range = 50 µm, scan rate = 100 µm s^{-1} (b) 3D projection of the seaweed surface. Representative images from triplicate analyses are presented.**

In Figure 7.4 (a) significant changes in the seaweed surface due to surface rearrangement were observed. Some traces of the parallel chains seen in the raw seaweed are still visible but circular depressions are also apparent on the 1 ng L^{-1} Cu (II)-loaded surface. The diameter of these depressions was measured and an average value 3.5 ± 0.8 µm (n=10) was obtained.

In addition to these surface depressions, Figure 7.4 (b) reveals the presence of surface mounds similar to those observed in SEM micrographs (Chapter 5). These mounds have an average diameter of 7.4 ± 0.5 μm (n=10). Surface measurements are summarised in Table 7.1.

Figure 7.5 (a) and (b) respectively illustrate the SFM images obtained for *Ulva lactuca* after exposure to 1 μg L^{-1} Cu (II) and the 3D projection of the seaweed surface.

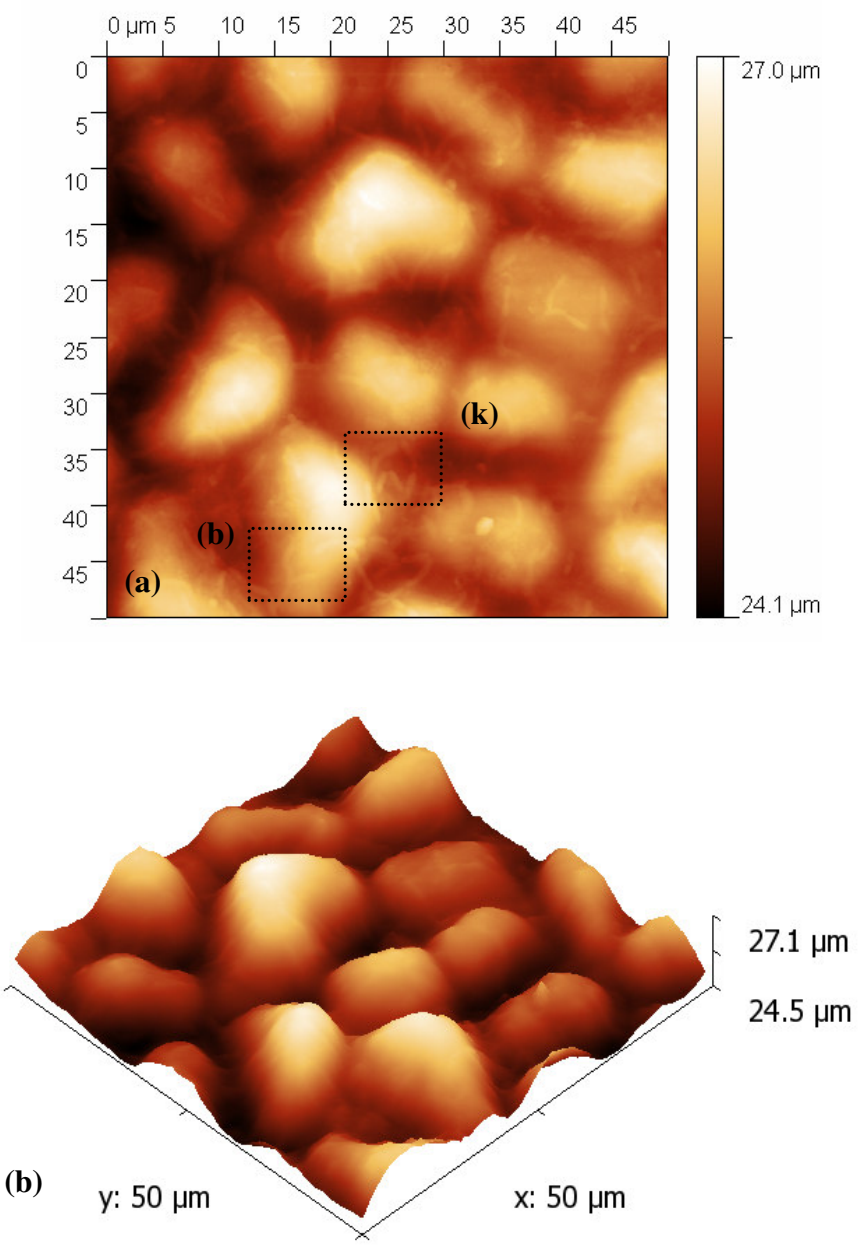

Figure 7.5 **(a) SFM image of *Ulva lactuca* exposed to 1 µg L^{-1} Cu (II). Scan range = 50 µm, scan rate = 100 µm s^{-1}, where k=kink and b=bifurcation of the polymer chain (b) 3D projection of the seaweed surface. Representative images from triplicate analyses are presented.**

The parallel chains observed in the raw and ng L^{-1} samples were not apparent in the 1 µg L^{-1} sample indicating that significant surface reconstruction has occurred at higher metal concentrations. The "rods" visible on the large mounds in Figure 7.5 (a) were not observed in either Figure 7.2 or 7.4. It is possible that these "rods" are actual fragments of

uncomplexed polymer chains which were not clearly visible at low concentrations. These chains are similar in appearance to the alginic acid chains observed by Decho [3] in his study on alginate polymers (Figure 1.20) where the width of single alginate strands in suspension varied between 1.41 nm and 4.65 nm (n=20). However, the thickness of the polymer strands in the gel matrix ranged from 3.74 to 18.2nm.

For *Ulva lactuca*, the average width of the observed rods was 0.53 ± 0.06 μm (n=10), which is significantly higher than those observed for alginic acid. This increased width may represent several polymer molecules arranged as an aggregate in a side-by side association.

Kinks **(k)** may represent an abrupt change in the polymer orientation in Figure 7.5. On the other hand, a bifurcation **(b)** may represent a region where there is unravelling of adjacent chains into individual strands [3].

Surface measurements are summarised in Table 7.1. Figure 7.6 (a) and (b) respectively illustrate the SFM images obtained for *Ulva lactuca* after exposure to 50 μg L^{-1} Cu (II) and the 3D projection of the seaweed surface.

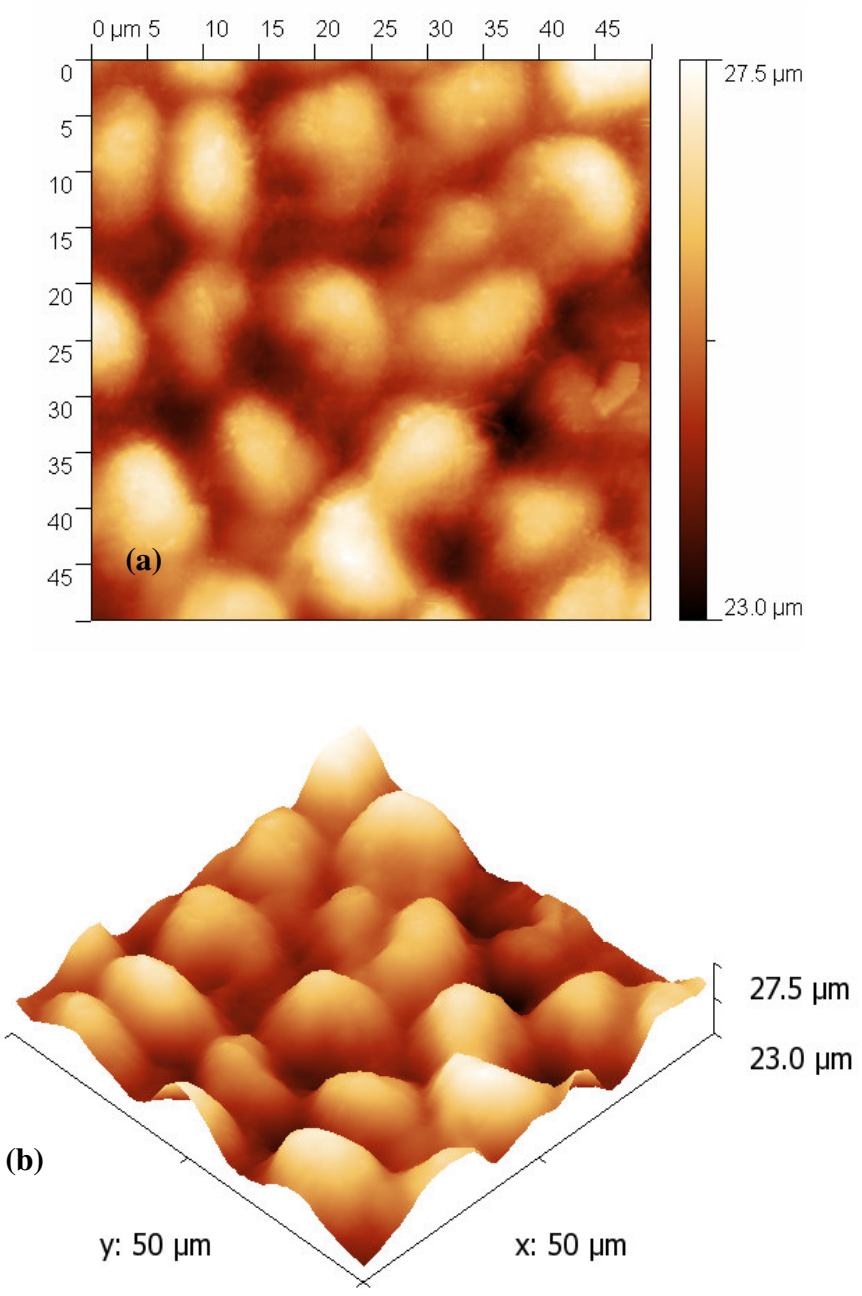

Figure 7.6 **(a) SFM image of *Ulva lactuca* exposed to 50 µg L^{-1} Cu (II). Scan range = 50 µm, scan rate = 100 µm s^{-1} (b) 3D projection of the seaweed surface. Representative images from triplicate analyses are presented.**

The chain fragments visible in Figure 7.5a are absent from the 50 µg L^{-1} loaded sample (Figure 7.6). This may be due to coordination of the Cu (II) ions by the polymer chains. Thus, these fragments are no longer available on the seaweed surface.

The surface roughness and average height values obtained from the 50μm scans of raw and metal loaded *Ulva lactuca* are summarised in Table 7.1.

Table 7.1 Surface roughness (R_a) and average heights of raw and Cu (II)-loaded *Ulva lactuca*. Average data (±SD) from triplicate analyses are presented.

	Raw	1 ng L^{-1}	1 μg L^{-1}	50 μg L^{-1}
R_a (μm)	7.49 ± 0.32	3.20 ± 0.50	4.04 ± 0.29	7.38 ± 0.10
Average Height (μm)	4.29 ± 0.41	1.08 ± 0.14	1.78 ± 0.67	2.36 ± 0.74

From Table 7.1, it is apparent that when the seaweed is exposed to ng L^{-1} quantities of Cu (II), some flattening of the surface occurs initially occurs with significant decreases observed in both surface roughness (from 7.49 ± 0.32 to 3.20± 0.50) and average height (from 4.29 ± 0.41 to 1.08 ± 0.14). Addition of Cu (II) to the system (even in trace amounts) appears to disrupt interactions between polymer chains, thus bringing about a reconstruction of the surface.

As the metal concentration increased, an increase in surface roughness and average height was observed with the R_a value of the 50 μg L^{-1} sample approaching that of the raw seaweed. However, despite the fact that the roughness values are comparable, the morphologies of the raw and metal loaded seaweeds are completely different.

Although SEM analyses in Chapter 5 were carried out at a metal concentration of 2000 mg L^{-1}, the SFM images obtained in the ng L^{-1} to μg L^{-1} range (Figure 7.4-7.6) were well matched with them. Therefore, both techniques again pointed to disruption of polymeric chains after metal binding. It was postulated that replacement of light metal ions such as Ca (II) with heavy metal ions such as Cu (II) brought about significant changes in polymer cross-linking by forming stronger coordinative bonds.

Scanning force microscopy results therefore imply that, even at low concentrations, the addition of a heavy metal ion has a significant effect on seaweed surface morphology.

Because significant changes occurred at low concentrations it is fair to assume that, at a metal concentration of 2000mg L^{-1}(as used in SEM analysis), almost complete metal complexation and surface reconstruction had taken place.

While surface roughness and height values gave an indication of the overall changes in morphology following metal exposure, it is also important to look at changes in individual surface structures after binding.

The most interesting surface features were observed in the 1 µg L^{-1} Cu (II) sample (Figure 7.5a). Figure 7.7 illustrates the 20 µm scan of this sample with various surface features highlighted.

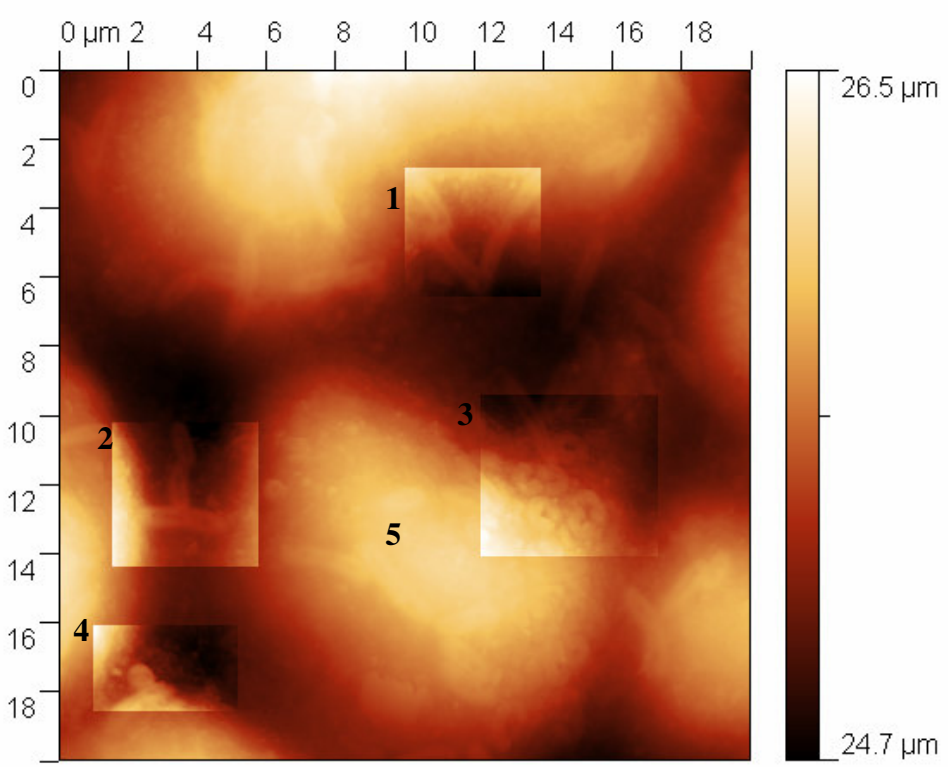

Figure 7.7 SFM image of *Ulva lactuca* exposed to 1 µg L^{-1} Cu (II). Scan range = 20 µm, scan rate = 40 µm s^{-1}

In Figure 7.7, polymer fragments such as **(1)** and **(2)** are arranged in a random configuration with an average length of 3.04 ± 0.07 µm and an average width of 0.53 ± 0.06 µm (n=10). These chains appear to either be hollow/ indented in the centre, thus

supporting the theory that these chains are aggregates containing a number of chains in a side by side arrangement. Chain **(2)** stretches across the grain boundary thus linking two adjacent mounds with an additional chain linked perpendicularly.

A folding or twisting of these chains is apparent in **(3)** with hollow circular particles of an internal diameter of 0.49 ± 0.04 μm and an external diameter of 1.04 ± 0.19 μm observed. The average chain width in this circular structure is therefore 0.55 ± 0.05 μm which corresponds well with the width observed for the straight chains (0.53 ± 0.06 μm). Thus it appears that polymer fragments are complexing around the metal ion in order to bind it. This agrees with the idea that polymer chains are twisted when coordinated with a metal ion (Chapter 5). Because the metal concentration is relatively low, the surface is not saturated with metal ions and therefore a mixture of free and complexed polymer is expected on the surface.

The small grain **(4)** has a diameter of 0.77 ± 0.12 μm and is apparently solid in appearance. It is possible that this grain **(4)** may be comprised of a number of circular polymer associations such as those in **(3)**. Possible dense packing of these chains around the metal ion may account for the solid appearance of the grain in the SFM image.

The large mound **(5)** is a possible agglomerate of smaller grains such as **(4)** and has a diameter of 13.36 μm. The formation of these grains and mounds at higher metal concentrations contributes to the increased surface roughness as illustrated in Table 7.1. The average distance between adjacent mounds is 1.55 ± 0.22 μm (n=10).

The observed features and their chemical composition require further SFM investigations to correlate them with the Cu (II) binding mechanisms as understood in the literature [14,15].

Figure 7.8 illustrates the 20 µm scan of the 50 µg L^{-1} Cu (II) sample. The progression of the surface features observed in Figure 7.7 is discussed below.

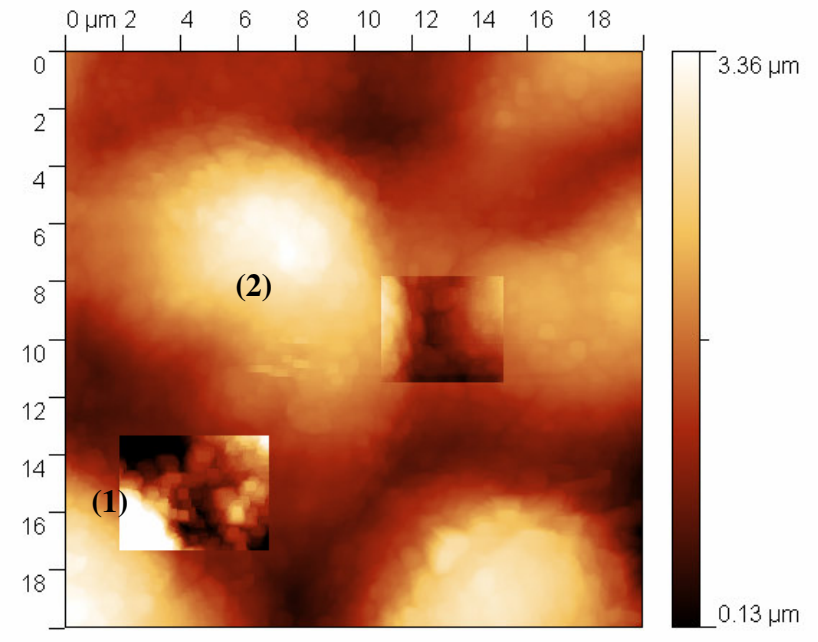

Figure 7.8 SFM image of *Ulva lactuca* exposed to 50 µg L^{-1} Cu (II). Scan range = 20 µm, scan rate = 40 µm s^{-1}

The mounds in Figure 7.8 have an average diameter of 15.38 ± 1.12 µm. This is larger than the value observed in Figure 7.7 for the 1 µg L^{-1} Cu (II) sample (13.36 µm) thus showing growth of these mounds with increasing metal concentration. This supports the idea that smaller grains agglomerate on the surface to form large mounds thus contributing to the increased surface roughness and height.

The small grains **(1)** on the edge of the large mound **(2)** (Figure 7.8) have an average diameter of 0.55 ± 0.08 µm while the distance between adjacent large mounds is 0.86 ± 0.15 µm. The distance between mounds in Figure 7.8 is lower than that observed in the 1 µg L^{-1} sample (Figure 7.7) thus indicating that the mounds are growing and aggregating with increasing metal concentration. Further growth of these structures at increased concentration would be expected with similar morphology to that seen in SEM images observed at high concentrations.

7.3 Conclusions

A novel SFM protocol for the analysis of seaweed surface morphology has been demonstrated in this chapter. Although only preliminary work has been carried out, this technique has the potential to provide an insight into the mechanism of heavy metal binding to the seaweed surface.

Significant reconstruction of the surface morphology of *Ulva lactuca* was observed after exposure to Cu (II) ions.

Exposure of *Ulva lactuca* to ng L^{-1} concentrations of Cu (II) resulted in significantly decreased roughness and height values. However, a subsequent increase in metal concentration brought about corresponding increases in surface roughness and height.

A proposed mechanism of Cu (II) may be as follows:

When the seaweed is exposed to low concentrations of Cu (II), the heavy metal may disrupt interactions between adjacent polymer chains. As seen in Chapter 5, the ionic radius of Cu (II) is less than that of Ca (II) and therefore Cu (II) incorporates a smaller number of functional groups into its coordination sphere. As the Cu (II) concentration increases, more Ca (II) is replaced with Cu (II) and thus some polymer fragments may become uncomplexed perhaps accounting for the high concentration of polymer fragments observed in Figure 7.6. Further increases in metal concentration may lead to complexation of the metal ions by ring closure (chelation) with surface polymers. These metal-ligand structures may then form into larger surface agglomerates thus accounting for the dramatic changes in surface morphology *in Ulva lactuca* after Cu (II) binding.

7.4 Future Work

Because the work in this chapter is preliminary with respect to the elucidation of Cu (II) binding mechanisms, there is huge scope for future work in the area. Some key areas of future work with this technique include:

- Further surface analysis at a variety of increased Cu (II) concentrations.
- A comprehensive analysis of the effects of Cr (III) and Cr (VI) on surface morphology.
- Application of the analysis protocol to the remaining seaweeds.
- Real time analysis of metal binding under liquid to investigate changes in surface morphology as metal binding occurs.
- Investigation into the changes in surface morphology brought about by chemical modifications.
- Multiple elemental analyses to match aggregation patterns and changes in surface roughness to a range of metals with varying ionic radii.

7.5 References

[1] ThermoMicroscopes., Scanning Probe Microscopy, In: Explorer Instrument Operation Manual 85-102444 Rev C, 1-11 (2001).

[2] Heinrich Horber, J. K., Local Probe Techniques, In: Atomic Force Microscopy in Cell Biology, Jena, B. P. and Heinrich Horber, J. K. (Ed.), Academic Press, San Diego, 1-31 (2002).

[3] Decho, A. W. *Carbohydrate Research*, **315**, 330-333 (1999).

[4] Hansma, H. G., Vesenka, J., Siegerist, C., Kelderman, G., Morrett, H., Sinsheimer, R. L., Elings, V., Bustamante, C. and Hansma, P. K. *Science*, **256**, 1180-1184 (1992).

[5] Vesenka, J., Guthold, M., Tang, C. L., Keller, D., Delaine, E. and Bustamante, C. *Ultramicroscopy*, **42**, 1243-1249 (1992).

[6] Drake, B., Prater, C. B., Weisenhorn, A. L., Gould, S. A. C., Albrecht, T. R., Quate, C. F., Cannell, D. S., Hansma, H. G. and Hansma, P. K. *Science*, **243**, 1586-1589 (1989).

[7] Gunning, A. P., Cairns, P., Kirby, A. R., Round, A. N., Bixler, H. J. and Morris, V. J. *Carbohydrate Polymers*, **36**, 67-72 (1998).

[8] Morris, V. J., Gunning, A. P., Kirby, A. R., Round, A., Waldron, K. and Ng, A. *International Journal of Biological Macromolecules*, **21**, 61-66 (1997).

[9] Hansma, H. G. and Hoh, J. H. *Annual Review of Biophysics and Biomolecular Structure*, **23**, 115-139 (1994).

[10] Kirby, A. R., Gunning, A. P. and Morris, V. J. *Biopolymers*, **38**, 355-366 (1996).

[11] Feng, D. and Aldrich, C. *Hydrometallurgy*, **73**, 1-10 (2004).

[12] Majidi, V., Laude, D. A. and Holcombe, J. A. *Environmental Science & Technology*, **24**, 1309-1312 (1990).

[13] Fujiwara-Arasaki, T., Mino, N. and Kuroda, M. *Hydrobiologia*, **116-117**, 513-516 (1984).

[14] Davis, T. A., Volesky, B. and Mucci, A. *Water Research*, **37**, 4311-4330 (2003).

[15] Schiewer, S. and Wong, M. H. *Chemosphere*, **41**, 271-282 (2000).

Chapter 8
Conclusions & Future Work

8.1 Introduction

According to the Marine Institute, there is considerable interest in the use of marine algae in bioremediation processes [1]. Given that increased urbanisation and industrialisation may contribute to metal pollution in the environment, identification of effective low cost sorbents for the removal of these contaminants is especially important.

A methodology for screening various seaweed biosorbents for the uptake of industrially significant metals has been demonstrated in this work. This research although fundamental in nature, has positive economic implications through potential exploitation of our natural seaweed resources for metal sequestration.

This research has taken standard techniques that have been previously used in studying metal biosorption and where possible these techniques have been adapted and refined for use to allow the results to be discussed more definitively e.g. The use of first derivative plots of potentiometric titration data has allowed us to more fully investigate the surface composition in terms of acidic functionalities as well as their corresponding pK_a values.

Characterisation of the seaweeds and their ability to bind heavy metals was carried out according to the following plan.

The first step in researching the metal uptake capability of the seaweeds was to determine the available sites on the biomass.

Once these parameters had been identified, factors such as the maximum binding capacity, optimum pH, equilibrium times, ionic strength and competition effects were subsequently investigated. The relationship between acidic sites and maximum uptake capacity was also determined. After this extensive study into the factors affecting metal biosorption, the functional groups involved in binding were identified using FTIR analysis.

ATR FTIR analysis demonstrated the use of a technique which reduces the need for sample preparation but also increases the sensitivity of the analysis. The absence of KBr

in the analysis also meant that chemical waste from the analysis was reduced. FTIR indicated the specific functionalities involved in binding, but a picture of how binding affected the structure of the seaweed was needed. Therefore SEM/EDX and XPS analyses were carried out.

SEM /EDX analysis was coupled with X-ray photoelectron spectroscopy to obtain more specific data regarding both cation and anion binding. SEM analysis provided an indication of seaweed surface morphology as well as changes after binding while EDX confirmed an ion-exchange mechanism for cation binding. However, EDX gave no indication of the Cr (VI) binding mechanism and as a result, further investigation by XPS was required.

XPS gave quantifiable results for the changes in constituent elements and could also differentiate between oxidation states. Therefore, it was used to follow the progress of Cr (VI) binding to the seaweeds.

As the seaweeds' binding capacity had previously been established and the functionalities responsible for binding identified, the next step was to identify treatments which could enhance the binding capacity of the seaweeds with the least damage to their structure. Chemical modifications revealed that acetone washing was the most effective modification technique for enhancing both cation and anion binding. Interactions of carboxyl and amino groups were also confirmed by blocking of these groups and preventing their participation in metal binding.

Although substantial changes in biomass structure were observed via SEM after metal binding, the need for a more quantitative estimation of these changes was required. The fact that scanning force microscopy (SFM) could fulfil this requirement coupled with its novelty in this type of application made it a suitable choice for analysis of the seaweed surface. Quantifiable changes in surface morphology were obtained with a possible indication of the Cu (II) binding mechanism to *Ulva lactuca* demonstrated.

8.2 Conclusions

While Section 8.1 detailed the rationale behind the chosen analysis programme, some of the resultant conclusions drawn from the work are given below.

Physical characterisation of the surface revealed that *Fucus vesiculosus* had the greatest number of acidic binding sites while *Palmaria palmata* had the least. The polyfunctional nature of the seaweed surface was demonstrated through the presence of various acidic groups with differing pK_a values.

Metal biosorption was pH dependent with an increase in pH resulting in increased cation and decreased anion uptake. Binding of anionic Cr (VI) required a longer equilibrium time than Cu (II) or Cr (III) but in all cases some correlation between the equilibrium time required and the quantity of acidic binding sites was found. Increased ionic strength had a negative effect on metal binding with the effect being most significant for Cr (III) and Cr (VI).

Palmaria palmata was most efficient at removing metal ions from solutions with low initial metal concentrations while at higher initial concentrations, *Fucus vesiculosus* exhibited superior performance. These results were in agreement with isotherm analysis which predicted the applicability of *Palmaria palmata* for metal removal in waste-streams containing low residual metal concentrations. The models predicted that *Fucus vesiculosus* and *Polysiphonia lanosa* would be the most suitable seaweeds for cation and anion removal respectively at higher residual metal concentrations.

Cu (II) and Cr (III) binding to *Fucus vesiculosus* in a competitive system had a depressive effect on the uptake of both metals. The effect of Cu (II) on Cr (III) binding was more significant than vice versa thus indicating that Cu (II) was more strongly bound to the seaweed than was Cr (III).

FTIR results revealed that the main groups involved in metal binding were carboxyl, amino and sulphonate groups with ether and alcohol groups interacting to varying degrees in different seaweed-metal combinations. Heavy metal binding to carboxyl groups was found to occur via bidentate complexation. A possible complementary relationship between the degree of ionic and covalent binding to biomass carboxyl groups was also found for some seaweeds. Novel analysis on the timescale of Cu (II) binding to the seaweeds was in agreement with equilibrium experiments.

SEM micrographs revealed significant changes in surface morphology after metal binding. Changes in seaweed morphology were most likely due to differences in the ionic radii and coordination spheres of the heavy metals under study. In most cases Cu (II) and Cr (III) brought about comparable changes in morphology but those found for Cr (VI) were unique, thus indicating further disparity between the mechanisms of cation and anion binding to seaweeds.

EDX analysis indicated an ion-exchange mechanism for cation binding and pointed to significant involvement of sulphur in Cu (II) binding to the red seaweeds. Additional XPS analysis verified this binding mechanism and also suggested cation complexation with carbon, oxygen, nitrogen and sulphur containing functionalities. Interactions between these functionalities and anionic Cr (VI) were also found. XPS studies revealed a reduction mechanism for Cr (VI) binding to the seaweeds with *Ulva* spp. having the ability to successful reduce large quantities of Cr (VI) to Cr (III).

Acetone treatment was the most successful modification technique in terms of increasing the seaweeds' binding capacity for both cations and anions. The importance of carboxyl and amino groups in Cu (II), Cr (III) and Cr (VI) was again demonstrated by blocking of these groups by modification. Titration of esterified samples confirmed that these groups were no longer available for binding and that there was good correlation between the degree of carboxyl blocking and the decrease in Cu (II) bound by *Ulva* spp. and *Polysiphonia lanosa*.

A novel methodology for investigating changes in surface morphology using scanning force microscopy was demonstrated in this work. Significant reconstruction of the surface was observed even at trace Cu (II) concentrations pointed to disruption of polymer chains on the surface by heavy metal ions as predicted in SEM analysis. Thus, a possible coordination mechanism between surface polymers and Cu (II) ions in *Ulva lactuca* was demonstrated.

8.3 Future Work

Some potential areas of future work directly arising from the work in this thesis are detailed below.

- Further physical characterisation of the seaweeds in terms of real and apparent densities, porosity, pore volume and pore size [2].
- Analysis of a range of metals with widely varying properties such as electronegativity and ionic radius to identify the link between these parameters and metal binding.
- Analysis of various other industrially significant metals such as Pb (II) and Ni (II) using the protocols tested in this work.
- Titration of metal bound seaweeds at various time intervals to determine the pattern of decrease in the number of available sites.
- Further titration of modified biosorbents to identify the effect of treatment on binding site availability.
- Testing of seaweed biosorption capacity under solvent conditions to establish its robustness in a potential industrial setting.
- Desorption studies to test the stability and reusability of the biomass after a number of sorption/desorption cycles.
- Far IR studies to investigate changes in the vibrations of the metal rather than changes in the ligands attached [3] i.e. seaweed functional groups. This would be particularly useful in investigations into metals with multiple oxidation states.
- Investigation into the reducing ability of various seaweeds with metals having multiple oxidation states e.g. Mo, Mn using a variety of techniques including XPS.
- Determination of the kinetics of Cr (VI) reduction in dead biomass using spectrophotometric methods.
- Further scanning force microscopy to examine changes in surface morphology after modification and the potential effects of modification on the mechanisms of heavy metal binding.

- Potential development of a predictive SFM model for surface roughness based on the metal concentration to which the seaweed is exposed.
- Real time analysis of Cr (VI) reduction in both live and dead seaweeds using a liquid cell for SFM to monitor changes in surface polymers as they occur.

8.4 References

[1] Marine Institute., Sea Change-A Marine Knowledge, Research and Innovation Strategy for Ireland (2007-2013). Part II: Research Measures, Research Programmes and Research Outcomes, Marine Institute, Galway, 58-112 (2006).

[2] Vilar, V. J. P., Botelho, C. M. S. and Boaventura, R. A. R. *Journal of Hazardous Materials*, **In Press, Corrected Proof**, -1579 (2007).

[3] Pons, M. N., Le Bonte, S. and Potier, O. *Journal of Biotechnology*, **113**, 211-230 (2004).

Appendix A

Cu(II) binding by dried biomass of red, green and brown macroalgae

WATER RESEARCH 41 (2007) 731–740

Available at www.sciencedirect.com

ScienceDirect

journal homepage: www.elsevier.com/locate/watres

Cu(II) binding by dried biomass of red, green and brown macroalgae

Vanessa Murphy, Helen Hughes, Peter McLoughlin*

Estuarine Research Group, Department of Chemical and Life Sciences, Waterford Institute of Technology, Cork Road, Waterford, Republic of Ireland

ARTICLE INFO

Article history:
Received 11 May 2006
Received in revised form
20 November 2006
Accepted 22 November 2006

Keywords:
Biosorption
Heavy metal
Marine algae
FTIR

ABSTRACT

Dried biomass of the marine macroalgae *Fucus spiralis* and *Fucus vesiculosus* (brown), *Ulva* spp. (comprising *Ulva linza*, *Ulva compressa* and *Ulva intestinalis*) and *Ulva lactuca* (green), *Palmaria palmata* and *Polysiphonia lanosa* (red) were studied in terms of their Cu(II) biosorption performance. This is the first study of its kind to compare Cu(II) uptake by these seaweeds in the South-East of Ireland. Potentiometric and conductimetric titrations revealed a variety of functionalities on the seaweed surface including carboxyl and amino groups, which are capable of metal binding. It was also found that, of the seaweeds investigated, *F. vesiculosus* contained the greatest number of acidic surface binding sites while *Palmaria palmata* contained the least. The metal uptake capacities of the seaweeds increased with increasing pH and kinetic behaviour followed a similar pattern for all seaweeds: a rapid initial sorption period followed by a longer equilibrium period. *P. palmata* reached equilibrium within 10 min of exposure while *F. vesiculosus* required 60 min. Correlation was found between the total number of acidic binding sites and the time taken to reach equilibrium. Fourier transform infra-red (FTIR) analysis of the seaweeds revealed the interaction of carboxyl, amino, sulphonate and hydroxyl groups on the seaweed surface with Cu^{2+} ions while time course studies established the relative contribution of each of these groups in metal binding.

1. Introduction

Heavy metal pollution is an environmental problem of worldwide concern with effluents from various industrial processes representing one of the most important sources of pollution. Copper is a metal commonly found in industrial wastewaters both in particulate form and as organic complexes. In aqueous environments, the speciation of the metal is dependant both on ligand concentration and pH (Elder and Horne, 1978). While the cupric ion (Cu^{2+}) is the metallic form most toxic to flora and fauna it is also a nutrient necessary for algal growth (Volesky and Holan, 1995).

If allowed to enter the environment Cu(II) can cause serious potential health issues. Even at low concentrations Cu(II) may be harmful to humans. It has been found that absorption of excess copper results in "Wilson's disease" where Cu(II) is deposited in the brain, skin, liver, pancreas and myocardium (Volesky, 1990).

Over the past two decades, attention has been concentrated on identifying materials that can effectively remove heavy metals from aqueous environments. These materials are known as biosorbents and the passive binding of metals by living or dead biomass is referred to as biosorption (Schiewer and Wong, 2000). Seaweeds have been shown to be extremely efficient biosorbents with the ability to bind a variety of

*Corresponding author. Tel.: +353 51 845514.
E-mail addresses: vmurphy@wit.ie (V. Murphy), hhughes@wit.ie (H. Hughes), pmcloughlin@wit.ie (P. McLoughlin).
0043-1354/$ - see front matter © 2006 Elsevier Ltd. All rights reserved.
doi:10.1016/j.watres.2006.11.032

metals (Volesky and Holan, 1995). In particular, the potential of non-viable seaweeds in the recovery of heavy metal ions from aqueous effluents has been studied (Yun et al., 2001; Davis et al., 2003).

Seaweeds possess a high metal-binding capacity (Ramelow et al., 1992; Holan and Volesky, 1994) with the cell wall playing an important role in binding (Crist et al., 1988, Kuyucak and Volesky, 1989). This is due to the presence of various functional groups such as carboxyl, amino, sulphate and hydroxyl groups, which can act as binding sites for metals. The main mechanisms of binding include ionic interactions and complex formation between metal cations and ligands on the surface of the seaweeds (Yun et al., 2001). Biosorption may be based on one or more of the following mechanisms: ion-exchange, physical adsorption, complexation and precipitation. These mechanisms may differ quantitatively and qualitatively according to the type of biomass, its origin and the processing to which it has been subjected. In many biosorption processes more than one of these mechanisms takes place simultaneously and it is difficult to distinguish between the single steps (Smith and Lacher, 2002).

This study adopts a systematic approach by studying Cu(II) binding to dried biomass of seaweeds from each of the three main seaweed classes (red, green and brown) that are available off the South-East coast of Ireland (52.39°N, 6.94°W). The seaweeds under investigation are *Fucus vesiculosus*, *Fucus spiralis*, *Ulva* spp., *Ulva lactuca*, *Palmaria palmata* and *polysiphonia lanosa* and were selected because of their abundance in this geographic environment.

While the seaweeds in this study have all previously been studied regarding their ability to bind metals (Crist et al., 1992; Fourest and Volesky, 1997; Cordero et al., 2004; Sheng et al., 2004) they have not been compared in terms of their Cu(II) binding ability.

Sheng et al. (2004) studied heavy metal binding to various seaweeds including the binding of copper. While kinetic, pH and Fourier transform infra-red (FTIR) studies were carried out, the authors did not estimate the number of binding sites on the seaweed surface or investigate the effect of exposure time on FTIR band shifting as has been done in this work.

Some key objectives of this study are as follows:

- To determine the quantity and nature of the seaweed binding sites and compare Cu(II) binding between red, green and brown seaweeds.
- To investigate the extent to which manipulation of experimental parameters influences Cu(II) binding in the selected seaweeds.
- To identify the functional groups present on the seaweeds and their relative contributions to Cu(II) binding as well as determining the timescale of binding to each.

2. Materials and methods

2.1. Biomass

Seaweeds were identified (Brightman, 1979) and collected from Fethard-on-Sea, Co. Wexford, Ireland (52.39°N, 6.94°W). The samples were rinsed thoroughly with distilled water in order to remove any adhering debris. The various plants collected within each species were combined before drying and grinding to give composite batches. Samples were oven-dried at 60 °C for 24 h, then subsequently ground and sieved to a particle size of 500–850 μm. This particle size fraction was used for all experiments. The biomass was stored in airtight polyethylene bottles until required.

2.2. Metal solutions

Standard metal solutions (analytical grade) containing 1000 mg L^{-1} Cu(II) (as copper nitrate) were purchased from Sigma–Aldrich (Ireland). Working solutions were prepared by diluting the stock solution with distilled water and adjusting the solutions to the appropriate pH using 0.1 M NaOH or 0.1 M HCl. The metal concentrations in solution were determined using Atomic Absorption Spectrophotometry (SpectrAA-600 VARIAN, Software version 4.10, flame mode).

2.3. Potentiometric and conductimetric titrations

2.3.1. Protonation of biomass

Biomass particles (5 g) were protonated by washing with 250 mL of 0.1 M HCl. This treatment ensured that any remaining ions e.g. Ca^{2+}, Mg^{2+}, Na^{+} and K^{+} were removed from the seaweed surface. The suspension was allowed to stir for 6 h to ensure that equilibrium had been reached. The biomass was filtered under vacuum and washed with distilled water until a constant conductance was obtained for the filtrate. The protonated biomass was oven-dried at 60 °C for 24 h and stored in polyethylene bottles until required.

2.3.2. Titration of biomass

For each titration, 200 mg of protonated biomass was dispersed in 100 mL of a 1 mM NaCl solution. Titration was carried out by stepwise addition of 0.25 mL of 0.1 M NaOH to the flask while the suspension was stirred under a nitrogen atmosphere. After each addition of titrant, the system was allowed to equilibrate until a stable pH reading was obtained. Conductivity was measured using a WTW LF 538 Conductivity metre with WTW TetraCon® 325 probe. pH measurements were recorded using a Mettler Toledo MP 220 pH meter with a Mettler Toledo Inlab® 413 pH electrode The pH electrode was calibrated with buffers pH 4 (±0.02) and pH 7 (±0.02) supplied by Riedel-de Haën. Potentiometric titrations were carried out in triplicate with conductimetric titrations carried out singly.

2.4. Optimum pH determination

In order to investigate the effect of pH on Cu(II) sorption, 50 mg L^{-1} metal solutions of various initial pH values were prepared using 0.1 M NaOH or 0.1 M HCl. Approximately 100 mg of biomass was added to flasks containing 50 mL of Cu(II) solution at the required pH. Flasks were shaken for 6 h at 200 rpm and room temperature (21 ± 1 °C). The samples were analysed via AAS and the equilibrium

metal uptake q_{eq} (mmol g^{-1}) was calculated according to Eq. (1):

$$q_{eq} = \frac{V(Ci - C_{eq})}{1000 m_s}, \quad (1)$$

where V is the volume of the copper solution (mL), C_i and C_{eq} are the initial and equilibrium concentration of copper in solution (mmol L^{-1}) and m_s is the mass of the alga (g) (Lodeiro et al., 2004)

2.5. Determination of equilibrium time

A quantity of 100 mg of biomass was added to 50 mL of a 50 mg L^{-1} Cu(II) solution adjusted to pH 5. Flasks were shaken at 200 rpm and room temperature (21± 1 °C). Samples were taken at t = 5, 10, 30, 60, 120 and 240 min and analysed by AAS. The equilibrium metal uptake q_{eq} (mmol g^{-1}) was calculated as before.

2.6. Fourier transform infra-red spectroscopy

2.6.1. FTIR analysis of biomass

For FTIR analysis, protonated seaweed was used as the free biosorbent control. The biomass (at a concentration of 1.0 g L^{-1}) was exposed to a 200 μg L^{-1} Cu(II) solution over a 4-hour period. Samples were taken at t = 5, 10, 30, 60, 120 and 240 min and oven-dried at 60 °C for 24 h. Samples were subsequently analysed using a Digilab Scimitar Series infra-red spectrometer employing a MIRacle™ Single Reflection HATR accessory.

3. Results and discussion

3.1. Potentiometric and conductimetric titrations

Figs. 1a and b show the respective potentiometric and conductimetric titration curves resulting from the addition

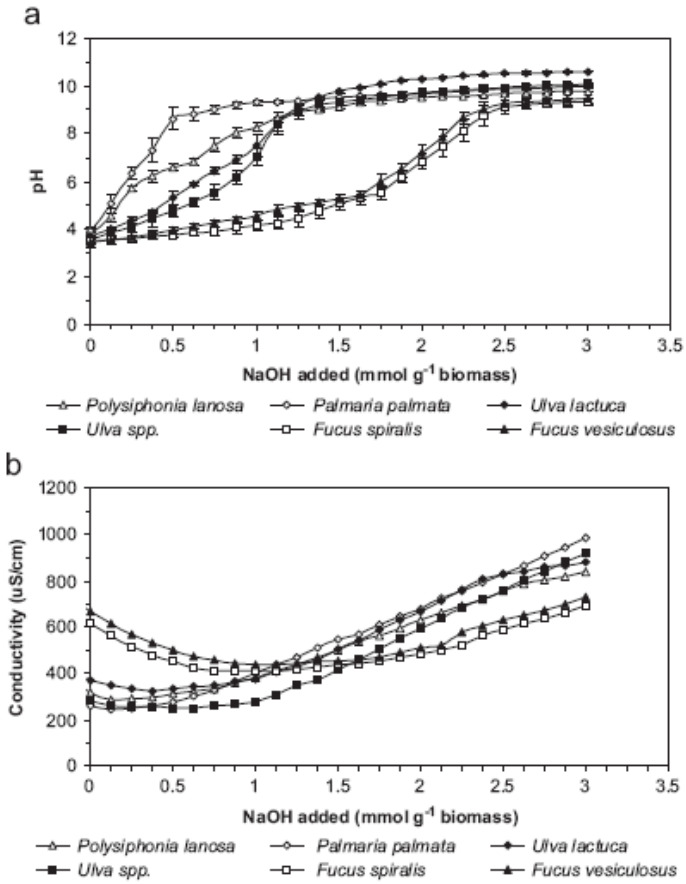

Fig. 1 – (a) Potentiometric and (b) conductimetric titration curves for six seaweed species. Error bars are calculated based on triplicate runs with 95% confidence intervals.

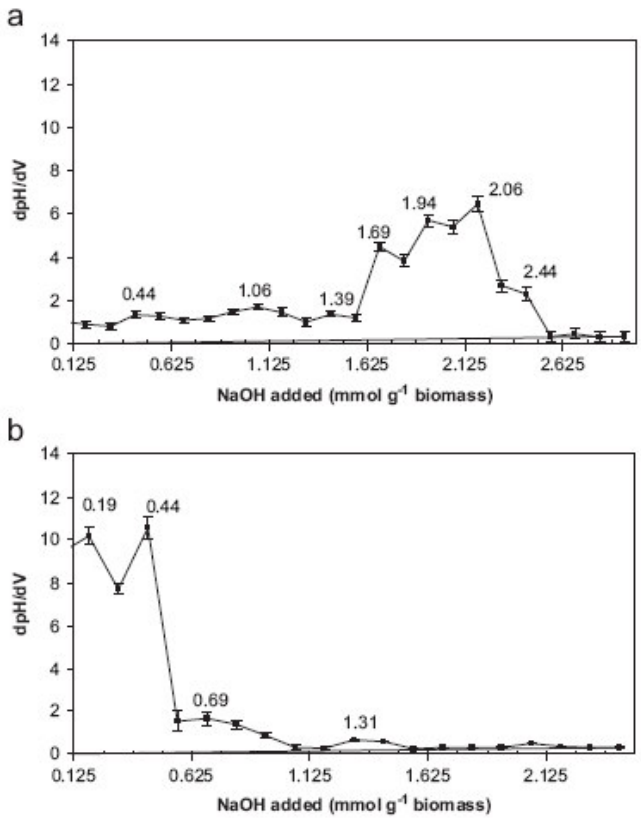

Fig. 2 – First derivative plots of average pH titration data for (a) *Fucus vesiculosus*, (b) *Palmaria palmata*. Error bars are calculated based on triplicate runs with 95% confidence intervals.

of NaOH. The various amounts of acidic groups in the biomass and their corresponding pK_a values were evaluated by identifying the inflection points of the titration curves (Fig. 1a). However, this can be quite difficult and a better indication of the position of these inflections was obtained from first derivative plots of average pH titration data (Fig. 2). The first derivative plots consist of the midpoint of successive amounts of NaOH added (*x*-axis) versus dpH/dV (*y*-axis). Reading the location of each peak on the *x*-axis gave the number of acidic groups on the biomass surface.

The number of strong acidic groups was determined from the first peak in Figs. 2a and b (0.44 and 0.19 mmol g^{-1} for *F. vesiculosus* and *P. palmata*, respectively) while the total number of acidic groups was determined from the final peak (2.44 for *F. vesiculosus* and 1.31 mmol g^{-1} for *P. palmata*). The number of weak acidic groups was then calculated by difference. Once these values were established, the corresponding pK_a values were then identified from the original titration curve. The pK_a values and the number of acidic groups on the biomass surface are summarised in Table 1.

It was shown that the brown seaweeds contained the greatest number of acidic functionalities (both total and weak) on the seaweed surface. Since it is thought that carboxyl groups (weak) are primarily responsible for metal sorption, especially in brown seaweeds, it was expected that the brown species would exhibit superior biosorption performance over the other seaweeds. Subsequent pH experiments showed that the brown seaweeds did in fact exhibit superior metal uptake relative to the other seaweeds. This finding is also in agreement with the work of various authors comparing brown, red and green seaweeds (Hashim and Chu, 2004; Jalali et al., 2002).

Sulphonate groups usually only contribute to metal binding at low pH and their typical pK_a values are in the range 1.0–2.5 (Sheng et al., 2004). Apparent pK_a values in this range were not detected by titration, but the presence of sulphonate groups on the seaweed surface was later confirmed by FTIR analysis. Hydroxyl groups in seaweed cell wall polysaccharides are considerably weaker than carboxyl groups and therefore may only interact with cations at a higher pH. This usually occurs at pH > 10. Therefore, surface hydroxyl groups only play a significant role in binding at very high pH values (Davis et al., 2003).

Algal proteins have also been known to interact with metal ions, particularly between pH 6–9 and protonated amino groups have a pK_a value of around 8 (Percival and McDowell,

1967). Each of the seaweeds displayed at least one pK_a value in this region e.g. *F. vesiculosus* had a pK_a value of 8.25 while *F. spiralis* displayed a value of 8.11.

Table 1 – pK_a values and quantity of acidic groups determined by titration

Seaweed	pK_a values	Quantity of acidic groups (mmol g^{-1} biomass)		
		Total	Strong	Weak
Fucus vesiculosus	3.85±0.1 4.68±0.2 5.70±0.2 6.82±0.3 8.25±0.2	2.44	0.44	2.00
Fucus spiralis	3.6±0.1 4.3±0.2 5.3±0.3 8.11±0.3	2.31	0.31	2.00
Polysiphonia lanosa	4.19±0.1 6.71±0.2 8.16±0.2 9.06±0.1	1.81	0.19	1.62
Palmaria palmata	4.47±0.2 8.71±0.3 9.35±0.2	1.31	0.19	1.12
Ulva lactuca	3.83±0.1 4.52±0.2 6.66±0.3 8.76±0.3 10.01±0.2	1.81	0.19	1.62
Ulva spp.	3.69±0.3 4.59±0.2 7.20±0.3 9.25±0.2	1.94	0.44	1.50

Error bars are calculated based on triplicate runs with 95% confidence intervals.

Conductimetric curves have been used in previous investigations as a standard procedure (Fourest and Volesky, 1996; Davis et al., 2000) and have been included in this work for comparative purposes only. The general trends observed in the conductimetric curves were similar to those observed previously by various authors (Fourest and Volesky, 1996; Figueira et al., 2000).

Fig. 1(b) illustrates that conductivity initially decreased sharply due to the neutralisation of free protons from strongly acidic groups. When all of the strong acidic groups were neutralised, the weaker acidic groups began to dissociate and contribute to measured conductivity. The neutralisation of weak acids was characterised by a gentle increase in solution conductivity. When all the weak acid groups were neutralised, the conductivity of the solution increased in proportion to the excess sodium hydroxide added. The transition between the decreasing and increasing portion of the conductivity curve should correspond to the first equivalence point on the potentiometric titration curve. However, in most cases an equivalence range rather than a specific point was obtained.

3.2. *Optimum pH determination*

Various authors have observed that solution pH is an important parameter affecting heavy metal biosorption by seaweed species (Chen et al., 2002; Figueira et al., 1999; Matheickal and Yu, 1999). The surface groups of seaweed species e.g. carboxyl and sulphonate display weakly acidic characteristics. Therefore, the optimum pH for metal uptake is related to the pK_a of these functionalities. However, the solution chemistry of the metal complexes involved must also be considered, as the speciation of metals in solution is pH dependant. Sheng et al. (2004) determined that in a system where copper is present as copper nitrate, Cu^{2+} remained as the dominant species if pH was maintained below 5.2. Kratochvil and Volesky (1998) also found that most heavy metals tend to precipitate out at pH > 5.5.

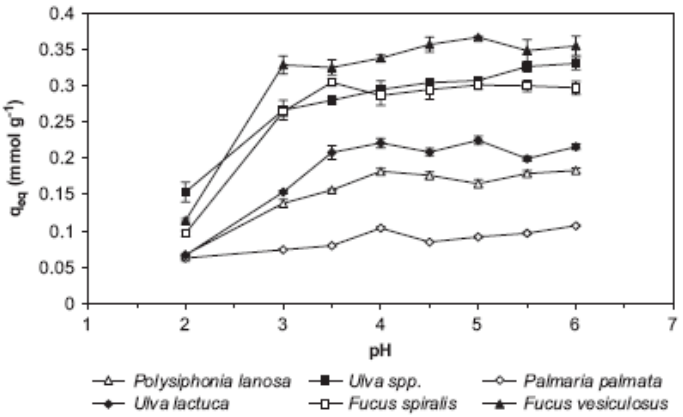

Fig. 3 – Optimum pH determination for Cu(II) sorption. Error bars are calculated based on triplicate runs with 95% Confidence Intervals. Initial Cu(II) ion concentration = 50 mg L^{-1}, concentration of biomass = 2 mg mL^{-1}.

Fig. 3 illustrates the relationship between metal uptake and solution pH for the seaweeds. It is clearly seen that higher pH values led to higher metal uptake. Determination of the optimum sorption pH was carried out only to a maximum pH of 6 because above this pH insoluble copper hydroxide was seen to precipitate out.

At low pH, the positively charged hydrogen ions may compete with metal ions for binding ligands on the cell wall and this leads to fewer sites being available to bind metal ions. As the pH increases there are fewer H^+ ions in solution and this means that there is less competition for binding sites thus freeing up more ligands leading to enhanced biosorption.

At pH 2, some metal uptake was observed and this may be due to the presence of sulphonate groups that are dissociated at this pH. At pH 3.5–5 carboxyl groups on the seaweed generate a negatively charged surface and electrostatic interactions between cationic species and this surface can be responsible for metal biosorption.

This pH dependence of biosorption demonstrates that seaweeds can potentially be developed as multi-use biosorption products. As seen, metal sorption is greatly reduced at lower pH thus facilitating removal of metal ions by simple pH adjustment.

Fig. 4 illustrates the relationship between the quantity of total acidic sites and physical parameters such as maximum metal uptake and the time required to reach sorption equilibrium. Each point on the *x*-axis represents the overall number of acidic groups as determined by titration for each seaweed species (Table 1).

Regression analysis of metal uptake on total acidic groups was carried out and Eq. (2) was obtained:

$$\text{Metal uptake} = -0.193 + 0.226\,(\text{total acidic groups}). \quad (2)$$

Correlation between the maximum Cu(II) sorbed and the total number of acidic binding sites available on the seaweed surface was found ($r^2 = 0.862$). The standard *t*-test on the coefficient of total acidic groups had a *P* value of 0.007, indicating that it is highly unlikely that the true coefficient is zero. Therefore, it appears that metal uptake is almost certainly positively related to the number of sites. The *t*-test takes into account the sample size ($n = 6$). Thus, even allowing for the small sample size, the relationship seems to be established.

Ulva spp. performed extremely efficiently in sequestering metal ions (0.326 mmol g^{-1}). The high binding capacity of non-living *Ulva* spp. has not previously been investigated, but Dodson and Aronson (1978) found that specific fractions of *Ulva* (formerly *Enteromorpha* as classified by Hayden et al., 2003) were high in uronic acid content. This may account for the increased metal uptake observed for *Ulva* spp. in this study. *Ulva* spp. are plentiful in the geographic location of this study relative to some of the other seaweeds studied. The abundance of these species points to their potential usage as a biosorbent material because removing them from the sampling site would not be as detrimental to the ecosystem as would removing a different species. It is therefore proposed that *Ulva* spp. warrants further study as potential bioremediation products for heavy metal removal.

Table 2 – Time required for sorption equilibrium in Cu(II)-biomass systems

Seaweed	Equilibrium time (min)
Fucus spiralis	60
Fucus vesiculosus	60
Ulva spp.	30
Ulva lactuca	30
Palmaria palmata	10
Polysiphonia lanosa	30

Initial Cu(II) ion concentration = 50 mg L^{-1}, concentration of biomass = 2 mg mL^{-1}, pH = 5.

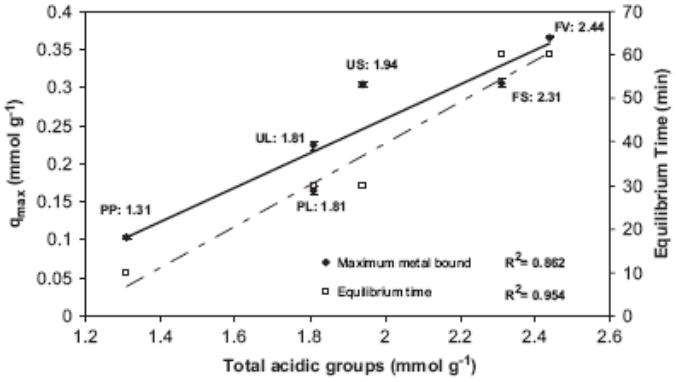

Fig. 4 – Relationship between (1) maximum Cu(II) bound (◆), (2) equilibrium time (□) and number of acidic binding sites. (FS: *Fucus spiralis*, FV: *Fucus vesiculosus*, PP: *Palmaria palmata*, PL: *Polysiphonia lanosa*, UL: *Ulva lactuca*, US: *Ulva* spp.). Errors bars are calculated based on triplicate runs with 95% confidence intervals. Initial Cu(II) ion concentration = 50 mg L^{-1}, concentration of biomass = 2 mg mL^{-1}, pH = 5.

3.3. Determination of equilibrium time for Cu(II) sorption

Equilibrium experiments were carried out at pH 5, where maximum uptake capacity was achieved and metal precipitation was avoided. Table 2 summarises the equilibrium time required for the uptake of Cu(II) ions by the various seaweeds.

Similar kinetic behaviour was observed for all seaweeds with rapid initial sorption followed by a period of much slower uptake. The equilibrium time needed for the different biomass-metal systems ranged from approximately 10–60 min. Therefore, in subsequent experiments 4 h was deemed more than sufficient to establish equilibrium.

An issue relating to the kinetics of Cu(II) binding is whether or not the time taken to reach equilibrium is linked to the physical structure of the seaweed in terms of the number and type of binding sites. Results from this study indicated that there was strong correlation ($r^2 = 0.954$, $P < 0.005$) between the total number of acidic binding sites and the time taken to reach sorption equilibrium (Fig. 4).

The large number of binding sites in the brown seaweeds means that once initial sorption has taken place there may potentially be some steric hindrance of the surface functionalities resulting in the longer time required to reach sorption equilibrium. This also points to possibility of a mechanism other than ion exchange taking place e.g. coordination between adjacent carboxyl groups.

Various authors have observed kinetic behaviour similar to that found in this study. Rapid uptake of nickel by the alga *Chlorella vulgaris* within the first 10 min of contact has been reported with equilibrium established in 30–60 min (Aksu, 2002). Matheickal and Yu (1999) also found that 90% of the total soluble cadmium was removed from solution by pretreated *Durvillaea potatorum* within 30 min of exposure with a gradual decrease in the cadmium concentration occurring over a 5-h period.

3.4. Fourier transform infra-red spectroscopy

3.4.1. FTIR analysis of biomass

FTIR spectroscopy has been frequently used to detect vibrational frequency changes in seaweeds (Park et al., 2004; Sheng et al., 2004; Figueira et al., 1999). It offers excellent information on the nature of the bonds present and allows identification of different functionalities on the cell surface. The main stretching frequencies observed by various authors and the sources of these stretches are summarised in Table 3.

Numerous chemical groups have been proposed to be responsible for the biosorption of metals by macroalgae. These include carboxyl, sulphonate, hydroxyl and amino (Smith and Lacher, 2002). Their relative importance in metal sorption may depend on factors such as the quantity of sites, their accessibility, chemical state and affinity between site and metal.

FTIR analysis of the seaweeds was carried out using Attenuated Total Reflectance techniques. Various authors have favoured the use of KBr methods for FTIR analysis, using either diffuse reflectance (Sheng et al., 2004; Chen et al., 2002) or by incorporating the sample into a KBr pellet (Figueira et al., 1999; Raize et al., 2004). The advantages of using an ATR method over KBR methods are the ease of sample preparation as well as increased sensitivity due to a lack of dilution.

Table 3 – Commonly observed stretching frequencies in seaweed FTIR spectra

Wavenumber (cm^{-1})	Assignment
3280	Bonded –OH, –NH stretching[a]
2920	Asymmetric stretch of aliphatic chains (–CH)[b]
2854	Symmetric stretch of aliphatic chains (–CH)[b]
1740	C=O stretch of COOH[c]
1630	Asymmetric C=O[c]
1530	Amide II[a]
1450	Symmetric C=O[c]
1371	Asymmetric $-SO_3$ stretching[d]
1237	C–O stretch of COOH[c]
1160	Symmetric $-SO_3$ stretching[d]
1117	C–O (ether)[a]
1033	C–O (alcohol)[a]
817	S=O stretch[d]

References: (a) Sheng et al. (2004), (b) Pons et al. (2004), (c) Fourest and Volesky (1996), (d) Figueira et al. (1999).

FTIR data presented in this study are more robust than those which have been found in the literature as all spectra are supported by triplicate analyses. In all cases, excellent wavenumber repeatability was observed between replicate scans with any differences being one wavenumber or less. Because the resolution of the instrument is 2 cm^{-1}, wavenumber changes greater than this value are considered to be valid. The extent of band shifting gives an indication of the degree of interaction of functional groups with metal cations.

The assignment of FTIR bands and detailed wavenumber shifts for the protonated and Cu(II)-loaded biomasses are summarised in Table 4 while the average FTIR spectra obtained for protonated and Cu(II)—loaded *F. vesiculosus* and *F. spiralis* are shown in Fig. 5.

FTIR studies revealed that Cu(II) binding to brown seaweeds occurred primarily through biomass carboxyl groups accompanied by significant interactions of the biomass amino groups. Although some sulphonate group interaction occurred for both *F. vesiculosus* and *F. spiralis*, only the latter showed some participation of biomass alcohol (hydroxyl) and ether groups in Cu(II) binding.

Similarly to the brown seaweeds, significant carboxyl and amino group participation was seen for Cu(II) binding to *Ulva* spp. and *U. lactuca*. Sulphonate groups also played a greater role in Cu(II) binding to both green species, than seen for the brown seaweeds. However, in contrast to the brown seaweeds, major interactions between biomass alcohol groups and metal cations took place in *Ulva* spp. but not *U. lactuca*.

Binding of Cu(II) to both *P. lanosa* and *P. palmata* involved participation of carboxyl and sulphonate functionalities. However, while amino and hydroxyl groups took part in Cu(II) binding in *P. lanosa*, this was not the case for *P. palmata*.

Table 4 – FTIR bands observed for protonated and Cu(II)-loaded seaweeds exposed to a 200 μg/L Cu(II) solution over a 4-h period

	Wavenumber (cm^{-1})					
	Fucus vesiculosus	*Fucus spiralis*	*Ulva* spp.	*Ulva lactuca*	*Polysiphonia lanosa*	*Palmaria palmata*
Free C=O	(1744)	(1740)	(1719)	(1723)	(1722)	(1722)
	1729	1726	1726	*	1708	1715
C=O (asymmetric)	(1623)	(1619)	(1632)	(1636)	(1641)	(1634)
	1613	1619	1596	1630	1634	1629
Amide II	(1511)	(1511)	(1525)	(1533)	(1515)	(1522)
	1525	1533	*	1525	1536	1523
C=O (symmetric)	(1455)	(1455)	(1448)	(1420)	(1446)	(1445)
	1458	1455			1446	1457
	1409		1409	1409		
$-SO_3$ (asymmetric)	(1370)	(1369)	(1361)	(1371)	(1375)	(1373)
	1378	1374	1314	1339	1391	1381
C–O (carboxyl)	(1205)	(1210)	(1212)	(1200)	(1216)	(1240)
	1210	1211	1216	1221	1223	1237
$-SO_3$ (symmetric)	(1152)	(1155)	*	(1157)	(1156)	(1162)
	1153	1153	(1163)	1156	1150	1153
C–O (ether)	(*)	(*)	(*)	(*)	(*)	(*)
	*	1111	*	*	*	*
C–O (alcohol)	(1029)	(1033)	(1007)	(1026)	(1034)	(1033)
	1029	1028	1034	1027	1025	(1033)

Wavenumbers obtained for protonated biomass controls are shown in parentheses. Number of scans = 40, resolution = 2.
Average values from triplicate runs are shown.
* Band not observed.

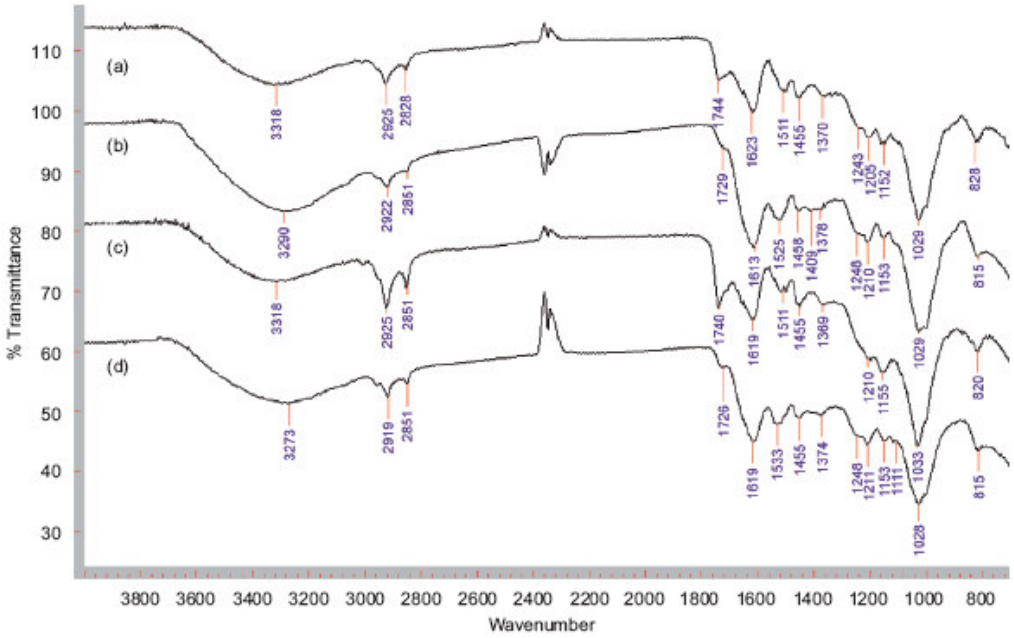

Fig. 5 – Stretching frequencies observed for (a) protonated, (b) Cu(II)-loaded *Fucus vesiculosus*, (c) protonated and (d) Cu(II)-loaded *Fucus spiralis* (number of scans = 40, resolution = 2). Sample spectra from triplicate runs are shown.

All seaweeds showed contributions from carboxyl and sulphonate functionalities in Cu(II) binding. Of the seaweeds studied, *P. palmata* was the only species not to show interaction of biomass amino groups with metal cations. *F. spiralis*, *Ulva* spp. and *P. lanosa* revealed interactions between Cu(II) ions and biomass alcohol groups with *F. spiralis* being the only seaweed to display participation of biomass ether groups in binding.

FTIR studies have therefore indicated that many of the same functional groups are responsible for Cu(II) binding to red, green and brown seaweeds. However, results showed that the relative contribution of these groups can vary not only between seaweed type but also within species. To investigate relative effect of each functional group, time-course analyses were carried out.

3.4.2. FTIR time-course analysis

FTIR time-course experiments identified the time scale of interaction of the various functionalities with Cu(II) over a 4-h period. The relationship between rate of metal uptake and the movement of FTIR stretching bands has not previously been investigated and so this element of the work is completely novel. Table 5 shows the FTIR bands observed over the first 30 min of Cu(II) exposure to *P. palmata* while Table 6 details those shifts observed after 120 min of exposure in *F. vesiculosus*.

P. palmata showed initial involvement of carboxyl groups with sulphonate groups interacting at a later stage. No significant band movement was observed after 10 min. In the case of *F. vesiculosus*, both carboxyl and amino interactions were dominant for the initial 10 min of metal exposure, while after this time, amino and sulphonate groups preferentially interacted with metal cations. After 60 min no further band movement was apparent in the FTIR spectrum. These results were in agreement with equilibrium studies (Section 3.3) which indicated that *F. vesiculosus* required 60 min to reach Cu(II) sorption equilibrium.

For all seaweeds, the results of the FTIR time-courses were in agreement with the equilibrium behaviour observed i.e. once equilibrium had been achieved, no further band shifting was observed in the FTIR spectra. This study, although preliminary in nature points to differences in binding affinity of the various functional groups for Cu(II) and indicates the feasibility of further studies which may be carried out on the relationship between seaweed composition and FTIR behaviour at a variety of metal concentrations.

Table 5 – Average stretching frequencies observed for protonated *Palmaria palmata* exposed to 200 μg L^{-1} Cu(II) over 30 min period

FTIR band (cm^{-1})	Time (min)			
	t = 0	t = 5	t = 10	t = 30
Free C=O	1722	1722	1715	1715
C=O (asymmetric)	1634	1631	1629	1629
Amide II	1522	1524	1523	1523
C=O (symmetric)	1445	1454	1457	1456
		1409		
$-SO_3$ (asymmetric)	1373	1377	1380	1379
C–O (carboxyl)	1240	1242	1237	1237
$-SO_3$ (symmetric)	1162	1160	1153	1153
C–O (alcohol)	1033	1035	1033	1033

Number of scans = 40, resolution = 2.
Average values from triplicate runs are shown.

4. Conclusions

A methodology for screening various seaweed biosorbents for the uptake of the heavy metal Cu(II) has been demonstrated in this work. The comparison of metal biosorption performance was based on expressing metal uptake against the key equilibrium biosorption parameters such the number of active sites, solution pH and time required for sorption equilibrium. Investigations into the surface functionalities involved in metal binding also provided an indication of

Table 6 – Average stretching frequencies observed for protonated *Fucus vesiculosus* exposed to 200 μg L^{-1} Cu(II) over a 120 min period

FTIR band (cm^{-1})	Time (min)					
	t = 0	t = 5	t = 10	t = 30	t = 60	t = 120
Free C=O	1744	1742	1733	1729	1729	1729
C=O (asymmetric)	1623	1617	1615	1613	1613	1613
Amide II	1511	1525	1525	1525	1525	1525
C=O (symmetric)	1455	1457	1457	1458	1458	1458
		1409	1409	1409	1409	1409
$-SO_3$ (asymmetric)	1370	1370	1371	1371	1378	1378
C–O (carboxyl)	1243	1244	1244	1248	1248	1248
	1205	1210	1210	1210	1210	1210
$-SO_3$ (symmetric)	1152	1153	1153	1154	1153	1153
C–O (alcohol)	1029	1028	1028	1028	1028	1028

Number of scans = 40, resolution = 2.
Average values from triplicate runs are shown.

differences in biosorption behaviour between the seaweeds. The results obtained in this study warrant further investigation into the practical applicability of dried seaweed biomass as a biosorbent for metal-loaded waste streams.

Acknowledgements

The authors gratefully acknowledge the support of:

- The Irish Research Council for Science, Engineering and Technology under the Embark Initiative.
- Technology Sector Research—(Strand III).

REFERENCES

Aksu, Z., 2002. Determination of the equilibrium, kinetic and thermodynamic parameters of the batch biosorption of nickel (II) ions onto *Chlorella vulgaris*. Process Biochem. 38 (1), 89–99.

Brightman, F.H., 1979. The Oxford Book of Flowerless Plants: Ferns, Fungi, Mosses, Liverworts, Lichens and Seaweeds. Oxford University Press, Oxford.

Chen, J.P., Hong, L.A., Wu, S.N., Wang, L., 2002. Elucidation of interactions between metal ions and Ca alginate-based ion-exchange resin by spectroscopic analysis and modeling simulation. Langmuir 18 (24), 9413–9421.

Cordero, B., Lodeiro, P., Herrero, R., De Vicente, M.E.S., 2004. Biosorption of cadmium by *Fucus spiralis*. Environ. Chem. 1 (3), 180–187.

Crist, R.H., Oberholser, K., McGarrity, J., Crist, D.R., Johnson, J.K., Brittsan, J.M., 1992. Interaction of metals and protons with algae. 3. Marine-algae, with emphasis on lead and aluminum. Environ. Sci. Technol. 26 (3), 496–502.

Crist, R.H., Oberholser, K., Schwartz, D., Marzoff, J., Ryder, D., Crist, D.R., 1988. Interactions of metals and protons with algae. Environ. Sci. Technol. 22 (7), 755–760.

Davis, T.A., Volesky, B., Vieira, R.H.S.F., 2000. *Sargassum* seaweed as biosorbent for heavy metals. Water Res. 34 (17), 4270–4278.

Davis, T.A., Volesky, B., Mucci, A., 2003. A review of the biochemistry of heavy metal biosorption by brown algae. Water Res. 37 (18), 4311–4330.

Dodson, J.R., Aronson, J.M., 1978. Cell wall composition of *Enteromorpha intestinalis*. Botanica Marina 21 (4), 241–246.

Elder, J.F., Horne, A.J., 1978. Copper cycles and copper sulphate algicidal capacity in two Californian lakes. Environ. Manage. 2 (1), 17–30.

Figueira, M.M., Volesky, B., Mathieu, H.J., 1999. Instrumental analysis study of iron species biosorption by *Sargassum* biomass. Environ. Sci. Technol. 33 (11), 1840–1846.

Figueira, M.M., Volesky, B., Ciminelli, V.S.T., Roddick, F.A., 2000. Biosorption of metals in brown seaweed biomass. Water Res. 34 (1), 196–204.

Fourest, E., Volesky, B., 1996. Contribution of sulfonate groups and alginate to heavy metal biosorption by the dry biomass of *Sargassum fluitans*. Environ. Sci. Technol. 30 (1), 277–282.

Fourest, E., Volesky, B., 1997. Alginate properties and heavy metal biosorption by marine algae. Appl. Biochem. Biotechnol. 67, 33–44.

Hashim, M.A., Chu, K.H., 2004. Biosorption of cadmium by brown, green, and red seaweeds. Chem. Eng. J. 97 (2–3), 249–255.

Hayden, H.S., Blomster, J., Maggs, C.A., Silva, P.C., Stanhope, M.J., Waaland, J.R., 2003. Linnaeus was right all along: *Ulva* and *Enteromorpha* are not distinct genera. Eur. J. Phycol. 38 (3), 277–294.

Holan, Z.R., Volesky, B., 1994. Biosorption of lead and nickel by biomass of marine-algae. Biotechnol. Bioeng. 43 (11), 1001–1009.

Jalali, R., Ghafourian, H., Asef, Y., Davarpanah, S.J., Sepehr, S., 2002. Removal and recovery of lead using nonliving biomass of marine algae. J. Hazardous Mater. 92 (3), 253–262.

Kratochvil, D., Volesky, B., 1998. Advances in the biosorption of heavy metals. Trends Biotechnol. 16 (7), 291–300.

Kuyucak, N., Volesky, B., 1989. The mechanism of cobalt biosorption. Biotechnol. Bioeng. 33 (7), 823–831.

Lodeiro, P., Cordero, B., Grille, Z., Herrero, R., De Vicente, M.E.S., 2004. Physicochemical studies of cadmium (II) biosorption by the invasive alga in Europe, *Sargassum muticum*. Biotechnol. Bioeng. 88 (2), 237–247.

Matheickal, J.T., Yu, Q.M., 1999. Biosorption of lead (II) and copper (II) from aqueous solutions by pre-treated biomass of Australian marine algae. Bioresour. Technol. 69 (3), 223–229.

Park, D., Yun, Y.S., Cho, H.Y., Park, J.M., 2004. Chromium biosorption by thermally treated biomass of the brown seaweed, *Ecklonia* sp. Ind. Eng. Chem. Res. 43 (26), 8226–8232.

Percival, E.G.V., McDowell, R.H., 1967. Chemistry and Enzymology of Marine Algal Polysaccharides. Academic Press, London, UK, pp. 99–126.

Pons, M.N., Bonte, S.L., Potier, O., 2004. Spectral analysis and fingerprinting for biomedia characterisation. J. Biotechnol. 113 (1–3), 211–230.

Raize, O., Argaman, Y., Yannai, S., 2004. Mechanisms of biosorption of different heavy metals by brown marine macroalgae. Biotechnol. Bioeng. 87 (4), 451–458.

Ramelow, G.J., Fralick, D., Zhao, Y.F., 1992. Factors affecting the uptake of aqueous metal-ions by dried seaweed biomass. Microbios 72 (291), 81–93.

Schiewer, S., Wong, M.H., 2000. Ionic strength effects in biosorption of metals by marine algae. Chemosphere 41 (1–2), 271–282.

Sheng, P.X., Ting, Y.P., Chen, J.P., Hong, L., 2004. Sorption of lead, copper, cadmium, zinc, and nickel by marine algal biomass: characterization of biosorptive capacity and investigation of mechanisms. J. Colloid Interface Sci. 275 (1), 131–141.

Smith, R.W., Lacher, C., 2002. Sorption of Hg (II) by *Potamogeton natans* dead biomass. Min. Eng. 15, 187–191.

Volesky, B., 1990. Biosorption of Heavy Metals. CRC Press, Boca Raton, FL.

Volesky, B., Holan, Z.R., 1995. Biosorption of heavy metals. Biotechnol. Progress 11 (3), 235–250.

Yun, Y.S., Park, D., Park, J.M., Volesky, B., 2001. Biosorption of trivalent chromium on the brown seaweed biomass. Environ. Sci. Technol. 35 (21), 4353–4358.

Appendix B

Comparative study of chromium biosorption by red, green and brown seaweed biomass

ARTICLE IN PRESS

Available online at www.sciencedirect.com

ScienceDirect

CHEMOSPHERE

ELSEVIER

Chemosphere xxx (2007) xxx–xxx

www.elsevier.com/locate/chemosphere

Technical Note

Comparative study of chromium biosorption by red, green and brown seaweed biomass

V. Murphy *, H. Hughes [1], P. McLoughlin [2]

Estuarine Research Group, Department of Chemical and Life Sciences, Waterford Institute of Technology, Cork Road, Waterford, Ireland

Received 2 February 2007; received in revised form 8 August 2007; accepted 9 August 2007

Abstract

Dried biomass of the macroalgae *Fucus vesiculosus* and *Fucus spiralis* (brown), *Ulva* spp. (comprising *Ulva linza*, *Ulva compressa* and *Ulva intestinalis*) and *Ulva lactuca* (green), *Palmaria palmata* and *Polysiphonia lanosa* (red) were studied in terms of their chromium biosorption performance. Metal sorption was highly pH dependent with maximum Cr(III) and Cr(VI) sorption occurring at pH 4.5 and pH 2, respectively. Extended equilibrium times were required for Cr(VI) binding over Cr(III) binding (180 and 120 min, respectively) thus indicating possible disparities in binding mechanism between chromium oxidation states. The red seaweed *P. palmata* revealed the highest removal efficiency for both Cr(III) and Cr(VI) at low initial concentrations. However, at high initial metal concentrations *F. vesiculosus* had the greatest removal efficiency for Cr(III) and performed almost identically to *P. lanosa* in terms of Cr(VI) removal. The Langmuir Isotherm mathematically described chromium binding to the seaweeds where *F. vesiculosus* had the largest q_{max} for Cr(III) sorption (1.21 mmol g^{-1}) and *P. lanosa* had the largest Cr(VI) uptake (0.88 mmol g^{-1}). *P. palmata* had the highest affinity for both Cr(III) and Cr(VI) binding with *b* values of 4.94 mM^{-1} and 8.64 mM^{-1}, respectively. Fourier transform infrared analysis revealed interactions of amino, carboxyl, sulphonate and hydroxyl groups in chromium binding to *Ulva* spp. The remaining seaweeds showed involvement of these groups to varying degrees as well as ether group participation in the brown seaweeds and for Cr(VI) binding to the red seaweeds.

Keywords: Chromium; Macroalgae; Langmuir; FTIR; Heavy metal

1. Introduction

Heavy metal pollution is one of the most significant problems of this century (Park et al., 2006). Chromium has found widespread use in electroplating, leather tanning and metal finishing with Cr(VI) being a suspected carcinogen and mutagen (Costa, 2003). Thus, the discharge of Cr(VI) into surface water is regulated to below 0.05 mg l^{-1} by the U.S. EPA (Baral and Engelken, 2002). Conventional chromium removal processes including ion-exchange, activated carbon adsorption, reverse osmosis, and membrane filtration can be expensive or ineffective at low concentrations and may also lead to secondary environmental problems from waste disposal (Arslan and Pehlivan, 2007). Thus, much research has been focussed on identifying biological materials that can efficiently remove heavy metals from aqueous environments. These materials are known as biosorbents and the passive binding of metals by living or dead biomass is referred to as biosorption (Schiewer and Wong, 2000).

Seaweeds are extremely efficient biosorbents with the ability to bind various metals from aqueous effluents (Davis et al., 2003; Tsui et al., 2006). Numerous chemical groups may be responsible for metal biosorption by seaweeds e.g. carboxyl, sulphonate, hydroxyl and amino (Smith and Lacher, 2002) with their relative importance depending on factors such as the quantity of sites, their accessibility and the affinity between site and metal. The

* Corresponding author. Tel.: +353 51 845514.
E-mail addresses: vmurphy@wit.ie (V. Murphy), hhughes@wit.ie (H. Hughes), pmcloughlin@wit.ie (P. McLoughlin).
[1] Tel.: +353 51 302064.
[2] Tel.: +353 51 302056.

0045-6535/$ - see front matter © 2007 Elsevier Ltd. All rights reserved.
doi:10.1016/j.chemosphere.2007.08.015

Please cite this article in press as: Murphy, V. et al., Comparative study of chromium biosorption by red, green and ..., Chemosphere (2007), doi:10.1016/j.chemosphere.2007.08.015

main metal binding mechanisms include ion-exchange and complex formation (Davis et al., 2003) but these may differ according to biomass type, origin and the processing to which it has been subjected.

This paper studies chromium binding to seaweeds from each of the three main classes available off the South-East coast of Ireland. The seaweeds under investigation are *Fucus vesiculosus* and *Fucus spiralis* (brown), *Ulva* spp. and *Ulva lactuca* (green), *Palmaria palmata* and *Polysiphonia lanosa* (red). Cr(III) and Cr(VI) binding to dead seaweed biomass is described in terms of binding capacity and affinity while the effects of manipulation of experimental parameters e.g. pH, equilibrium time and initial metal concentration on binding are also investigated. Fourier transform infrared spectroscopy (FTIR) is also employed to identify the specific functionalities involved in chromium binding to these seaweeds.

2. Materials and methods

2.1. Biomass

Seaweeds were harvested from Fethard-on-Sea, Co. Wexford, Ireland (52°11′53.68″N, 6°49′34.36″W), rinsed thoroughly with distilled water, oven-dried at 60 °C for 24 h, then subsequently ground and sieved to a particle size of 500–850 μm (Raw biomass).

2.2. Metal solutions

Working solutions were prepared by dilution of chromium stock solutions (19 mM) with distilled water. Solution pH was adjusted using 0.1 M NaOH and HCl as required. Initial and equilibrium metal concentrations were subsequently determined using AAS (SpectrAA-600 VARIAN, Software version 4.10, flame mode).

2.3. Optimum pH determination

One hundred milligrams of raw biomass were added to 50 ml of 1 mM Cr(III) and Cr(VI) solutions adjusted to pH 1.5–6. Flasks were shaken for 6 h at 200 rpm and room temperature (RT) (21 ± 1 °C). Samples were filtered under vacuum and the filtrate was analysed via AAS. The equilibrium metal uptake q (mmol g^{-1}) was calculated according to an equation used by Lodeiro et al. (2004).

2.4. Determination of equilibrium time

One hundred milligrams of raw biomass were added to 50 ml of 1 mM Cr(III) and Cr(VI) solutions adjusted to pH 4.5 and pH 2, respectively. Flasks were shaken at 200 rpm and RT with samples removed at intervals of 5, 10, 30, 60, 120, 240, 300 and 360 min and subsequently analysed by AAS. The metal uptake at time t (q_t) was calculated according to an equation adapted from Lodeiro et al. (2004).

2.5. Batch adsorption experiments

One hundred milligrams of raw biomass were added to 50 ml of Cr(III) and Cr(VI) solutions of various concentrations (0.09–4.8 mM) adjusted to pH 4.5 and pH 2, respectively. Flasks were shaken for 4 h at RT and 200 rpm. After suitable dilution, metal uptake was measured using AAS and q was then calculated. Data was analysed using the linearised Langmuir equation which yielded q_{max}, the maximum metal uptake (mmol g^{-1}) and b, an affinity parameter (mM^{-1}).

2.6. Fourier transform infrared spectroscopy

Protonated biomass was used as the biosorbent control during FTIR analysis and was prepared according to a procedure adapted from Fourest and Volesky (1996). Protonated biomass (at a concentration of 2 mg ml^{-1}) was exposed to 4 μM Cr(III) and Cr(VI) solutions (adjusted to pH 4.5 and 2, respectively) over a 4 h period. Samples were filtered under vacuum, oven-dried at 60 °C for 24 h and analysed directly using a Digilab Scimitar Series infrared spectrometer (MIRacle™ Single Reflection HATR diamond accessory). A background scan with the diamond in place was run before each analysis. Triplicate samples were analysed over 40 scans at a resolution of 2 cm^{-1}.

3. Results and discussion

3.1. Optimum pH determination

Chromium-containing wastewaters are usually acidic and thus, pH experiments in this study were conducted in the pH range 1.5–6. Various authors (Figueira et al., 1999; Chen et al., 2002; Davis et al., 2003) have shown that solution pH greatly influences metal biosorption by seaweeds. Functional groups such as sulphonate (–OSO_3) and carboxyl (–COOH) display acidic characteristics and therefore, the pH at which maximum metal uptake occurs is related to the pK_a of these groups. The point of zero charge (PZC) of the seaweeds was determined from potentiometric titrations in a previous study by Murphy et al. (2007). *F. vesiculosus* and *F. spiralis* were shown to have PZC values of 6.05 and 5.85, respectively, *U. lactuca* and *Ulva* spp. had values of 6.45 and 6.13 while the values for *P. palmata* and *P. lanosa* were 6.18 and 6.41. These results are comparable with those reported by Romero-Gonzalez et al. (2001) for dealginated seaweed waste where the PZC was 6.36. Therefore, below the PZC, the biomass still has a net positive charge despite the presence of dissociated negatively charged functionalities.

Cr(III) is cationic in solution (Cr^{3+} and $CrOH^{2+}$) while Cr(VI) occurs as anionic species such as CrO_4^{2-} and $HCrO_4^-$. Therefore, changes in pH should have significantly different effects on the binding behaviour of the chromium species. The relationship between chromium uptake and solution pH is illustrated in Fig. 1.

Please cite this article in press as: Murphy, V. et al., Comparative study of chromium biosorption by red, green and ..., Chemosphere (2007), doi:10.1016/j.chemosphere.2007.08.015

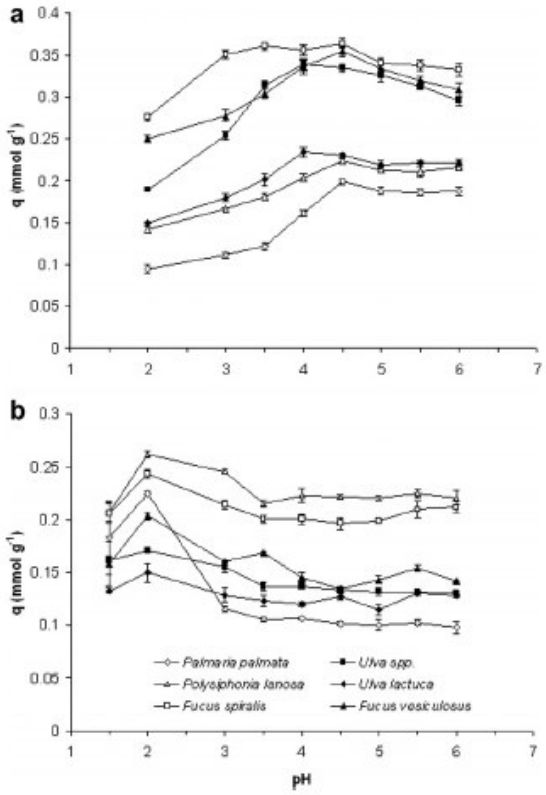

Fig. 1. Determination of the optimum pH for (a) Cr(III) and (b) Cr(IV) sorption. Error bars are calculated based on triplicate runs with 95% confidence intervals. Initial metal concentration = 1 mM, biomass concentration = 2 mg ml^{-1}.

It is clearly seen that, in Fig. 1a, up to pH 4.5, an increase in pH resulted in increased Cr(III) uptake. At pH values <3, competition from H^+ ions in solution for available biomass binding sites contributes to decreased Cr(III) binding. However, as pH increases, fewer H^+ ions are present in solution resulting in less competition for binding sites and hence increasing Cr(III) uptake. The pH dependence of Cr(III) uptake suggests that carboxyl groups (pK_a 3.5–5.0) are important in binding (Sheng et al., 2004). Murphy et al. (2007) identified various carboxyl functionalities with pK_a values in this range for the seaweeds under investigation e.g. *F. vesiculosus* (3.85 ± 0.1 and 4.68 ± 0.2) and *Ulva* spp. (3.69 ± 0.3 and 4.59 ± 0.3). Therefore, it was expected that carboxyl groups would significantly influence metal binding in these seaweeds. Sheng et al. (2004) also showed that sulphonate groups (pK_a 1.0–2.5) may contribute to metal binding at low pH. The interaction of these functionalities with Cr(III) is evident in Fig. 1a, where there is decreased, but not negligible metal uptake at low pH.

At pH >3.5, dissociation of sulphonate and carboxyl functionalities leads to increased negative charge on the biomass, so, while anionic Cr(VI) species are repelled, cationic Cr(III) experiences an increased attraction to the biomass resulting in improved metal binding.

From Fig. 1a, pH 4.5 was chosen as the optimum pH for Cr(III) sorption. At this pH, maximum uptake was achieved and metal precipitation as $Cr(OH)_3$ was avoided (Yun et al., 2001). Haug and Smidsrod (1970) showed that, in the pH range 1–5, Cr^{3+} and $CrOH^{2+}$ are the major species present in solution with the affinity of Cr^{3+} for biomass binding sites being significantly larger than that of $CrOH^{2+}$. At pH values <3.5, $CrOH^{2+}$ binding remains at a level lower than that of Cr^{3+} but gradually increases with increasing pH and eventually exceeds the level of Cr^{3+} binding at pH >4.5, possibly explaining the decreased Cr(III) binding observed above this pH.

The optimum pH for Cr(VI) sorption was pH 2 (Fig. 1b). Increased solution pH increases the negative charge on the biomass thus repelling anionic Cr(VI) species. As solution pH decreases, amino and carboxyl groups may become protonated, thus making the biomass more positively charged and hence creating an electrostatic attraction with Cr(VI) species.

3.2. Determination of equilibrium time for Cr(III) and Cr(VI) sorption

Fig. 2 illustrates the equilibrium time required for chromium uptake by the six seaweeds. Both Cr(III) and Cr(VI) binding resulted in similar kinetic patterns with rapid initial sorption followed by a long period of equilibrium. After this equilibrium period, metal uptake did not change considerably with time. This result is in agreement with those found for a number of similar biosorbent types (Aksu, 2002; Sheng et al., 2004).

The equilibrium time required for different biomass–metal systems in this study ranged from 30 to 180 min with Cr(III) binding requiring shorter equilibrium times in all cases. The red seaweeds each required 30 min for Cr(III) uptake, *U. lactuca* required 60 min while, *Ulva* spp, *F. vesiculosus* and *F. spiralis* each took 120 min to reach equilibrium. Conversely, Cr(VI) equilibrium required 120 min for *Ulva* spp., *U. lactuca* and *P. palmata* with the remaining seaweeds reaching equilibrium within 180 min of exposure. Disparities in equilibrium time between Cr(III) and Cr(VI) point to obvious mechanistic differences in binding but this finding requires further investigation which is outside the immediate scope of this paper.

3.3. Adsorption isotherms

Fig. 3 illustrates the experimental isotherm plots obtained for Cr(III) and Cr(VI) binding. Using the data in Fig. 3, removal efficiencies (RE) at high and low initial metal concentrations (C_i) were calculated (Table 1).

At low C_i (0.09 mM), *P. palmata* displayed the greatest RE for Cr(III) and Cr(VI). This value was significantly decreased at high C_i (3.84 mM) thus indicating the

Please cite this article in press as: Murphy, V. et al., Comparative study of chromium biosorption by red, green and ..., Chemosphere (2007), doi:10.1016/j.chemosphere.2007.08.015

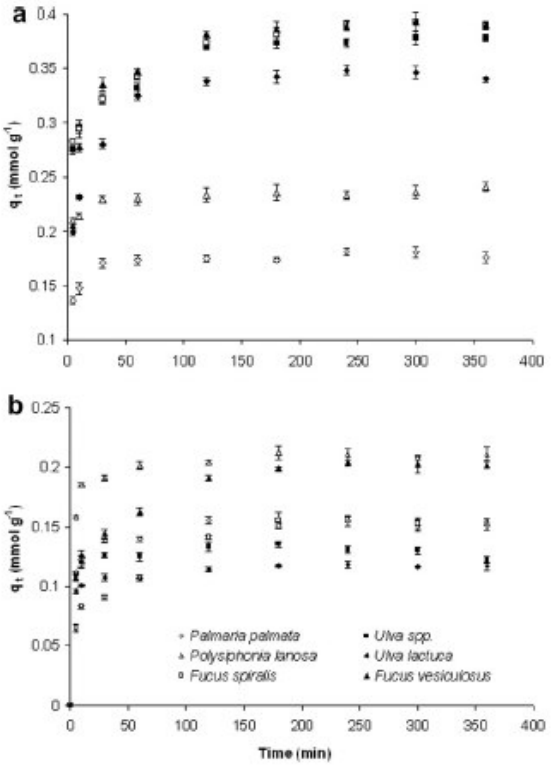

Fig. 2. Determination of equilibrium binding time for (a) Cr(III) and (b) Cr(VI) sorption. Error bars are calculated based on triplicate runs with 95% confidence intervals. Initial metal concentration = 1 mM, biomass concentration = 2 mg ml^{-1}, pH = 4.5 and 2, respectively.

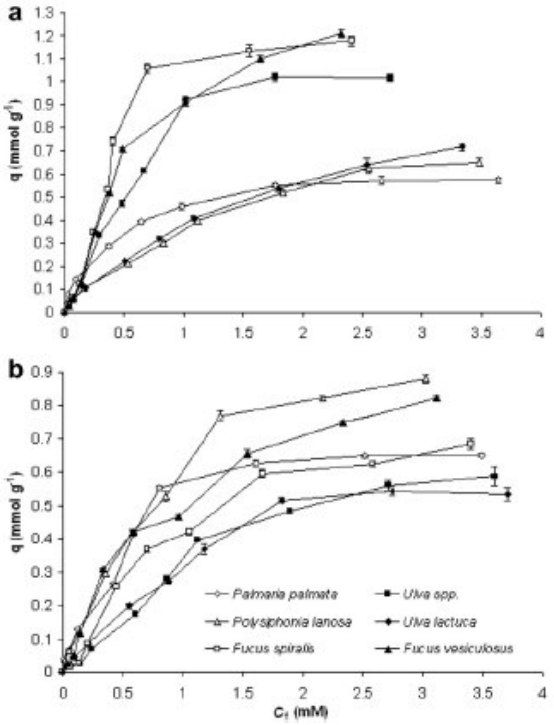

Fig. 3. Experimental isotherm data for (a) Cr(III) and (b) Cr(VI) sorption. Biomass concentration = 2 mg ml^{-1}. pH = 4.5 and 2, respectively. Error bars are calculated based on triplicate runs with 95% confidence intervals.

suitability of this seaweed for treatment of dilute metal solutions. On the other hand, at high C_i, *F. vesiculosus* displayed the highest RE for Cr(III), but for Cr(VI), both *F. vesiculosus* and *P. lanosa* had the same RE (within error) indicating their potential applicability for treatment of more concentrated metal solutions. RE values reflect the increased number of metal ions competing for available binding sites at high C_i. At low C_i, the number of available binding sites on the biomass is high (relative to the metal concentration) and hence metal uptake is very efficient.

The Langmuir isotherm was also used to model experimental isotherm data in Fig. 3. Langmuir parameters provide useful information regarding the sorption process in terms of maximum uptake capacity (q_{max}) and affinity (b). Although q_{max} is dependent on experimental conditions such as solution pH and temperature, it is a good measure for comparing different sorbents for the same metal.

The initial isotherm gradient indicates the sorbent affinity at low metal concentrations. In the Langmuir equation, this initial gradient corresponds to the affinity constant b. Davis et al. (2003) showed that a high b value indicates a steep desirable beginning of the isotherm which reflects high affinity of the sorbent for the metal.

Table 1
Removal efficiencies for chromium binding to six seaweeds

	Cr(III) (%) C_i (mM)		Cr(VI) (%) C_i (mM)	
	0.09	3.84	0.09	3.84
Fucus vesiculosus	74 ± 1	50 ± 2	76 ± 3	39 ± 1
Fucus spiralis	70 ± 3	43 ± 2	56 ± 3	35 ± 1
Ulva lactuca	73 ± 1	30 ± 1	50 ± 3	23 ± 1
Ulva spp.	71 ± 1	43 ± 2	45 ± 1	25 ± 1
Palmaria palmata	87 ± 1	24 ± 1	91 ± 2	28 ± 1
Polysiphonia lanosa	63 ± 2	27 ± 1	81 ± 2	37 ± 2

Errors are calculated based on triplicate analyses with 95% confidence intervals.

Plots of $1/q$ vs. $1/C_f$ were constructed according to the linearised Langmuir equation resulting in a straight line with a slope of $(1/(b \cdot q_{max}))$ and an intercept of $(1/q_{max})$. Langmuir parameters q_{max} and b are summarised in Table 2.

The q_{max} values obtained for Cr(III) binding decreased in the order: brown > green > red with *F. vesiculosus* and *P. palmata* having the highest and lowest values, respectively. The q_{max} values obtained by Tsui et al. (2006) for Cr(III) binding to *Sargassum hemiphyllum* (1.39 mmol g^{-1})

Please cite this article in press as: Murphy, V. et al., Comparative study of chromium biosorption by red, green and ..., Chemosphere (2007), doi:10.1016/j.chemosphere.2007.08.015

Table 2
Langmuir parameters for chromium biosorption by six seaweeds

	Cr(III)			Cr(VI)		
	q_{max} (mmol g^{-1})	b (mM^{-1})	r^2	q_{max} (mmol g^{-1})	b (mM^{-1})	r^2
Fucus vesiculosus	1.21 ± 0.12	1.88 ± 0.20	0.98	0.82 ± 0.04	1.76 ± 0.16	0.98
Fucus spiralis	1.17 ± 0.09	1.77 ± 0.13	0.99	0.68 ± 0.05	1.47 ± 0.15	0.97
Ulva lactuca	0.71 ± 0.04	1.98 ± 0.19	0.94	0.53 ± 0.07	1.97 ± 0.19	0.99
Ulva spp.	1.02 ± 0.10	1.38 ± 0.12	0.99	0.58 ± 0.07	1.20 ± 0.12	0.97
Palmaria palmata	0.57 ± 0.03	4.94 ± 0.34	0.98	0.65 ± 0.09	8.64 ± 0.31	0.86
Polysiphonia lanosa	0.65 ± 0.03	1.34 ± 0.11	0.99	0.88 ± 0.11	2.44 ± 0.23	0.94

Errors are calculated based on triplicate analyses with 95% confidence intervals.

are well matched with those found for the brown seaweeds in this study while a q_{max} of 0.54 mmol g^{-1} for *Spirogyra* biomass (Bishnoi et al., 2007) was also comparable with the results obtained for *P. palmata* in this study.

Although q_{max} indicates overall capacity, biomass performance is likely to be determined by both q_{max} and b values. For example, a biosorbent with a low q_{max} and a high b could outperform a biosorbent with a high q_{max} and a low b, especially in cases where metal ions are present in trace amounts (Hashim and Chu, 2004). In this study, despite *P. palmata* having a q_{max} of less than half that of *F. vesiculosus*, it possessed the largest b value thus indicating its high affinity for Cr(III) at low equilibrium concentrations. Therefore, the most suitable seaweed for Cr(III) sorption depends on its final application with *F. vesiculosus* being most suitable for high concentration applications and *P. palmata* being most suitable for low residual concentrations. In the case of *P. palmata*, its potential suitability as a biosorbent for Cr(III) is not readily apparent if the seaweeds are compared purely on the basis of q_{max}.

In contrast to Cr(III), isotherm analysis of Cr(VI) binding (Table 2) revealed that the red seaweed *P. lanosa* had the greatest q_{max}. However, similarly to Cr(III) binding, the affinity parameter, b, was highest for Cr(VI) binding to *P. palmata*. Therefore, *P. palmata* has high affinity for both cations and anions at low residual concentrations. From the values obtained in this study, it appears that the most suitable seaweed for Cr(VI) biosorption is *P. lanosa* as it possessed comparatively large q_{max} and b values. This result is in agreement with those found by various authors detailing the improved sorption performance of red seaweeds for Cr(VI) (Nourbakhsh et al., 1994; Cabatingan et al., 2001).

3.4. Fourier transform infrared spectroscopy (FTIR)

FTIR spectroscopy has previously been used to detect vibrational frequency changes in seaweeds and allows identification of the functionalities capable of interacting with metal ions (Figueira et al., 1999; Park et al., 2004; Sheng et al., 2004). Assignment of the FTIR peaks to specific functional groups is based on the work of Clothup et al. (1990). FTIR spectra of protonated, Cr(III) and Cr(VI) loaded *Ulva* spp. are shown in Fig. 4 and detail the significant band shifts observed after chromium binding to the seaweed.

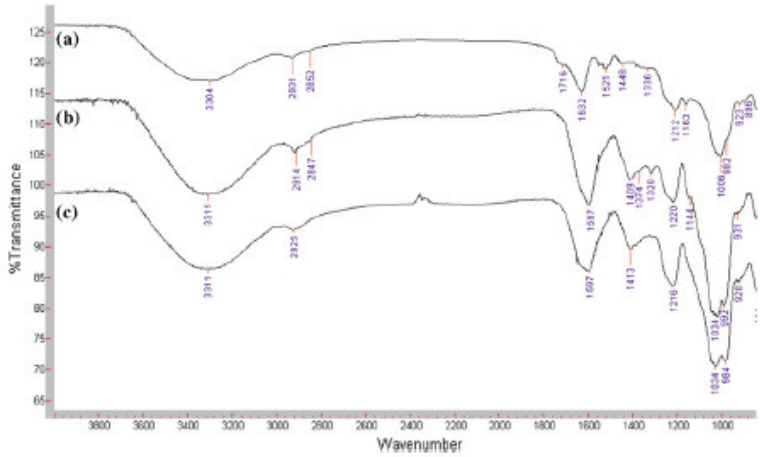

Fig. 4. Stretching frequencies observed for (a) protonated and (b) Cr(III)-loaded (c) Cr(VI)-loaded *Ulva* spp. Number of scans = 40, resolution = 2. Sample spectra from triplicate analyses are shown.

Please cite this article in press as: Murphy, V. et al., Comparative study of chromium biosorption by red, green and ..., Chemosphere (2007), doi:10.1016/j.chemosphere.2007.08.015

Considerable amino interaction was evident from the disappearance of the –NH stretching band (1525 cm^{-1}) in the Cr(III) and Cr(VI)-loaded spectra (Fig. 4b and c). "Free" carboxyl groups gave rise to a stretching band at 1716 cm^{-1} (Fig. 4a) which was not present after chromium exposure indicating participation of these functionalities in metal binding. A strong asymmetric C=O stretch initially present at 1632 cm^{-1} in (a) was also shifted to 1597 cm^{-1} in (b) and (c) thus pointing to changes in carboxyl symmetry after chromium binding. The symmetric C=O stretch was similarly shifted from 1448 cm^{-1} in (a) to 1409 cm^{-1} and 1413 cm^{-1} in (b) and (c), respectively. This decrease, coupled with a wavenumber increase of the C–O (carboxyl) stretch from 1212 cm^{-1} after binding pointed to coordination between seaweed carboxyl groups and chromium ions.

Sulphonate groups also contributed to both Cr(III) and Cr(VI) binding to *Ulva* spp., with slight differences in band shifting observed between oxidation states. Cr(III) binding resulted in a large wavenumber decrease for both the asymmetric (1336–1320 cm^{-1}) and symmetric (1163–1144 cm^{-1}) $–SO_3$ bands while Cr(VI) binding resulted in the disappearance of these bands, possibly indicating greater involvement of $–SO_3$ in Cr(VI) binding.

Biomass hydroxyl groups also played a major role in chromium binding as shown by changes in peak wavenumber and shape. Large wavenumber increases of the C–O (alcohol) band from 1006 cm^{-1} (a) to 1034 cm^{-1} (b) and (c) were observed with the appearance of an additional peak shoulder at 992 cm^{-1} in the Cr(III)-loaded sample and 984 cm^{-1} in the Cr(VI)-loaded sample.

While all seaweed–metal combinations showed significant contributions of carboxyl, amino and sulphonate groups, their relative importance varied between species and metal oxidation state. Participation of hydroxyl and ether functionalities in chromium binding also varied greatly between species. Only the green seaweeds and the red seaweed *P. lanosa* showed any interaction between chromium and biomass hydroxyl groups. On the other hand, ether participation occurred only in brown seaweeds and for Cr(VI) binding to the red seaweeds. Therefore, the effects of chromium binding to these seaweeds must be evaluated with both differences in species and metal ion in mind.

4. Conclusions

A methodology for screening various seaweeds for chromium biosorption was demonstrated in this work. Comparison of metal biosorption performance was based on expressing metal uptake against key biosorption parameters such as solution pH, equilibrium time and initial metal concentration. Chromium biosorption was highly pH dependent with higher and lower pH values favouring Cr(III) and Cr(VI) removal respectively. Cr(VI) binding also required longer exposure times than Cr(III) to ensure that equilibrium had been reached. It was shown that, at high C_i, RE values were related to the quantity of binding sites available on the seaweed. Langmuir Isotherm analysis indicated that consideration of both q_{max} and b values are necessary when determining the most suitable seaweed for chromium biosorption. FTIR analysis indicated involvement of a number of functionalities in chromium binding, the extent of which varied between seaweed species and metal oxidation state. The results obtained in this study therefore warrant further investigation into the practical applicability of dried seaweed biomass as a biosorbent for chromium-loaded waste streams.

Acknowledgments

The authors gratefully acknowledge the support of the Irish Research Council for Science, Engineering and Technology under the Embark Initiative in addition to that of Technology Sector Research – (Strand III).

References

Aksu, Z., 2002. Determination of the equilibrium, kinetic and thermodynamic parameters of the batch biosorption of nickel(II) ions onto *Chlorella vulgaris*. Process Biochem. 38, 89–99.

Arslan, G., Pehlivan, E., 2007. Batch removal of chromium(VI) from aqueous solution by Turkish brown coals. Bioresource Technol. 98, 2836–2845.

Baral, A., Engelken, R.D., 2002. Chromium-based regulations and greening in metal finishing industries in the USA. Environ. Sci. Policy 5, 121–133.

Bishnoi, N.R., Kumar, R., Kumar, S., Rani, S., 2007. Biosorption of Cr(III) from aqueous solution using algal biomass spirogyra spp. J. Hazard. Mater. 145, 142–147.

Cabatingan, L.K., Agapay, R.C., Rakels, J.L.L., Otters, M., van der Wielen, L.A.M., 2001. Potential of biosorption for the recovery of chromate in industrial wastewaters. Ind. Eng. Chem. Res. 40, 2302–2309.

Chen, J.P., Hong, L.A., Wu, S.N., Wang, L., 2002. Elucidation of interactions between metal ions and Ca alginate-based ion-exchange resin by spectroscopic analysis and modeling simulation. Langmuir 18, 9413–9421.

Clothup, N.B., Daly, L.H., Wiberley, S.E., 1990. Introduction to Infrared and Raman Spectroscopy, third ed. Academic Press, London.

Costa, M., 2003. Potential hazards of hexavalent chromate in our drinking water. Toxicol. Appl. Pharm. 188, 1–5.

Davis, T.A., Volesky, B., Mucci, A., 2003. A review of the biochemistry of heavy metal biosorption by brown algae. Water Res. 37, 4311–4330.

Figueira, M.M., Volesky, B., Mathieu, H.J., 1999. Instrumental analysis study of iron species biosorption by *Sargassum* biomass. Environ. Sci. Technol. 33, 1840–1846.

Fourest, E., Volesky, B., 1996. Contribution of sulfonate groups and alginate to heavy metal biosorption by the dry biomass of *Sargassum fluitans*. Environ. Sci. Technol. 30, 277–282.

Hashim, M.A., Chu, K.H., 2004. Biosorption of cadmium by brown, green, and red seaweeds. Chem. Eng. J. 97, 249–255.

Haug, A., Smidsrod, O., 1970. Selectivity of some anionic polymers for divalent metal ions. Acta Chem. Scand. 24, 843–847.

Lodeiro, P., Cordero, B., Grille, Z., Herrero, R., Sastre de Vicente, M.E., 2004. Physicochemical studies of cadmium(II) biosorption by the invasive alga in Europe, *Sargassum muticum*. Biotechnol. Bioeng. 88, 237–247.

Murphy, V., Hughes, H., McLoughlin, P., 2007. Copper binding by dried biomass of red, green and brown macroalgae. Water Res. 41, 731–740.

Nourbakhsh, M., Sag, Y., Ozer, D., Aksu, Z., Kutsal, T., Caglar, A., 1994. A comparative study of various biosorbents for removal of

Please cite this article in press as: Murphy, V. et al., Comparative study of chromium biosorption by red, green and ..., Chemosphere (2007), doi:10.1016/j.chemosphere.2007.08.015

chromium(VI) ions from industrial waste waters. Process Biochem. 29, 1–5.

Park, D., Yun, Y.S., Cho, H.Y., Park, J.M., 2004. Chromium biosorption by thermally treated biomass of the brown seaweed, *Ecklonia* sp. Ind. Eng. Chem. Res. 43, 8226–8232.

Park, D., Yun, Y.S., Kyung, H.Y., Park, J.M., 2006. Effect of Ni(II) on the reduction of Cr(VI) by Ecklonia biomass. Bioresource Technol. 97, 1592–1598.

Romero-Gonzalez, M.E., Williams, C.J., Gardiner, P.H.E., 2001. Study of the mechanisms of cadmium biosorption by dealginated seaweed waste. Environ. Sci. Technol. 35, 3025–3030.

Schiewer, S., Wong, M.H., 2000. Ionic strength effects in biosorption of metals by marine algae. Chemosphere 41, 271–282.

Sheng, P.X., Ting, Y.P., Chen, J.P., Hong, L., 2004. Sorption of lead, copper, cadmium, zinc, and nickel by marine algal biomass: characterization of biosorptive capacity and investigation of mechanisms. J. Colloid Interf. Sci. 275, 131–141.

Smith, R.W., Lacher, C., 2002. Sorption of Hg (II) by *Potamogeton natans* dead biomass. Miner. Eng. 15, 187–191.

Tsui, M.T.K., Cheung, K.C., Tam, N.F.Y., Wong, M.H., 2006. A comparative study on metal sorption by brown seaweed. Chemosphere 65, 51–57.

Yun, Y.S., Park, D., Park, J.M., Volesky, B., 2001. Biosorption of trivalent chromium on the brown seaweed biomass. Environ. Sci. Technol. 35, 4353–4358.

Please cite this article in press as: Murphy, V. et al., Comparative study of chromium biosorption by red, green and ..., Chemosphere (2007), doi:10.1016/j.chemosphere.2007.08.015